The interaction between metabolism and the plasma membrane potential, and intracellular pH

Mahmoud Farout, MSc

Thesis submitted for the double degree of

Doctor of Philosophy

undertaken at

Department of Physics
Lancaster University
Lancaster, UK

Department of Physics
An-Najah Nat. University
Nablus, Palestine

July 2019

Acknowledgements

I would like to thank my supervisor Professor Aneta Stefanovska for her help and unwavering support throughout my PhD. Without her help, support and time I would not have completed this thesis.

In addition, thanks go to Professor Lars Olsen who provided me with part of the data, and discussed with me part of the analysed results. Thanks also go to Dr Shakil Patel who provided me with the other part of the data analysed in this thesis. I would also like to thank Professor Peter McClintock and Professor Isobel Hook.

I would like to thank Dr Lawrence Sheppard who provided me with Matlab code of harmonics finder and discussed with me the results obtained from my study. Thanks go to Dr Gemma Lancaster for her support in the Matlab. Thanks also go to Dr Julian, Dr Will, Dr Phil, and Rosemary who helped me in proofreading of this thesis.

To my fellow, Aleksandra Pidde, for her time in discussing the results of a part of this work. Many thanks to Dr Yeheven Suprunenko for his help and interesting discussion. I would like also to thank my officemates and friends at Lancaster University; Dr Maxime, Miroslav, Yunus, Federico, Bastian, Hala, Sultan, Joe, Dr Valentina, Dr Boštjan and Dr Carlo.

Thanks go to my family who were patients within the period that I spent at Lancaster University. Specially, my wife Lara, my daughters Shushu and Ishraq, and my sons Shams and Habib.

Finally, I would like to thank Lancaster University and An-Najah National University (Nablus-Palestine) for funding my PhD research.

Declaration

This thesis is my original work and has not been submitted, in whole or in part, for a degree at this or any other university. Nor does it contain, to the best of my knowledge and belief, any material published or written by another person, except as acknowledged in the text.

Ethics Declaration

The data analysed within this work were collected in accordance with the appropriate permissions from their respective institutions or committees, as detailed below.

The resting membrane potential data from jurkat T cells used in chapter 5 was recorded by S. Patel as a part of his PhD study at Lancaster University. The data is available via DOI: https://doi.org/10.17635/lancaster/researchdata/249

The glycolytic oscillations data from population of suspensions of yeast cells were measured in Denmark by Professor Lars Olsen, and we received the data from him personally. The data is available via DOI:
https://doi.org/10.17635/lancaster/researchdata/248

List of publications

The following manuscripts are currently under preparation:

A. Pidde, M. Farout, and A. Stefanovska, Fluctuations in the membrane potential in Jurkat cells. In preparation (Work from chapter 5, section 5.1).

M. Farout, L. Olsen and A. Stefanovska, Interaction of metabolism, mitochondrial membrane potential and intracellular pH. In preparation (Work from chapter 5, section 5.2).

Parts of the work have also been presented at the following scientific meetings and workshops:

M. Farout, A. Pidde, S. Patel, J. Owen-Lynch, S. Roberts, and A. Stefanovska. Fluctuations in the resting membrane potential of jurkat T lymphocytes Sixth Palestinian Conference on Modern Trends in Mathematics and Physics PCMTMP-VI, 5-8 August 2018 Palestine, Oral presentation.

M. Farout, and A. Stefanovska, Interaction of metabolism, membrane potential and cell volume. POBO. 27-30 November 2018. Buckinghamshire, UK. Poster Presentation. I got the third prize at the conference.

Abstract

Hodgkin and Huxley won a Nobel Prize for their passive model of the squid axon. Their model describes the voltage across a cell plasma membrane, based on measurements in the squid axon. The model explains the generation of action potential. It was published over 60 years ago, however, their model still represents the paradigm in neurobiology [1]. Hodgkin and Huxley used the voltage-clamping method to do their measurements of currents across the membrane of the axon. All measured currents are caused by the diffusion of ions due to their electrochemical gradients. Due to the voltage-clamping method that they used, there was no need to include active transport in their model, therefore, metabolism was ignored in their study. In reality, metabolism is required to produce ATP, which is required to operate the ATPases that regenerates the electrochemical gradient of the cations Na^+ and K^+ and results in maintenance of the plasma membrane potential [2]. Therefore, it is still unknown how the energy state of a cell is involved in the generation of the plasma membrane potential, and what is the origin of the fluctuations in the voltage across the membrane of a cell. Here we discuss results of free-running whole-cell patch-clamp recordings of the resting membrane potential of jurkat T cells [3]. Since the voltage was not clamped in these experiments, it is plausible to assume that a metabolism is required to pump the cations against their electrochemical gradients. These pumps have been shown to be crucial in maintenance of the plasma membrane potential [3]. To study the interactions between the plasma membrane potential and metabolism, we analysed data recorded in yeast cells in suspension [4, 5]. The measurements include the energy state of the cell evaluated from the intracellular level of ATP in the yeast population, and the mitochondrial membrane potential obtained by a fluorescent recording [6]. In addition, nicotinamide adenine dinucleotide NAD and hydrogen H substance (NADH), plays a role in the chemical process that generates energy for the cell, as well as the intracellular pH were measured. All measured parameters were oscillating over time under aerobic/anaerobic shift. The results were

analysed using time series analysis methods that allow for time-localised analyses of the underlying dynamics [7, 8, 9]. We will present results of analysis of interaction between cellular functional processes and argue that the metabolism is driving them. The results suggest that the mitochondrial F_0F_1-ATPase might be involved in the mechanism by which glycolytic oscillations are driving the oscillations in the mitochondrial membrane potential and the cytosolic pH. The results were modelled as phase oscillators of glycolysis, cytosolic pH and the mitochondrial membrane potential. This model regenerates the signals measured from yeast cells and show approximately the same main mode frequency as the original data.

Glossary and abbreviations

ACA N-(p-amylcinnamoyl) anthranilic acid; TRPM2 cation channels inhibitor.

ADP adenosine diphosphate. It is required with phosphate to synthesize ATP.

Aerobic respiration a process require energy, therefore it produces energy more than Anaerobic respiration.

AMP adenosine monophosphate is simply the adenosine molecule bonded to only one phosphate group.

Anaerobic respiration a process that does not use oxygen, therefore produces less energy.

Antiporter a protein that is moving two types of ions or molecules in opposite direction using the energy of one of them to move the other one against it electrochemical gradient.

Apoptosis a programmed cell death, abnormally avoided by cancer cells.

ATP adenosine triphosphate, energy currency of the cell. ATP is used as an energy source for many cellular processes such as protein synthesis, maintenance of the membrane potential and cell volume regulation.

AVD apoptotic volume decrease.

CFTR cystic fibrosis transmembrane conductance regulator.

Cl^--mini small conductance of Cl^- channel.

Cl^--maxi big conductance of Cl^- channel.

$Cl^-_{swelling}$ a chloride channel which is activated by cell swelling and membrane stretching.

Crabtree effect a phenomenon of aerobic fermentation in a high external glucose concentration.

Cotransporter a protein that moves two or more ions or molecules in the same direction utilizing the energy of one or two of them to move the remaining against its electrochemical gradient.

CRAC calcium release-activated channel.

Cytosol the liquid enclosed by the cell membrane which contains the cellular organelles.

Depolarization a process in which the membrane potential becomes less negative.

$DiOC_2(3)$ carbocyanine dye which is used to evaluate the mitochondrial membrane potential.

ER Endoplasmic reticulum.

F_0F_1-ATPase a protein located in the inner membrane of the mitochondria that synthesize ATP from the proton gradient across that membrane.

FFT fast Fourier transform. An algorithm used to transform a signal from the time domain to the frequency spectrum.

FRET fluorescence resonance energy transfer.

Hyperchloremia an increase in chloride concentration in the blood.

GHK Goldman-Hodgkin-Katz.

HK the altered bath solution with elevated K^+ used in the jurkat cells experiment.

Hyperglycemia high blood sugar.

Hyperkalaemia an increase in K^+ concentration in blood.

Hypernatremia an increase in sodium concentration in blood.

Hyperosmotic stress an increase in the number of osmolytes in the medium relative to the cytosol.

Hyperpolarization a process in which the membrane potential becomes more negative.

Hypoglycemia a decrease in glucose level in blood.

Hypokalemia a decrease in potassium concentration in blood.

Hyponatremia a decrease in sodium concentration in blood.

Hypoosmotic stress a decrease in the number of osmolytes in the medium relative to the cytosol.

Hypoxia deprivation of oxygen in the tissues.

in vivo studies on intact living organisms.

Jurkat T cell an immortalized cells which is used as a model in biological studies.

KCa calcium-activated potassium channels.

Kv voltage-gated potassium channels.

Lactate the end product of the fermentation in mammalian cells.

LCl the bath solution with lowered Cl^- used in the jurkat cell experiment.

LNa the bath solution with lowered Na^+ used in the jurkat cell experiment.

MMP the mitochondrial membrane potential, which is usually more negative inside the matrix of the mitochondria with respect to the cytosol.

NAD^+ nicotinamide adenine dinucleotide.

NADH reduced form of nicotinamide adenine dinucleotide (NAD).

NKCC Na^+, K^+, $2Cl^-$ cotransporter.

OXPHOS oxidative phosphorylation. A process requires oxygen to produce approximately 90 % of the cell ATP.

Pasteur effect an inhibiting effect of oxygen on the fermentation process.

PFK Phosphofructokinase. It is used in glycolysis to convert fructose-6-phosphate to fructose-1,6-biphosphate.

PKTHPP 1-1-[6-(biphenyl-4-ylcarbonyl)-5,6,7,8-tetrahydropyrido[4,3-d]-pyrimidin-4-yl]piperidin-4-ylpropan-1-one; an inhibitor of leak K^+ (TASK) channels.

Plasma membrane a phospholipid bilayer encloses the cell, separating it from its surroundings and contain the pathways through which energy and matter pass into or out of the cell.

pH a logarithmic scale used to specify the acidity or basicity of an aqueous solution.

PMCA plasma membrane calcium pump.

PMP the plasma membrane potential, which represent the voltage difference between the cytosol and the cell surrounding. It is usually negative inside the cell with respect to outside.

Proliferation a process in which the cell number increases as a result of cell growth and division.

Pump or ATPase a protein that hydrolyze ATP to move ions against their electro-chemical gradients.

Pyruvate an end product of breakdown of glucose which can be converted in the cytosol to lactate or transported to the mitochondria and converted to acetyl-CoA to be used in the Krebs cycle.

RVD regulatory volume decrease. A mechanism used by the cell to regulate its volume when it is exposed to hypoosmotic stress.

RVI regulatory volume increase. A mechanism used by the cell to regulate its volume when it is exposed to hyperosmotic stress.

SS standard solution used in the pipette in jurkat cells experiment.

Std standard deviation.

Symport a protein that uses the energy from an ion (molecule) to move another against its electrochemical gradient in the same direction of the first ion.

TAWP time-averaged wavelet power.

TFR time-Frequency Representation.

TRAM-34 1-[(2-chlorophenyl)diphenylmethyl]-1H-pyrazole.

Turgor pressure the pressure exerted on cell membranes or walls by water passing into the cell by osmosis.

UV ultra violet spectrum.

VGSCs voltage-gated sodium channels.

Warburg effect a phenomenon in cancer cells which favor anaerobic glycolysis to produce ATP over the efficient respiratory process.

WFT widowed Fourier transform. Time-frequency representation.

WT wavelet transform. Time-frequency representation.

2DG 2-deoxy-D-glucose, differ from glucose by the removal of an oxygen atom from the hydroxyl group at the 2 position.

φ (driving force) electro-chemical gradient or a force that drives the ions to cross the membrane.

Notations

I	electrical current
F	Faraday constant (96,485 C/mol)
V	electrical voltage
C	electrical capacitance
G	the conductance
Q	electric charge
R	gas constant (8.314 J. K^{-}1 mol^{-}1)
T	temperature in Kelvin

Contents

List of Figures

List of Tables

Chapter 1

Introduction

In the period 1930s to 1950s, Hodgkin and Huxley had measured the currents through the membrane of the squid axon, using the voltage-clamping method. Then, they had modelled their measurements, which represent only the passive current through the membrane under the influence of the electrochemical gradient of the ions passing the patch. Their model won a Nobel prize in 1963 and still represents the paradigm in neurobiology [1]. Due to the voltage-clamping method that they used, active transport of the ions against their electrochemical gradient was not included in their model, therefore, metabolism was not considered. Meanwhile, it become obvious that in living organisms, metabolism is crucial in producing the energy, which is needed to operate the ATPases (pumps) that regenerate the electrochemical gradients of the major cations Na^+ and K^+ and result in the maintenance of the voltage difference across the plasma membrane of the cell [3]. However, it is still unknown how the energy state of the cell is involved in the generation and the maintenance of the plasma membrane potential. In addition, most previous studies [10, 11, 12, 13] ignored the dynamics (fluctuations) of the membrane potential and considered the cell in a steady state, which means that fluctuations were considered in previous studies as noise [1, 14]. On the other hand, it was reported by Nakaoka et al. [15] that fluctuations in the resting membrane potential are very important in Paramecium cell. They found that this unicellular

organism is changing direction of swimming exploiting these fluctuations. They also reported that the amplitude of the fluctuations is magnified when intracellular Ca^{2+} increased significantly. These results suggest that Ca^{2+} may activate Ca^{2+}-gated K^+ channels and, as a result, the membrane conductance may increase and may cause an increase in the amplitude of membrane potential fluctuations [15]. Majima [16] studied the fluctuations in the resting potential of Paramecium. Majima reported that the amplitude of the fluctuation was between 0.5 and 5.0 mV and the amplitude of fluctuations is proportional to the driving force of K^+. Moolenaar et al. [14] reported that the magnification in the amplitude of membrane potential fluctuation is the result of an increase in the motive force (driving force) of K^+. In another work by Oosawa et al. [17], it was indicated that the amplitude of fluctuation in the resting potential is proportional to the circulating current. Therefore, there are pieces of evidence that the fluctuations in resting potential are not an artefact of the method but represent an intrinsic mechanism.

The main questions that the present study would like to answer are:

- How the energy state of the cell is involved in the membrane potential maintenance?
- How the energy state affects the dynamics of the membrane potential in standard and altered conditions?
- How metabolism interacts with other cellular processes, such as intracellular pH and the mitochondrial membrane potential, to let the cell adapt and survive under altered states when metabolism is shifted from aerobic to anaerobic? These questions will be explored and answered through the analysis in this work.

1.1 Outline of the thesis

Chapter 2 introduces the physiological background of the work. It starts with the biology of yeast *Saccharomyces cerevisiae*, then metabolism is discussed, after that ion homoeostasis is introduced. Then, the plasma membrane potential (PMP), pH, cell volume, and the mitochondrial membrane potential (MMP) are discussed. In addition, glycolytic oscillations in yeast cells are also discussed.

Chapter 3 introduces the methods used to measure the dynamics in the plasma membrane potential in jurkat T cells and the methods used to measure the fluorescence of the oscillations in NADH, ATP, pH and the mitochondrial membrane potential.

Chapter 4 shows the methods used to analyse the data measured from jurkat T cells and the data measured from synchronized oscillatory yeast cells.

Chapter 5 presents the analysis of the data and the results obtained.

Chapter 6 shows a model of the interaction between glycolysis and both cytosolic pH and the mitochondrial membrane potential.

Chapter 7 summarises the work presented in this thesis and discusses possible directions for future research.

Finally, chapter 8 provides appendices which include the derivation of Goldman-Hodgkin-Katz equation and supplementary material for the two parts of chapter 5

Chapter 2

Biophysical review

2.1 Introduction

This chapter presents a biophysical review about the biology of yeast cells including cell structure, metabolism, ion homoeostasis, plasma membrane potential, cytosolic pH, cell volume, mitochondrial membrane potential and glycolytic oscillations. The structure of this chapter will be as follow; section 2.2 is about the biology of yeast *Saccharomyces cerevisiae*. Section 2.3 discusses cell metabolism. In section 2.4, ion homoeostasis is discussed. Section 2.5 is about the plasma membrane potential. Section 2.6 is about the intracellular pH and its regulation. Section 2.7 is about the mitochondrial membrane potential. The glycolytic oscillations are discussed in section 2.8. Finally, the chapter is summarized in section 2.9.

2.2 The biology of yeast *Saccharomyces cerevisiae*

To understand the fundamentals of eukaryotic cell biology, it is complex and difficult to work with human cells. It is more effective to concentrate on simple, robust

and rapidly reproducible cells such as *E. coli* or *Saccharomyces cerevisiae* yeast (budding yeast) [18], see figure 2.1, (B). Yeasts have been known and used for thousands of years in the fermentation process, like alcoholic beverages production [19]. S. cerevisiae is considered by scientists to be a "model organism" because it is both a unicellular and eukaryotic organism at the same time. It can be cultured in an economical manner and generated rapidly (less than 2h under optimal conditions) which make the biological material adequate.

Saccharomyces cerevisiae has become a unicellular model organism in several studies; in ageing [20], mitochondrial biology [21], human medicine such as in brain function, cancer and heart disease [22], osmotic stress [23, 24, 25, 26, 27], cell wall damage [28], numerous applications in the health food industry [19], and glycolytic oscillations and measurements of glycolytic intermediates [29, 30, 31, 32, 4, 33, 5, 34].

The budding or brewster's yeast *S. cerevisiae* are commonly employed as models in biomedical and physiological research. Because they are harmless, manipulated easily and their genetic systems are able to be traced in the laboratory using fabulous molecular tools [35, 36]. Karathia et. al. (2011) proposed a method to select a model organism and applied it on *S. cerevisiae* and showed that it is a good model for animals in general and *Homo sapiens* in particular [37].

2.2.1 Description and significance

Saccharomyces (literally 'fungi of the sugar') *cerevisiae* are ubiquitous in nature, with an apparent trend for vineyard and grove soils, where they grow on falling sugary fruits from plants [38]. It is, also known as baker's yeast, a eukaryotic unicellular microbe that belongs to the fungi kingdom [19]. They colonize a large variety of natural environments, such as plant surfaces (leaves, fruits, and flowers) or tree exudates, surfaces of warm-blooded animals and even intestinal parts, grotto dirt, surfaces of insects' bodies, fresh or salt water and many other environ-

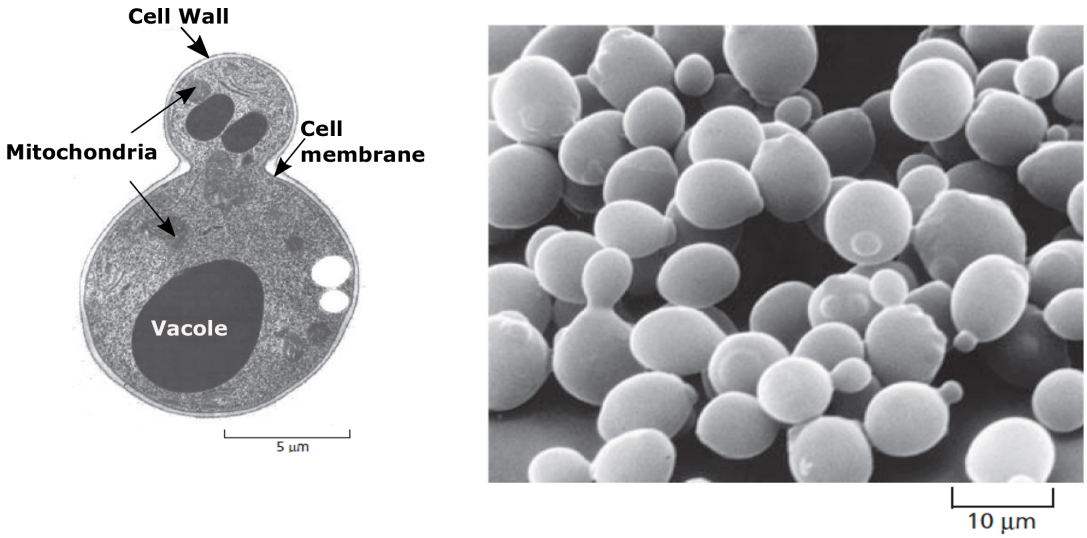

Figure 2.1: A) The structure of a budding yeast cell.B) The yeast *Saccharomyces cerevisiae* is a model eukaryote. A few yeast cells are seen in the process of dividing, which they do by budding. From [18]

ments [38].

2.2.2 Cell Structure

Saccharomyces cerevisiae is a unicellular microorganism. It is different from human cells by possessing a rigid wall, so it is relatively immobile and different from plant cells by not possessing chloroplast [18, 39].

However, yeasts, in fact, have the same subcellular structure as multicellular organisms' cells. Many scientists used it as a model for diverse fundamental and applied fields of life science, biotechnology, and medicine [40]. *S. cerevisiae* consist of approximately 30% of dry materials, 8% nitrogen, 50% of proteins, 40% of carbohydrates, 5% of lipids, 6% of minerals and vitamins amount depend on the growth condition and the type of the yeast [19].

Yamaguchi et. al. (2011) studied the cell structure of *S. cerevisiae* using freeze-substitution and serial ultrathin-sectioning electron microscopy. They found that there are 1-3 mitochondria, hundreds of thousands of ribosomes [41]. The cytoplasm occupied approximately 64% of the cell volume, cell envelope occupied 15-

17%, nucleus occupied 10.5%, vacuole occupied 5.8% and mitochondria occupied 1.7% in unbudded cells in its G1 phase.

The shape of yeast, as revealed by Leeuwenhoek in 1680, is small spherical or oval bodies [42]. Its mean diameter is ~ 3.2 μm (major axis ~ 3.6 μm and the minor axis ~ 3 μm), its mean volume is ~ 17 μm^3 and the wall thickness is 70-200 nm depending on growth conditions [43**?** , 41].

In the following, the most related parts of the structure are discussed; cell envelope, the cytoplasm and cytoskeleton, the nucleus, vacuoles, and the mitochondria.

Cell envelope

In *S. cerevisiae*, 15% of the cell volume is occupied by the cell envelope which plays a central role in governing the permeability and osmotic properties of the cell. This envelope compromises the plasma membrane, which is surrounding the yeast cytosol, the periplasmic space and cell wall [45].

The plasma membrane in all cells is a very important structure which prevents mixing of the intracellular cytoplasm with the aqueous milieu. It represents the main barrier for passages of hydrophilic molecules. In *S. cerevisiae*, the plasma membrane is about 7.5 nm thick. It can be depicted by a lipid bilayer interspersed with different functional proteins. These proteins comprise those implicated in solute transport, signal transduction, cell wall biosynthesis, and cytoskeletal anchoring [46].

Yeast plasma membrane structure is not considered fixed. But, it changes both its structure and function in response to the growth conditions. It can alter its thickness and the properties of proteins that dictate what enters or what leaves the cytoplasm. These properties are mediated by specific proteins which control nutrient uptake, ion movement, etc. [46, 47].

Signal transduction is another physiological function of the plasma membrane. It operates in response to external stimuli as heat shock, osmotic shift, toxicity, etc. In addition, endocytosis and exocytosis occur through the plasma membrane [47]. At any temperature, the fluidity of the plasma membrane increases with increasing unsaturated alkyl chain content. The length of these chains controls the bilayer thickness. When a cell is exposed to osmotic stress, the membrane lipid composition is altered to make the cell stronger. This suggests that the plasma membrane structure is dynamic to play a role in cell osmoregulation [48].

The periplasm is an outer region of 35-45 A^o that lies external to the plasma membrane and internal to the cell wall, see figure 2.1, (A). It involves the proteins which are secreted through the plasma membrane and are unable to pass the cell wall. These encompass the invertase and phosphatase which are responsible for catalysing substrates that cannot cross the plasma membrane [49]. In contrast to animal cells, yeasts possess cell walls which form a structural feature of all yeasts, see figure 2.1, (A) [40]. The cell wall of yeasts represents a thick (100-200 nm) structure, which forms 15-25% of the total dry mass of the cell. The dominant constituents of the cell wall are glucan (β-1,3 and β-1,6) and mannans which account for 80-90% [39, 50, 51, 52].

Glucan forms a strong 3D network which is responsible for the mechanical properties of the wall and provides the attachment sites for mannans which form the outer layer of the wall. Mannans forms a filter for large molecules and makes the permeability of the cell wall to be limited, thus shielding the plasma membrane from any perturbing compound or foreign enzymes. In addition, a third component of the cell wall known as chitin is present in small amounts (1-2%) which is essential in budding and for cell survival [53, 54, 39, 55, 56].

The cell wall is a strong structure which is responsible for the cell's mechanical stress resistance and supports it against osmotic changes [44, 45]. In addition, it plays an important role in transporting materials into or out of the cell and the

first line of defense against infections [40].

The cytoplasm and cytoskeleton

The yeast cytoplasm, as in all other cellular organisms, is an aqueous acidic fluid which forms the site for many activities happening in the cell. It represents the space for the intracellular low, intermediate molecules, glycogen, dissolved proteins, and other macromolecules. In addition, it contains all cell compartments; nucleus, mitochondria, etc. [47].

Compartmentalization inside the cell is an important property of all eukaryotic cells, banning improper meeting of certain compounds within the cytoplasm and facilitating reactions in an efficient order [44]. Each compartment possesses its own membrane to facilitate interactions of the cytoplasm with these compartments to increase the integrity of the cell.

The cytoskeleton network is important in providing an organized structure to the yeast cytoplasm. It comprises microtubules and microfilaments which is common in all eukaryotic cells [46]. The main compartments in cells are discussed in the text that follows.

The nucleus

In yeasts, the nucleus is an organelle of around 1.5 μm diameters which is located in the cytoplasm of the cell. The nucleus possesses a double membrane containing pores and other protein to facilitate transport between the cytoplasm and the nucleoplasm. The main function of the nucleus is to house, maintain and transcribe the DNA [18].

Vacuoles

A vacuole is one of the membrane-determined compartments in the yeast cytoplasm. In addition, it serves in cytoplasm's pH homoeostasis, osmoregulation, protein degradation, and it plays a central role in the storage of small ions, amino acids and phosphates [44].

Mitochondria

Another double membrane-determined compartment in yeasts is the mitochondrion which is found in higher eukaryotes. Mitochondria comprise an outer membrane which contains enzymes implicated in lipid metabolism. Another membrane, which is the inner membrane, contains cytochromes of the respiratory chain, NADH and succinate dehydrogenases and H^+-ATPase. The intra-mitochondrion space, known as the matrix, contains enzymes of fatty acids oxidation and the citric acid cycle, together with the machinery of protein synthesis and mitochondrial DNA [46].

Mitochondria number, size and shape in all cells are not fixed. They change according to several factors such as yeast species or strains, growth conditions and even within cell cycle [57].

Yeast mitochondria are involved in ATP production during respiration under aerobic conditions. But they become redundant under anaerobic condition due to the absence of oxygen which is required as electron acceptors. In addition, they are involved in adaptation to stresses caused by ethanol, toxic oxygen radicals and high sugar in non-respiratory function of brewing yeasts [46].

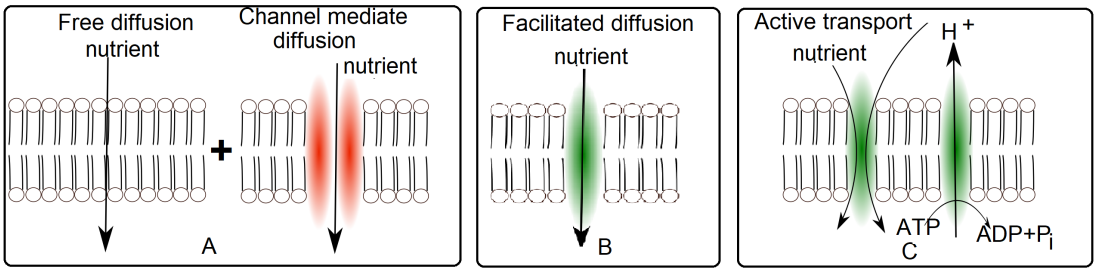

Figure 2.2: mechanisms of nutrients uptake in yeasts.

2.2.3 Translocation of the nutrients into the yeast cell

Solutes movement faces several barriers; the envelope of the cell which forms three layers; the cell wall, the periplasm and the plasma membrane, and the intracellular organellar membranes [47]. The cell wall cannot be considered as a freely porous structure despite unselectively properties. In addition, it may become weakened and lead to stretching when exposed to stresses. This may increase the permeability of the cell envelope [46].

A more selective barrier in yeasts is the plasma membrane. This barrier isolates the cell from the external environment. Therefore, it dictates nutrients that enter and metabolites that leave the cell [47]. Recognition of how these barriers regulate transport mechanism is very important in yeast physiology. Such mechanism controls the rates at which yeast cell can metabolize, grow, divide and adapt to external stresses [46].

There are three main types of processes that enable translocation of substrates across lipid bilayers:

Free diffusion These are the passive movements of lipid-soluble nutrients through the plasma membrane, see figure 2.2, (A). It is the simplest and slowest nutrient transport governed by the law of mass action from a higher concentration to a lower concentration until it reaches equilibrium. This mechanism does not need energy since it is driven by the tendency of the system to grow in entropy [47].

Facilitated diffusion This mechanism is faster than free diffusion. In addition, it is mediated by a carrier protein that undergoes conformational alterations to allow the passage of molecules, see figure 2.2(B). This mechanism is driven by the concentrations gradients and maybe an extra electric gradient in the case of ionic solutes [58, 47].

Active transport This is an energy-dependent chemiosmotic mechanism. It is responsible for the uptake of most required nutrients into yeasts. It moves nutrients against concentration gradients exploiting the membrane potential and the generated transmembrane hydrogen electrochemical gradient by the plasma membrane H-ATPase. The hydrogen (proton) gradient motive force enables uptake of nutrients with proton influx as in symport mechanism, or against proton efflux, as in antiport mechanism [47], see figure 2.2, (C).

Transport of water

As in all other organisms, in yeasts, water is essential as a solvent to facilitate the movement of solutes within the cell. In addition, water is important for the intracellular activity of the enzymes. The movement of the water both in and out of the yeast cell is limited by passage through both the plasma membrane and the cell wall through selective pathways known as aquaporins [59]. The force driving water influx in fungal cells is the turgor potential [60], which is created due to a difference between the osmotic potential of the cell and its water potential. In *S. cerevisiae*, the osmotic potential is generated by the accumulation of solutes from the external medium. When the water potential of the yeast cell is altered from a relatively steady-state condition, yeasts have to adopt this change by sometimes a very rapid response. These quick adjustments have to be by changing to a new osmotic potential by regulating their turgor potential or their cell volume [60].

For example, in the presence of higher salt or sugar concentrations, the water

potential of the growth medium decreases and cellular water will be lost, and the cell will be shrunk. But, when the converse situation happens by rising water potential, the cell will swell, and its volume will increase. In both cases, the cell will respond dramatically using unknown mechanisms to regulate its volume which is necessary for optimal metabolism and growth [46].

In the next sections, metabolism, ion homoeostasis, membrane potential, pH and cell volume will be discussed to understand a possible interaction between these processes through the transport system that derive the energy required to operate from metabolism to regulate the other processes.

2.3 Metabolism

Metabolism refers to the chemical reactions in which oxidation and reduction of nutrients are achieved by cells. In the oxidative process, catabolic pathways produce energy from intermediates by using electrons removed from them. This energy is consumed in the reductive process (anabolic pathways), in which new materials are synthesized. These processes are considered as crucial for cell growth and survival. Yeast cells are microorganisms that utilize the breakdown of many compounds to produce their chemical energy, in the form of ATP. These cells respond differently to diverse nutrients conditions (e.g. physiological or altered nutrition conditions). The energy produced by the catabolism of sugar is used to continuously fuel many cellular functional processes, such as maintenance of ionic balance across the plasma membrane, membrane potential, regulation of pH and cell volume, signalling, protein synthesis, and cell growth. On average, every day, we approximately turn over our body equivalent in ATP [61]. Therefore, our understanding of the main stages of cellular metabolism is crucially important. This importance increases when novel imaging techniques show growing correlations between many diseases with dysfunction of cell metabolism, including cancer [62, 63, 64, 65] and diabetes [66].

The production of the principal energy currency of the cell (ATP) can be achieved through two main cellular metabolic pathways: glycolysis, and oxidative phosphorylation (OXPHOS). The regulatory mechanism of cellular ATP level involves the mutual interactions between these pathways according to demand and supply [4]. In healthy cells, glycolysis, Krebs cycle and OXPHOS are required for ATP production where the later produces more than 90% of the produced energy [67]. In contrast, in metabolically altered cells, glycolysis may dominate the cellular energy production even in the presence of oxygen [68]. This phenomenon is known as Warburg effect [69, 70] and favoured in cancer cells [64, 71] and some fermentable yeasts as *S. cerevisiae* [72, 73]. The chemical reactions of glycolysis occur in the cytoplasm where OXPHOS and Krebs cycle occurs in the matrix of the mitochondria. These processes are considered as the powerhouse of the cell. The rate of ATP production depends on the type of the cell and the conditions of the cell. In physiological conditions, cells produce the higher rate of ATP using glycolysis and respiration. On the other hand, in metabolically altered cells respiration may decrease or is completely disabled, and thus, the rate of ATP production is reduced per glucose consumed. As an example, yeast cells and endothelial favour glycolysis which produces 2 ATP/1 glucose over respiration which produces 36 ATP/1 glucose when oxygen is absent, or the cell is in low energy requirements [74, 75].

2.3.1 Glycolysis

When hexose is taken up by the cell, it is converted into two molecules of pyruvate by glycolysis. A net of two molecules of ATP and two molecules of NADH are produced during this process. This process consists of 10 steps started by the consumption of 1 molecule of glucose. The sequence of reactions that catalyzed by enzymes, which oxidatively converts glucose to two molecules of pyruvates in the cytoplasm. Figure 2.3, (A) outlines these steps, which is summarized in the

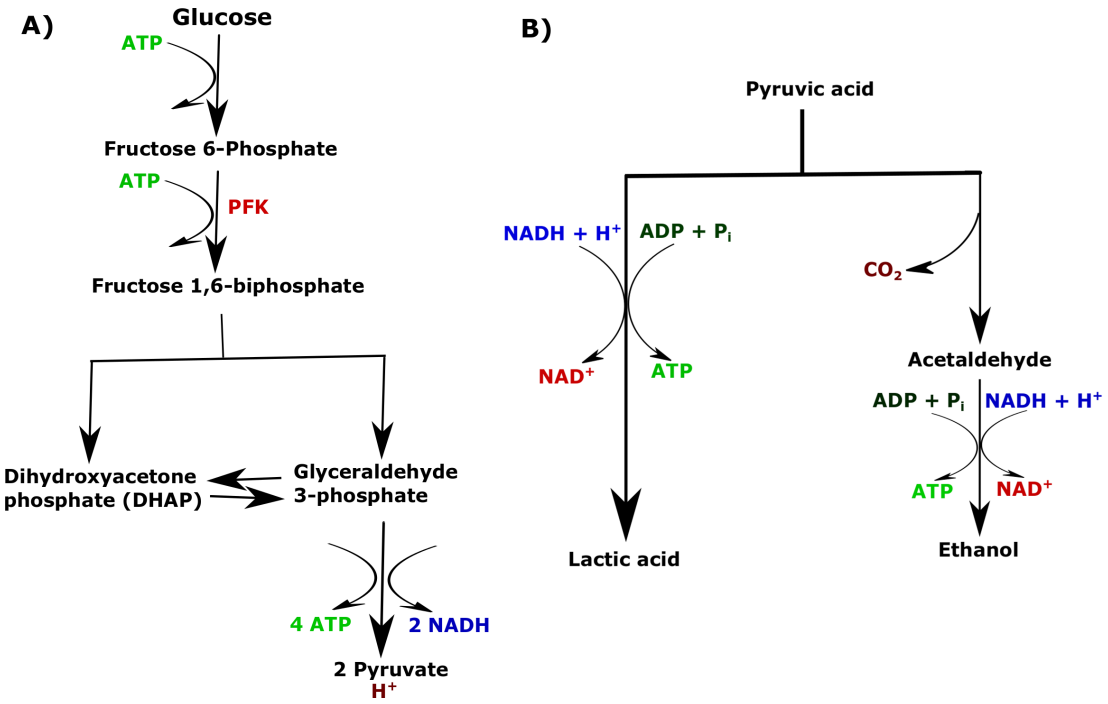

Figure 2.3: A) Glycolysis. Adapted from [46]. B) Fermentation in mammalian (left) and in yeast cells (right). Adapted from [76]

reaction [46].

$$Glucose \longrightarrow 2Pyruvate + 2ATP + 2NADH + H^{+}. \tag{2.1}$$

The enzymes that are considered as a key of regulation in glycolysis are phosphofructokinase and pyruvate kinase. The former activity is influenced by several effectors, including pH [77], ATP [78], AMP [79], and concentrations of intracellular ions such as K^{+}, ammonium and inorganic phosphate [80]. It was reported by Trivedi (1966) that PFK activity of skeletal muscles from mice and frogs is extremely sensitive to pH variations in the physiological range. Acidic pH decreases the affinity of PFK for fructose 6-phosphate (F6P) [81]. At alkali pH values, the affinity of PFK for ATP decreases. Therefore, control of glycolysis by ATP and pH may contribute to regulation of these factors. Any decrease in pH from physiological range causes a decrease in PFK affinity for F6P. And this may prevent more decrease in pH by slowing glycolysis. The concentration of other metabolites may contribute in slowing glycolysis since the decrease in PFK affinity for F6P

cannot by itself slow down the glycolysis. Sols and Salas (1966) proposed that the effect of pH on the PFK activity may be due to ATP inhibitory effect which is pH-dependent [82].

2.3.2 Respiration

Respiration is the process that involves chemical reactions that utilize nutrient molecules in living cells to produce energy. Respiration is composed of two types; aerobic and anaerobic. Aerobic respiration is the process that requires oxygen to break down nutrients and release energy. The chemical reaction that represents aerobic respiration is summarized by the equation,

$$Glucose + oxygen \longrightarrow water + carbondioxide. \tag{2.2}$$

These reactions occur in all cells all the time where most of these reactions happen in the mitochondrial matrix. In the presence of oxygen, after the conversion of glucose to pyruvates, ATP and NADH, NAD^+ is regenerated by the transfer of NADH electrons to the respiratory chain proteins. The subsequent respiratory process reduces the oxygen to water and generates a proton gradient along the inner membrane of the mitochondria. This proton gradient forms a motive force to drive the mitochondrial membrane-enzyme complex, ATP-synthase [83]. Additional ATP molecules, as well as redox equivalents, are produced by the dissimilation of pyruvates, produced by glycolysis, to carbon dioxide and water via the pyruvate dehydrogenase and the tricarboxylic acid cycle. In total, 36 ATP molecules are produced when a one glucose molecule is dissimilated completely [84].

Control of glycolytic flux in *S. Cerevisiae* has been considered to occur mainly at the level of both phosphofructokinase and pyruvate kinase. Phosphofructokinase is activated by fructose-2,6-bisphosphate [81] and AMP [79] and is inhibited by ATP [78]. Meanwhile pyruvate kinase activity is modulated by its activation

by fructose-1,6-bisphosphate [85]. However, since phosphofructokinase does not catalyze the first irreversible step in the utilization of glucose, and so, some mechanism should exist to regulate the rate of glucose transport, phosphorylation, or both. As reported by Thevelein (1995) glucose influx into glycolysis is controlled by trehalose-6-phosphate, which may be connected to the mechanism of sensing glucose by cells [86]. Therefore, glycolysis rate can be controlled at the level of the linear reaction pathway starting from extracellular glucose to intracellular pyruvate. In addition, this process may be controlled by the hydrolysis of ATP produced by the process itself, by the maintenance of ion balance, or regulation of pH or cell volume [87]. Another factor that may regulate glycolysis is the re-oxidation of NADH, which is formed by glycolysis, either by respiration or by fermentation [88].

The other respiration type is anaerobic, in which glucose is dissimilated without oxygen to produce ATP. This process is known as fermentation in which ethanol is produced by yeast cells and lactic acid by mammalian cells and is outlined in figure 2.3(B). The switch from aerobic respiration to fermentation is usually controlled by the depletion of oxygen. In this process NADH molecules, which are produced by glycolysis are re-oxidized and pyruvate is converted into ethanol and CO2 by the enzymes pyruvate decarboxylase and alcohol dehydrogenase in the cytoplasm. As a result, 2ATP and $2NAD^+$ are produced from one glucose molecule. This process produces the NAD^+ required by glycolysis to continue, and this may result in a coupling between glycolysis and fermentation through the oxidation-reduction of NADH molecules [89].

There are several mechanisms that may affect the balance between fermentation and respiration. These mechanisms involve Crabtree effect long-term and short-term, and the Pasteur effect. In the long-term Crabtree effect, aerobic alcoholic fermentation occurs because respiratory routes are insufficient to dissimilate pyruvate. Short-term Crabtree effect is an instantaneous aerobic alcoholic fermentation due to transition from sugar-limited to an excess of sugar, which causes a

saturation in respiratory routes and an overflow of pyruvate flux. In contrast, Pasteur effect is a high affinity of respiratory routs for pyruvate, acetaldehyde and/or NADH in the presence of oxygen, therefore alcoholic fermentation is suppressed [88].

The energetically favourable process is respiration, in which dissimilation of carbohydrates requires glycolysis coupling to the Krebs cycle. This route produces approximately 10 times the ATP produced by the fermentation route [84]. Despite the variation in adaptation mechanisms for metabolic needs of each cell, the biochemistry of most metabolic routes is conserved from microorganisms to human. Oxygen depletion switches the metabolic state of the cell from respiration to fermentation. However, *S. cerevisiae* yeasts switch between metabolic states in response to external glucose level [90, 91]. When the concentration of the external glucose exceeds 0.83 mM, the yeast *S. cerevisiae* switches the metabolic state to a mixed respire-fermentative state resulting in the production of ethanol [92]. At low external glucose concentration, when oxygen is available, *S. cerevisiae* inhibits fermentation completely and switches to respiration.

Since yeast cells are usually living in a medium with fluctuating nutrient levels, they require active and rapid mechanisms for adaptation of their metabolism. These mechanisms may ensure sufficient energy supply from various carbon sources to ensure the balance between production and demand to avoid death due to catastrophic loss of energy [93, 86]. Despite respiration being highly energetically favourable, at high growth rate, *S. cerevisiae* switches to fermentation which can produce ATP at a high rate per mass of enzymes [94]. The enzyme F_0F_1-ATPase may play the coordinator role in metabolic trade-off in yeast cells [83].

As an example of metabolic coordination, yeast cells grown on glucose first convert the glucose to ethanol by fermentation then they undergo a diauxic shift, a mechanism they developed to remodel their protein composition and continue their growth on the ethanol produced at a lower rate [83]. If they are fed again

with glucose and due to the alteration in metabolic state, glycolytic oscillations are initiated which may represent a mechanism of metabolic coordination [95]. All these metabolic adaptive mechanisms are developed by yeast cells to ensure that they can support their functional processes with the energy required (e.g. balance of ions across the plasma membrane, regulation of pH and cell volume, protein synthesis, and growth).

Metabolism is the main source of the energy required by the cell to survive, to proliferate and to function properly through the regulatory processes. These processes are the ion homoeostasis, which is required in maintenance of the membrane potential, and intracellular pH regulations.

2.4 Ion homoeostases

One of the most important processes for the survival of all organisms is the homoeostasis of ions. High intracellular K^+ and low intracellular Na^+ are substantial for different functional processes (e.g. enzyme activation 'PFK', membrane potential, cell volume and internal pH regulation, and protein synthesis [96, 97, 98, 99]. Therefore, yeast cells spend a high percentage of its energy to accumulate K^+ and to extrude toxic cations such as Na^+ and Li^+ [100] to get a high ratio of K^+/Na^+.

Many physiological processes can be affected by the movement of the ions across the plasma membrane and may also affect the transport process itself. These processes include the cell volume, membrane potential, and pH [100]. The influx of Na^+ may be accompanied by a movement of water into the cell and an increase of cell volume and this may be followed by an efflux of K^+ which results in a membrane hyperpolarization. Another scenario may be an extrusion of Na^+ accompanied by an influx of H^+ and K^+, which result in an acidification of the cell with a depolarization of the plasma membrane. To study the effect of ion transport on the cell functional processes mentioned above and how cells maintain

ion homoeostasis, it is recommended to understand the relation of these processes to the process of ions transport across the plasma membrane. As a starting point, the transport of cations and anions is discussed to answer the following questions:

i. How is electroneutrality maintained by the cell?

ii. What are the mechanisms used by the cell to translocate ions to maintain ion homoeostasis and electroneutrality?

iii. What are the sources of transport energization?

iv. What intracellular processes are coupled to let the cell function properly?

2.4.1 Monovalent cations transport

Nutrients such as amino acids are taken up by symport meaning the translocation of the component moving against its concentration gradient is thermodynamically coupled to movement of a component along its concentration gradient. In the case of amino acids, amino acid movement is coupled to H^+ uptake or to K^+. Therefore, the uptake and efflux of these components are discussed in this section. The uptake of these ions is important in the generation of the plasma membrane and pH regulation in yeast cells [101, 47].

Proton efflux

In all living cells, electrochemical gradients of ions across membranes are present as universal features. Different methods of energizations are involved in generating these electrochemical gradients and the most widely used is ATP hydrolysis to pump H^+, Na^+, K^+ or Ca^{2+}. These gradients have very crucial physiological roles: to drive nutrients and ions transport (see fig 2.4), to regulate turgor pressure and cell volume, and to regulate the activity of sensitive cytosolic enzyme, which may be affected by the change in intracellular ion concentrations (i.e. PFK) [102].

The first indication that yeast cells contain a proton-ATPase is the acidification

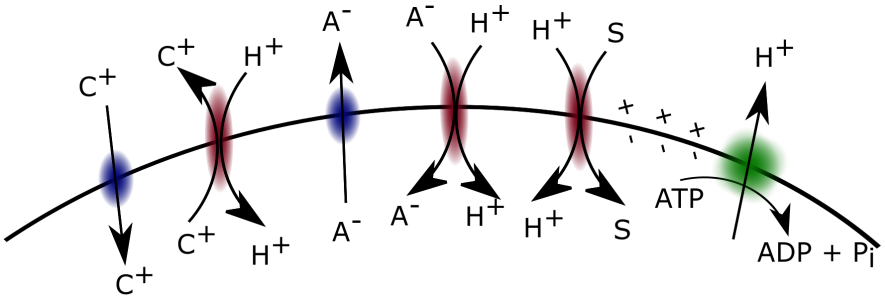

Figure 2.4: The role of the electrochemical proton gradient generated by the primary active transport of the H^+-ATPase in driving secondary active transport processes; S: neutral solute (e.g. neutral amino acids), A-: anionic solute (e.g. Cl^-) and C^+: cationic solute (e.g. K^+). From [102].

of the medium observed by fermentable yeast cells [102]. Addition of glucose to the medium results in medium acidification, which suggests an activation of the proton pump by glucose. The addition of arsenate or H^+-ATPase inhibitors to the medium reduces the acidity because both reduce the proton efflux, but arsenate mechanism is completely different from ATPase inhibitors; arsenate reduces the level of ATP which results in a reduction of the ATPase activity [103].

The H^+-ATPase has a very high capacity with a maximum flux ranging from 30 picomole/cm^2/sec in yeast [103] to 200 picomole/cm^2/sec in Neurospora [104]. With stoichiometry of 1proton/ 1ATP [105], the maximum activity may consume 40-60% of the total ATP produced [102]. The activity of this pump is controlled by two factors:

- The intracellular/extracellular H^+ ratio (or pH in and out of the cell with the membrane potential).
- Glucose concentration, which activates the pump when added to the yeast cells [102].

Therefore, when glucose is added to a medium containing K^+, a high activity of the ATPase is observed as a decrease in medium pH and an increase in cytosol pH, then the ATPase activity slows down corresponding to a decrease in intracellular proton concentration [103, 102]. The activity of the pump can be inhibited by

membrane depolarization when the extracellular concentration of K^+ is elevated [103]. As mentioned before the proton pump is a major ATP consumer in yeast cells. This was observed by the decrease in ATP level after activation of the pump by the addition of glucose [5], raising medium pH [106], adding potassium [107] or addition of uncouplers diethylstilbestrol and dicyclohexylcarbodiimide which inhibit the plasma membrane ATPase with interference with the energy metabolism of the cell [103].

The H^+-ATPase plays a substantial role in the survival of the cell by the production of the proton gradient and membrane potential which drive three electrical types of nutrient uptake [47]. The first type is the uptake of sugars and neutral amino acids via protons, which is driven by both the membrane potential and pH gradient. The second type is the uptake of anions (Cl^-, phosphate, sulphate and anionic amino acids) via protons, which may be driven by pH gradient or with membrane potential dependent on the stoichiometry of the cotransporter. The third type is the uptake of cations (K^+, Na^+, Ca^{2+}, Mg^{2+} and cationic amino acids), which is driven by the membrane potential and affected by pH gradient as will be discussed later in this section [102]. The uptake of nutrients coupled to protons is activated by the acidity of the medium and inhibited by the acidity of the cytosol in energy-deprived yeast cells.

In addition to nutrient uptake, the proton gradient is involved in the extrusion of undesirable or toxic substances; Na^+ and Ca^{2+} effluxes are affected by exchange with H^+ [47].

The activity of enzymes such as PFK is sensitive to intracellular pH [77] and therefore the activity of the proton pump can affect the activity of these enzymes. The proton pump (pma1) inhibitor, omeprazole, inhibits the growth of *S. cerevisiae*. This may be due to the inhibitory effect of low intracellular pH on PFK activity which results in the reduction of glycolysis and limitation in ATP production [108]. On the other hand, the inhibitory effect of omeprazole on pma1

may result in in-establishment of proton gradient and would mainly affect proton coupled transport. Therefore, due to the complexity of the cell's cytosolic contents the interaction of omeprazole with cell growth is not easily linked with one of these processes.

In conclusion, the activity of pma1 is a prerequisite for the growth of yeast cells. Since the proton gradient generated by the activity of pma1 is involved in nutrient uptake, turgor pressure [109], pH [110] and ionic distribution, all are necessary for cell growth. A transient cytosolic alkalinization was observed at the initiation of the cell cycle in yeast cells [111], which supports the inhibitory effect of omeprazole on *S. cerevisiae* growth [108]. The maintenance of electroneutrality during proton extrusion can be achieved by an influx of K^+ or an efflux of succinate [112]. But, since the biosynthesis of succinate from glucose is very slow and the proton extrusion is very rapid, the exchange with K^+ is the more efficient option. This exchange has been observed [113]. If the K^+ is absent, then the electrical balance is absent. Therefore, the proton pump will generate an electrical potential which will inhibit further activity of the pump. In the presence of K^+, the potential created by the pump will drive the influx of K^+, which will discharge potential, and the activity of the pump will continue; this indicates that K^+ plays a role in the regulation of the pump's activity [102].

Proton uptake

The proton gradient, generated by the H^+-ATPase, is the major source of energy for nutrient uptake and toxic ion extrusion. Amino acids, sugars, anions, and cations are transported across the membrane into the cytosol, by being coupled to the uptake of protons through different transporters. Nha1 is an antiporter which is involved in sodium homoeostasis under salt stress and pH regulation. This transporter is activated when the medium pH is very low, or the cell is growing in a saline medium. Nha1 uses the proton gradient to extrude Na^+ or K^+ from the

cytosol [114]. Therefore, the increase in the Nha1 activity results in counterbalance of K^+ uptake and restores the cytosolic pH [115, 116]. Two protons are taken into the cell when one Na^+ or K^+ is extruded, which suggests that this antiporter is electrogenic [117]. Therefore, Nha1 may contribute to the maintenance of the plasma membrane potential, pH regulation and cell volume regulation in saline or osmotic stresses [118, 119].

Phosphate uptake is coupled to protons through the cotransporter Pho84 which is involved in pH regulation. When pH of the medium becomes lower the activity of the Pho84 cotransporter increases and therefore, the cytosolic pH decreases which may reduce the rate of further phosphate uptake [120, 121]. Cockburn et. al. (1975) have reported that the uptake of one phosphate is accompanied by the uptake of three protons and an extrusion of two K^+ in a non-metabolising cell [122]. But, in metabolising cells, the stoichiometry is different; with the uptake of one phosphate, it is found that the cell uptakes two protons and extrudes one K^+ [123]. This cotransporter may result in membrane depolarization and therefore stimulation of H^+ pump in metabolising cells.

To sum up, the uptake of protons and other nutrients is coupled to the activity of the proton pump (see Fig. 2.4). Potassium uptake and efflux form part of these activities, since the increase in extracellular K^+ stimulates the activity of the proton pump and the efflux of K^+ is involved in nutrients uptake driven by the proton gradient. In the next two subsections, K^+ uptake and influx are discussed.

Potassium uptake

Fungal cells usually thrive in media with variable compositions. Therefore, the concentration of extracellular K^+ is highly variable, whereas the intracellular K^+ must be strictly regulated due to its effect on many physiological processes in the cell. Since these species can grow in either high and low concentration of K^+ (10 μM-2.5 M), these cells possess different types of K^+ transporters which are tightly

coordinated. While fungal cells have different putative K^+ uptake transporters which belong to four families, two transporters (TRK and HAK) and two ATPases (ACU and PAT), *S. cerevisiae* only have TRK transporters [124, 125].

TRK transporters are strictly regulated to maintain the proper intracellular concentrations of K^+ in yeast cells (around 200-300 mM) [126, 101, 127, 128, 98]. TRKs are similar to ion channels in their function but they still have the possibility to function as symport [129]. In addition to K^+ uptake, TRKs might mediate the transport of Cl^- across the plasma membrane of yeast cells [130, 131, 132, 128, 127]. The activity of TRK uniporters is driven by the membrane potential, which is generated by the activity of the plasma membrane H^+-ATPase (PMA1) [100]. The high affinity of K^+ uptake and the high velocity was attributed to the TRKs. In trk1,2 mutants, a low-affinity K^+ uptake was observed and attributed to the non-specific channel Ncs1, which is blocked by Ca^{2+} [133, 134, 135].

The uptake of K^+ may be affected by the extracellular concentration of K^+, intracellular pH, membrane potential and the surface potential [121]. In addition, an increase in the extracellular Na^+ may enhance K^+ efflux and inhibit the uptake of K^+. Potassium starvation of yeast cells results in a reduction of K^+ concentration to around 100 mM [128]. Acidification of the cytoplasm results in an acceleration of the H^+ pump and K^+ uptake [136, 137, 138]. The membrane potential is the driver of the K^+ uptake by the TRK system, and thus, it is one of the main factors that control K^+ uptake in yeast cells. The last factor that might affect the uptake of K^+ is the surface potential. The binding sites in the vicinity of the transporters consist of groups with negative charges which may play a crucial role in ion transport. These groups lead to an accumulation of cations near the transporters which result in an increase in anion dissociation constant and a decrease in cation dissociation constant and a decrease of cation uptake [121]. Therefore, when the activity of the pump increases or a salt is added to the medium the surface potential becomes less negative and an increase in the cation dissociation constant with a decrease in the anion dissociation constant is

achieved, which result in cation uptake to maintain electroneutrality. Through this mechanism, the cell prefers TRK system over a symport due to a decrease in the anion dissociation constant.

The K^+ gradient observed usually with the hyperpolarised membrane potential can be explained by the existence of the TRKs uniports. But, under certain conditions of low external pH with very low potassium, the membrane potential is less hyperpolarised. Therefore, the uniport could not explain the K^+ gradient, and a symporter mediating H^+ with K^+ influxes was proposed, and this was supported by the existence of a K^+/H^+ symport in Neurospora crassa [139].

To maintain a tightly regulated amount of internal K^+ which is required by the cell to function properly, efflux of K^+ is required and is discussed in the next section.

Potassium efflux

In a yeast cell with diameter of for example 5 μm, and with the accepted value for the biological membrane capacity of about 1 $\mu f/cm^2$, when 1 million of monovalent cations enter the cell a membrane potential of about 100 mV is generated. If this charge translocation is not compensated by a movement of another charge (anions or cations), the velocity of uptake of that cation will decrease and the change in the number of osmolytes inside the cell will cause water influx and an increase in cell volume. Therefore, when the cell uptakes cations, an influx of anions or an efflux of cations is necessary to compensate the change in charge and turgor pressure.

At least three different types of transporters are involved in the K^+ efflux. The only specific K^+ efflux channel is Tok1, which is present in the plasma membrane of *S. cerevisiae* and gated by the membrane potential. This channel is activated at very low negative and positive voltages and can be modulated by the extracellular K^+ concentrations [140, 141, 142, 143]. The other two transporters that contribute

to K^+ efflux were identified as Na^+ efflux systems. These are Ena1 and Nha1 which represent an Na^+ pump and an Na^+/H^+ antiporter respectively, but both can also mediate the efflux of K^+ [144, 145, 146]. The lack of these three transporters causes membrane potential depolarization and the overexpression of Nha1 and Tok1 result in membrane hyperpolarization [147, 118, 119].

In mammalian cells, there are many types of K^+ ion channels that participate in K^+ efflux dependent on the physiological conditions. As an example, in jurkat T cells, the voltage-gated K^+ channel is activated under physiological conditions (for more detail, see section 2.5.9). But the number of activated ion channels is very small and increasing with membrane depolarization. Another example, also in jurkat T cells, the Ca^{2+}-gated K^+ channels which are inactive under physiological conditions (~50 nM Ca^{2+}). But, these channels are activated when the intracellular concentration of Ca^{2+} is elevated over 200-300 nM and saturated when cytosolic Ca^{2+} concentration reaches 1 μM (for more details see section 2.5.9).

2.4.2 Divalent Cations Transport

For optimal growth, yeast cells require divalent cations (e.g. Mg^{2+}, Ca^{2+}, Zn^{2+}, Fe^{2+} and Cu^{2+}). Ca^{2+} may stimulate metabolism and it is one of the main signal transduction in most cells. The transport system of most divalent cations involves phosphate absorption by yeast cells [121]. Divalent cations uptake appears to be pH dependent. The uptake of Ni^{2+} by *S. cerevisiae* increases with increasing extracellular pH and the uptake of Mn^{2+} by *S. cerevisiae* is optimal at pH 5. Additionally, the rate of uptake of Ca^{2+} and Sr^{2+} by the yeast *S. cerevisiae* increases as the medium pH increases up to pH 8 [148] then decreases at higher pH values which make the dependency of divalent uptake on medium pH to be complex. This increase in monovalent and divalent cations uptake may be interpreted by the change in surface potential and the increase in cation dissociation constant due to H^+ -pump activity which increases when pH of the medium increases [121].

Ca^{2+} uptake is stimulated by K^+ efflux induced by DI09 [148]. This may be attributed to the negative potential generated by the diffusion of K^+, or to the change in surface potential caused by efflux of K^+, or to the requirement in charge compensation by the cell to maintain electroneutrality. In contrast, at low FCCP concentration, the cytosol pH increases and the Ca^{2+} uptake increases, which is not well understood [148, 4].

Ca^{2+} is essential in growth of *S. cerevisiae*, therefore, its regulation is crucial. Ca^{2+} is abundant in yeasts, but the cytosolic Ca^{2+} concentration is low (50-200 nM) to serve it's signalling function [149]. To maintain this low concentration, exchangers and pumps are required to sequester the surplus of Ca^{2+} in intracellular compartments [149]. Cytosolic Ca^{2+} may increase transiently in some specific conditions, such as hypertonic shock [150]. Ca^{2+} signals are generated by the entrance of Ca^{2+} through the plasma membrane transporters [151] and/or release from intracellular storage [152]. Vacuole represents the main Ca^{2+} store in yeast cells [153].

To maintain electroneutrality, cells extrude monovalent cations when divalent cations are translocated into the cell. In most cases, K^+ efflux accompanied the maintenance of electroneutrality.

2.4.3 Intracellular transport

Other systems that are involved in Na^+ detoxification and maintenance of K^+ homoeostasis are present at the organellar level (vacuolar, mitochondrial and endosomal and Golgi apparatus). Organellar pH and volume regulations are attributed to the alkali metal cation transport across the membranes of these organelles. Four systems of antiporters that exchange protons with K^+ and/or Na^+ were described in the internal compartments of *S. cerevisiae*: the endosomal Nhx1 and the Golgi apparatus Kha1 transporters which belong to Na^+/H^+ exchangers [154, 155], Mkh1 which is localized in the inner membrane of the mitochondria and exchange K^+ for

H^+, and the vacuolar cation/H^+. exchanger (Vnx1). The vacuolar proton pump generates the proton gradients across the endosomal, Golgi apparatus and vacuolar membranes, and so the activity of their cation/H^+ antiporters are functionally interconnected to that pump [156].

Transport across the vacuolar membrane

Rapid Na^+ detoxification and intracellular K^+ storage is attributed to the vacuole cation sequestration. The vacuolar cation/H^+ antiporter (Vnx1) sequence corresponds to a member of Ca^{2+}/H^+ exchange family [157]. Despite that, Vnx1 has been shown to mediate Na^+ and K^+ for protons, but not Ca^{2+}. This exchanger plays different functional roles that are related to the vacuole. These roles include vacuolar volume and pH regulation. In addition, it is expected to be involved in cytosolic pH regulation and ion homoeostasis [100].

Endoplasmic and Golgi apparatus transport system

Yeast cells have three Na^+/H^+ antiporters (Nha1, Nhx1 and Kha1), all are involved in pH regulation and Na^+ detoxification under high salt stress. Kha1 is localized to the Golgi body membrane and has the highest similarity to the cation/H^+ antiporter of the bacteria [158, 155]. This antiporter is crucial for growth at high extracellular pH. Kha1 mutants show growth deficiency at high medium pH, but this can be suppressed by the addition of KCl which suggest that K^+ may be a major substrate of this exchanger [147].

The first intracellular antiporter discovered in yeast cells was Nhx1, an endosomal antiporter exchanging Na^+ and/or K^+ with protons [159, 160]. This exchanger is involved in Na^+ detoxification and surplus K^+ sequestration. The deletion of Nhx1, results in an increase in cell sensitivity to low medium pH and salts [154]. In addition, the activity of this antiporter is involved in intracellular pH regulation and cell adaptation to hyperosmotic stress [160, 161, 154]. Nhx1 and Kha1 are

functionally close but in different organelles.

Transport across the mitochondrial membrane

An exchange of K^+ and H^+ was predicted by Mitchell (1961) [162], and then was confirmed by direct measurements of H^+ and K^+ fluxes in isolated mitochondria from yeast and other organisms. Mkh1, is an exchange of K^+ and H^+ localized in the inner membrane of the mitochondria. This exchanger is involved in pH regulation and maintenance of cells membrane potentials [100].

2.4.4 How can cells maintain electroneutrality?

After the previous discussion of the ion transport in *S. cerevisiae*, it is possible to answer this question. As mentioned in the previous sections, the movement of one of the ions is not separated from the movement of other ions. Therefore, the movement of an ion is coupled to the movement of, at least, another ion to maintain the electroneutrality of the process. As an example, movement of phosphate is accompanied by H^+ movement through a symport. Another example is the extrusion of H^+ using the pump is accompanied by the uptake of K^+. The cell employs the transport system (see figure 2.5) that discriminates between different cations, extrudes toxic and surplus cations and sequesters a part of these cations in internal organelles to provide the cell with sufficient K^+/Na^+ ratio. This ratio is essential in maintaining cell electroneutrality, preserving membrane potential, regulating cell pH, and keeping higher intracellular turgor pressure.

2.4.5 What are the sources of transport energization?

Through the previous discussion of ion transport, it was realized that the main source of the energy required in the translocation of ions is metabolism which is responsible for the ATP production that is required by Pma1 pump to extrude H^+

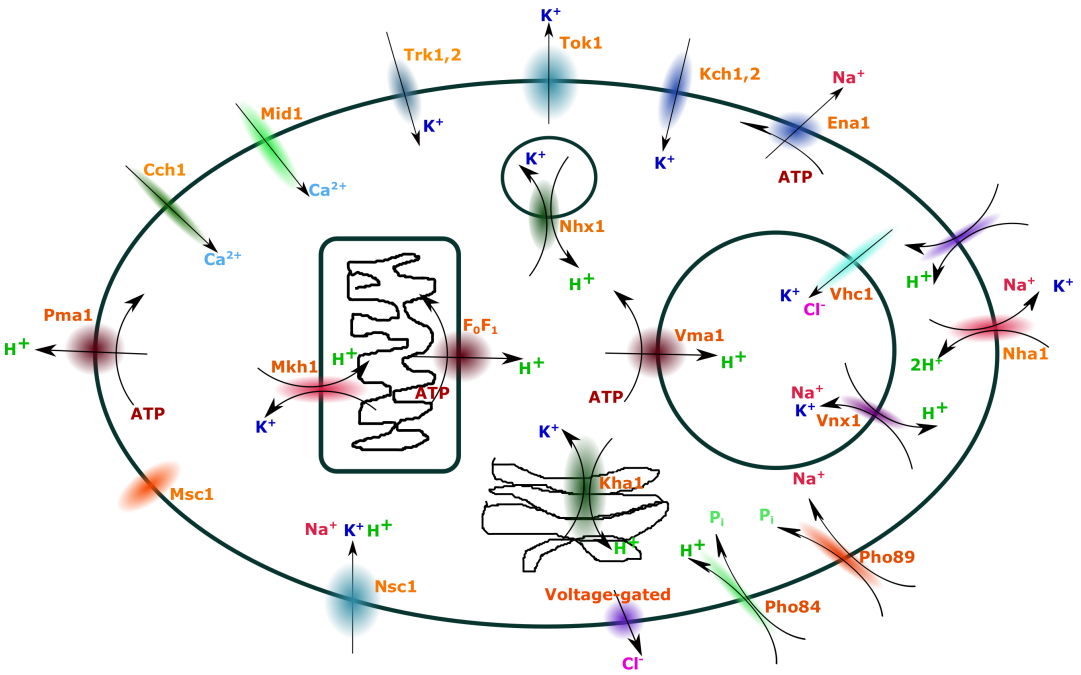

Figure 2.5: The major plasma membrane and intracellular ion transporters in *S. cerevisiae*. This system is responsible for most cellular activities such as pH regulation, ion homoeostasis, etc. The intracellular granules are shown; the vacuole is the larger sphere, the smaller sphere is the nucleus and the other two granules are the mitochondrion and the endoplasmic reticulum.

out of the cell. The extrusion of H^+ generates a proton gradient and a potential across the plasma membrane that form other sources of energy that might be used by the transport system to uptake or extrude nutrients, ions and undesirable substances. The uptake of K^+ through trks transporters is driven by a hyperpolarised membrane potential where the electrical force dominates the diffusion force and results in an uptake of potassium across the plasma membrane. On the other hand, the efflux of K^+ is driven by the diffusional force produced by the K^+ gradient that is created by K^+ homoeostasis system.

While the extrusion of H^+ is driven by the hydrolysis of ATP, the uptake of H^+ is a diffusion-dependent process. In contrast, the uptake of Na^+ is driven by diffusion and the extrusion of toxic Na^+ is driven by the energy produced by the hydrolysis of ATP. The uptake of anions like phosphate and Cl^- is driven by the H^+ gradient through symports in the plasma membrane.

Since the translocation of most ion is pH-dependent, it also affects the intracel-

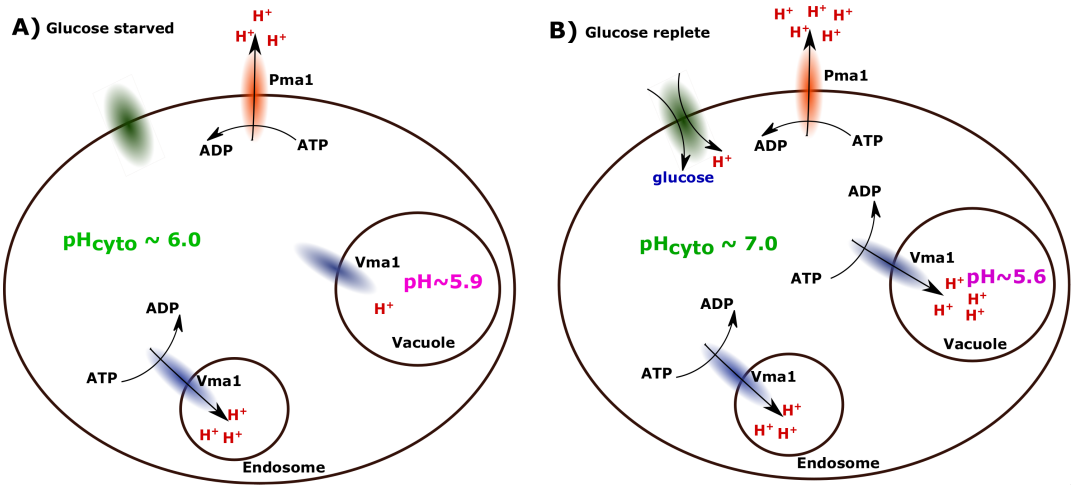

Figure 2.6: pH may serve as a signaling function. A) In glucose-starved cells, cytosolic pH is low (pH 6.0) due to a decrease in Pma1 activity. B) In the presence of glucose, the activities of Pma1 and Vma1 increase, and so, the cytosolic pH increases to 7 and the vacuolar pH decreases to 5.6. Both the vacuole and the endoplasmic reticulum have proton pumps which are responsible of protons sequestration to regulate cytosolic pH.

lular pH value. Therefore, the energy state of the cell may affect the cytosolic pH value. As reported by Cyert et al (2013), in the presence of glucose, the ATPases in the plasma and vacuolar membranes are active, and so, cytosolic pH is 7.0-7.2 and vacuolar pH is 5.6. On the other hand, in glucose-starved cells these pumps are inactive due to the limitation in ATP production, and so, cytosolic pH drops to 6.0 and vacuolar pH increases to 5.9 [163], see fig 2.6.

Ion homoeostasis is one of the processes that are strictly regulated in healthy cells to maintain the cell membrane potential. How is cell homoeostasis involved in the maintenance of the membrane potential in an altered cells? To answer this question, ion homoeostasis is discussed in apoptosis and cancer cells.

Ion homoeostasis is a very important process that is used by the cell to regulate its pH and volume and to maintain the plasma membrane potential. In the following section the membrane potential is discussed and the role of ions is explored.

2.5 Membrane potential

2.5.1 Introduction

All cells, in a unicellular organism (e.g. yeast) and multicellular organisms (i.e. animals and plants), manifest a voltage difference between the intracellular solution and the surrounding medium. This voltage difference is termed *membrane potential* since it is a potential difference between two solutions separated by the plasma membrane of the cell. The membrane potential is a measure of the potential inside the cell relative to the outside ($V_{out}= 0$) and it is usually negative under physiological conditions which means that the cytoplasm is negative relative to the extracellular solution. When a cell is stimulated, the membrane potential is changed significantly, but when it is at rest (no stimulation) the membrane potential does not significantly changed and this potential is termed the resting membrane potential [164, 165, 166]. However, as we will see below, even unperturbed it continuously fluctuates/oscillates over time.

The resting membrane potential is usually negative under physiological conditions. In most mammalian cells, the resting membrane potential is around -50 mV and its value varies between cells and ranges from -100 mV to -10 mV. For example, in muscle cells, it is around -90 mV, in neurons, it is around -70 mV it is around -50 mV in lymphocytes [167, 168, 169] and around -10 mV in human red blood cells [170]. This membrane potential comes about due to asymmetry distribution of ions across the plasma membrane (ions concentration gradients) and due to the selectivity of the membrane to some ions, and the continuous opening and closing of ion channels and movements of ions across the membrane. The negativity of cytoplasm is caused by the asymmetry of charge across the membrane, as a result, the membrane is said to be polarized. When the cytoplasm becomes more negative than the resting potential, it is said to be hyperpolarised and when it becomes more positive, it is said that the membrane is depolarized. In addition,

repolarization refers to the process in which the membrane returns to its normal resting potential [166].

Living cells are continuously regulating their intracellular concentrations of permeable ions to avoid osmotic stress and changes in cell volume, which affect many cellular functional processes. Consequently, the membrane potential fluctuates around a resting value. While the resting potential was studied extensively in most cells, the fluctuations are mainly ignored and are usually considered as noise in membranes [14, 1]. However, if the opening and closing were only random, a resting membrane potential fluctuations with large amplitude would not be generated. Some feedback regulation to amplify the fluctuation seems to be involved in the generation process [15]. In addition, it was proved that they are not an artefact of the method but represent an intrinsic mechanism, when the fluctuation in membrane potential was absent during ionomycin-induced hyper-polarization [171]. These fluctuations may convey information that may help in determining the dynamical behaviour of these cells.

Since ion channels are known to control many physiological processes as heartbeat generation, conduction of nerve impulses, initiation of muscle contraction and hormone secretion, the dysfunction of ion channels is connected with clinical signs in 80% of diseases [172, 173, 174]. The study of electrical properties of the membrane and proteins spanning it becomes very important. One of these properties is the resting membrane potential dynamics.

The structure of this section will be as follows. Subsection 2.5.2 will be about the establishment of the membrane potential. Subsection 2.5.3 is about membrane composition and ion transporters. In subsection 2.5.4, resting membrane potential is presented. Subsection 2.5.5 is about the deviation of the membrane potential from its resting value. Subsection 2.5.6 details the categorization of cells relative to ion permeabilities. In subsection 2.5.7, membrane resistance and the electronic model of the cell membrane are presented. Subsection 2.5.8 is about the fluctua-

tions in resting potential and finally, ion channels in jurkat cell are presented in subsection 2.5.9.

2.5.2 Establishment of the membrane potential

To understand how the membrane potential is established, a hypothetical example is assumed which is composed of two conducting solutions separated by a membrane. A sensitive device was added to measure the membrane potential between the two solutions. Suppose that the membrane permeability can be changed and in the first case, the membrane is impermeable to all ions. Assume that the left solution composed of 150 mM KCl and 10 mM NaCl is close to the intracellular cytoplasm and the right solution composed of 150 mM NaCl and 10 mM KCl mimics the extracellular medium of most mammalian cells (Figure 2.7). The values we used are to avoid osmotic forces since the number of solutes used on both sides are equals. In this case, we have electro-neutrality on both sides, and so, the membrane potential will be zero, because the membrane does not allow ions to move in order to create charge separation.

In real cells, the concentration of chloride in extracellular solution is high relative to intracellular. In addition, large proteins carry a high portion while chloride carry a low portion of the intracellular negative charge.

Imagine now that the membrane is permeable to all ions without selectivity (Figure 2.8). In this case, K^+ will move from left to right and Na^+ will move in the opposite direction, both are moving in the directions of their chemical gradient. Chloride in both sides has the same concentration so it is in equilibrium, and will not move. The movement of K^+ and Na^+ will continue until equilibrium is established. At equilibrium, the concentration of each ion will be equals on both sides and the system will get neutrality again on both sides, which means that the membrane potential will be zero again due to membrane non-selectivity.

It is emphasized that without membrane selectivity and ion concentration

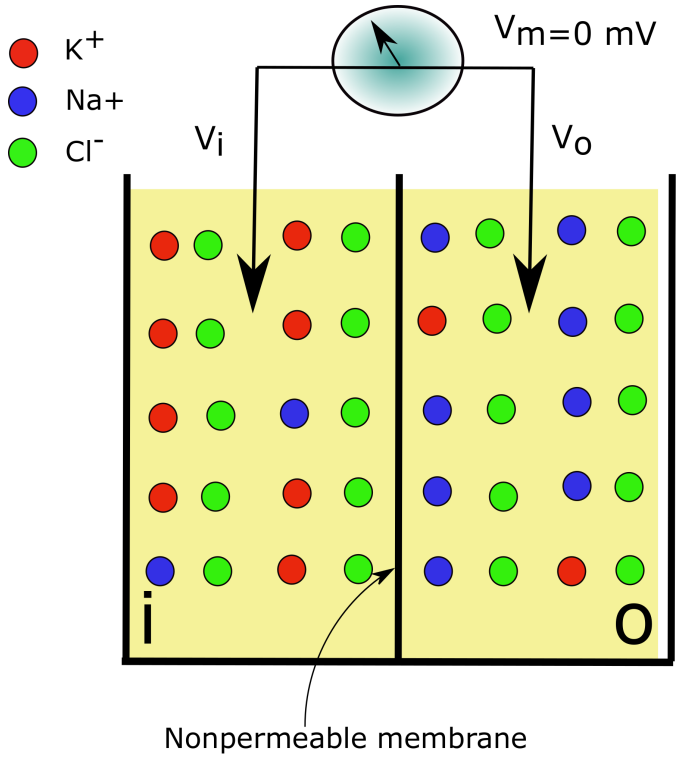

Figure 2.7: A Non-permeable membrane separating two electro-neutral solutions composed of 150 mM KCl and 10 mM NaCl in the left side (i) and 150 mM NaCl with 10 mM KCl in the right side (o), supported by a sensitive device to measure the voltage difference between both sides, $V_m = V_i - V_o$. -ve: means negative.

gradients, there will not be charge separation and no membrane potential is established. To confirm these conclusions, let us propose a new scenario closer to reality in which the membrane is permeable to K^+ only (Figure 2.9). In this case, K^+ will move from the left to the right leaving the negative charge in the left side and creating a positive charge on the right side. As a result, a membrane potential is established which will create a force opposite in direction to the movement of the moving K^+ ions. This force will increase as more K^+ ions move from the left side to the right until this force becomes equal to the chemical (diffusion) force. At this moment, equilibrium is reached at a certain value of the membrane potential known as the resting membrane potential, which is equal to the K^+ equilibrium potential or Nernst potential (E_K).

From this case, we can define a force termed as driving force of ions, which is the difference between the diffusional (chemical) force (created by the concentration gradient of ions) and the electrical force (created by charge separation). For

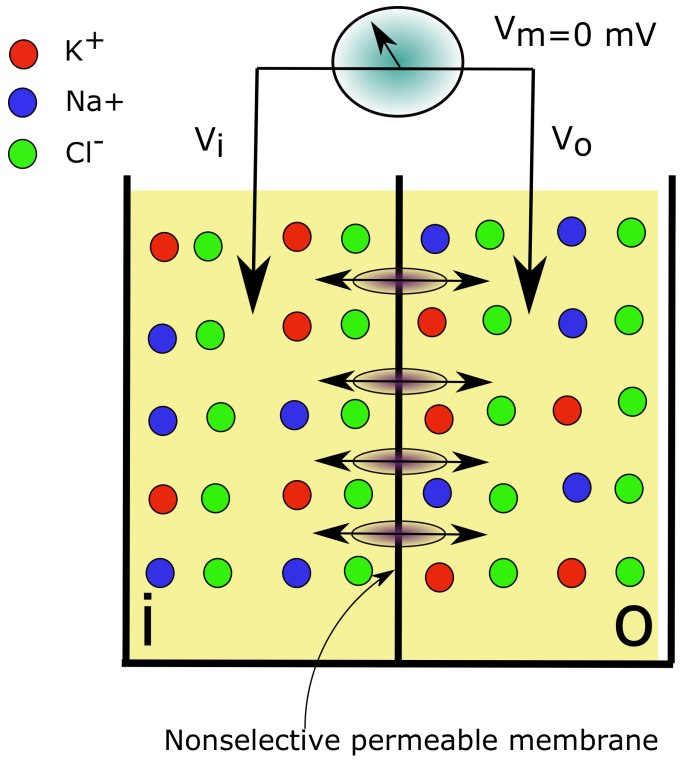

Figure 2.8: A non-selective permeable membrane separating two electro-neutral solutions composed of 150 mM KCl and 10 mM NaCl in the left side (i) and 150 mM NaCl with 10 mM KCl in the right side (o), supported by a sensitive device to measure the voltage difference between both sides, $V_m = V_i - V_o$.

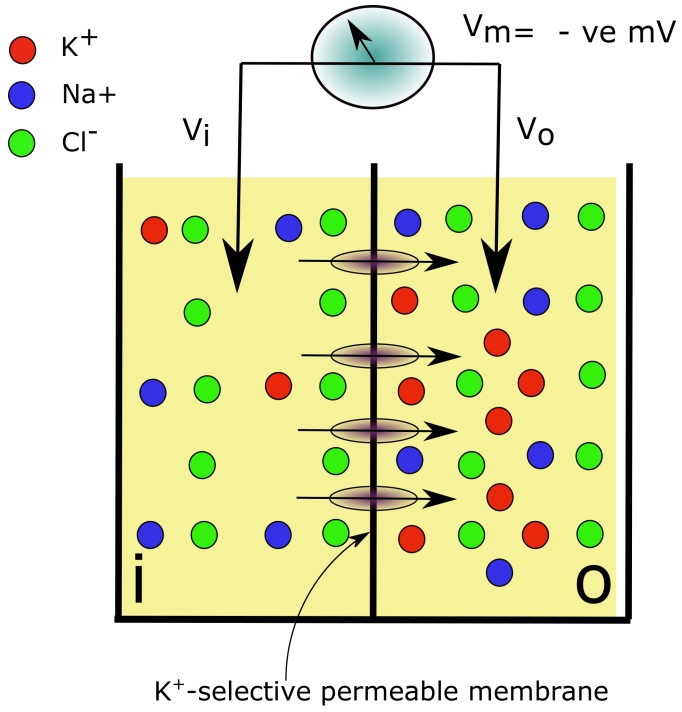

Figure 2.9: A K^+ selective membrane separating two electro-neutral solutions composed of 150 mM KCl and 10 mM NaCl in the left side (i) and 150 mM NaCl with 10 mM KCl in the right side (o), supported by a sensitive device to measure the voltage difference between both sides, $V_m = V_i - V_o$. -ve: means negative.

simplicity, this force can be written in terms of the potentials, and so, the driving force can be written as:

$$D.F. = V - V_r, \tag{2.3}$$

where D. F. is the driving force, V is the membrane potential and Vr is the Nernst potential (will be discussed later in this chapter) of an ion which is given by the relation:

$$V_r = \frac{RT}{zF} \ln(\frac{[C]_o}{[C]_i}), \tag{2.4}$$

where R is the gas constant, T is the temperature in Kelvin, F is Faraday constant, z is the valence of an ion, $[C]_i$ and $[C]_o$ are the intracellular and extracellular ion concentrations respectively [175].

Now we can imagine the real case. In most mammalian cells the permeability to K^+ is very high relative to Cl^-, and Na^+ permeability is very low in non-excitable cells. Therefore, the resting membrane potential will be closer to K^+ equilibrium potential and will be located between the equilibrium potential of these ions. The resting membrane potential can be calculated if we know the concentrations of all ions inside and outside the cell and the permeability of the membrane to each ion (the resting value of the membrane potential will be discussed later in this chapter). In the next section, we discuss the membrane composition and ion transporters, then we show how the resting membrane potential of a cell can be calculated and categorize cells upon their permeability using resting membrane potential [175].

2.5.3 Membrane composition and ion transporters

All living cells are composed of cytoplasm separated from their milieu by a lipid bilayer membrane. Since living cells require the exchange of materials with the surrounding to remain alive, the membrane is essentially permeable to nutrient and waste products. The structure of membranes (hydrophobic) prevent the movement

of charged ions or molecules across the lipid bilayer. Therefore, the passage of ions and polar nutrient across the plasma membrane requires special paths termed as transporters. Because of cell variability, cell requirements differ from cell to cell. Thus, each cell contains a specific set of membrane transport proteins [164].

Most cells' membranes contain three major classes of proteins: ion channels, carriers, and ATP-powered pumps, see figure (2.10).

Ion channels

Ion channels are hydrophobic pathways through which specific ions pass at a very rapid rate down their electrochemical gradients, and so, ions' movement is termed as facilitated diffusion. A small part of the ion channels are open all the time and these are known as non-gated ion channels. Most ion channels open in response to specific electrical signals such as voltage-gated channels, or chemical such as Ca^{2+}-gated K^{+} channels and these are known as gated channels [164].

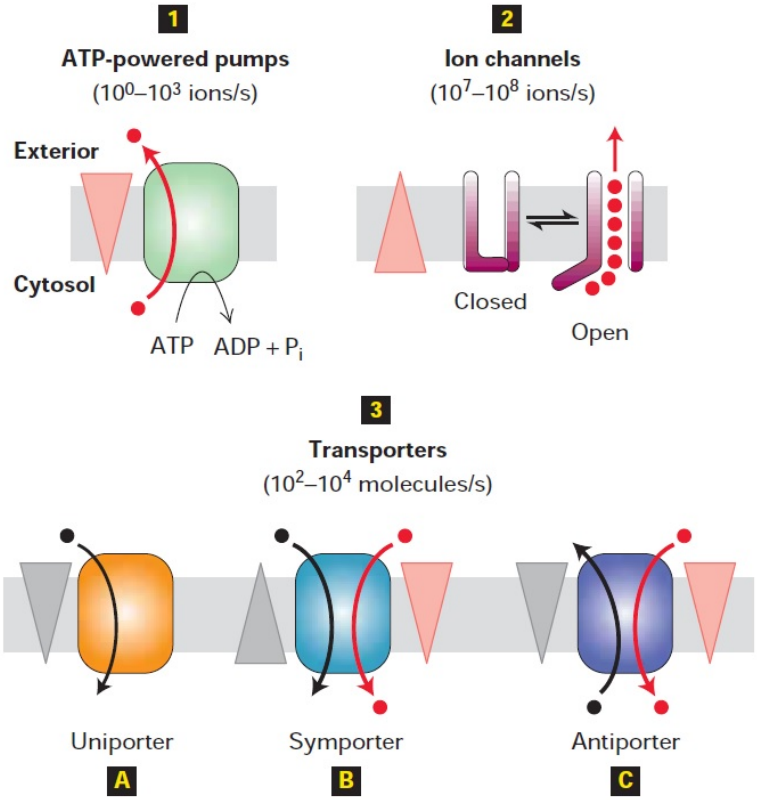

Figure 2.10: Membrane transport proteins. 1) Pumps utilize the energy released by ATP hydrolysis to power movement of specific ions (red circles) or molecules against their electrochemical gradients. 2) Channels permit movement of specific ions down their electrochemical gradient. 3) Transporters fall into three groups A) Uniporters, B) Symporters and C) Antiporters. Copied from [164]

Transporters

As already discussed in Section 2.2.3 for yeast cells, cells have various types of transport. Transporters are divided into three types: uniporters, antiporters, and symporters. Uniporters are proteins that transport only single molecule down its concentration gradient in facilitated diffusion, such as glucose [176]. In contrast, symporters and antiporters couple the movement of one molecule against its concentration gradient with another molecule (sometime more than one molecule) down their concentration gradients such as Cl^-/HCO_3^- and Na^+/H^+ exchangers and Na^+- K^+- $2Cl^-$ cotransporter [177, 178, 179]. These proteins are called co-transporters and are considered as secondary active transport because they exploit

the energy stored in the electrochemical gradient of one or two molecules to move another molecule against its electrochemical gradient [164]. The interaction of the ions with the transporters is stronger than the interaction with ion channels, and so, the rate of transport in carriers is low relative to ion channels.

ATPases

Pumps are proteins that hydrolyse ATP and use its energy to move ions against their electrochemical gradients. Examples are Na^+/K^+-pump, H^+-pump and Ca^{2+}-pump. Their transport process is termed as active transport, in which the movement of ions uphill is coupled to the hydrolysis of ATP. The rate of flow of ions through active transport is very slow (10-1000 ion/sec) relative to passive transport (10^8 ion/sec) [180, 164].

Since all functional processes of the cell are strict, the transport process is important to keep the cytosol composition to be approximately constant. Therefore, all three classes of transport work together to regulate pH [181], cell volume [182] and maintenance of membrane potential [183]. In all cells, intracellular K^+ is usually 10-fold or more than extracellular but, Na^+ and Cl^- are very high outside the cell relative to inside. These distributions with membrane transporters are very important to generate voltage difference across cells membranes [164].

2.5.4 Resting membrane potential

In section 2.5.2, we have shown that the membrane potential is established due to membrane selectivity to some ions and due to the concentration gradients of these ions. The concentration gradients result in a force that acts on ions and diffuses them from the side of high concentration to the side of low concentration. Due to the selectivity of the membrane to some ions (i.e. K^+), K^+ ions will move from one side leaving a negative charge to the other side creating a positive charge, as a result, generating an electrical gradient. The chemical gradient ($\triangle\ g_{chemical}$) and

the electrical gradient ($\triangle$ $g_{electrical}$) are defined as [184]:

$$\triangle\ g_{chemical} = RT \ln\left(\frac{[C]_o}{[C]_i}\right), \tag{2.5}$$

$$\triangle\ g_{electrical} = zFV, \tag{2.6}$$

where R, T, z, F and V as defined before, and $[C]_o$ and $[C]_i$ are the extracellular and intracellular C concentrations, respectively.

The membrane potential is established and acts on the moving ions in opposite direction. As more ions move, the membrane potential increases and the opposite force increases until it equalizes the chemical force that is moving the ions. At that moment equilibrium is established. Therefore,

$$\triangle\ g_{chemical} = \triangle\ g_{electrical}, \tag{2.7}$$

substituting from equations 2.5 and 2.6 gives

$$zFV_r = RT \ln\left(\frac{[C]_0}{[C]_i}\right), \tag{2.8}$$

solving to equilibrium potential

$$V_r = \left(\frac{RT}{zF}\right) \times \ln\left(\frac{[C]_0}{[C]_i}\right). \tag{2.9}$$

This result is known as the equilibrium potential of the ion C. Doing the same for other ions, we can derive their equilibrium potential which is also known as Nernst potential.

In living cells, it is impossible to get equilibrium. Instead, the steady state can be established for all ions, at a moment where the total current through the membrane is zero. At that moment, the resting membrane potential is established and has a value that lies between the equilibrium potentials of the permeable ions, such

as K^+, Na^+ and Cl^-. The value of the resting membrane potential is usually closer to the equilibrium potential of the ion that has higher permeability, mostly K^+. To calculate the resting membrane potential we can use the Goldman-Hodgkin-Katz (GHK) equation. They assumed that the electric field is constant across the lipid membrane, the Nernst-Plank equation can hold within the membrane and the ions move independently across the membrane [184].

GHK equation is defined as [185] (for derivation see appendix A)

$$V_r = \frac{RT}{F} \ln\left(\frac{P_K[K^+]_o + P_{Na}[Na^+]_o + P_{Cl}[Cl^-]_i}{P_K[K^+]_i + P_{Na}[Na^+]_i + P_{Cl}[Cl^-]_o}\right), \tag{2.10}$$

where V_r is the resting membrane potential, $[x]_i$ and $[x]_o$ are the intracellular and the extracellular concentration of ion x, respectively and P_x is the membrane permeability to ion x.

2.5.5 Deviation of membrane potentials from resting values

In the previous section, it was shown that the theoretical value of the resting membrane potential can be calculated using GHK equation, which is a theoretical value and represents a theoretical steady state. In this section, we discuss two factors that may deviate the membrane potential from its resting value, which cause dynamics in the resting membrane potential, in contradiction to the theoretical assumption. The first factor is the permeability of the membrane to some ions such as K^+, Na^+ and Cl^-. The membrane permeability value for each ion depends on the number of open channels, which is selective to that ion. For example, the permeability of the membrane for K^+ depends on the number of K^+ open channels. When the number of open channels increases due to activation, the membrane permeability for K^+ increases and the membrane becomes more selective to K^+. An example is Kv1.3 (voltage-gated K^+ channel), a channel which opens due

to membrane depolarization. When the membrane depolarises the probability of Kv1.3 channels to be open increases and the membrane becomes more selective to K^+ ions. As a result, the K^+ ions move out of the cell and cause membrane hyperpolarization. Therefore, the membrane resting potential becomes closer to K^+ equilibrium potential. But, if the number of Na^+ open channels increases, the membrane becomes selective to Na^+. As a result, an influx of Na^+ ions cause depolarization of the membrane and the membrane resting potential becomes closer to Na^+ equilibrium potential.

The second factor that may change the membrane potential is the concentration of ions inside or outside the cell. To deal with living cells, we should discuss extracellular changes that may occur due to hydration, cell injury or nutrition time. These processes may cause a dramatic change in extracellular ion concentrations. As a result, the equilibrium potential of ions change and the conductance may change. Therefore, the resting potential of the membrane deviates from it physiological value.

We previously defined the driving force of an ion as the difference between the membrane potential and the equilibrium potential of that ion. When the membrane potential is changed, the driving force of that ion is also changed. As a result, a change in the current may occur, if the ion channels are open. As a consequence, the membrane potential will fluctuate around the resting value. Resting membrane potentials were thought to be static values. But, due to opening and closing of gated ion channels and the change in driving force, they are fluctuating around steady-state values. Fluctuations in resting membrane potentials will be discussed later in this chapter.

The driving force can be used to predict the direction of the current (ion flow) across the plasma membrane. In the case of cations a positive driving force predicts an efflux (positive ions moving out of the cell, such as K^+) in the direction of their electrochemical gradients, and a negative driving force predicts an influx (positive

ions are moving into the cell, such as Na^+ and Ca^{2+}) in the direction of their electrochemical gradient. In case of anions such as Cl^- and HCO_3^-, the situation is reversed. A positive driving force predicts an influx and a negative driving force predicts an efflux.

In some cases, the membrane potential is to be found exactly the same as the equilibrium potential of one of the ions. As a result, the driving force of that ion is zero, which means no flow of ions into or out of the cell and that ion is said to be in electrochemical equilibrium.

In the next section, the result of this section and those from the previous one can be used to categorize cells with respect to their permeabilities.

2.5.6 Cells categorization with respect to their permeabilities

In the previous two sections, we show how to calculate the resting membrane potential using GHK equation, and how the change in extracellular concentrations of ions causes a change in the membrane potential. We can exploit these characteristics to categorize cells into three groups relative to the currents that dominate the membrane of the cell under control conditions. For example, if the permeability of the membrane of one cell is highly selective to K^+, then the resting membrane potential is closer to the equilibrium potential of K^+. To confirm that the cell is dominated by K^+, we can change the extracellular concentration of one of the ions. Changing the concentration of each of Na^+ or Cl^- causes an insignificant change in the resting membrane potential because their permeabilities are very low relative to K^+. But changing the extracellular K^+ concentration can cause a significant shift in the membrane potential towards the new equilibrium potential of K^+.

In the same way, we can determine if the cell is dominated by Na^+ current or

Cl^- current through the shift in the membrane potential parallel to a change in the extracellular concentration of one ion. If the shift is parallel to a change in Cl^- extracellular concentration, then the cell is dominated by Cl^- current. And so on. Using this method in this thesis, jurkat T cells were categorized into three groups; cohort 1 (K^+ dominant), cohort 2 (Cl^- dominant) and cohort 3 (Na^+ dominant).

The next section discusses the electrical circuit which is equivalent to the cell membrane and helps us to study the factors that cause the fluctuation in resting membrane potentials.

2.5.7 Membrane resistance and electronic model of the plasma membrane

As mentioned in section 2.5.3, the membrane bilayer of lipids form a barrier, which resists the movement of ions across the membrane. In contrast, the solutions separated by the membrane are very conductive. Therefore, the membrane forms an insulator between two conductors, which is electrically an analogy to a capacitor. Since ion channels are conductive and span the membrane, they make the membrane a non-perfect conductor. Thus, the membrane resistance to movement of ions is finite.

Ions are subjected to two forces; one due to diffusion from high to low ion concentration and another due to electrical membrane potential. Their net force is termed as driving force [175]. Ions can flow across the membrane if the driving force is different from zero. In electronic terms, ions flow is expressed in terms of current as a flow of charge,

$$I = \frac{\mathrm{d}q}{\mathrm{d}t}, \tag{2.11}$$

where I is current in amperes and $\mathrm{d}q/\mathrm{d}t$ is the rate of charge flow across the membrane in coulomb/sec. The flow of charge (ions) is determined by the driving force and the membrane resistance (or from now on we will use conductance, the recip-

rocal of resistance). The magnitude of the driving force can be calculated from the membrane potential and the equilibrium potential of ions. As the membrane potential becomes far from equilibrium for an ion, say K^+, the ions' driving force becomes larger and ions' flow becomes larger. Therefore, the current is directly proportional to the driving force. Ion flow is also limited by the membrane conductance; if there are more K^+ channels that are open then more K^+ ions can pass through the membrane. Thus, the flow of ions is also directly proportional to the membrane conductance. Thus, current can be written as,

$$I_K = G \times \phi, \tag{2.12}$$

where I_K is the K^+ current, G is the membrane conductance to K^+ in siemens, and ϕ is the driving force of K^+ ions in volts. This equation is a special case of Ohm's law [175].

As mentioned earlier (section 2.5.3), the membrane forms a capacitor and since the intracellular side is negatively charged relative to outside, then an electromagnetic field is generated across the membrane. The attraction of charge on both sides of the membrane causes charge storage,

$$Q = V \times C, \tag{2.13}$$

where Q is the charge stored in the membrane in coulomb, V is the membrane potential in volts and C is the membrane capacitance in farads. Differentiating equation 2.13 gives the current charging the membrane,

$$I_c = C\frac{\mathrm{d}V}{\mathrm{d}t}, \tag{2.14}$$

I_c is the capacitive current, C is the membrane conductance and $\mathrm{d}V/\mathrm{d}t$ is the change in membrane potential.

Since the membrane lipid bilayers can be modelled by a capacitor, ion channels

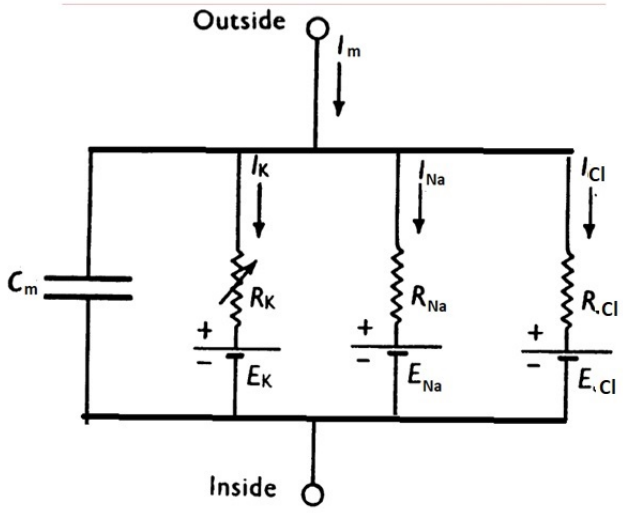

Figure 2.11: The electrical equivalent circuit proposed for cell membrane. The variable resistance represents gated channel conductance, batteries represent the driving forces of ions and capacitor represent the insulating property of the membrane bilayer of lipid. From [1].

by resistors and the driving forces by batteries, the membrane can be modelled as an electric circuit (see figure 2.11). The total current of the membrane is given by the sum of individual ion currents (HGK assumptions) and the capacitive current of the membrane [186],

$$I_{total} = C\frac{\mathrm{d}V}{\mathrm{d}t} + I_K + I_{Na} + I_{Cl}. \tag{2.15}$$

At steady state I_{total}=0, Thus

$$-C\frac{\mathrm{d}V}{\mathrm{d}t} = I_K + I_{Na} + I_{Cl}. \tag{2.16}$$

Substitutions from equations 2.12 and 2.3 in equation 2.16 give the relation of membrane potential dynamics with membrane conductance and the driving force of each ion. This equation is given by

$$-C\frac{\mathrm{d}V}{\mathrm{d}t} = G_K(V - V_K) + G_{Na}(V - V_{Na}) + G_{Cl}(V - V_{Cl}), \tag{2.17}$$

where G_x is the conductance of ion x, V is the membrane potential and V_x is the

equilibrium potential of ion x.

Any current through the membrane generates dynamics in the resting potential (fluctuations). The main sources of fluctuations are the opening and closing of gated ion channels and any change in the driving force of an ion. In the next section, fluctuations in membrane potential are discussed.

2.5.8 Fluctuations in resting membrane potentials

As discussed in previous sections of this chapter, the permeability of membranes to specific ions together with ion concentration gradients generate a voltage difference across cell membranes. Cells in resting state can generate a potential which is constant if they do not express gated ion channels. In living cells, even under physiological conditions, cells have gated ion channels which are opening and closing continuously [171]. Therefore, ions can flow through them when they are open if the driving force of that ion is not zero, causing fluctuations in the current of that ion. Equation 2.16 illustrates how any change in current may cause a change in membrane potential. Thus, any fluctuation in currents can generate fluctuations in membrane potential.

Fluctuations were considered in previous studies as noise [14, 1]. But these fluctuations are the consequences of cell homoeostasis, consisting of cell volume regulation, pH regulation, etc. Fluctuations and oscillations were reported in several previous studies. Spontaneous oscillations were reported in K^+ channels activity in transformed Madin-Darby Canine kidney cells. These oscillations were sensitive to Ca^{2+} [187]. In another study, the same type of cells show spontaneous oscillations in membrane potential under sustained alkaline stress (pH 7.7). The measurements were done using microelectrodes. These oscillations are caused by periodic opening of Ca^{2+}-activated K^+ channels [188]. And Fluctuations in the membrane potential were observed in EGFR-T17 (a clone of mouse NIH-3T3 fibroblasts overexpressing EGF receptors; epidermal growth factor receptors), A431

and KB (two human carcinoma lines). These fluctuations follow a marked hyperpolarization caused by an activation of Ca^{2+}-activated K^+ channels [189].

It was reported by Nakaoka et al. [15] that fluctuations in the resting membrane potential are very important in Paramecium cell. They found that this unicellular organism is changing his direction of swimming by exploiting the fluctuations in his membrane potential. They also reported that the amplitude of fluctuations is magnified when intracellular Ca^{2+} increased significantly. These results suggest that Ca^{2+} activates Ca^{2+}-gated K^+ channels and, as a result, the membrane conductance increases and causes an increase in the amplitude of membrane potential fluctuations. The amplitude of fluctuation reported, with low intracellular Ca^{2+}, was 0.42 mV but, when Ca^{2+} was elevated inside the cell the amplitude reaches several millivolts [15]. Majima [16] studied the fluctuations in the resting potential of Paramecium. Majima reported that the amplitude of the fluctuation was between 0.5 and 5.0 mV and the amplitude of fluctuations is proportional to the driving force of K^+.

Moolenaar et al. [14] reported that the magnification in the amplitude of membrane potential fluctuation is the result of an increase in the motive force (driving force) of K^+. In another work by Oosawa et al. [17], it was indicated that the amplitude of fluctuation in the resting potential is proportional to the circulating current, which is consistent with equation (2.16). Next section, ion channels that jurkat T cells contain are discussed, to increase our understanding of ion channels that may contribute to fluctuations generation.

2.5.9 Ion transporters in jurkat T lymphocytes

As discussed in previous sections, the potential difference across a cell's plasma membrane depends mainly on the electric charge distribution within the intracellular cytosol and the extracellular solution. This charge distribution is created mainly by the movement of ions across the membrane. The ions that play the

most important role in creating the membrane potential include K^+, Na^+, Cl^-, and Ca^{2+}. Since the membrane is a dielectric lipid, the charged molecules cannot pass through it, even small ions. Ions can traverse the plasma membrane by facilitated diffusion through open ion channels along their electrochemical gradient, by an active pump against the electrochemical gradient, or by passive carrier mechanisms, as discussed in section 2.5.3. Ion channels are integral membrane proteins with pores filled with aqueous, which can exist in one of two states, open or closed. Ion channels can change between these states by a conformational mechanism. This mechanism is termed "gating" in which a transition from the closed to open state allows ion transport across the membrane. This mechanism can be regulated in different ways. In some ion channels, the gating mechanism is sensitive to the membrane potential and these are therefore termed voltage-gated ion channels. One example is voltage-gated potassium channels [190]. Some channels change their state from closed to open when a ligand binds to a specific extracellular or intracellular receptor and these are called ligand-gated ion channels such as GABA receptors or the P2x family of ATP receptors [191]. Others are sensitive to the concentration of an intracellular substance, such as Ca^{2+}-gated potassium channels, in which Ca^{2+} binds to calmodulin which attached to a CAM-binding site at the C terminus of that channel [192]. In addition, there are channels which are gated by the change in cell volume. These channels are opened due to cell swelling and the mechanical forces caused by the tension in the plasma membrane. An example of this type is $Cl^-{}_{swell}$ [193]. Ion channels are characterized with respect to their selectivity to specific ions, their gating mechanism, and their sensitivity to drug molecules or toxins. For example, voltage-gated potassium channels are selective to K^+, they activate and then deactivate when the plasma membrane is depolarized, and they are sensitive to Tetraethylammonium (TEA), noxiustoxin (NTX), Kaliotoxin (KTX), the scorpion toxin maurotoxin (MTX), charybdotoxin (CTX) and dalazatide [194, 171, 195].

The most commonly known ion channels in the different type of cells include

the voltage-gated K^+ channels, Ca^{2+}-gated K^+ channels, Ca^{2+} channels, Cl^- channels, Na^+ channels, and chemically-activated receptors. Since ion channels are known to control many physiological processes as heartbeat generation, conduction of nerve impulses, initiation of muscle contraction and hormone secretion, the dysfunction of ion channels is connected with clinical signs in some diseases. Muscle disorders are caused by a mutation in voltage-gated sodium channels, and mutation in ATP-sensitive potassium channels in pancreatic β cells can cause persistent hyperinsulinemic hypoglycemia in infancy (for other diseases related to ion channels dysfunction see reviews [172, 173, 174]).

Cells such as nerves and muscles are well studied; they fire action potentials and are therefore termed "excitable cells". They use voltage-gated ion channels to propagate these electrical signals along their axons. In contrast, "non-excitable cells" do not generate electrical pulses like action potentials. Non-excitable cells like lymphocytes, fibroblasts, and epithelial cells, like excitable cells, express an intricate mix of transporters conducting K^+, Ca^{2+}, Cl^- and non-selective combinations of cations. Expression of these ion channels varies between types of cells and sometimes varies even between the same type of cells. As an example, 10% of jurkat T cells express sodium voltage-gated channels [196]. One of the fundamental requirements for the processes of life within the cell is the influx of Ca^{2+}, which relies on the regulation of the plasma membrane calcium ion channels. Therefore, K^+ channels are very important since they regulate Ca^{2+} signalling by maintaining a negative membrane potential and thus allow calcium channels to carry larger currents during the activation of the cell (see review [197]).

The patch-clamp technique is the best technology to study the function of ion channels, which are excellent drug targets since they play the main role in many common diseases [174, 198]. The two major drawbacks of the patch-clamp technique are the high personal cost due to the labour-intensive evaluation of individual drugs and the low throughput. Several methods are available today to test ion channel active drugs (ICADs): patch-clamp [199], ion-sensitive dyes

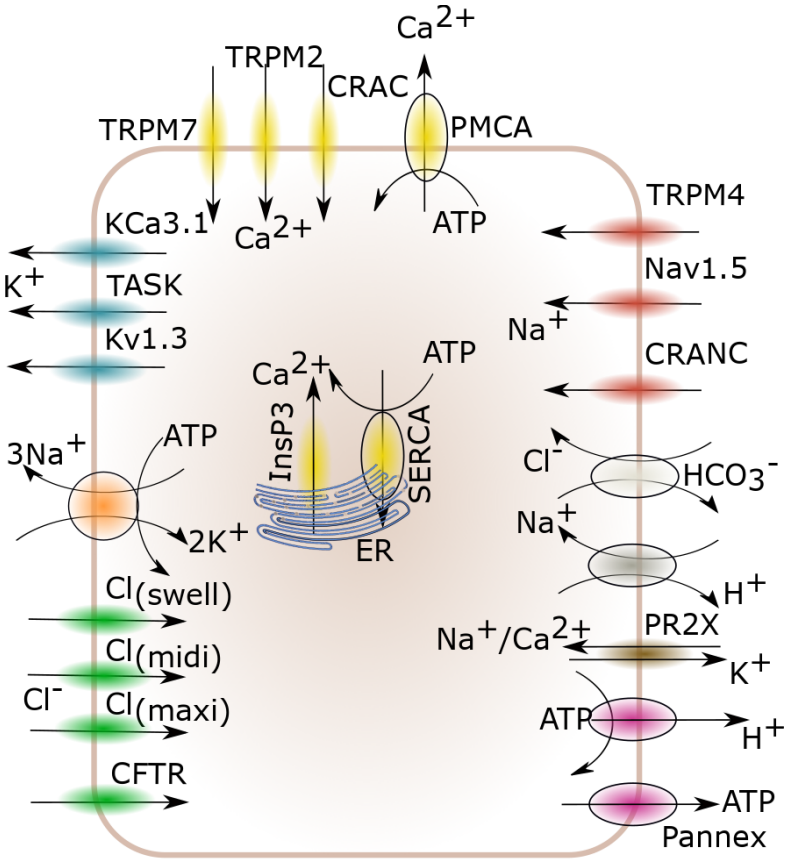

Figure 2.12: A model of most transporters expressed in jurkat T Lymphocytes. Concentration gradients are shown as triangles, K^+ is the only one directed outward. K^+ transporters are in blue, Na^+ transporters are in red, Ca^{2+} transporters are in yellow, Cl^- transporters are in green and others are not specific to one colour.

[200], membrane potential-sensitive dyes [201], voltage-sensing based on fluorescent resonant energy transfer (FRET) [202], binding assays [203] and radioactive flux assays [204]. It is well known that patch-clamp represents the best method for the evaluation of the action of compounds. In the whole-cell patch-clamp configuration, one can manipulate the intracellular solution (e.g. adding a molecule under inspection) by diffusion through the pipette solution and can manipulate the extracellular solutions [205]. In the next sections, we will review the K^+, Na^+, Cl^-, Ca^{2+}, and other ion channels expressed in jurkat T lymphocytes (see figure 2.12 and table 2.1).

K^+ ion channels

The development of new technologies has increased the number of identified ion channels in jurkat T cells (see table 2.1); the predominant ion channel present in jurkat T lymphocyte under whole-cell configuration employed was a voltage-gated K^+ channel, Kv1.3 (n-type). It was estimated that 400 channels/cell (equivalent to a density of 3 channels/μm^2 of the cell membrane) were present in T lymphocytes. The conductance of a single ion channel was estimated from the current-voltage relation to be 12 pS [190]. These channels are sensitive to membrane potential, temperature, and intracellular Ca^{2+}. Voltage-gated K^+ channels are activated by depolarization of the membrane to more positive potentials than its physiological resting potential. The rate of activation, the rate of deactivation, recovery from deactivation and the peak conductance are all increased with temperature. However, these channels may be deactivated as a result of an increase in intracellular Ca^{2+}, under whole-cell conditions [206]. Kv1.3 channels are involved in different processes of lymphocytes cell life; in cell volume regulation (RVD), deactivation of lymphocyte, and, the most related to our study, in sustaining the resting membrane potential. Blockade of Kv1.3 channels induces depolarization, diminishing the influx of Ca^{2+}, and, as a result, inhibiting the activation of lymphocyte, which is driven by antigen. Voltage-gated K^+ channels are sensitive to any type of inhibitors such as TEA (in mM), NTX, KTX, MTX, and CTX (last 4 in nM) [195, 171].

Another type of K^+ channels presents in jurkat T cells is the Ca^{2+}-gated K^+ (KCa3.1) channels. This channel operates with Kv1.3 in cooperatively and compensatory method to regulate Ca^{2+} influx. Grissmer et al. [192] identified two types of KCa3.1 channels in jurkat T cell using whole-cell patch clamp. Intracellular Ca^{2+} activates both KCa3.1 channels in the same manner. The threshold of activation, for both, is 200-300 nM of Ca^{2+} and full activation occurs with 1 μ M of Ca^{2+}. Since the intracellular physiological concentration of Ca^{2+} is between

50 - 100 nM, then KCa3.1 channels are inactive under physiological conditions. The differences between these two channels are their conductance and sensitivity to drugs. One of them has a conductance of 2-8 pS, is sensitive to TEA (mM) and apamin (pM), is dominant (more than 500 channels/cell) and is therefore called SK (small KCa). Another one has a conductance of 11-35 pS, is sensitive to TEA (mM), quinine and CTX (nM), less dominant (5-50 channels/cell) and is therefore called IK (intermediate KCa). The BKCa channel (big KCa) does not exist in jurkat cells [195, 191, 192].

In contrast to Kv1.3, KCa3.1 channels do not appear to contribute significantly in resting membrane potential of lymphocytes under physiological conditions but induce a membrane hyperpolarization when intracellular Ca^{2+} concentration is increased over the threshold. KCa3.1 channels are involved in lymphocytes activation by inducing Ca^{2+} influx as a result of the resting membrane hyperpolarization when activated. The hyperpolarization of the membrane potential increases the driving force of Ca^{2+} and causes an influx of Ca^{2+}.

In addition to these two types of K^+ channels, there is a leakage K^+ current through TASK (K_{2p}) channels. When any K^+ channel is open, there will be a K^+ efflux controlled by the electrochemical gradient of K^+. This efflux will cause a hyperpolarization of the membrane potential. Therefore, K^+ channels in lymphocytes possess a substantial role in facilitating Ca^{2+} influx through mitogen-stimulated Ca^{2+} channels by maintaining membrane potential hyperpolarization [191, 192], [207]-[208].

Na^+ ion channels

Jurkat T cells expressed several types of Na^+ ion channels (see table 2.1), most of these are inactive under physiological conditions. Like excitable cells, 10% of jurkat cells expressed voltage-gated Na^+ channels (VGSCs), which carry an inward current when the membrane is depolarized to more positive voltages relative to

physiological resting membrane potentials [190, 196]. Most voltage-gated sodium ion channels are sensitive to tetrodotoxin (TTX) in the range of nanomolar concentrations. Therefore, they are known as TTX-sensitive. In contrast, the subset expressed in jurkat T cells (Nav1.5, Nav1.7, and Nav1.9) are sensitive to concentrations in the micromolar range, and so they are known as TTX-resistant. These ion channels have a threshold of activation about -50 mV, and are involved in cell invasion but they have no effect on proliferation and cell migration [209].

Na^+ may enter the cell through other ion channels such as CRANC and TRPM4. The former is a non-selective cation channel, activated by thapsigargin, ionomycin, ADP-ribose and Inositol trisphosphate receptor (IP_3). CRANC ion channels have unitary conductance of about 23 pS. They are termed as Ca^{2+} release activated the non-selective channel. [210]. TRPM4 ion channels are activated by intracellular Ca^{2+}. They are highly selective to Na^+ relative to other monovalent cations. These channels depolarize the membrane when activated, and thereby limit the influx of Ca^{2+} [191].

Another channel that may facilitate the entrance of Na^+, is CRAC. This is a Ca^{2+} channel that carries the main part of Ca^{2+} influx when the Ca^{2+} store is depleted. CRAC channel also has a very low conductance to Ca^{2+}, 24 fS, but has a very high expression in jurkat cells $\sim$ 5000-10000 channels/cell. It facilitates the entrance of Na^+ only in particular circumstances, namely in the absence of extracellular divalent cations [211, 210]. Sodium is one of the main ions that are involved in creating the membrane potential together with potassium and chloride.

Since Na^+ concentration inside the cell is very low relative to outside, the cell requires a mechanism to remove the sodium enters the cell through cell processes. To move Na^+ from the intracellular region to the extracellular media, cells need to extrude Na^+ ions against their electrochemical gradient (uphill). This process requires energy that can be taken from the hydrolysis of ATP. In each cycle, cells couple the hydrolysis of one ATP to the extrusion of $3Na^+$ and the uptake of

$2K^+$ in an electrogenic process. The result of this process is a hyperpolarization of the membrane and a rebuilding of the gradients of these ions [212, 183, 213, 214]. This pump can be partially inactivated by an increase of intracellular Ca^{2+} concentrations [215, 216, 217].

Cl^- ion channels

Jurkat T cells usually possess modest chloride current since they have a relatively high intracellular concentration of Cl^- [191]. However, chloride channels are involved in many functional cellular processes, such as ion homoeostasis, cell volume regulation, pH regulation etc., these channels have different gating and complex activation mechanisms. The most studied is the $Cl^-_{swelling}$ which has a small conductance of about 1-2pS, therefore it is known as Cl^--mini [207, 193]. Cl^--mini is activated by cell swelling and intracellular ATP. When cells are exposed to hypotonic medium the Cl^--mini is activated and the efflux of Cl^- depolarises the membrane, as a result, it limits the influx of Ca^{2+}. In cell volume regulation, the depolarization of the plasma membrane by the Cl^- efflux causes an efflux of K^+. When the cell loses a resultant of KCl, it will be followed by water efflux and cell volume decrease (RVD) [193].

Another Cl^- channel is activated by cAMP or prolonged membrane potential and has a conductance of 40 pS in symmetrical Cl^- solutions. Its conductance is higher than that of Cl^--mini. Therefore, it is termed midi Cl^- channels. This channel requires a threshold of intracellular concentration of Ca^{2+} approximately 10^{-7}M to be activated [218, 207]. It is probably the same Cl^- channel reported by Guggino [219, 220]. They termed it as outwardly rectifying Cl^- channel (ORCC).

Table 2.1: Ion channels in jurkat T cell

Type of ion channels	Ions	Inhibitors	Activation	References
Voltage-gated K^+ (Kv1.3) channel	K^+	TEA^+, Scorpion venoms	Membrane depolarization	[190, 206, 192, 195, 171, 221, 222]
Calcium-gated K^+ channels (SKCa, IKCa)	K^+	Charybdotoxin, TRAM-34	increase in $[Ca^{2+}]_i$	[207, 195, 171, 223, 224, 225]
Leakage (TASK) K^+ channels	K^+	PKTHPP		[191, 226, 208, 227]
voltag-gated Na^+ (Nv) channel	Na^+	Jingzhaotoxin-III	membrane depolarization	[209, 196, 228]
TRPM2	Na^+	ACA	ADP-ribose	[229]
TRPM4	Na^+, Ca^{2+}	9-phenanthrol	Ca^{2+}	[191, 230, 231]
CRAC	Ca^{2+}, Na^+	Divalent and trivalent cations	Ca^{2+}-store depletion	[226, 232, 233, 234, 235]
CRANC	Na^+, Ca^{2+}		Store-depletion, thapsigargin, ionomycin, ADP-ribose and IP3	[210]
TRPM7	Ca^{2+}	Carvacrol	Mg^{2+} ions	[236, 237]
Ca^{2+} ATPase (PMCA)	Ca^{2+}	Caloxin 1b1	ATP	[191, 238, 239]
Voltage-gated Ca^{2+} channel	Ca^{2+}	Kurtoxin	membrane depolarization	[240, 241]
Serca	Ca^{2+}	Thapsigargin	ATP	[191, 242]
InsP3	Ca^{2+}		Inositol trisphosphate	[191]
CFTR	Cl^-	Sulfonylurea glibenclamide	cAMP	[191, 243]
Cl_{swell} or (mini)	Cl^-	Glibenclamide	Cell swelling	[218, 244]
Cl (intermediate)	Cl^-		Prolonged depolarization	[193]
Cl (maxi)	Cl^-		Prolonged depolarization	[193]
GABA	Cl^-	Guvacine	external GABA	[191, 245]
$Cl^-/HCO_3{}^-$	Cl^-, $HCO_3{}^-$	Cyclic AMP	Change in pH	[246, 247]
H^+/Na^+ exchanger	H^+, Na^+	SM-20550 (Amidines)	ATP regulated	[248, 249]
Voltage-gated H^+ channel	H^+	pH-dependent divalent cations	membrane depolarization	[250, 251, 252]
Na^+/K^+-ATPase	Na^+, K^+	Ouabain	ATP	[213, 253]
Pannexin	ATP release	S-Nitrosylation		[254, 255, 256, 257, 258]
Pr2X	Ca^{2+},K^+,Na^+		Extracellular ATP	[259]

A higher conductance Cl^- channels of about (300-400 pS) are termed as Cl^--maxi. The activation of these channels is complex. Cl^--maxi channels are activated by membrane depolarization for several minutes (>0 mV) and they show voltage dependence [207]. Other Cl^- channels expressed in jurkat cells are GABA A, CFTR, and Cl^-/HCO_3^- anti-porter. The latter often involved in cell volume regulation and pH homoeostasis [260, 261].

Ca^{2+} ion channels

All channels discussed before may be involved in membrane potential to regulate Ca^{2+} influx by changing the driving force of Ca^{2+}. When the membrane is hyperpolarised by the K^+ efflux, calcium ions enter the cell through Ca^{2+} open channels in the direction of Ca^{2+} electrochemical gradient. Jurkat T cells express several types of Ca^{2+} channels, which is responsible for the entrance of Ca^{2+} ions. The sources of the intracellular calcium are partially from the release of Ca^{2+} that stored in the endoplasmic reticulum (ER) and the other part is the influx through the plasma membrane Ca^{2+} channels. This influx is triggered, by the depletion of the internal storage, through a very low conductance with very high selectivity Ca^{2+} channels, termed as CRAC channel [226, 235].

Another Ca^{2+} inward current was activated by the membrane depolarization, which suggests an expression of voltage-gated Ca^{2+} channels in jurkat T cells [240]. Stockes et al [262] reported that this channel is a non-voltage-gated Ca^{2+} channel related to the classical Ca^{2+} voltage-gated channels. TRPM2 is a Ca^{2+} channel non-selectively permeable to cations. It can be activated by ADP-ribose and high concentration of concanavalin A and inhibited using the antifungal agents clotrimazole and econazole, N-(p-amylcinnamoyl)anthranilic acid, and by 2-aminoethoxydiphenyl borate (2-APB) [229, 263, 230, 264].

Regulation of the intracellular Ca^{2+} requires a movement of Ca^{2+} against its electrochemical gradients. The extrusion of Ca^{2+} from the cytoplasm to the

extracellular solution or to the store (ER) requires energy which is taken from the breakdown of ATP. SERCA in the ER and (PMCA) the plasma membrane Ca^{2+}-ATPase hydrolyse ATP to get the energy required to move Ca^{2+} against its electrochemical gradient [265, 266, 267].

Other ion channels

Ion channels are involved in most functional processes in the cell. Ion channels were discussed in previous subsections are involved in regulation of Ca^{2+} and maybe in other ions' homoeostasis. But, other ion channels which are expressed in jurkat T cells are involved in pH regulation, ion homoeostasis and cell volume regulation such as H^+-ATPase, Na^+/H^+ antiporter, Pannexin and P2X [254, 255, 256, 257, 259]. Pannexin releases ATP when the cell exposed to the hypotonic medium. This ATP will activate P2X channels that facilitate the entrance of cations such as Ca^{2+}, K^+ and Na^+. This suggests that P2X channels may be involved in cell volume regulation and ion homoeostasis.

A proton pump is expressed in the plasma membrane of jurkat cell that is involved in the regulation of pH. In addition, Na^+/H^+ antiporter, which exploits the electrochemical energy of sodium to pump protons to the external medium, might be involved in cell volume regulation and pH homoeostasis [251, 250, 248].

In conclusion, the integrity of the ion channels expressed in jurkat T cells is involved in regulation of the function of ion channels in physiological conditions. The expression of these ion channels may vary under altered state to maintain the regulation of the new steady state of the cell. Understanding the role of these ion channels in the physiological and pathophysiological states may help in producing medicines which are required to treat the cell in altered states.

The membrane potential was discussed mainly in jurkat T cells, in what follows the role of the membrane potential in apoptosis and cancer cells is discussed.

Plasma membrane potential in apoptosis

As mentioned before, ion homoeostasis is linked to apoptosis and bioelectrical properties can be used as indicators for cell characterization and can control cell development, therefore the plasma membrane potential is apt to be linked to apoptosis.

Many studies reported a plasma membrane depolarization accompanied cell apoptosis [268, 269]. However, the role of this depolarization during cell death is still not clear. PMP depolarization through apoptosis may be a consequence of ionic imbalance or it may be a signal required in initiating the required factors of apoptotic. Cell apoptotic is reported to be initiated with an imbalance in major ions such as K+, Na+, Ca2+, and Cl-, and these ions are known to be correlated with the generation of the resting membrane potential (see section 2.5) [270, 271, 272, 273, 274, 275, 276, 277]. Therefore, the PMP is favoured to be correlated with apoptosis. A huge reduction in intracellular K+ concentration was reported in the development of cell apoptosis. In addition, an increase of Na+ and Ca2+ intracellular concentrations were observed in the apoptotic process [268, 270]. These results may support that the PMP is a result of ionic imbalance during apoptosis. But, lowering extracellular Cl- which causes membrane depolarization and apoptosis may correlate apoptosis to the depolarization of the membrane. The depolarization of the membrane causes the efflux of K+, which result in an osmotic imbalance and shrinkage of the cell volume.

From all these studies it is not obvious if the depolarization is a required factor in apoptosis even it precedes K+ efflux and shrinkage. In addition, shrinkage and apoptosis may be initiated by a dysfunction of regulatory volume increase which may result in shrinkage due to upregulation of aquaporins (APQs see reviews by Borgnia [278, 279, 280, 281], and inactivation of these water pathways. Therefore, the depolarization of the PM may be required in cases where apoptosis is initiated by the huge loss of K+ due to the depolarization of the PM, which results in

shrinkage and cytochrome release.

Plasma membrane potential in cancer

Cone et al (1971) reported that hyperpolarizing CHO cells to -45mV induces mitotic arrest and further hyperpolarization to -75 mV fully blocked cell division. In contrast, membrane depolarization, by applying Na+, K+-ATPase inhibitor, to -10 mV results in cell cycle resume [282]. It was found that the cytosolic concentration of Na+ is higher in tumours compared to normal cells [283, 284]. These results support the correlation between tumour and membrane depolarization regardless the ion channel or the types of ions involved [277].

The involvement of ion channels in the generation of the membrane potential and its dynamics was discussed. In the next section, the role of ion channels in intracellular pH regulation will be discussed in healthy and altered cells. The effect of pH on the membrane potential, glycolysis, cell growth and ion homoeostasis also will be explored.

2.6 Intracellular pH

The international convention of pH is regarded as the negative logarithm of the hydrogen activity [285, 286]. It is measured on a scale between 0 and 14 to describe the degree of acidity and alkalinity, where the value 7.0 represents the neutrality, lower values correspond to acidity and higher values correspond to alkalinity. Contrary to this scale, pH value can be negative or greater than 14 for very strong acids and bases respectively [287]. The pH scale was established by international agreement to trace a set of standard solutions; therefore, the modern pH scale is a measure of the proton's chemical potential [286].

It is only possible as a first approximation to treat the inverse antilog pH as the proton activity or concentration. Using this classical definition of pH in watery

solutions, one can estimate the concentration of H^+ in a cell cytosol if assumed to be a watery solution. As an example, in a single cell with a volume of 48 μm^3 [288, 289] at neutral pH (7.0) [290], the estimated free proton number is not more than 3000 in all compartments. In contrast, protein analysis in yeast cells tells us that the proteins number in a cell is in the order of millions [291]. Each protein usually has multiple protonatable groups which means that millions of protons can be donated or taken up. In addition, cells contain an excess of acidic metabolites compared to free protons, as an example, the concentration of inorganic phosphate in yeasts is estimated to be around 50 mM [292]. Therefore, the classical definition of pH to be related to the concentration of protons does not seem to be applicable.

pH regulation is one of the most crucial processes in cell function, therefore it is strictly regulated in a small range even when cells are exposed to extreme changes in medium pH value. Cells maintain a pH value close to neutrality by the cytosol high buffer capacity produced by proteins and utilizing a powerful mechanism of ion exchange (H^+/Na^+) at the plasma membrane [119]. In addition, pH plays a crucial role in yeast growth, glycolysis, gluconeogenesis, fermentation and proliferation [293, 294].

Cells have adaptive regulatory pH mechanisms to keep the value of pH within a physiological small range. Cellular compartmentalization, buffer capacity and proton sequestration form part of these mechanisms. In addition, pH homoeostasis can be achieved by the operation of ATPases that extrude protons from the cytosol into the mitochondrial matrix or out to the external medium [295, 296]. Glycolysis and cell membrane potential are two factors that account for cytosolic acidification. The electrical charge distribution across the plasma membrane, which generate the membrane potential, drives the uptake of positively charged protons and extrude HCO_3^- and result in a reduction of the intracellular pH. Net acid equivalents that produced by metabolic reactions account for cytosolic acidification. To prevent cytosolic acidification, protons must be extruded continuously out of the cytosol across the plasma membrane through the H^+-ATPase (Pma1) using the energy

released from ATP hydrolysis [297].

As mentioned above, pH has different effects on the functional processes of the cell. In the following, these effects are discussed in detail. Starting by the effect of pH on glycolysis and cell growth, followed by the effect on ion homoeostasis, then the effect on the plasma membrane potential and finishing by the effect on the mitochondrial membrane potential. After that, the mechanism of pH regulation is discussed.

2.6.1 The effect of pH on glycolysis

Glycolysis is a process in which carbon source molecules are broken down to produce energy that are required by the cell to survive. These reactions are catalysed by many enzymes, which are enhanced by some metabolites and inhibited by others. One of the most important enzymes in glycolysis is phosphofructokinase (PFK), which play a crucial role in the regulation of glycolysis [77]. In addition, PFK is extremely sensitive to small changes in cytosolic pH; a low physiological pH (acidic pH) decreases the affinity of PFK for F6P and an increase in pH (alkalinization) results in a decrease in PFK affinity for ATP. The effect of the decrease of pH may be to stop pH from more decrease by glycolysis to prevent cell damage. In a similar way, the increase in pH cause enhancement of glycolysis to prevent more increase in pH which may cause uncontrolled glycolysis. These coupled mechanisms may contribute to the regulation of both pH and glycolysis simultaneously [298].

2.6.2 The effect of pH on cell growth

Growth inhibition is linked to a severe decline in pH. This was attributed to the decrease in cytosolic ATP/ADP ratio due to the increase in the activity of pma1, caused by the decrease in intracellular pH. But, with amphotericin B a direct

correlation between growth inhibition and pH decline was found. Amphotericin B causes a disruption of the plasma membrane and a proton influx which result in a decrease in cytosolic pH and inhibition of growth without a change in ATP/ADP ratio [110, 298].

The regulation of cytosolic pH is very crucial for the optimal activity of several critical metabolic processes. To maintain a physiological range of intracellular pH, yeast cells require an intact plasma membrane. Any minor change in cytosolic pH can regulate important processes in the cell such as division, synthesis of the RNA and DNA, and thermo-tolerance [299, 300, 301, 302, 303]. In yeast, maintenance of cytosolic pH in the physiological range can be partly achieved by the activity of pma1 which couples the extrusion of protons to the hydrolysis of ATP. This enzyme may consume up to 60% of the cellular energy to regulate the intracellular pH, which is crucial for cell growth. Therefore, the plasma membrane H^+-ATPase is essential for cell growth [102, 304].

2.6.3 The effect of pH on the plasma membrane potential

The membrane potential (MP) was discussed in section 2.5. It depends mostly on the distribution of K^+, Na^+ and Cl^- in most mammalian cells. But, in yeast, the MP depends mostly on the distribution of protons and may be the K^+ ions [130, 305].

In yeast cells, the acidification of the cytosol that may occur when glucose is added may depolarize the plasma membrane potential. Therefore, the activity of the pma1 increases to regulate both pH and the membrane potential by translocating the protons out of the cell utilizing more than 50% of the cell energy as discussed in section 2.4.1. Since the pump pma1 is electrogenic and it regulates the intracellular pH, its activity results in changes in both the membrane potential and the intracellular pH. Translocation of protons out of the cytosol cause alkalinization of the cytosol and hyperpolarization of the MP. The Na^+, K^+/H^+-antiporter

and Nha1, which are pH dependent transporters, influence the plasma membrane potential of *S. cerevisiae* yeast cells [119].

This suggests that pH might play a role as an electrical signal to communicate between cells.

2.6.4 Regulation of cytosolic pH

Since PFK activity is extremely sensitive to small changes in pH, it is a crucial requirement to maintain the pH value in the physiological range. One of the most important regulatory processes is the control of glycolysis by pH to prevent more change in pH; a decrease in pH results in a reduction in the PFK affinity for fructose 6-phosphate this may slow down glycolysis and result in preventing more decrease in pH. In a similar process, an increase in pH results in glycolysis stimulation, which results in preventing more increase in pH [77].

These mechanisms cannot regulate pH completely by itself, therefore other mechanisms are required. When glucose is added to yeast culture, pH decreases [306] and the activity of pma1 increases to extrude protons out of the cytosol to prevent a severe drop in cytosolic pH. Yeast cell utilize 40-60 % of their total ATP to regulate pH through pma1 activity [102]. The H^+-ATPase (pma1) is activated by glucose in a self-regulatory process; the addition of glucose causes an increase in glycolysis process, which result in pH fall and cause an increase in pma1 activity to prevent the fall in pH [297].

The regulatory system of intracellular pH consists of several processes; buffer capacity and a transport system.

Buffer capacity

The buffer can be defined as a solution that resists changes in pH value when acid or alkali substrates are added. In cytosolic solution, almost all proteins and

metabolites can act as buffers [295]. The number of proteins within the cytosol is more than a million each has protonatable groups which means that proteins can detach millions of protons if the pH value of the cytosol increases suddenly [291]. By contrast, when intracellular pH decreases rapidly, proteins can be protonated with millions of protons from the cytosol. The total buffering capacity may be insufficient to counteract long-term stresses, therefore more dynamical and sustainable mechanisms are required to regulate pH [307].

Transport system

Almost all cells have mechanisms to extrude protons to maintain a physiological pH range which is above H^+ equilibrium distribution across the plasma membrane. Therefore, this mechanism must be an active transport, which requires energy to move protons against their electrochemical gradient [102]. Cells with quiescent states are usually associated with cytosolic acidification while intracellular pH increase usually accompanies activation of cells [77]. Therefore, it is crucial for cell activation to have a mechanism to extrude H^+ and raise pH or to sequester protons in the internal organelles. Main systems that extrude protons at the expense of ATP hydrolysis are ATPases; pma1, F_0F_1-ATPase, and Vma1.

(1) The plasma membrane H^+-ATPase) The first observation that indicates that fungi and plants contain H^+-ATPase in their plasma membrane was the acidification of the fermenting media by yeast cells [102]. This acidification was inhibited by arsenate, which suggests ATP requirement and ATPase involvement in the extrusion of protons out to the media [103]. Pma1 is activated by the addition of glucose to the medium, which results in acidification of the cytosol and activation of the ATPase. This pump has a very high maximum capacity ranging from 30 pico-mole/cm^2/sec in yeast cells [103] to 200 pico-mole/cm^2/sec in Neurospora [104]. With a stoichiometry of 1 H^+/ 1 glucose and an area of 10x10 nm^2 occupied by each pma1 molecule, this rate may result in a consumption of 40-60% of the

produced ATP in a yeast cell.

Pma1 can be controlled by two types of factors; intrinsic factors identified by the proton gradient and the membrane potential and an extrinsic factor such as glucose in yeast cells [102]. The addition of glucose increases the activity of the pump, which results in a fall of ATP level in the cytosol. In acidic media, the proton efflux is inhibited and also inhibited by the depolarization of the plasma membrane [103]. The pma1 is a major ATP consumer in yeast cells [5], this can be observed by raising the medium pH [106] or adding K^+ [107] which result in a rapid activation of the pump and a fall in the cytosolic ATP level. These results suggest that this pump is very important in the energy balance of the cell and represent a major regulator of intracellular pH.

(2) Intracellular ATPases Both the vacuole and the mitochondria contain H^+-ATPases. The vacuolar ATPase (V-ATPase) consumes ATP to sequester protons in the vacuole to maintain cytosolic pH in physiological range. V-ATPase in metabolising yeast cells collaborate with pma1 to maintain pH homoeostasis [307], see figure 2.13. The result of the activity of this pump is the acidification of the vacuole, which creates a pH gradient with the cytosol and a membrane potential like pma1. The addition of K^+ is important in balancing the plasma membrane potential and stimulation of pma1 to increase cytosolic pH [307]. The generation of pH gradient and membrane potential by both pma1 and vma1 is very important in driving the transport of other ions across their respective membranes.

While plasma membrane and vacuolar ATPases are important in generating pH gradient to drive other ions transport, the mitochondrial ATPase, which shares some characteristics with those ATPases, is doing a different work by utilizing the proton gradient as an energy source to produce ATP in the mitochondrial inner membrane [308]. This process is very important and produces a high portion of the total ATP in the cell. In non-respiring cells, this ATPase consumes ATP to generate a pH gradient across the inner membrane of the mitochondria, which

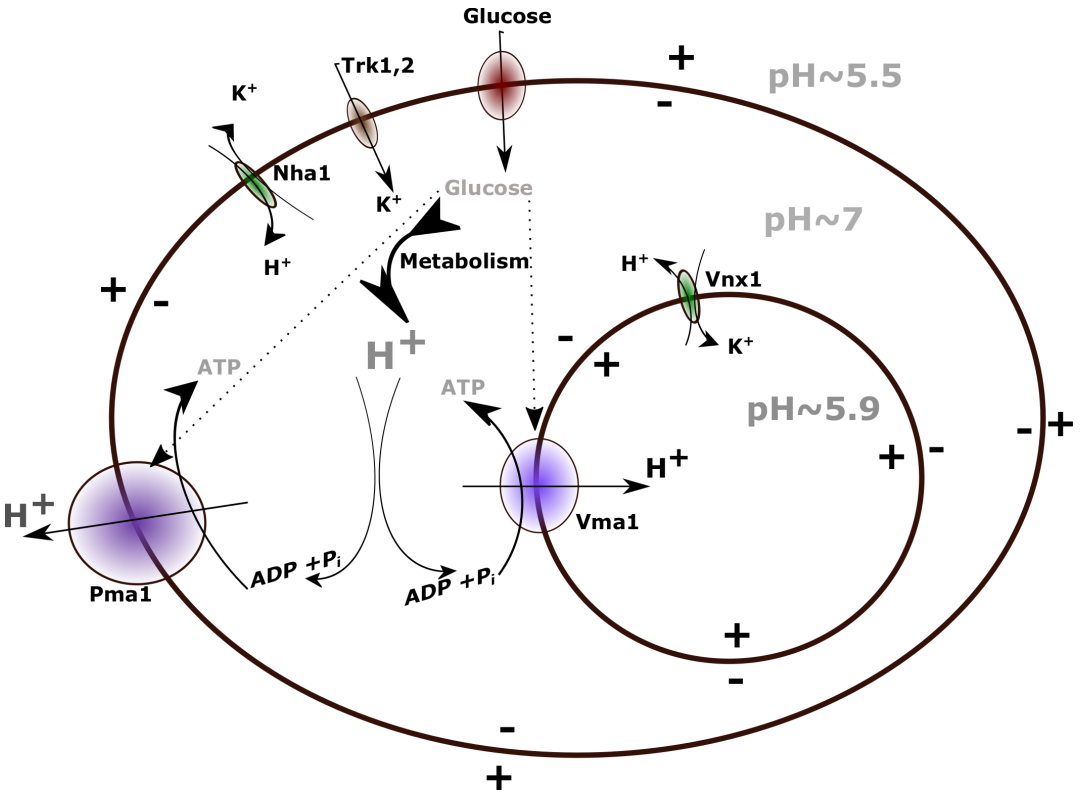

Figure 2.13: A Model of collaboration between vacuolar and plasma membrane ATPases in intracellular homoeostasis. Adapted from [307].

participate in the maintenance of the mitochondrial membrane potential (MMP) [309, 4].

(3) Na^+/H^+ antiport This transporter is usually involved in pH regulation under sudden changes of intracellular pH. After sudden alkalinization of microorganism's cytosol, this antiporter utilizes the K^+ outward gradient to uptake protons in a regulatory process of intracellular pH. [310, 145, 311].

Nha1 is often activated under NaCl stress in yeast cells to eject the toxic Na^+ and maintain high K^+/Na^+ ratio, which is crucial for optimal cellular function [118]. This system is normally translocating Na^+ outwards utilizing the energy stored in the proton gradient, which is created by the pma1 activity that utilizes the free energy of the ATP hydrolysis to eject protons [312, 313, 314]. It was proposed by West and Mitchell (1974) that this antiporter is electroneutral [312], but Taglicht et al. found that an imposed membrane potential with negative

inside the cell can accelerate the extrusion of Na^+ at all pH values tested [315]. This result suggests that this antiporter is electrogenic ($2H^+$ are exchanged for each Na^+) at acidic and alkali pH values and is influencing the plasma membrane potential [119]. But, it is usually activated at high intracellular pH values and it ejects Na^+ or K^+ to regulate pH and may regulate the K^+ content of the cell [145, 146]. It was mentioned in previous sections that the extrusion of toxic Na^+ at acidic and neutral intracellular pH can be achieved by the Na^+-pump (Ena1). In S. cerevisiae, the overexpression of Nha1 gene results in an increase in pH-dependent Na^+ tolerance [114].

2.7 Mitochondrial membrane potential

The mitochondrial membrane potential (MMP) represents part of our study. Therefore, MMP from previous studies is revised here.

The voltage difference across the mitochondrial inner membrane is referred to the mitochondrial membrane potential (MMP). This potential represents one of the two components that are produced by the proton gradients, which exist across the inner membrane of the mitochondria. H^+ gradient, across the inner membrane of the mitochondria, is generated by protons pumped by the respiratory chains which are located in the inner membrane of the mitochondria itself [316, 317, 318, 319]. The other component represents the pH gradient across that membrane. Each component of the proton gradient can drive the synthesis of ATP by F_0F_1-ATPase [320, 321, 322].

2.8 Glycolytic oscillations

Rhythmic behaviour is prevalent in living systems, which is often related to external oscillatory process such as annual cycle, daily cycle or cell cycle. However,

glycolysis exhibits an oscillatory process which is related to the chemical reactions that form glycolysis. In 1920, Lotka described one of the earliest chemical reactions mechanisms [323]. The mechanism was represented by chemical equations based on a law of mass action. Hess and Boiteux have listed many oscillatory examples in living systems [324]. In the 1950s, Duysens and Amesz reported fluctuations in NADH fluorescent in intact yeast cells [6]. And then Chance et al reported in the 1960s, for the first time, an oscillation in the concentration of intracellular reduced pyridine nucleotide in cell extracts [325] and in intact cells [326]. In this background, a small part of huge number of researches on oscillatory process in glycolytic metabolites is presented [327, 328, 329, 330, 331, 332, 29, 32, 4, 5, 333, 334].

Most the reported oscillations in glycolysis was in population of yeast cells and they measured only macroscopic oscillations. In 2012, Gustavsson et al., observed sustained oscillations in individual isolated intact yeast cells [335]. The results of Gustavsson et al. confirmed that the macroscopic oscillations measured before were due to the synchronization of individual cell when the density of cells reaches a threshold. The metabolite that was proposed to be a synchronizer in the process is acetaldehyde [330]. In this background, a review of glycolytic oscillation is present in intact cells.

2.8.1 Glycolytic oscillations in intact cells

Many reports on oscillations in NADH in intact cells goes back early in 1960s [326]. Yeast cells are starved until they reach a shift from glucose to ethanol utilization as a substrate in cell growth. And then, a pulse of glucose is added followed by cyanide, to cause a shift from aerobic to anaerobic glycolysis, which results in an oscillation in the metabolites, such as NADH, ATP, etc. The oscillations observed in metabolites were around phosphofructokinase, which is similar to what was reported in cell extracts [324]. But there was a difference in the frequency and the shape of the oscillations. The frequency in intact cells was higher than

that in cell extracts while the shape in intact cells was sinusoidal. On the other hand, there was a similarity between both cell extracts and intact cells metabolite frequency. In both, the frequency was affected by several factors such as the rate of addition of glucose, temperature and pH [336]. Glycolytic oscillations in yeast cells was found to be density dependent. Therefore, the oscillations are induced in whole population at the same time by the addition of glucose followed by KCN. Cells then synchronize and oscillate with the same frequency. But, if individual cells oscillate with different frequencies, the macroscopic oscillation, due to cells desynchronization, will die out [327]. The glycolytic oscillations can last longer, due to mutual interaction between cells, at a high cell density [327, 329].

Olsen (2009) measured simultaneous oscillations of NADH and mitochondrial membrane potential (MMP) in a population of yeast cells, S. cerevisiae. It was shown that both NADH and MMP were oscillating with the same frequency and in phase. Using different protein inhibitors, the result show that the MMP is driven by the glycolytic oscillations [4]. In addition, intracellular pH was found to be oscillating with the same frequency of NADH and MMP. The interaction between these processes is still unclear. Ozlap et al. have reported oscillations in ATP with the same frequency of NADH and found that they were out of phase [5].

It was reported that acetaldehyde plays the role of the synchronizer in yeast cells population [330]. Since yeast cells produce acetaldehyde when ethanol is used as a substrate and secrete this molecule to the medium. Then, other cells uptake this molecule passively and sense the oscillations in that cell. It was reported that acetaldehyde is oscillating with same frequency of other metabolites. This way, acetaldehyde play the role of synchronizer between cells. And this makes the density of the cells as an important factor to generate macroscopic oscillation in yeast population. Poulsen et al (2004) used argon gas instead of KCN, which was reported to inhibit respiration and found that any volatile molecule as argon gas or CO_2 can interact with acetaldehyde and initiate oscillations [29]. Poulsen reported that their measurements failed to detect oscillations in isolated cells under

conditions where glycolytic oscillations were observed in the suspension.

Gustavsson et al. (2012) reported glycolytic oscillation at the microscopic scale in individual yeast cells. A champer was used with laser tweezers to trap cells in the solution. The cells were fed by glucose at a constant rate and KCN was used to shift glycolysis from aerobic to anaerobic. Sustained oscillations that last more than an hour were observed and the number of cycles exceeds 40 in some cells [335]. Understanding these oscillations and the interaction between different oscillating cellular processes may help in distinguishing between the cell in healthy and altered state.

To study fluctuations in the plasma membrane potential and the oscillations in intracellular processes, measurements were done using jurkat T cells and yeast cells. In the next chapter, measurements methods and the conditions of the measurements are discussed.

2.9 Summary

This chapter reviews the biophysical background of cellular functional processes in healthy and altered state of the cell. The characteristics of yeast cell and jurkat cells were also revived. The review is initiated by a biological background of yeast cells followed by metabolism. Then, ion homoeostasis, PMP, pH, cell volume and the MMP are discussed. In addition, oscillations in glycolytic metabolites are reviewed. The discussion show that the interaction and the mechanisms by which these processes interact are not clear and need more study. Therefore, in this thesis, the dynamics in the resting membrane potential is studied under different conditions. The sources of these dynamics are studied and the factors that may affect the resting membrane potential and the amplitude of the fluctuations in the resting membrane potential are studied. The analysis and the results of this study are presented in chapter 5.

Chapter 3

Measurements methods

Methods used in measurements are discussed in this chapter. The structure of this chapter is as follow:

Section 3.1 discuss the whole-cell patch-clamp, details the protocol used in the measurements, and explore the solutions used in the experiments. Section 3.2 shows the techniques used to measure NADH, ATP, mitochondrial membrane potential and cytosolic pH. Finally, section 3.3 summarises the chapter.

3.1 Whole-cell patch-clamp

Patch clamping refers to imposing a defined voltage (voltage-clamp) on a small piece of cell membrane to measure the current through that piece or imposing a defined current (current-clamp) to measure the voltage difference across that piece. But it is rarely used for small patches of membranes. Following Neher and Sakmann introduction [337], patch-clamp most often refers to voltage clamp of a membrane patch.

The main step in patch-clamp is pushing the tip of 1-2 μm-diameter glass micropipette against a cell. After that the clamp is completed dependent on the type of patch-clamp configuration; in whole cell, a weak suction pulse is applied

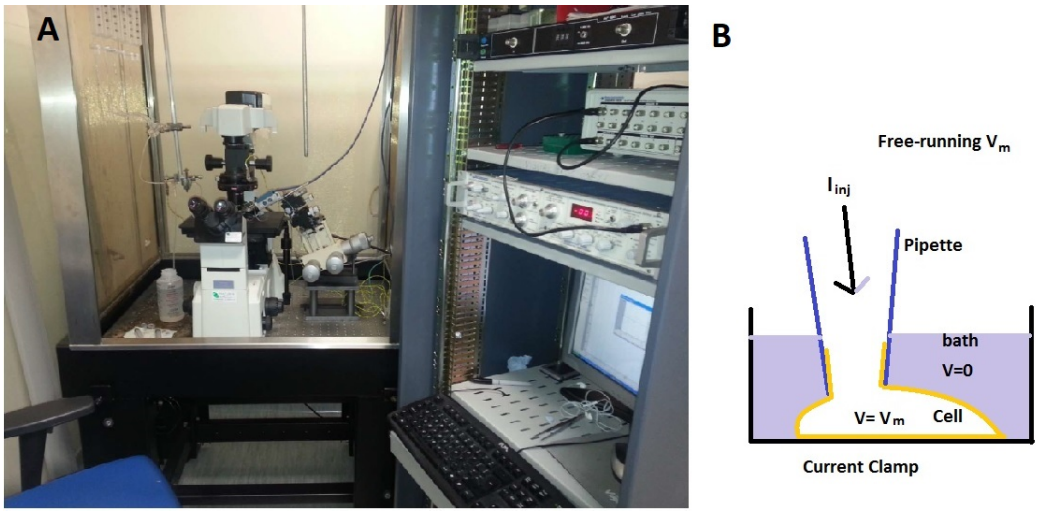

Figure 3.1: A) A picture of the patch clamping rig at Lancaster University, UK. From [2]. B) Current-Clamp configuration.

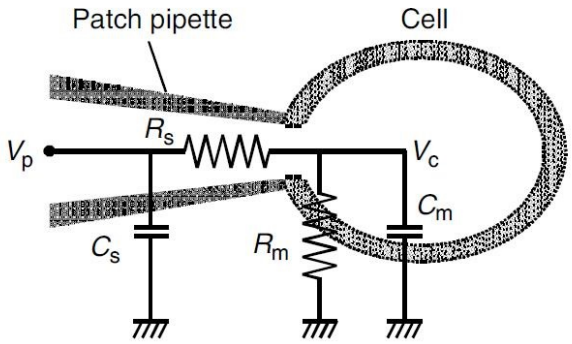

Figure 3.2: Whole-cell patch-clamp equivalent circuit. R_s: series (access) resistance; R_m: membrane resistance; C_m: membrane capacitance; C_s: stray (pipette) capacitance; V_c: cell potential V_p: pipette potential. From [205]

to rupture the patch and maintain a tight seal. An amplifier is used to inject current into the cell to current-clamp the whole-cell membrane and to measure the membrane potential, which is impossible without the giga-seal[338].

The giga-seal, is a seal whose electrical resistance is more than 10GΩ, which is required to isolate the membrane electrically from the external solution to record the currents through the membrane or to record the membrane potential dynamics. A high seal is required to make the electrical isolation of the membrane more complete and to reduce the noise in the recordings [339].

Figure 3.1(A) show the patch-clamping rig at Lancaster University used in the

measurements of this study, done by Shakil Patel [2]. Figure 3.1(B) illustrates the current-clamp principle in whole-cell patch-clamp configuration. As shown, the experimenter injects a current if required in the pipette using an amplifier and the membrane potential is recorded while the current is clamped to a certain value (I=0). Any difference is compensated by current injection using an amplifier. An equivalent circuit to the whole-cell patch-clamp is shown in figure (3.2). Two resistors are connected in series; the pipette resistance ($R_{pipette}$) (the access resistance (R_{access})) and the membrane resistance (R_m). Since the membrane resistance is very high relative to the access resistance, the voltage drop across the access resistance is very small [175]. To correct for this error, a tricky compensation is usually done using the amplifier by adding a compensating current to the injected one.

To calculate that current, we need V_p to be equal to V_c after the compensation. Before compensation we get,

$$V_p = I_{inj} \times R_s + V_c. \tag{3.1}$$

After compensation we get,

$$V_p^{'} = I_{inj}^{'}(R_s + R_m). \tag{3.2}$$

What is required from compensation is to let V_p to be equal the actual value of the plasma membrane potential. In other words, we need

$$V_p^{'} = V_c. \tag{3.3}$$

The result of this compensation will be a change in injected current. The new injected current can be related to the current before compensation by the relation,

$$I_{inj}^{'} = I_{inj}\frac{R_m}{R_m + R_s}. \tag{3.4}$$

R_{access} is in series with the membrane capacitance. Thus, they form RC circuit, which means that any change in holding potential will be delayed by the capacitance. The effect of this RC is usually compensated or reduced through the experiment.

This method has advantages of controlling electrical and chemical gradients governing membrane ion fluxes and measurement of ion currents and membrane potential of very small cells (thanks to giga-seal configuration). In contrast, it has limitations, such as the lack of control over intracellular ionic composition within experiments and spatially nonuniform voltage control [340, 341, 205]. In addition, wash out of main cytosol contents may cause significant run-down problems.

3.1.1 Measurement protocol and the solutions used

The protocol used in these experiments is illustrated in details in [2]. Briefly,

- Find a cell to patch.
- Fill the pipette with an intracellular solution (see table 3.1) using a syringe and a filter, then tap the pipette several times to remove any air bubbles that might exist in the pipette tip [205].
- Place the pipette in the holder, then place the tip of the pipette in the bath and focus it towards your cell target.
- Using a micro-manipulator, move the tip of the pipette to be closer to the cell membrane.
- Release the positive pressure and through the software on the computer watch the change in seal resistance until it reaches the giga value.
- After giga-seal is formed, change the voltage-clamp to negative voltages, to a value which is close to the expected resting membrane potential of the cell (-70 to -60 mV) to do fast correction and to compensate for the pipette

capacitance.

- Apply a light and short suction to break through the membrane and to create electrical access to cell cytosol [342].
- A compensation for the membrane capacitance needs to be done, just as for the pipette capacitance case [341].
- A compensation for the access resistance is needed using the amplifier, by inducing a current change to the injected current through a feed-back loop to compensate for the voltage drop caused by the access resistance [342].
- For current-clamp experiment, the mode is changed to current clamp. Then the resting membrane potential is measured at zero current and the membrane potential is adjusted to the expected value of the resting membrane potential by current injection if required. A free-running voltage record is done over a period of time (i.e. 10 min) [205].

Table (3.1) details the pipette solutions used in all experiments with jurkat T cells. The intracellular concentration of ions resulting from the solutions used in pipette are present in table (3.2). The baths and the concentrations of extracellular ions are present in tables 3.3 and 3.4 respectively. The osmolarity of the solutions was between 280 mOsm and 310 mOsm and was measured using a Vapro osmometer (Wescor, USA) [2].

Table 3.1: Intracellular solution used in experiments with jurkat T cell

Substance	Standard pipette solution (mM) (I1)	Standard pipette solution with elevated calcium (mM) (I2)	Standard pipette solution with ATP (mM) (I3)	Standard pipette solution with elevated Ca and ATP (mM) (I4)
KCl	120	120	120	120
NaCl	20	20	16	16
$CaCl_2$ free	10 nM	1 μM	10 nM	1 μM
Hepes	5	5	5	5
EGTA	11	5	11	11
ATP-Na	0	0	4	4

Table 3.2: Intracellular solution used in experiments with jurkat T cell

Substance	Standard pipette solution (mM) (I1)	Standard pipette solution with elevated calcium (mM) (I2)	Standard pipette solution with ATP (mM) (I3)	Standard pipette solution with elevated Ca and ATP (mM) (I4)
K^+	120	120	120	120
Na^+	20	20	20	20
Cl^-	140	140	136	136
Ca^{2+}	0.00001	0.001	10 nM	0.001
ATP	0	0	4	4

Table 3.3: Extracellular solution used in experiments with jurkat T cell

Substance	Standard bath solution (mM) (E1)	Standard bath solution with elevated K^+ (mM) (E2)	Standard bath solution with lowered Cl^- (mM) (ECl2)	Standard bath solution with lowered Na^+ (mM) (ENa2)
KCl	6	6		6
NaCl	150		10	150
$CaCl_2$	2	2	2	2
Hepes	10	10	10	10
$MgCl_2$	1	1	1	1
Glucose	10	10	10	10
Na-Gluconate		150		
K-Gluconate		6		54
Choline-Cl			140	

Table 3.4: Extracellular solution used in experiments with jurkat T cell

Substance	Standard bath solution (mM) (E1)	Standard bath solution with elevated Cl^- (mM) (ECl2)	Standard bath solution with lowered Na^+ (mM) (ENa2)	Standard bath solution with lowered K^+ (mM) (E2)
K^+	6	6	6	60
Na^+	150	150	10	150
Cl^-	162	6	162	162
Ca^{2+}	2	2	2	2
Mg^{2+}	1	1	1	1

3.1.2 Preparation of Jurkat T cells

Jurkat cells were cultured in RPMI-1640 medium supplemented with 1% FBS and 100 units/ml penicillin and streptomycin and used at 48 hours. Briefly, the cells were sub-cultured from the T25 flask containing the main stock of Jurkat cells by centrifuging the cells at 600RPM for 5 minutes. The supernatant was removed, and the pellet was resuspended in warm RPMI-1640 medium. Trace amounts of FBS was removed by centrifuging the cell suspension at 600RPM for 5 minutes. The cell pellet was then resuspended in warm RPMI-1640 and the volume of medium containing 2X105 cells/ml was transferred to a T25 flask containing RPMI-1640 medium supplemented with 1% FBS and 100 units/ml penicillin and streptomycin. These cells were used at 48 hours [2].

3.2 Fluorescence spectroscopy

3.2.1 Introduction

Over the last 30 years, there has been a remarkable growth in the use of fluorescence in biological science. The major research tools in biophysics and biochemistry are fluorescence spectroscopy and time-resolved fluorescence. The dominant methodology, which is extensively used in biological aspects, is fluorescence. This method is now ubiquitous and used in flow cytometry, DNA sequencing, genetic analysis and biotechnology. Fluorescence is now low cost and high sensitive, therefore, it is used for cellular and molecular imaging.

Luminescence, is a light emitted from any substance which is excited electronically. When a molecule absorbs an appropriate light and after the electron returns following a vibrational relaxation of the molecule, it will emit a light with longer wavelength accompanied with heat. While, not all molecules are capable of producing fluorescence, aromatic molecules usually can. The molecules that can

emit fluorescence are called fluorophores and are divided into intrinsic and extrinsic. Intrinsic fluorophores are molecules that can emit fluorescence naturally (i.e., NADH). Extrinsic fluorophores are substances that are added to a sample that does not have the ability to show the desired spectrum properties (i.e., ATP, pH, DNA and membranes) [343].

3.2.2 Measurements of NADH fluorescence

NADH refers to reduced nicotinamide adenine dinucleotide. In this thesis, NADH autofluorescence were made in a QE65000 spectrometer (Ocean Optics, Dunedin, FL) fitted with a temperature-controlled cuvette holder. The temperature was 25 $\pm$ 0.02 C. The light used in excitation of NADH was supplied by two Hg-lamps (model St75: Heraeus, Hanau, Germany) powered by two NT HgSt power supplies (Duratee Analysentechnik, GmBH, Hockenheim, Germany). The light was guided to the sample using optical fibres (Rapp Optoelectronic, GmBH, Hamburg, Germany) mounted perpendicular to the emitted light. An interference filter (355/20 nm) (Edmund Optics Inc., Barrington, NJ) was used to excite NADH, and the emitted fluorescence was measured as the average intensity in the wavelength range 445-470 nm [4]. NADH fluorescence also was measured by an FS910 Spectrofluorometer (Edinburgh Instruments, Edinburgh, Scotland) using excitation (366/3 nm) and emission (450/10 nm).

3.2.3 Measurements of ATP

The energy-coupling agent, ATP, is a universal molecule used as energy currency by cells to fuel cell functions (e.g., mechanical work; muscle contraction, transport work; ion homeostasis and chemical work; gene replication, protein synthesis and producing light in fireflies) [344, 345].

Due to the importance of this molecule in assessing metabolic states of cells,

measurements of cellular ATP levels become crucial. Therefore, several techniques were developed to measure the concentrations of ATP with high sensitivity, selectivity and monitoring the time and spatial change in concentrations [344, 346, 347, 348, 349, 350, 5, 351].

Luciferin-luciferase

Luciferin-luciferase is one of the earliest methods, which uses firefly's luciferase to assess ATP levels in cells extracts [352]. The bioluminescence of luciferase method is rapid, sensitive (0.1 femto-mole), and reproducible assay [353]. This method exploit the oxidation of luciferase given by the reactions [354],

$$\text{Luciferase} + \text{Luciferin} + \text{ATP} \rightarrow \text{luciferase} - \text{luciferin} - \text{AMP} + P_i, \tag{3.5}$$

$$\text{Luciferase} - \text{luciferin} - \text{AMP} + O_2 \rightarrow \text{luciferase} + \text{oxyluciferin} + \text{AMP} + CO_2 + h\nu. \tag{3.6}$$

These reactions result in the production of a flash of yellow-green light, with a maximum peak emitted at 562 nm when pH is 7.75 and temperature is 25 ^{0}C [353]. Lower pH (i.e., 6.0) will cause a shift in the peak to 620 nm. This shift represent one of the limitations performed in this method [355]. Other drawbacks are the low throughput, the time between readings reaches 10 seconds and the utilization of ATP in the reactions. Consumption of ATP may result in high errors in the measurements. In addition, luciferase method was used with population of permeabilized cells until it was extended to the modulation of confined nanotube fluorophores [349].

Magnesium-sensitive fluorescent indicator

The affinity of ATP for magnesium is higher than ADP, therefore, the hydrolysis of ATP will cause an increase in cytosolic Mg^{2+} concentration. Due to this affinity,

magnesium-sensitive fluorescent indicator (Magnesium Green, MgG) can be used as an index that can provide us with the change in ATP concentration [356, 357, 345]. This method has limitations due to the sensitivity of the MgG to Ca^{2+}. In addition, permeabilization of the plasma membrane causes efflux of Mg^{2+} and a rapid fall in the MgG signal [347, 357]. The main drawback in MgG is that it is very sensitive to Ca^{2+}, therefore, interpretation of the results required caution when Ca^{2+} is increasing[347].

Förster resonance energy transfer

A Förster resonance energy transfer (FRET)-based fluorescent ATP probe is one of the recently methods developed for imaging ATP concentration in single living cells. This probe is named ATeam and it is stable against acidification [350]. This method depends on the energy transfer from an excited fluorophore to another fluorophore by means of intermolecular long-range dipole-dipole coupling [358]. It is one of the highly sensitive and spatially and temporally improved techniques. One drawback in this method is the availability of genetically encoded fluorescent proteins, which is used combined with light microscopy imaging to provide the tools required to increase the spatial and temporal resolutions [358, 359]. The other drawback is that the time between readings reaches 10 seconds.

Aptamer-based biosensors

Aptamers are single-stranded nucleic acids isolated from oligonucleotide (RNA or DNA) and synthesized chemically using SELEX method (systematic evolution of ligands by exponential enrichment), which was described in 1990 [360, 361]. Aptamers are a class of high-affinity molecules of small size, which is chemically stable at room temperature and cost effective [362]. They offer remarkable selectivity and high sensitivity of biosensors designed by labeling their 3' and 5' termini with a fluorophore and a quencher [363]. Therefore, they can distinguish between closely

related compounds (e.g. ATP and ADP) [5, 364]. The simplest format of aptamers can be destabilized by truncating DNA then labeling their termini by a quencher and a fluorophore. This format can undergo significant conformational change which result into a measurable physical signal (e.g. light) when binding to their targets [348, 362]. They can bind with a high affinity to a great variety of molecular targets with high selectivity [365]. This method is widely employed due to the availability of many different fluorophores and quenchers and their capability for real-time detection [362].

When coupled to nanoparticles, aptamers offer a significant improvement to the performance of biosensors and result in signal amplification and target specificity.

In this thesis, ATP concentrations were measured using aptamers coupled to nanoparticles. ATP concentration in the yeast S. cerevisiae was monitored using the aptamers-based ATP nanosensors with a sampling frequency of 1 Hz. A black Hole 1 quencher and an Alexa Flour 488 (AF488) fluorophore were attached to the 3' and 5' of the aptamer, and then polyacrylamide nanoparticles were prepared in the presence of the aptamer switch probe [5]. These nanoparticle were inserted into yeast cells using electroporation; a short high voltage pulses to conquer the plasma membrane barrier [366].

Since the sensors were not specific for ATP, and the binding of ADP was lower than ATP, the change in the fluorescence from Texas Red was measured (605 nm); the fluorescence from Alexa Flour 488 was measured at 520 nm. The fluorescence signals of AF488 was normalized by the fluorescence signals of Texas Red as given by the equation,

$$\Phi_A = \frac{F_{520}}{F_{605}} - 1. \tag{3.7}$$

The ATP concentration can be calculated from equation 3.8 results from the curve

fitting of the data to a three-parameter sigmoidal form [5],

$$\Phi_{\text{measured}} = \frac{2.27}{1 + exp(-\frac{[ATP]-3.22\text{mM}}{1.45\text{mM}})} + \frac{1.55}{1 + exp(-\frac{([A]_0-[ATP])-4.37\text{mM}}{1.85\text{mM}})}, \quad (3.8)$$

where $[A]_0$ represent the total concentration of ATP and ADP which was considered to be fixed to 2.5 mM [5]. This method suffers from a drawback due to the accuracy of the sensor to ATP concentrations. The accuracy of the sensor is low at lower concentrations of ATP than at higher concentrations. But, the sensor can measure changes in readings that reaches less one second.

3.2.4 Measurements of MMP

Mitochondrial membrane potential measurements were done using an extrinsic fluorophore, the potential-dependent DiOC2(3), using a QE65000 spectrometer fitted with temperature cuvette holder [4]. The DiOC2(3) fluorophore was excited using an Edmund Optics interference filter at 500/24 nm wavelengths, and the emission was measured as the average intensity from the suspension of yeast cells in the range 580-620 nm or as the average of the intensity in the range 530-550 nm. These ranges have no influences from NADH fluorescence.

3.2.5 Measurements of cytosolic pH

Measurements of the cytosolic pH in a glycolytically oscillating suspension of yeast cells were described in [367]. Briefly, a 3 μL of 4.5 mM 5- (and 6-) carboxylfluorescein diacetate succinimidyl ester (CFSE) in dimethyl sulfoxide was added to 2 mL suspension of yeast cells (10% wet weight). The mixture of the suspension was stored at 40 ^{0}C for 20 min, and then centrifuged at 7000 X g for 3 min. The resulting pellet was suspended in 100 mM phosphate buffer, pH 6.8, and stored at 4 ^{0}C until use.

The value of the cytosolic pH was measured as the ratio of the emission at

520/1 nm, using excitations of 490/3 nm and 435/3 nm, respectively. To calculate the value of pH from the ratio measured, a calibration curve was constructed by permeabilizing the cells with 70% ethanol for 30 min at 30 ^{0}C [367]. Then the permeabilized cells were resuspended in a citric acid/Na^+ phosphate buffet at pH values ranging from 5.5 to 8.5 and CFSE. The data were fitted to Henderson-Hasselbalch type equation [368, 369],

$$R_{490/435} = 2 + \frac{10^{(\mathrm{pH}-7)}}{1 + 10^{(\mathrm{pH}-7)}}, \tag{3.9}$$

the number 2 represents the ratio (R) limit at low pH values.

3.2.6 Preparation of yeast cells

Yeast cells, S. cerevisiae diploid strain X2180, were grown and harvested as described in [30]. The cells were starved at room temperature for 3 h in 100 mM sodium phosphate buffer, pH 6.8, before use. Cells were suspended in phosphate buffer, pH 6.8, except for measurements of cytosolic pH.

The yeast cells (Saccharomyces cerevisiae X2180) were harvested at the diauxic shift, washed, starved, and kept cold (2–4°C) in a phosphate buffer at pH 6.8 as previously described [328, 370]. A diauxic shift can be monitored by the measurements of glucose level in the medium. When glucose is absent the diauxic shift is reached to be sure that cells are not using glucose from internal pool through the experiment. The shift in metabolism from aerobic to anaerobic is important in initiation of glycolytic oscillations.

3.3 Summary

This chapter introduces the methods used to do the measurements of the data in this thesis and show how cells were prepared for each measurement. Due to

limitations in the whole-cell patch-clamp protocols, the pipette solution was not changed within the experiment while the extracellular solution was changed once. In addition, the measurements of the fluorescence of each of NADH, pH, ATP, and the mitochondrial membrane potential were done for two of them simultaneously due to limitations in the devices used in the measurements.

The data result from these measurements require convenient methods for analysis. These methods are discussed in the next chapter.

Chapter 4

Analysis of dynamical systems

In physics, any phenomena or some variables evolving in time can be termed as a dynamical system. Since most natural phenomena are evolving in time, it is of great interest to study these systems. Biological living systems are the best examples of systems that progress in time. Due to their openness, living systems exchange mass and energy with the surroundings, and therefore, represent non-linear dissipative dynamical systems. In other words, living systems are usually kept away from thermodynamical equilibrium and belong to a broader class of self organizing [371].

This chapter comprises four main sections. Section 4.1 presents theoretical background of dynamical systems. Section 4.2 reviews the inverse approach to dynamical systems. Statistical tests are described in section 4.3, and finally, the inverse approach methods are applied to numerical simulations are introduced in section 4.4.

4.1 Introduction

If we define a system by x, then a dynamical system describes the change in x over time as given by the equation:

$$\frac{\mathrm{d}x}{\mathrm{d}t} = f(x), \tag{4.1}$$

where f is some function acting on the previous state of x and f describes the infinitesimal change in the state x in an infinitesimal time interval t. Equation 4.1 describes the progress of systems in cases of the continuous time. Iterated maps may be used when dealing with system progressing in discrete time [372]. In this thesis, only continuous time and, therefore, differential equations are taken into consideration. In living systems, the system explicitly depends on time and this is known as nonautonomous, and the simplest case can be described mathematically by the differential equation:

$$\frac{\mathrm{d}x}{\mathrm{d}t} = f(x, t). \tag{4.2}$$

Dynamical systems can be categorized into linear and nonlinear systems. Linear dynamical systems are completely solvable, therefore, exhibit simpler features and properties than the nonlinear dynamical systems. In linear systems, the evolution of the output is proportional to the evolution of the input, but in nonlinear dynamical systems, this proportionality does not exist. A clear majority of living systems are nonlinearly dynamical [373], making them difficult to be solved or analyzed, but very interesting. Nonlinear dynamical systems may manifest self-sustained oscillations which may be represented, in the phase space of the system, by a stable limit cycle. A limit cycle is defined by an isolated closed trajectory with neighboring trajectories are not closed, but instead, spiral either away if it is unstable or towards the limit cycle if stable; in the latter case, the limit cycle is said to be an attractor. Stable limit cycles are scientifically very important since they model systems' oscillations even without external periodic forcing. Examples of self-sustained oscillations are the beating of a heart; daily rhythms in human

body temperature, the periodic firing of a pacemaker neuron, and hormone secretion. Slightly perturbing the system will result in a return to the standard cycle due to the stability of the system [372]. Deterministic models' considerations are of vast importance in biological oscillations dynamics.

4.2 Inverse approach to dynamical systems

A vast collection of biological systems' properties is explicitly time-dependent [374]. Therefore, these properties are considered as non-autonomous systems. Due to the difficulties in the analysis of non-autonomous systems, many ineffective methods suited to autonomous systems were applied to them. One of these methods is the reconstruction of the attractor in phase space. This method works well for systems that do not explicitly depend on time but does not consider time-varying attractors [375]. To solve the problem of time-dependence of these systems, extra dimensions in phase space is required to incorporate time-dependency into the phase space, but this method introduces more unnecessary complexity to the system.

Dynamical systems can be tackled using the inverse problems approach in two ways: making direct measurements from the system itself or modeling the system in a set of differential equations. Both approaches are useful in understanding the features of the system. The only difference is the source of limitations; in the first approach, the source of limitation is the data while in the second the limitation appears from approximation and simplification of the model.

Non-autonomous systems are time-varying, therefore, signal analysis methods that assume stationarity are not valid to be used with these systems. Nonstationarity is a feature that defines a complex time series. Statistically, nonstationarity exhibited as a change either in the time series mean or variance or both [376]. One of the common methods of visualizing the dynamical properties of a time series is to represent its frequency spectrum. The discrete Fourier transform (DFT) is

one of the earliest methods applied to analyse time series. This method appears first in 1805 in the work of Carl Friedrich, when he tried to determine the orbits of asteroids by analysing data of their locations [377]. Application of the DFT to nonstationary time series will produce blurred or misleading power spectra, as will be seen later in this chapter (section 4.4), this will indeed limit its usefulness. Windowing approaches like windowed Fourier transform (WFT) and wavelet transform (WT), proved a success when applied to time series analysis. The former exhibits limitations due to the fixed window size that badly limits the usefulness of the method in the analysis of slow oscillations, while the later form a solution of that limitation by introducing an adapting window size [378]. The simultaneous visualization of the time-frequency representations of data is extremely useful in observing the dynamical features of the system and their time evolution.

As a result, progress in development of wavelet based methods for the treatment of nonautonomous dynamics is now very active [7], including finding harmonics [379], extracting modes [380], wavelet phase coherence [381], wavelet bispectrum [382] and Bayesian inference [383].

4.2.1 Time-domain

Data measured from living systems can be represented in time-domain as a starting point. But, the dynamical features of nonautonomous systems are faded inside the data and cannot be easily visualized in time-domain representations. Therefore, other methods are required to observe the dynamics characterized by the time variability of the amplitudes and frequencies of modes present in the time series. Before using other ways of representation, pre-processing of the time series is required to provide optimal conditions for analysis. In time series recorded from biological systems, artefacts may appear due to movements, missed measurements, or any non-physical influence. If the duration of these artefacts is much shorter than the frequency range of interest, linear modulation can be applied to remove

them from the data. But, if their duration is long relative to the frequencies of interest and they are close to either end, then they should be cut from the data.

Detrending of the data to remove trends and effects of slower frequencies than frequencies under study is another thing to be considered in pre-processing. This can be carried out using a moving average method, in which a window moved along the signal. This window has a defined width in time when moved along the data, the central value is set to the mean of that window. This method is usually used to smooth signals, depending on the size of the window used with the data. It is usually necessary to subtract the average of the data when doing frequency, or time-frequency analysis. As an example, a window of size 50 sec is used to remove frequencies lower than 0.02 Hz.

4.2.2 Frequency-domain

Any data measured as a time series can be represented in both time domain and frequency domain. In the former, the data represents a function of time (in seconds); $F(t)$, while in the later the data will be represented as the distribution of the dynamics of the system on the frequency domain. The maximum frequency observed in the signal equals half the sampling frequency (f_s) used to measure the data, defined as the Nyquist frequency. And the time between two consequent measurements is equal to the reciprocal of the sampling frequency, $\Delta t = 1/f_s$. The lowest observable frequency depends on the length of the data (L); $fmin = 1/L$. Therefore, the data must be longer than one period of oscillations and one also cannot distinguish between two oscillations if the difference in their frequencies less than fmin. Practically, the reliable minimum frequency in data from biological systems is defined to be as $1/5L$ [384].

One of the common methods of visualizing the dynamics of a signal is by representing it in the frequency domain to observe the frequency spectrum. This way, one can observe how oscillations and fluctuations in the signal are distributed

over different wavelengths.

The discrete Fourier transform (DFT) is one of the earliest methods applied to analyze signals. To understand this method, it is better to consider first the Fourier series. A Fourier series of a periodic function can be expressed as an infinite series of sines and cosines,

$$F(t) = a_0 + \sum_{w=1}^{\infty} [a_w \cos(wt) + b_w \sin(wt)], \tag{4.3}$$

where ω represents the angular frequency and a_0, a_w, and b_w are constants known as Fourier coefficients. The values of these coefficients depend on the shape of the function, $F(t)$, with the largest values corresponds to components (modes) in the signal that have stationary frequencies.

Signals of variables measured from living systems usually involve discrete sampling. For the basis described above, the DFT of a signal $F(n)$ can be defined as:

$$F(w) = \sum_{n=0}^{N-1} F(n) e^{-\frac{2\pi i w n}{N}}. \tag{4.4}$$

This equation can transform a signal from time domain to frequency domain representations, which means that periodic terms in the signal will appear as peaks in the frequency domain at the corresponding frequencies. The Fourier transform is symmetric in the range $0 \leq w \leq N-1$, for real-valued signals the transform is reflected in the point $w = N/2$, with coefficients correspond to positive frequencies for $w < N/2$ and the negative frequencies coefficients correspond to $w > N/2$. Therefore, the negative-frequency coefficients are usually not represented in the final plot.

One of the limitations in this method is that Fourier transform assumes that the time series on which it is performed is stationary, i.e. that the frequency and amplitude of the modes do not vary with time. But, in signals recorded from living systems, there is some degree of time variance. Other limitations in Fourier

transform will be shown at the end of this chapter with implementations of the methods using simulated signals.

4.2.3 Time-frequency analysis

Windowed Fourier transform

The Windowed Fourier transform (WFT) or Short Time Fourier Transform (STFT) was developed to overcome the limitations in the Fourier transform when dealing with nonstationary signals [378]. This was done by producing time-frequency representations of signals.

The WFT works in an intuitive way by dividing the signal into equal parts 'windows' within which the signal can be treated as a stationary one. Then, the Fourier transform (FFT) is calculated for each window, and the value in the middle of the window in the WFT representation set to the resultant FFT values.

The WFT method still has its limitations. The window size is constant when dealing with fast or slow oscillations. The size of the window is determined by the user and depend on whether the user requires good frequency resolution or good time resolution, therefore, one cannot get both simultaneously [378]. Also, the frequency resolution is linear in the WFT, which means that it performs poorly in resolving separate low-frequency oscillatory components in the signal.

Continuous wavelet transform

Due to the limitations in WFT, a solution to the fixed window size was required. The optimal solution to that limitation is wavelet transform (WT), which allows the window size to change inversely with the frequencies in the data; the size of the window is wide when dealing with very slow oscillations and a small window size when dealing with very fast oscillations, which is known as an adaptive window. If the process is accomplished in discrete steps, it is known as the discrete

wavelet transform (DWT). In this method, the window is applied to the signal parts without overlap between frequency bands. If continuous steps are carried out, it is known continuous wavelet transform (CWT).

The CWT is given by [385],

$$W_T(s,t) = \frac{1}{\sqrt{s}} \int_{-\frac{L}{2}}^{\frac{L}{2}} \Psi(s, u-t) f(u) du, \tag{4.5}$$

where $\Psi(s,t)$ is the mother wavelet (a basis of the CWT method), s is a scaling parameter to change the wavelet frequency distribution and shifting its time according to t. The frequency scale in CWT is continuous, therefore for any arbitrary frequency, the wavelet components can be calculated.

The wavelet transforms (WT) performs calculations using a new wavelet and window size, exploiting the scaling factor and the time shifting to calculate each scale. A small window (wavelet) is used for fast oscillations (high frequencies) and larger ones for slow oscillations (low frequencies). Hence, the time resolution at high frequency is not limited by the large window required for detecting low frequencies.

The calculation of WT can be achieved by a moving adaptive window along with all locations of the signal. For each location, a complete range of scales of the wavelet (huge number of wavelet basis) is used and is adaptive to the range of the frequencies to be investigated.

If there is a good match between the wavelet basis used and the data, the value obtained from their convolution will be large. In this way, a time-frequency representation of the whole signal can be generated by plotting time, frequency and amplitude on a three-dimensional graph (see examples later in section 4.4).

The wavelet power spectrum can be found by calculating the integration of

the square of the wavelet transform modulus over frequency [7, 385]

$$P_W(w,t) = \int_{w-\frac{dw}{2}}^{w+\frac{dw}{2}} |W_T(w,t)|^2 dw, \tag{4.6}$$

this will produce a vector representing the power of the whole-time series, which can be plotted versus frequency to be used to compare power spectra between different signals. This provides a good starting point in the analysis since it can be used to identify the frequency range of the main oscillatory components in the signal under investigations.

Wavelet types

There are many wavelet forms, each has its properties and applications. Complex wavelets, i.e. Morlet wavelet, are useful, they allow the separation of the phase and amplitude components of the transformed signal. In this thesis, the Morlet wavelet was used in all analyses. The Morlet wavelet, which is closest to the Fourier basis, is a complex wave within a Gaussian envelope that has a unit standard deviation

$$\Psi(s,t) = \frac{1}{\sqrt[4]{\pi}}(e^{\frac{2\pi i w_c t}{s}} - e^{\frac{2\pi {w_c}^2}{2}})e^{-\frac{t^2}{2s^2}}, \tag{4.7}$$

where $s = w_c/w$. The parameter w_c is the central frequency, which determines the trade-off between time and frequency resolution in the wavelet coefficients calculated from the signal under study; values higher than $w_c = 2$ give good frequency but poor time resolution while values below $w_c = 1$ give poor frequency but good time resolution. At very small values, which is less than $w_c = 0.2$, the wavelet becomes meaningless.

The coefficients obtained from wavelet transform using morlet are complex numbers, which define the amplitude and instantaneous phase for each frequency and time [386].

The signals obtained from real systems have finite lengths, while CWT inte-

grates over infinite time. Therefore, the wavelet transform at the boarders becomes ill-defined close to $t = 0$ or when t approaches the end of the signal. This limitation was solved by signal padding; made longer at both ends during wavelet transform, and then the added regions are removed to retain only the original period. Several types of padding regimes are available, i.e. zero padding, periodic padding and predictive padding [8]. When the wavelet transform is running at the boarders of original signals, a boundary effect is still observed even after padding. The portion of the wavelet transform which is not affected is known as the cone-of-influence.

Mode-extraction

The best in time-frequency representation of signals is proved to be the morlet wavelet transform which can be used to track the time variability of oscillations. Since wavelet transform is still a linear method it inherits the problem of generating harmonics when nonlinear oscillations are represented using wavelets.

Identifying the harmonics generated by time-frequency representation on non-linear oscillations makes it possible to separate modes in the time domain and even reconstruct them. This can be achieved using the time-dependent phase information of the modes,

$$\phi(s,t) = arg[W_T(s,t)]. \tag{4.8}$$

If the shape of the waveform of the oscillation is the same during the whole signal, the phases of the harmonics of this mode will share the same dynamics. The relation between the two modes can be defined as,

$$\phi(s_1,t) = \frac{s_1}{s_2}\phi(s_2,t), \tag{4.9}$$

where s_1 and s_2 are the scales of these two harmonics.

Wavelet method can be used to separate the modes of the signal from the noise

by distinguishing between the noise fluctuations for the harmonics from the noise fluctuations for the fundamental mode if they are different, the real dynamics of the mode can be separated from the noise. Another method based on ridge extraction is known as nonlinear mode decomposition. Information from the harmonics is used in this method to improve the mode extraction [8, 380]. In ridge extraction, by tracing the time variability of the highest peak over a defined frequency range in the wavelet transform, the main mode can be extracted and subtracted from the signal. Then the algorithm is repeated for the highest peak remaining in the signal after removal of the main mode. The algorithm looks at both the phase and amplitude variations of several oscillations to distinguish harmonics, which share the same dynamics, from other modes that do not share dynamics with the main mode (genuine modes).

Harmonics detection

Since CWT inherits the problem of high harmonics caused by nonlinearity and the wavelet transform obtains time-dependent phase information, it is possible to detect relations between oscillations and identify the harmonics of any mode in the signal [379, 7]. The method introduced by Sheppard et al [379] enables distinguishing genuine modes from harmonics of nonsinusoidal oscillations. This method based on the mutual information between harmonics that share the same dynamics and surrogate testing. The wavelet transform is used to trace the time variability of the modes and the harmonics exist in the signal. Harmonic detection can provide information about the underlying physiology of the system under investigation and can show the level of nonlinearity in the response of the system.

The mutual information is related directly to entropy. It is a measure of the missing entropy from a conditional distribution while considering information about another variable. The Shannon entropy is a measure of unpredictability (see [379] and references therein). If the distribution is uniform then it has high

entropy, whereas sharply peaked distributions have low entropy.

Wavelet transforms were introduced to determine the phase at each point in time of each frequency in data. The phases were divided into 24 bins, the mutual information is calculated for each possible pair of the signal phases. To check for significant cross-correlations between the pairs surrogates were used (see section 4.3 [379].

The entropy of the 24 phases discretized is given by,

$$H(\phi_1) = -\sum_{\phi_1=1}^{24} p(\phi_1)\log_2(\phi_1). \tag{4.10}$$

And the mean entropy of the conditional distribution is calculated using the equation,

$$H(\phi_1||\phi_2) = -\sum_{\phi_1=1}^{24} p(\phi_2)\sum_{\phi_1=1}^{24} p(\phi_1||\phi_2)\log_2 p(\phi_1||\phi_2). \tag{4.11}$$

The mutual information of the signal is given by the difference between equation 4.10 and equation 4.11,

$$M(\phi_1,\phi_2) = H(\phi_1) - H(\phi_1||\phi_2). \tag{4.12}$$

The proportion of the mutual information of two phases approaches 1 when the two frequencies of the phases are approaching each other [379]. Since the mutual information calculated between pairs of phases is biased by the correlations exist in short phase signals caused by binning, surrogates testing is required.

4.2.4 Interactions

Wavelet phase coherence

Synchronization is a phenomenon observed in interacting systems. It is a good indicator of interaction and does not necessarily happen with system coupling.

This phenomenon refers to when the phases or amplitudes of two oscillators remain in a fixed relationship due to their weak interaction [387]. Oscillators can be phase synchronized, phase and amplitude synchronized or generalized synchronized and they may have n:m synchronization relation, which means that there are n cycles of one oscillator in m cycles of the other. Phase coherence is a special case of phase synchronization where $n = m = 1$, or in other words phase coherence can result in 1:1 phase synchronization. Phase coherence can be defined [379],

$$\Pi(s) = \frac{1}{N} \left| \sum_{n=1}^{N} e^{i\Delta\phi(s,t_n)} \right|, \tag{4.13}$$

where $\Delta\phi(s, t_n) = \phi_1(s, t_n) - \phi_2(s, t_n)$ is the phase difference between the two oscillatory components from two different signals at the same scale s and time t_n.

If the phases of the two oscillations remain locked for all the time, then the oscillations are coherent ($\Pi(s) = 1$), whereas if there is no tendency to have a fixed relationship between the phases then $\Pi(s) = 0$ and the two oscillations are not coherent. Instead of getting a time-independent phase coherence at each frequency, the time variation of phase coherence can be traced by performing the calculations over time using a sliding window along each frequency (or scale). The phase coherence is usually biased towards lower frequencies and this can be accounted for using surrogates of the signals [388, 389] (see later in section 4.3). While the phase coherence is biased towards lower frequencies, the time-localized phase coherence can avoid this problem since the window in wavelet transform is adaptive and can be scaled to always contain the same number of cycles [390].

4.3 Statistical tests

4.3.1 Wilcoxon signed-rank and sum-rank tests

Wavelet transform and windowed Fourier transform enable the calculations of the time-averaged power, which is more physically meaningful than the spectra calculated using the Fourier transform for data from nonautonomous dynamical systems. This enables more meaningful results when using statistical tests to test for statistical hypothesis using Wilcoxon signed-rank (paired) and sum-ranked (unpaired) tests.

If we measured bivariate data (x(t), y(t)) from the same population P and both values have the same units, i.e. millivolts, then the spectra calculated from them can be compared. Assume we want to test for each frequency-value the null hypothesis that the median over P of the signed difference between the spectra of each data measured at each frequency is equal to 0. And if we suppose that the distribution of this signed difference is symmetric about some value then we can use the Wilcoxon signed rank test. In this thesis, this test was used when the resting membrane potential was measured by a group of Jurkat cells then the measurements were repeated by altering the extracellular medium while using the same cells. Both data must be equal in a number of samples and must have the same length and the same sampling frequency. The results were considered significant when $p < 0.05$ [391, 392, 393].

When the measurements of the two-compared data were taken from two different populations, the null hypothesis to test is the median of the time-averaged power at frequency f for the first population is equal to the median of the time-averaged power of the second population. The test applied then is the rank sum test. In this case, the number of samples need not be the same. Again, the results were considered significant when the p-value is <0.05 [391, 392, 394].

4.3.2 Surrogates

Two signals or even two components of one signal may have possible connection generated by the interaction between the processes from which these signals were recorded or may be a common external influence on these processes. Analyzing possible connections can be achieved using methods such as wavelet phase coherence, wavelet bispectrum, and dynamical Bayesian inference. Values produced from these methods to quantify the possible level of connection between processes are of no use unless one can do the same tests when the interaction or the common influence was absent. One way to test for significance of the obtained values from these methods is to use surrogate time series [395].

Also, when detecting for harmonics generated in the time-frequency representation due to nonlinearity using the mutual information between pairs of phases extracted from the data. Surrogate testing is required because the values obtained from mutual information are strongly biased by the correlations present in the relatively short phase data and by the discretization of the phases time series into bins which were used to speed up the computation [379].

In this thesis, surrogates required to test for significance in wavelet phase coherence and harmonic detections are the amplitude adjusted Fourier transform (AAFT) and the iterative amplitude adjusted Fourier transform (IAAFT). The null hypothesis for both is that the phases in the time series are independent for all frequencies, which means that surrogates can be generated by the randomization of the time-phase information [385].

In the case of phase coherence, the baseline for significance detection was the phase coherence calculated between the generated surrogates using IAAFT. While, in harmonics detection, a local maximum in the values of the mutual information calculated for a pair of phases from the original data is deemed to indicate a harmonic if it occurs some number of the standard deviation above the mean

value of the surrogates' mutual information [379].

To test a null hypothesis using surrogates at a level of significance α, $1/(1-\alpha)-1$ surrogates should be generated for a one-sided test, and $2/(1-\alpha)-1$ surrogates for the two-sided test. Comparing the value of the static from the data under study with the distribution of the values computed from the surrogates, the null hypothesis may be rejected when the data deviates from the surrogates. Otherwise, it may not [396, 397]. To increase discrimination power, one may use more surrogates. AAFT and IAAFT are the most commonly used surrogates. Both conserve the amplitude distribution (AD) in real space and the power spectrum (PS) of the original signal. In both, the basic assumption is that higher-order correlations can be destroyed by randomization of Fourier phases in time while preserving the linear correlations [398].

AAFT algorithm:

- Sort the original data Sort $(x(1:N))$.
- Compute the Fourier transform of the original data $z(\mathrm{n}) = fft(x(\mathrm{t}))$.
- Generate a ranked time series from the original data $r(x(\mathrm{t}))$ that satisfies sort $x(r(x(\mathrm{t}))) = x(\mathrm{t})$.
- Create a random data set $g(\mathrm{t})$ with the same length as the original data.
- Sort $g(\mathrm{t})$.
- Define a new time series $y(\mathrm{t}) = sortg(r(x(\mathrm{t})))$.
- Generate a surrogate $y'(\mathrm{t})$ by randomisation of the phases. Then taking the inverse Fourier transform.
- Make a ranked time series from y'; $r(y'(\mathrm{t}))$.
- The surrogate of $x(\mathrm{t})$ is given by $x'(\mathrm{t}) = \mathrm{sort}x(r(y'(\mathrm{t})))$. In the final time series, the amplitude of the original time series was preserved and the spectrum while the phases were randomized.

IAAFT is an iterative procedure of the AAFT version to preserve the histogram of the data in addition to AAFT preserved linear correlations.

4.4 Implementation of analysis using simulated examples

4.4.1 Time-representation

When analyzing any signal, one starts by representing the data using time-domain representation. The output of this representation may show complexity in the signal, oscillations if present and trends. But, separation of oscillating modes from these results cannot be easily achieved. Three examples of different simulated systems are shown in figure 4.1. From this figure, one can observe the shape of waves obtained from these systems.

The systems in figure 4.1 are given by:
Example (1):A square wave with a modulated frequency defined by the equation,

$$x = sgn(\sin(2\pi ft + \frac{a_m}{f_m}\sin(2\pi f_m t))), \tag{4.14}$$

where f=0.5 Hz, $a_m = 0.1$, $f_m = 0.008$ and the sampling frequency is 200 Hz.

Example (2): The sum of two sine waves with modulated frequencies defined as,

$$x = \sin(2\pi f_1 t + \frac{a_m}{f_m}\sin(2\pi f_m t)) + \sin(2\pi f_2 t + \frac{a_m}{f_m}\sin(2\pi f_m t)), \tag{4.15}$$

where f_1 =0.7 Hz, f_2= 1.0 Hz, a_m=0.1, f_m=0.008 and the sampling frequency is 200 Hz.

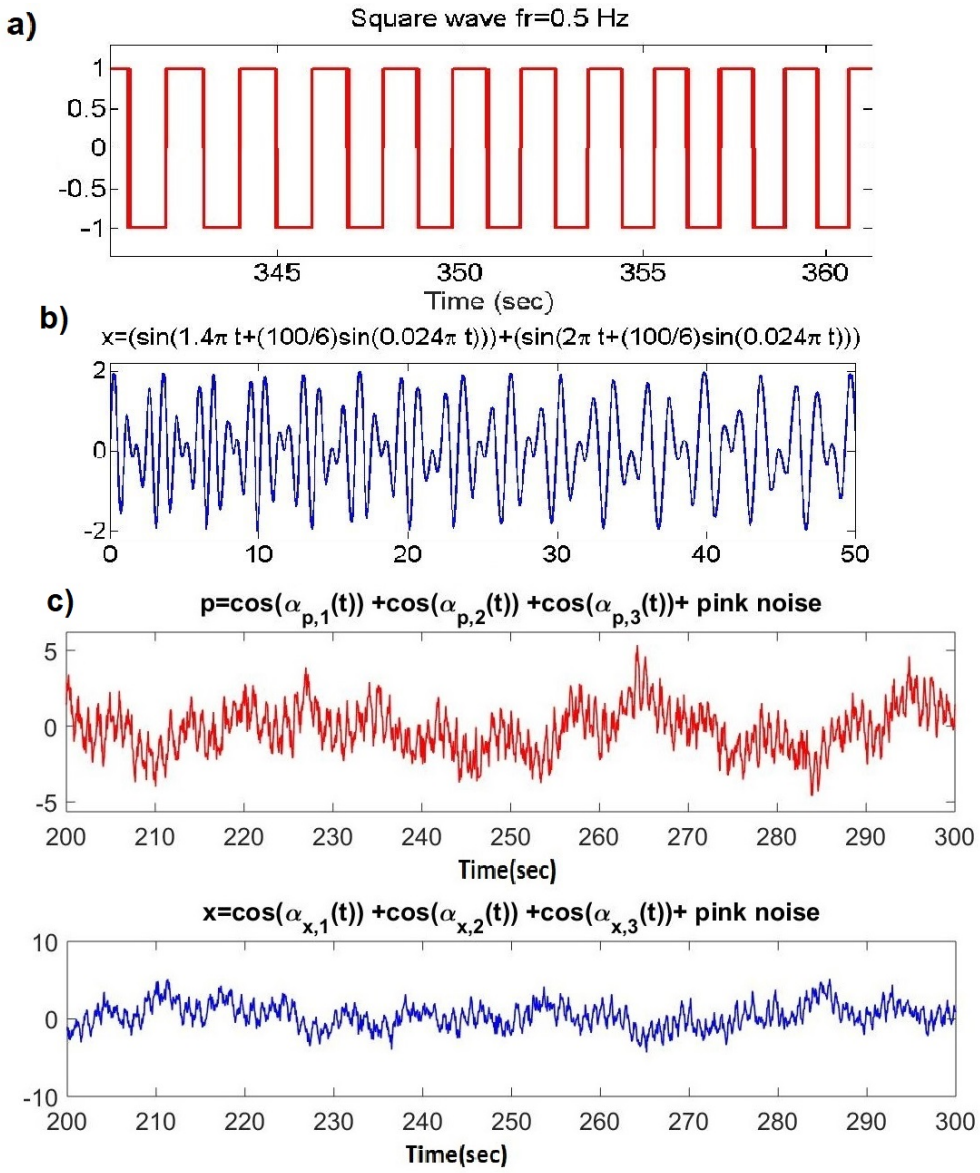

Figure 4.1: Three simulated examples represented in time scale, a) square wave, b) the sum of two sine waves with a modulated frequencies, and c) Two interacting systems; up is the driver and down is the driven system, each one contains three oscillating modes. The sampling frequency is 200 Hz in a and b, while in c it is 20 Hz. Pink noise is a random noise having equal energy per octave, and so having more low-frequency components than white noise. Or a process with a frequency spectrum such that the power spectral density (energy or power per frequency interval) is inversely proportional to the frequency of the signal. Pink noise is the most common signal in biological systems [399].

Example (3): Two interacting systems; x(t) is driven by y(t),

$$y(t) = \sum_{i=1}^{3} \cos(\alpha_{yi}(t)) + pinknoise, \tag{4.16}$$

where $\alpha_{yi}(t)$ is given by,

$$\frac{d\alpha_{yi}}{dt} = \omega_{0i}, \tag{4.17}$$

and

$$x(t) = \sum_{i=1}^{3} \cos(\alpha_{xi}(t)) + pinknoise, \tag{4.18}$$

where $\alpha_{xi}(t)$ is given by,

$$\frac{d\alpha_{xi}}{dt} = \epsilon\omega_{0i} \sin(\alpha_{xi}(t) - \alpha_{yi}(t)) + \eta(t), \tag{4.19}$$

where ϵ=1.5, η is a white Gaussian noise with strength=0.2 and standard deviation= $\sqrt{2E}$ and ω_{0i} is defined as

$$\omega_{0i} = \omega_{1i} + A_i \sin(\omega_{2i}t), \tag{4.20}$$

and $\omega_{1i} = 2\pi f_{1i}$, $\omega_{2i} = 2\pi f_{2i}$, the sampling frequency is 20Hz and other parameters are listed in table

Table 4.1: Parameters of example (3); $(.)_i$: represents A_i, f_{1i} or f_{2i}

Parameter	$(.)_1$	$(.)_2$	$(.)_3$
A	1	0.15	0.025
f_1 (Hz)	1.5	0.25	0.05
f_2 (Hz)	0.008	0.0025	0.0005

4.4.2 Frequency-representations

Frequency domain analysis is another choice to be used in analysing data, using Fourier transform. As mentioned before, this method assumes stationarity of signals. Therefore, this method may be a misleading way in interpreting the spectrum

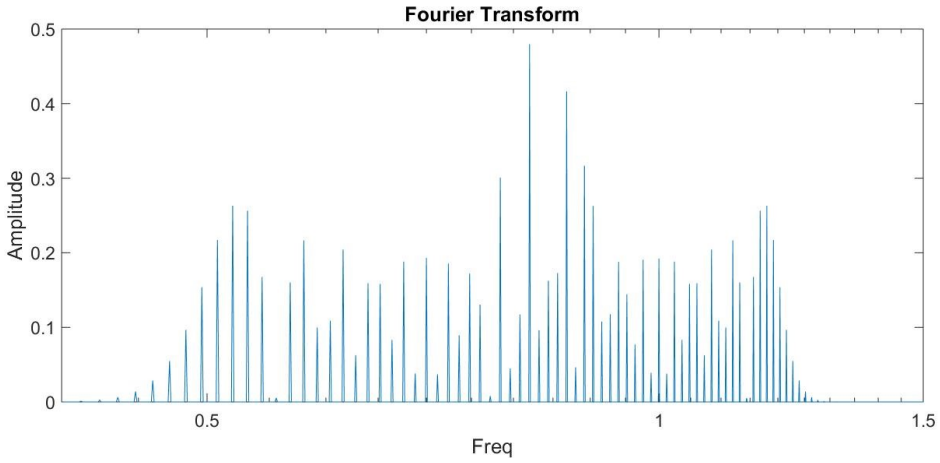

Figure 4.2: The Fourier transform of example 2 given in equation 4.15; the region shown is only the one contains components of the transformed signal. The sampling frequency is 200 Hz. The original signal contains two modes with frequencies 0.7 and 1 HZ.

produced from data using this method. Figure 4.2 show the Fourier transform of system 2. The spectrum does not appear to represent a signal that composed of only two components. Time-frequency representation show a better representation of non-stationary signals.

4.4.3 Time-frequency representations

Due to the openness of living systems, the data recorded result in time evolving amplitudes and frequencies of oscillations. Therefore, using Fourier transform will result in a misleading interpretation of these systems (see figure 4.2). The introduction of time-frequency analysis solved that problem, allowing the representation of the full dynamics of the oscillatory components present in living systems. Figure 4.3 shows the time-frequency representation of example 2. Comparing the results from Fourier transform and the time-frequency representation using WT and WFT show how the Fourier transform was a misleading result which may result in wrong interpretations of the data. As observed in figure 4.3, time-frequency representations show an optimal analysis of the signal by obtaining two components around 1 Hz and 0.7 Hz.

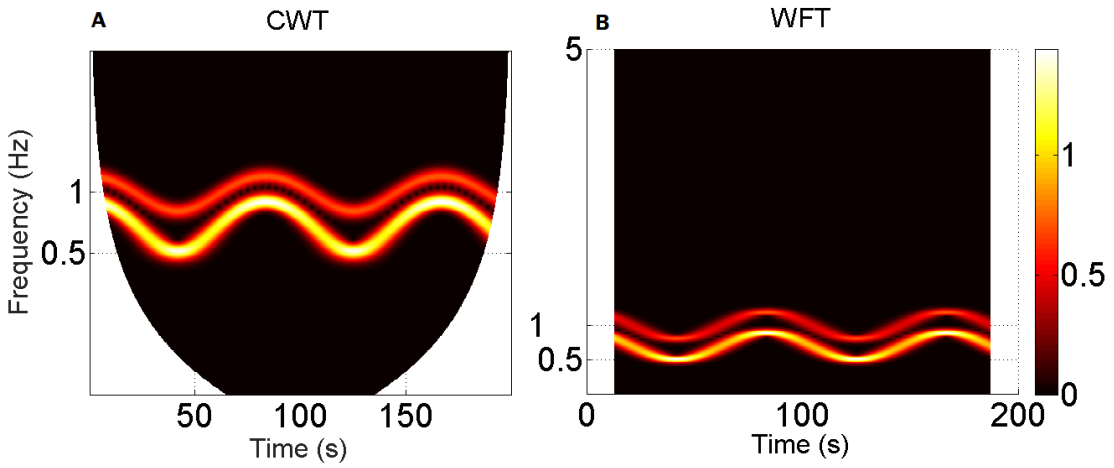

Figure 4.3: The time-frequency representation of example 2 given in equation 4.15; A) continuous wavelet transform, optimal central frequency=2, and B) windowed Fourier transform representation, window size=50 sec. The sampling frequency is 200 Hz, the frequencies of the main modes are 0.7 and 1 Hz.

WFT and WT, mentioned before, are two methods which can be used to represent signals in time-frequency space. The main difference between these two methods is the size of the window used in representations. In WFT, the size of the window is fixed which form a drawback in good resolution for both time and frequency at different frequency levels. In contrast, the window size in WT is inversely proportional to the frequency of the mode analysed; at low frequencies, the window size is big while at high frequencies it is smaller, therefore this window is adapted to the components present in the signal. In figure 4.4, it is observed from the representation that WFT resolution at low frequency has a poor frequency resolution with smaller window size (50 sec); the method cannot separate the lowest two modes, while the resolution increases when the size of the window increases to 250 sec. Unfortunately, increasing the frequency resolution, by increasing the window size, results in poor time resolution (see figure 4.4 a and b).

Figure 4.4 (c, d) show how the WT is better to represent the dynamics of modes from example 3; all modes were separated exploiting the logarithmic scale of the frequency. The time-frequency representation of data can show details of high harmonics due to nonlinearity as seen in figure 4.5. Square wave with 0.5 Hz

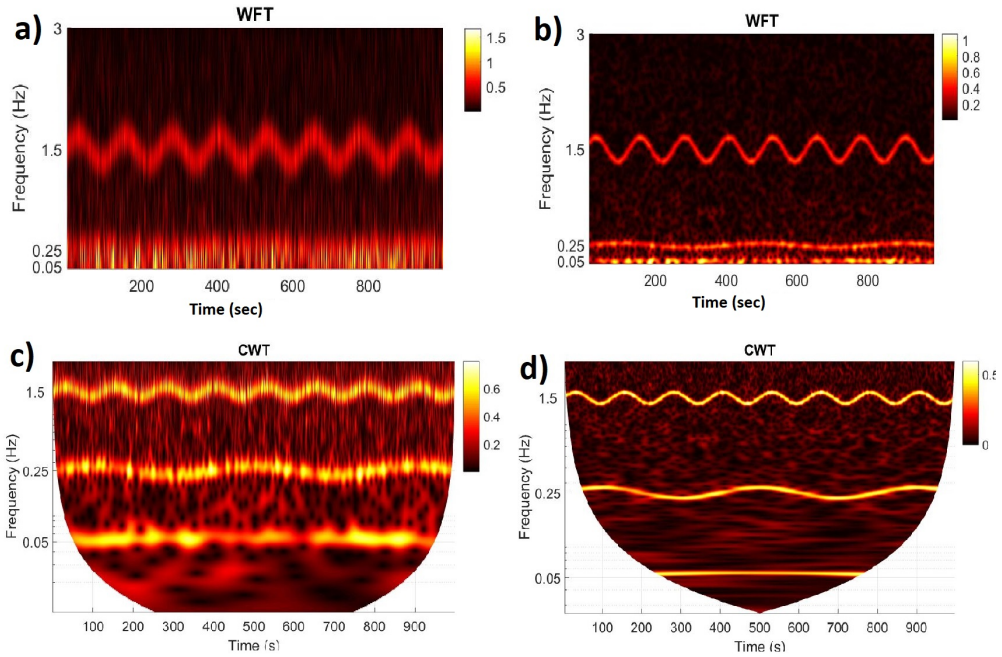

Figure 4.4: The time-frequency representation of example 3 given in equation 4.16; Windowed Fourier transform representation with window size = 50 sec in (a), and 250 sec in (b). Continuous wavelet transform (c) with central frequency (f_0)=1, and d) f_0 =5. The sampling frequency is 20 Hz. The frequencies of the main modes are 0.05, 0.25 and 1.5 Hz.

frequency show many high harmonics when represented using wavelet transform (WT) or windowed Fourier transform (WFT).

4.4.4 Harmonic detection

As mentioned before, the time-frequency representation with mutual information between the pairs of phase data extracted from WT, the higher harmonics brought about by nonlinearity can be distinguished from independent modes. AAFT surrogates were used to detect significance in harmonic detection. Figure 4.6 show the mutual information M(ϕ_1, ϕ_2) relative to the surrogate distribution. Regions more than 5σ above the 500 surrogate mean are remarked with blue, and local maxima are marked with +. The data is simulated from example (1), a square wave defined by the equation 4.14. The main component in the signal is around 0.5 Hz, while other peaks appear at higher harmonics.

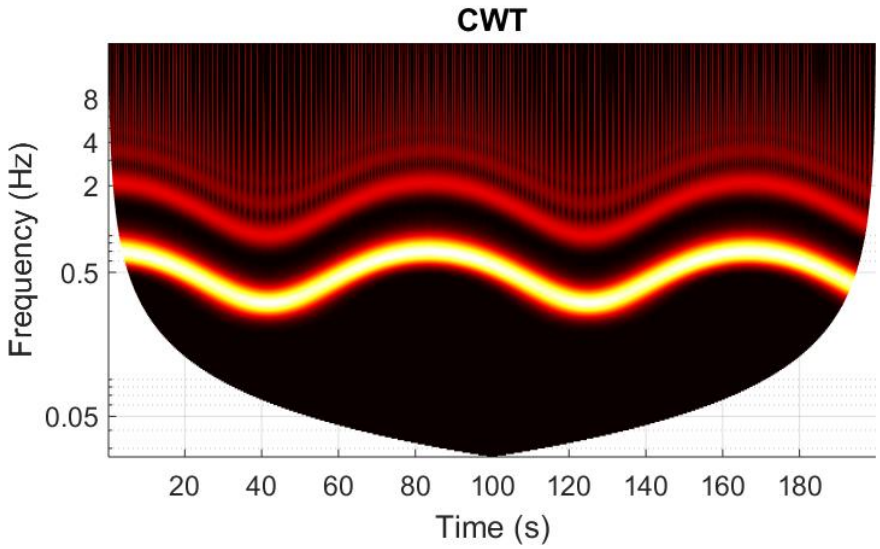

Figure 4.5: The time-frequency representation (continuous wavelet transform CWT) of example 1 given in equation 4.14; several high harmonics appear in the representation due to nonlinearity in the data; the range of frequency plotted is (0.01-20 Hz), the sampling frequency is 200 Hz and the central frequency is 1 Hz. The signal contains only one mode with frequency 0.5 Hz.

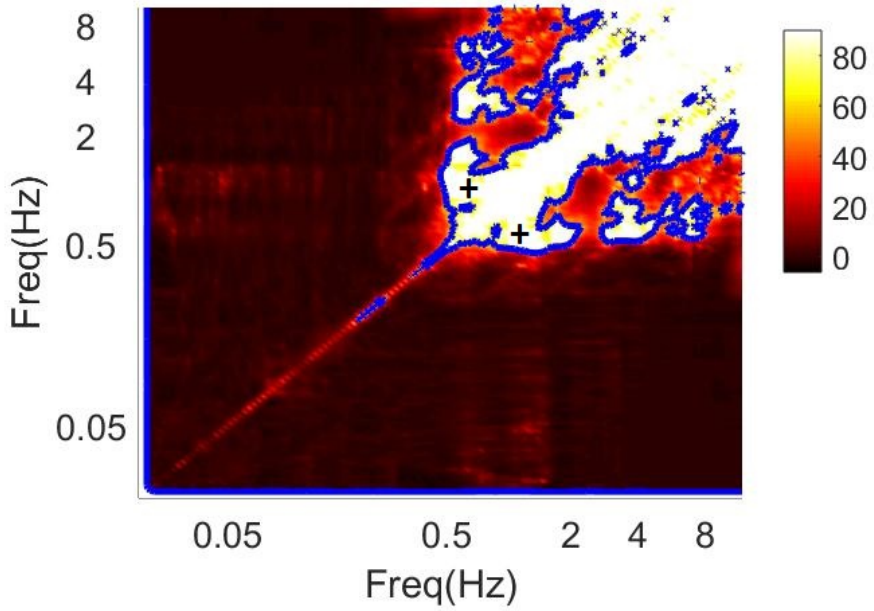

Figure 4.6: The mutual information $M(\phi_1, \phi_2)$ relative to the surrogate distribution. Regions more than 5σ above the 500 surrogate mean are remarked with blue, and local maxima are marked with +. The data is simulated from example 1 given in equation 4.14; several high harmonics appear in the representation due to nonlinearity in the data. The central frequency used in calculations is 1.

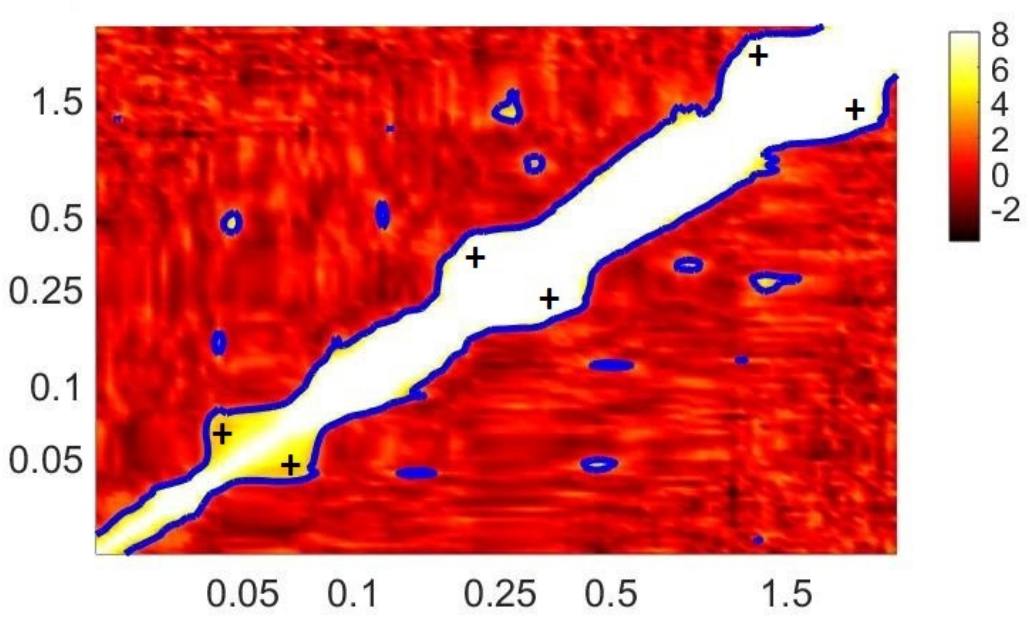

Figure 4.7: The mutual information $M(\phi_1, \phi_2)$ relative to the surrogate distribution. Regions more than 5σ above the 500 surrogate mean are remarked with blue, and local maxima are marked with +. The data is simulated from x(t) given in equation 4.16. The sampling frequency is 20 Hz and the central frequency is 1.

In figure 4.7, the harmonics produced from example 3 data are shown and can be distinguished easily from the main components. The data is simulated from x(t) given in equation 4.16. As shown, the mutual information $M(\phi_1, \phi_2)$ relative to the surrogate distribution is plotted. Regions more than 5σ above the 500 surrogate mean are remarked with blue, and local maxima are marked with +. The main components appear at 0.05, 0.25 and 1.5 Hz, while higher harmonics correlated to each component appear in blue circles on the line approximately perpendicular to the axes at that frequency.

4.4.5 Interactions: phase coupling

In example 3, bivariate data is simulated which represent two interacting signals, each of these data contains 3 components. One of these data is driving the another and phase coherence here is used to detect the interactions between these components. The null hypothesis in phase coherence case is that the phases are independent for all frequencies. Therefore, the time-phase information is to be

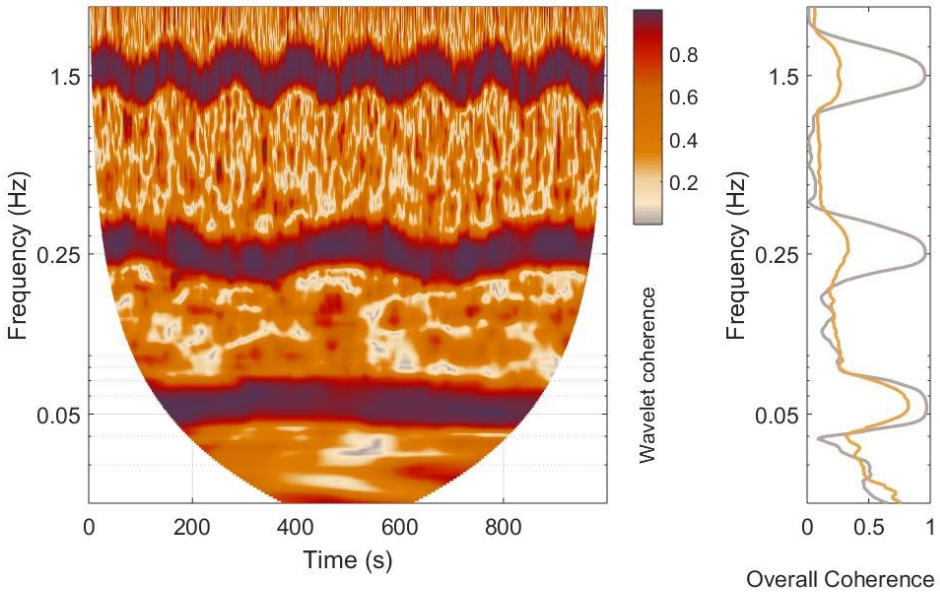

Figure 4.8: Wavelet phase coherence between the time series x(t) and y(t) given by the equations 4.18 and 4.16 respectively. On the right, significant phase coherence is shown when the original data coherence (black line) is greater than 95th percentile of 100 pairs od IAAFT surrogate coherence (red line). On the left, the windowed wavelet phase coherence reveals the time variability of the mode coherence. The central frequency is 2.

randomized in the surrogates. IAAFT surrogates were used to test for significance since these surrogates fit this null hypothesis.

To track time-variation in the calculated phase coherence, this can be achieved using a sliding window along each frequency. Figure 4.8 shows both the phase coherence and the time-averaged wavelet coherence. In both cases, the coherence was significant between the three components of y(t) and x(t) simulated data.

Chapter 5

Analysis and results

This chapter introduces the analysis and results of the data in chapter 3. This chapter is divided into two parts. The first part 5.1 is discussing the analysis of the fluctuations measured in the resting membrane potential of jurkat T cells. The second part 5.2 is discussing the analysis of the oscillations in NADH, ATP, pH, and the mitochondrial membrane potential measured from populations of S. cerevisiae yeast cells.

5.1 Membrane potential

The Resting membrane potential is usually considered to be static. In this chapter, it is shown that resting membrane potential is dynamic. To do this data measured by Shakil Patel [2] is analysed using the techniques discussed previously to investigate the factors that generate the dynamics observed in resting membrane potentials. The results show that these dynamics are created by the fluctuations in membrane conductance (opening and closing of gated ion channels) and due to the change in ions' driving forces that are created due to alteration in the concentration gradients of the permeable ions from physiological values. These fluctuations may convey information within the cell; in processes such as proliferation, motility,

metabolism or cell volume regulation.

The first part of this chapter is structured as follows; section 5.1.1 discusses the fluctuations in the resting membrane potential, the hypotheses and experimental protocols are presented in sections 5.1.2 and 5.1.3 respectively. In section 5.1.5, data analysis is discussed. Section 5.1.6 details the time-averaged wavelet power analysis of the data. Finally, a discussion and summary are presented in sections 5.1.7 and 5.1.8 respectively.

5.1.1 Fluctuations in resting membrane potential

Fluctuations as defined previously are deviations in the value of the membrane potential from a steady state. These dynamics are mainly generated by opening and closing of gated ion channels such as Kv1.3 channel under physiological conditions in Jurkat T lymphocytes [171].

Most previous studies and proposed models assume that under physiological conditions the resting membrane potential is static, see for example [400, 401, 11, 402], which means that all gated ion channels are closed. In this work, we show that, even under physiological conditions, the resting membrane potential fluctuates around a steady state value. As a result, we conclude that part of the gated ion channels is opening and closing under physiological conditions. These gated ion channels differ between different types of cells and even between the three groups of Jurkat cells categorized in this work (see categorization later).

While previous studies show that Jurkat T cell are K^+ dominant, this work shows that there are three different groups of Jurkat T cells categorized with respect to their permeabilities; one group is K^+ dominant, the second is Cl^- dominant and the third is Na^+ dominant. In addition, this work shows that fluctuations in the resting membrane potential of Jurkat T cells are generated by the fluctuations in the number of open ion channels and may get magnified by introducing activating molecules, such as Ca^{2+} or ATP. Another factor that may generate fluc-

tuations in resting membrane potential is the driving force. These two factors form the main points of our hypotheses, next section.

5.1.2 Hypotheses

The time-domain and the time-averaged wavelet power analysis of resting membrane potential dynamics provide the tools used to test the hypotheses:
1) The resting potential dynamics are created by the fluctuation in membrane conductance and the driving force of ions or ions concentrations.
2) The amplitude of fluctuations in the resting membrane can be magnified by molecules such as ATP or ions such as Ca^{2+} that increase the membrane conductance.
3) A change in the ionic driving force, participating in resting potential fluctuations, leads to a change in the amplitude of the fluctuation.

5.1.3 Experimental Protocol

To test the hypotheses presented in the previous section, a whole-cell patch-clamp configuration was used to measure the resting membrane potential at Lancaster University from (2015) to (2016) by Shakil Patel. The cells were categorised into three groups depending on their permeabilities to K^+, Cl^- and Na^+.

Control cells are defined such that the pipette and bath solution which mimic the physiological intracellular and extracellular environments of real living cells. Attempts to categorize cells into groups were done by changing the bath solution; elevating K^+, lowering Cl^- or Na^+. The average number of cells in each group was 6 cells. In this section, we also present the cells categorization criteria and the test of the second hypothesis.

To test the second hypothesis, molecules such as ATP and ions such as Ca^{2+} were introduced in the pipette solutions and the resting membrane potential was

recorded for 10 min in each case. The data was sampled using a sampling frequency of 20 KHz which is equivalent to a recording rate of 1 record per 50 μsec.

5.1.4 Cells categorisation criteria

As mentioned in the previous section, Jurkat T cells were categorized after measurements into three groups. The first group is K^+ dominant (Cohort 1). This group was characterized by a resting membrane potential which is close to K^+ equilibrium potential in both control and altered solutions. The Nernst equation is used to calculate the theoretical equilibrium potential of each ion which was compared to the resting potential of each group in control and altered cases. The same method was used with Cl^- and Na^+ groups.

In the next subsection, analysis of all groups is given to provide confirmation of our hypotheses that the dynamics in resting membrane potential values are intrinsic properties of the membrane itself.

5.1.5 Analysis and results

Pre-processing

Down-sampling Down-sampling is a process of reducing the sampling rate of the data. Since the sampling frequency is 20 KHz, then the Nyquist frequency is 10 KHz. Signals were down-sampled using a window of 1000 points (0.05 sec), which means that one point was picked from every 1000 points, to remove frequencies higher than 10Hz which is out of the range of interest. Therefore, the Nyquist frequency of the downsampled data becomes 10 Hz. No aliasing filter is needed to be used with the original data.

De-trending Prior to the analysis of the fluctuation in the resting membrane potential, all data were detrended using a moving average. Then, the standard deviation

of the resting membrane potential is considered as a fluctuation in the detrended data of the resting membrane potential.

Statistics

All data are plotted as the mean of the recorded membrane potential and the Wilcoxon signed-rank test is used [391]. The Wilcoxon signed-rank test is usually used to test whether two-paired data comes from the same distribution. For example, to compare the resting membrane potential of two groups of cells recorded with an alteration in solution composition outside the cell, the signed-rank test is used.

The difference between the means of two groups is considered significant when the test gives p value less than 0.05 ($p < 0.05$). Different groups were used in measurements when the intracellular solution was changed (due to a limitation in the method) the Wilcoxon rank-sum test was used. This test is also known as the Mann-Whitney U test. Wilcoxon rank-sum test is a non-parametric test used with non-paired data selected from populations having the same distribution.

Analysis: time-domain representation

As discussed earlier, cells were categorized into three groups with respect to the ionic species that dominate the current. First, a categorization criterion is discussed. Second, the results from the three groups are analysed. Therefore, the results presented here are as follows; categorization analysis, the results of K^+-dominant Jurkat T cells (cohort1), the results of Cl^--dominant (cohort2) and finally, the results of Na^+-dominant Jurkat cells (cohort3). The final two cohorts are present in the appendices.

Analysis of cells categorizations

The equilibrium potential of each ion was calculated using the Nernst equation (2.9) in standard and altered ion concentrations. Then, the measured membrane potential was compared for each cell with the calculated equilibrium potential of each ion. If the recorded membrane potential is shifted in parallel to one of the ions, as for example K^+, the cell is considered K^+-dominant, and so on. Table (5.1) details the calculated and measured membrane potential of three groups of jurkat cells; each one is a member of a different group. The calculations were done using Matlab codes that I wrote at the beginning of the analysis.

As illustrated in table (5.1), cells were grouped in K^+-dominant because the membrane potential of this group was shifted with the shift of K^+ equilibrium potential when the extracellular concentration of K^+ was shifted from 6 to 60 mM. Na^+-dominant membrane potentials were shifted with Na^+ equilibrium potential due to a decrease in the extracellular Na^+ concentration from 150 to 10 mM. And, Cl^--dominant cells' membrane potentials were shifted with Cl^- equilibrium potential as extracellular Cl^- concentration was lowered from 162 to 6 mM. Other cells were excluded from categorization, because there was no shift in the membrane potential when an ion concentration in the bath was altered, which means that this cell is related to the other two non-altered ions (Results are not shown). This method of categorization can be confirmed using GHK equation (2.10) and by assuming the permeabilities of the ions to be known. In K^+-dominant, the permeability of K^+ is high relative to others, and by changing the extracellular concentration of each ion, the membrane potential will be shifted significantly only when $[K^+]_o$ is altered. In the same way other groups can be tested.

Table 5.1: Measured resting membrane potential and equilibrium potential of ions K^+, Cl^- and Na^+ in 3 different groups of jurkat cells, E_r is equilibrium potential, V_r is measured resting potential

	Standard		Altered	
Cohort	V_r mV	E_r mV	V_r mV	E_r mV
K^+	-32.68	-79.4	-9.2	-17.3
Cl^-	-3.9	-3.65	15.56	78.75
Na^+	-5.8	50.4	-19.35	-17.3

Cohort 1: K^+-Dominant

The mean of the resting membrane potential was calculated from the recordings for each group of Jurkat T cells and the standard deviation using Matlab codes that I wrote specially for this study. Both are presented in table (5.2) as a mean ±standard error of the mean (SEM). A significant difference in the mean and in the standard deviation of the resting membrane potential is found between groups and presented in (Figure 5.1). The fluctuations in the resting membrane potential were considered as the standard deviations of the detrended data of the resting membrane potential of each cell in each group.

Figure 5.2(a) represents the recorded resting membrane potentials of group (G1) of Jurkat cells (N= 7), where the pipette and the bath solutions were standards (I1 and E1); for pipette and bath solutions, see measurement protocols (section 3.1.1). This case was considered as the control. Each cell in the group has a different resting membrane potential and a different fluctuations' amplitude. Therefore, the mean was calculated for each of the resting membrane potential and the amplitude of fluctuations. The mean of the resting membrane potential was -32.6 mV and the mean of the amplitude of fluctuations was 1.87 mV. Figure 5.2(b) shows the recordings of the resting membrane potential from the same cells presented in figure (1a) after elevating the extracellular K^+ from 6 mM to 60 mM (E2). As before cells show variability in both the resting membrane potential

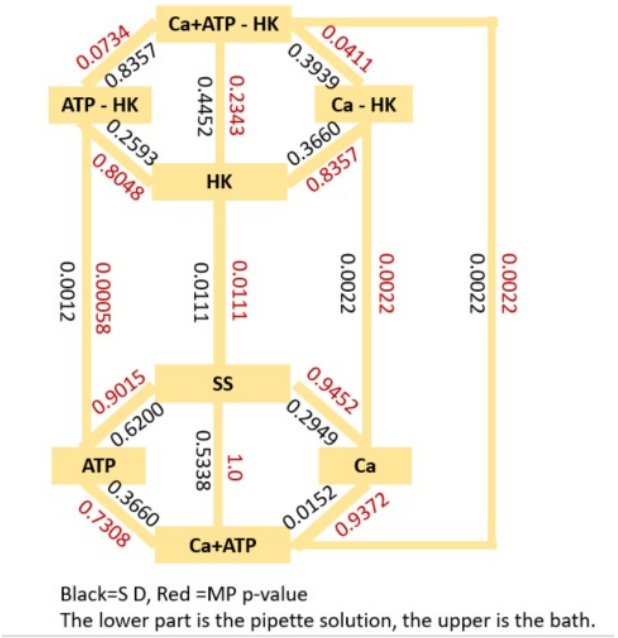

Figure 5.1: Significance between each two cases in K-dominant groups of Jurkat T cells was checked using Wilcoxon signed-rank test and the significant value is considered for p <0.05, SD:standard deviation (p-value in black) and MP: membrane potential (p-value in red). SS:Standard medium and standard solution in the pipette, HK: Standard solution in the pipette and elevated K^+ in the bath, ATP: ATP is introduced in the pipette, Ca: Ca^{2+} is introduced in the pipette

and the amplitude of fluctuations. The mean of the resting membrane potential significantly (p=0.0111) depolarises (becomes more positive) to -9.2 mV and the amplitude of the fluctuation significantly (p=0.0111) decreases to 0.41 mV.

Table 5.2: Resting membrane potential and standard deviation in K^+-dominant jurkat T cells (Cohort 1), HK: high $[K^+]_o$, see solutions used in methodology

Solution	Membrane potential mV (Mean ±SEM)	Standard Deviation mV (Mean ±SEM)
Standard (I1+ E1)	-32.576±6.82	1.869±0.428
HK (I1+ E2)	-9.19±1.725	0.409±0.135
Ca^{2+} (I2+ E1)	-34.132±2.654	2.803±0.369
Ca^{2+}-HK (I2+ E2)	-10.087±0.403	0.664±0.126
ATP (I3+ E1)	-32.348±3.78	2.323±0.431
ATP-HK (I3+ E2)	-9.146±1.004	0.538±0.109
Ca^{2+}+ATP (I4+ E1)	-35.256±4.003	1.545±0.185
Ca^{2+}+ATP-HK (I4+ E2)	-12.951±1.061	0.494±0.083

1 μM of Ca^2+, an activator of KCa channels, is introduced in the pipette solu-

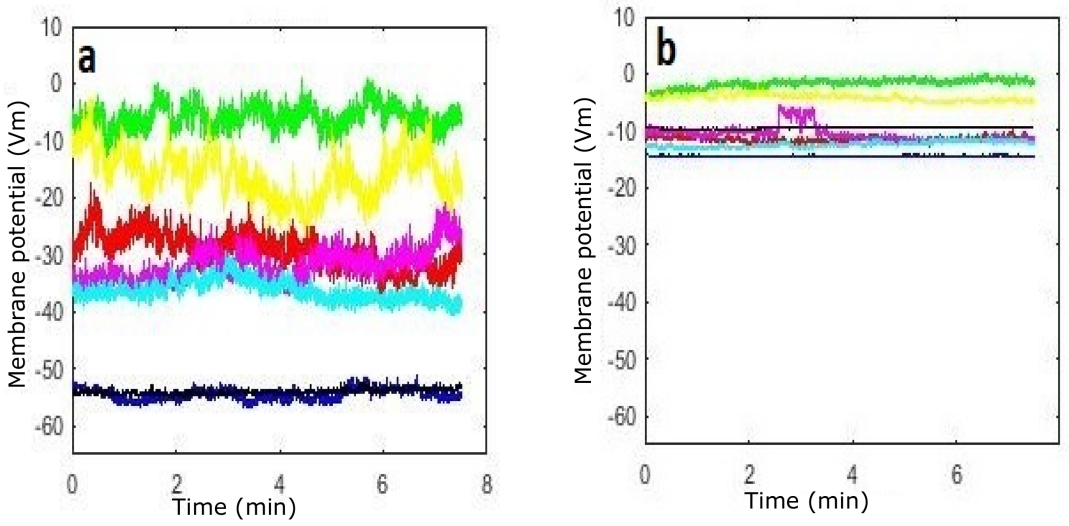

Figure 5.2: Recordings of the resting membrane potential of Jurkat T cells group G1 using whole-cell patch-clamp, a) the pipette solution is standard (I1) and the bath is standard (E1), b) the pipette solution is standard (I1) , and the bath with high extracellular concentration of K^+ (E2), N=7, p=0.0011.

tion (I2) in a new group (G2) of Jurkat T cells (N=7) and the bath used is standard (E1). The recordings from these cells are shown in Figure 5.3(a). The mean of the resting membrane potential is slightly hyperpolarised to -34.13 mV(p=0.945) relative to the control and the amplitude of the fluctuations increases insignificantly to 2.8 mV (p = 0.295), the highest amplitude of fluctuations in all measurements. But, when the bath was changed from standard to a solution with high extracellular concentration of K^+ (E2), the membrane depolarizes significantly to -10.1 mV (p= 0.0022) and the amplitude of fluctuations decreases significantly to 0.66 mV (p=0.0022), see figure 5.3(b).

In a new group of jurkat cells, G3, 4 Mm of ATP is added to the pipette solution (solution I3) and the bath used is standard (E1). The time series of the resting membrane potential recorded from this group (G3, N=7) is presented in figure 5.4(a). The membrane potential, approximately, does not change from the control (standard) case (p=0.9), but the amplitude increases insignificantly (p=0.62) to 2.32 mV. In figure 5.4(b), the pipette solution remains the same as in figure 5.4(a) but the bath was replaced by the solution (E2); which contains

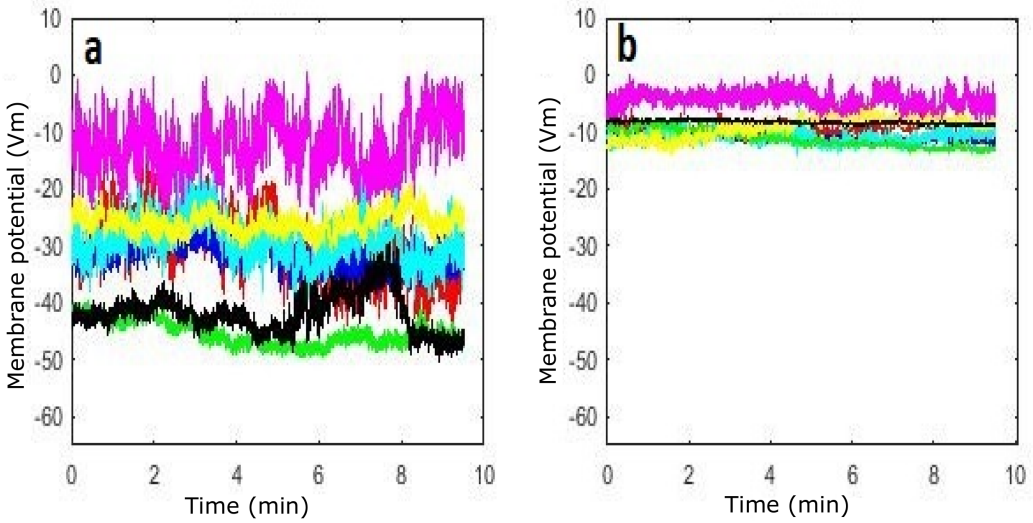

Figure 5.3: Recordings of the resting membrane potential of Jurkat T cells group G2 using whole-cell patch-clamp, a) the pipette solution is standard + 1μ M Ca^{2+} (I2) and the bath is standard (E1), b) the pipette solution is standard + 1 μ M Ca^{2+} (I2) , and the bath with high extracellular concentration of K^+ (E2), N=7, p=0.0022

a high extracellular concentration of K^+. The mean of these data is found to be -9.14 mV (p= 0.00058) and the standard deviation is 0.538 mV (p= 0.0012).

In the last group (G4, N=6), 4 mM ATP and 1 μM of Ca^{2+} are introduced together in the pipette solution (I4) and the bath solution was standard (E1). The resting membrane potential is recorded and the results are plotted in figure 5.5(a). The value of the resting membrane potential increases insignificantly (p=1) to the maximum hyperpolarized value (-35.26 mV) and the standard deviation decreases to 1.54 mV (p=0.53). Measurements using the same group of cells are repeated using the bath (E2) with a high extracellular concentration of K^+ (Figure 5.5(b)). The membrane depolarizes to -12.95 mV (p=0.0022) and the standard deviation decreases significantly to 0.49 mV (p=0.0022).

The p-value is calculated to differentiate between all cases in the groups, as an example, the significance is found in the addition of Ca^{2+} with ATP in HK bath compared to the addition of Ca^{2+} alone, using the same bath solution (HK), p-value= 0.0411. To see more cases, all significances are shown in figure 5.1. These

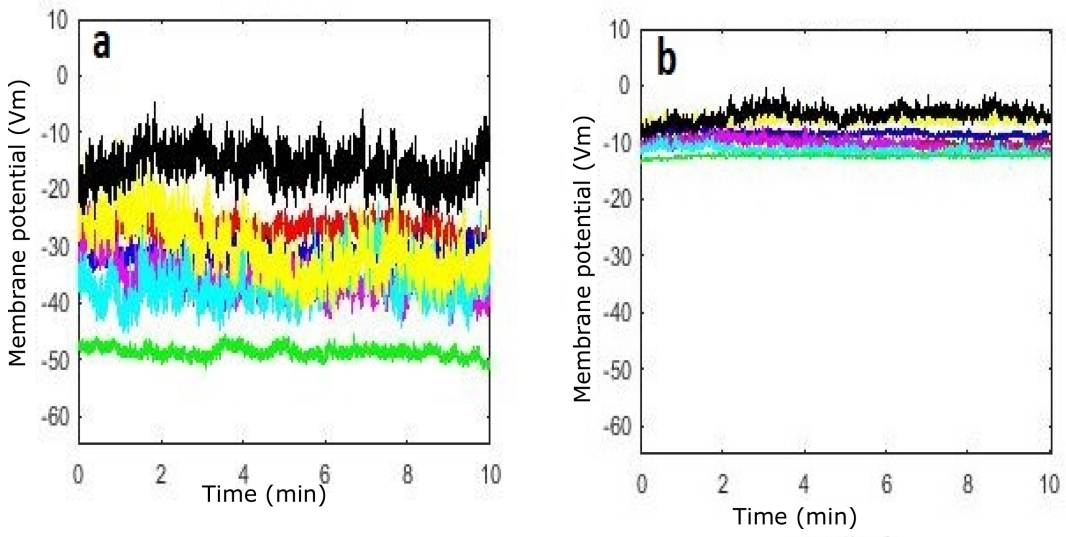

Figure 5.4: Recordings of the resting membrane potential of Jurkat T cells group G3 using whole-cell patch-clamp, a) the pipette solution is standard + 4mM ATP (I3) and the bath is standard (E1), b) the pipette solution is standard + 4mM ATP (I3) , and the bath with high extracellular concentration of K^+ (E2), N=7, p=0.00058

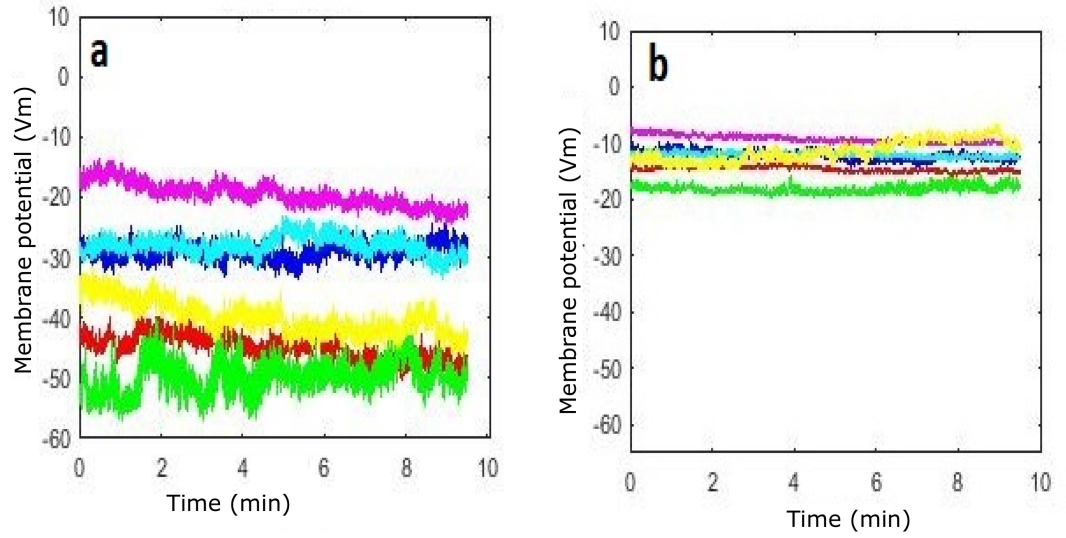

Figure 5.5: Recordings of the resting membrane potential of Jurkat T cells group G4 using whole-cell patch-clamp, a) the pipette solution is standard + 4mM ATP+1 μ M Ca^{2+} (I4) and the bath is standard (E1), b) the pipette solution is standard + 4mM ATP +1 μ M Ca^{2+} (I4) , and the bath with high extracellular concentration of K^+ (E2), N=7, p=0.0022

calculations were handled using Matlab codes that I wrote to perform this study.

The other two cohorts are analysed and are presented in appendix 8.2.

5.1.6 Time-averaged wavelet power analysis

To test our hypotheses using another analysis approach, time-frequency analysis was performed on downsampled data using a custom Matlab code (these code were generated by students in biomedical group at Lancaster University [8, 385] and I edited it to work with my signals), with a Morlet mother wavelet of central frequency f_0=1. Time-averaged wavelet power was calculated for each signal. The mean of the time-averaged wavelet power was also calculated for all signals over the frequency interval of interest (0.01-10 Hz). The significance was checked, as previously mentioned, using Wilcoxon signed-rank and sum-ranked tests in accordance with paired and non-paired data, respectively. The results were considered as significant when $p < 0.05$ (Highlighted in orange; table 5.3). All means of the time-averaged wavelet power with the significance are tabulated and divided with respect to cells cohorts. Table 5.3 shows the results of the significance in time-average wavelet power analysis of K^+-dominant jurkat cells. It is obvious that there is a significant difference in the spectra when K^+ was elevated in the bath in all cases, except one, when ATP and Ca^{2+} were introduced together in the pipette.

While the addition of ATP or Ca^{2+} to the pipette solution with standard bath conditions was insignificant, their addition to the pipette with the altered bath by elevation of K^+ from 6 to 60 mM was significant. The last case, when ATP and Ca^{2+} are introduced together in the pipette solution, there was no significant change in the time-averaged wavelet power when compared with the standard (control) case. The same result was obtained when both ATP and Ca^{2+} are introduced together in the pipette solution when the bath was altered with elevating K^+ (see figure 5.8).

The addition of both ATP and Ca^{2+} to the pipette solution when compared to

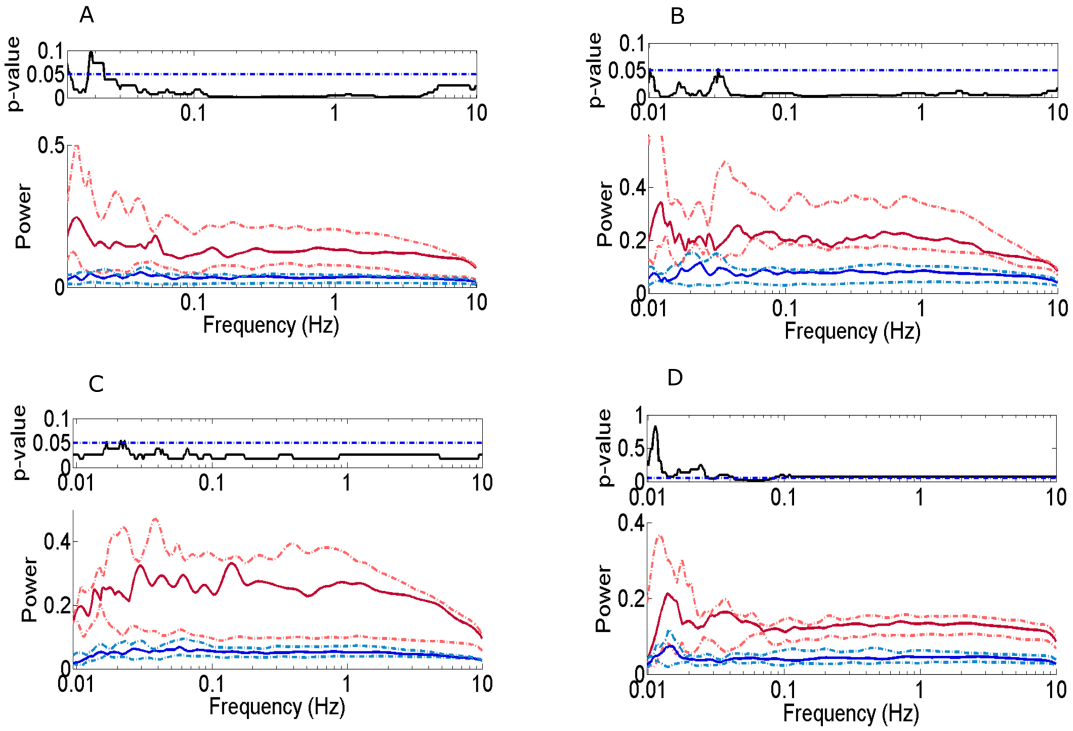

Figure 5.6: Time-averaged wavelet power resting membrane potential of K^+-dominant jurkat cells. The median for each group is plotted and the dashed lines represent the 25% and the 75% quantiles A) Standard pipette solution with standard bath (red) compared with standard pipette solution with altered bath (K^+ increased from 6 mM to 60 mM) (blue). B) Calcium is added to the pipette solution with standard bath data (red) compared with the same pipette solution with altered K^+ in the bath (blue). C) ATP is added to the pipette solution with standard bath data (red) compared with the same pipette solution with altered K^+ in the bath (blue). D) ATP and Calcium are added together to the pipette solution with standard bath data (red) compared with the same pipette solution with altered K^+ in the bath (blue). Significance is plotted separately over each graph in the figure. The p-value <0.05 was considered as significant (dashed-blue line) (See table 5.3). Morlet wavelet is used with central frequency 1.

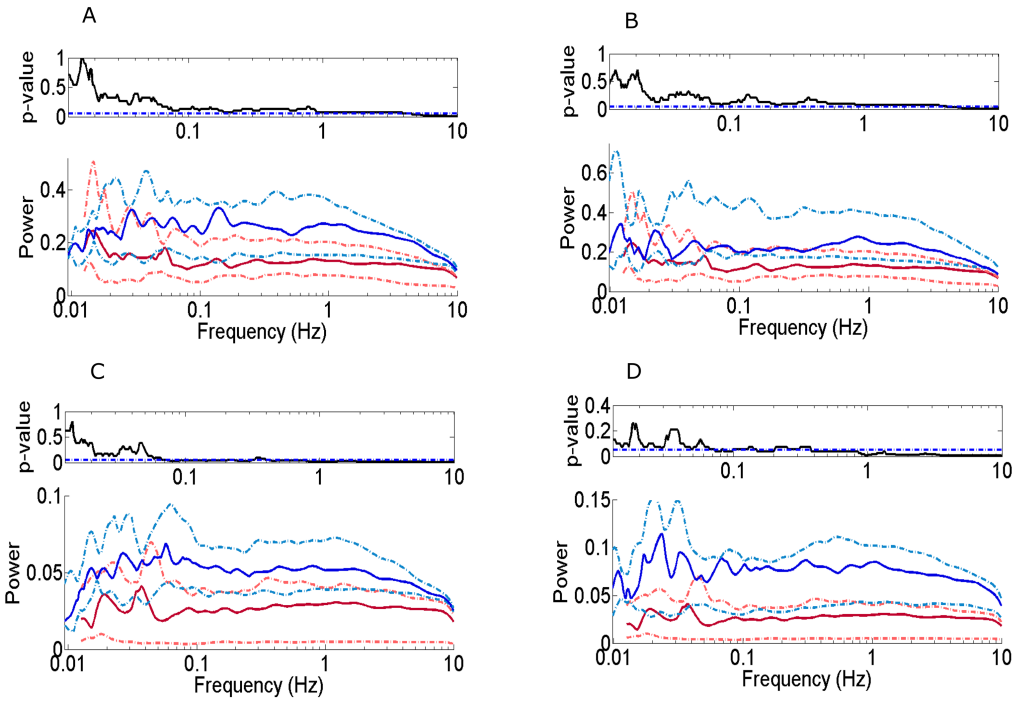

Figure 5.7: Time-averaged wavelet power resting membrane potential of K^+-dominant jurkat cells. The median for each group is plotted A) Groups G1 and G2; with standard bath and pipette solutions (red) vs ATP added to the pipette with standard bath (blue). B) Groups G1 and G3; Ca^{2+} is introduced in the pipette with standard bath (blue) vs standard bath and pipette solutions(red). C) Groups G1 and G2; The same as in A, except the bath in both groups was altered by increasing K^+ concentration from 6 to 60 mM. D)Groups G1 and G3; The same as in D, except the bath in both groups was altered by increasing K^+ concentration from 6 to 60 mM. Significance is plotted is plotted separately over each graph in the figure. The p-value <0.05 was considered as significant (dashed-blue line) (See table 5.3). Morlet wavelet is used with central frequency 1.

the addition of ATP or Ca^{2+} with each of the extracellular solutions; standard or high extracellular K^+ were insignificant using time-averaged wavelet power analysis. For more details, see figure 5.8 (C-F) and table 5.3.

Table 5.3: The mean of time averaged wavelet power calculated to each case in jurkat T cells (Cohort1) and the significance between each two cases was calculated using Wilcoxon signed-rank test , HK: High $[K^+]_o$, SS:standard solution, SCa: Ca^{2+} was added to pipette,ATP: ATP was added to pipette, CaATP: Ca and ATP were added to the pipette, CaK: Ca was added to the pipette and K^+ was elevated in the medium, ATPK: ATP was added to the pipette and K^+ was elevated in the medium, CaATPK: Ca and ATP were added to the pipette and K^+ was elevated in the medium. Significant differences ($p < 0.05$) are highlighted in orange.

Solutions (X-Y) (i.e. X=SS and Y=HK in first row)	Mean of the time averaged wavelet power of X mV^2/s	Mean of the time averaged wavelet power of Y mV^2/s	p-value
SS-HK	0.141	0.0236	0.0041
Ca-CaK	0.2506	0.0722	0.0012
ATP-ATPK	0.2268	0.0545	0.0262
CaATP-CaATPK	0.1283	0.0447	0.0649
SS-Ca	0.141	0.2506	0.1282
SS-ATP	0.141	0.2268	0.0973
SS-CaATP	0.141	0.1283	0.7308
HK-CaK	0.0236	0.0722	0.0379
HK-ATPK	0.0236	0.0545	0.0262
HK-CaATPK	0.0236	0.0447	0.1014
ATPK-CaATPK	0.0545	0.0447	0.5338
CaK-CaATPK	0.0722	0.0447	0.1807
ATP-CaATP	0.2268	0.1283	0.1320
Ca-CaATP	0.2506	0.1283	0.0734

The analysis of cohorts 2 and 3 are presented in Appendix 8.2. The results from these two cohorts are consistent with the results from cohort 1.

5.1.7 Discussion

The present study was designed to determine the factors that generate the dynamics in the resting membrane potential in jurkat T lymphocytes. The main question in this work is whether membrane conductance and the ionic driving force may generate the dynamics in the membrane potential or not. All measurements were

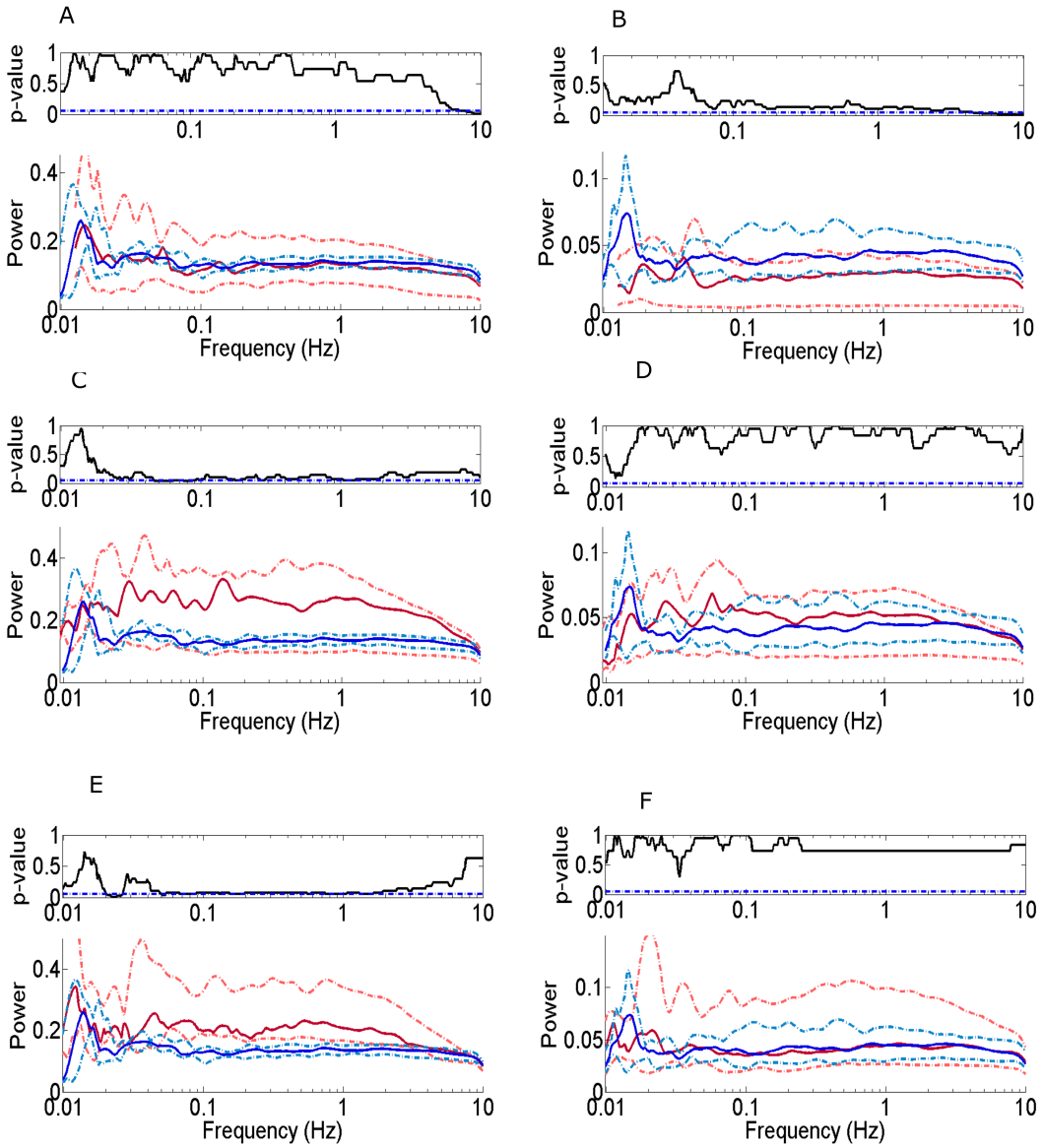

Figure 5.8: Time-averaged wavelet power resting membrane potential of K^+-dominant jurkat cells. The median for each group is plotted A) Groups G1 and G4; with standard bath and pipette solutions (red) vs ATP and Ca^{2+} were added to the pipette with standard bath (blue). B) Group G1 and G4; Same as in A except the bath was altered by elevating extracellular K^+. C) and D) The addition of ATP and Ca^{2+} together to the pipette (red) compared with cases when ATP added alone to the pipette with standard (blue) and altered HK baths (blue), respectively. E) and F) The addition of ATP and Ca^{2+} together to the pipette (red) compared with cases when Ca^{2+} added alone to the pipette (blue) with standard and altered HK baths, respectively Significance is plotted is plotted separately over each graph in the figure. The p-value <0.05 was considered as significant (dashed-blue line) (See table 5.3). Morlet wavelet is used with central frequency 1.

done to answer this question. The jurkat cells used for this purpose were grouped into 3 cohorts to simplify the analysis.

Cohort 1: K^+-dominant

Prior studies showed that jurkat cells, under physiological conditions, are dominated by voltage-gated K^+ channels. A small fraction of these channels are open [171]. The opening and closing of gated ion channels cause fluctuations in the current passes across the membrane, and this generates fluctuations in the membrane potential. While the opening and closing process is essential to the generation of membrane potential dynamics, these fluctuations cannot be created without the driving force that moves the ions through open channels. Therefore, both factors are proposed, in our hypotheses, to be responsible for the generation of fluctuations in the resting membrane potential.

Table 5.4: Driving force and the amplitude of fluctuation in K^+-dominant jurkat T cells (Cohort1), HK: high $[K^+]_o$

Solution	Driving Force (mV)	Amplitude of fluctuations (mV)
Standard (I1+ E1)	42	1.869
HK (I1+ E2)	8	0.409
Ca^{2+} (I2+ E1)	43.6	2.803
Ca^{2+}-HK (I2+ E2)	8.04	0.664
ATP (I3+ E1)	42.3	2.323
ATP-HK (I3+ E2)	8.14	0.538
Ca^{2+}+ATP (I4+ E1)	39.6	1.545
Ca^{2+}+ATP-HK (I4+ E2)	4.25	0.494

Effect of the driving force

To study the effect of the driving force on the amplitude of the fluctuations, extracellular concentration of K^+ was elevated from 6 mM to 60 mM, and this results

in membrane depolarization, which is consistent with [171], and results in a reduction of the driving force of K^+. Table (5.4) shows the calculated driving force in each case. When the driving force of K^+ ions decreases by increasing $[K^+]_o$, the amplitude of fluctuations in membrane potential, as expected, decreases significantly despite what intracellular solution is used; four intracellular solutions (I1, I2, I3, and I4) were used while altering the concentration of K^+ in the medium. All cases show the same result; a decrease in the driving force cause a decrease in the amplitude of the fluctuations of the resting membrane potential. These results support our hypothesis that the driving force is one of the factors that generate the fluctuations in the resting membrane potential and can affect them.

In the other three cases, when ATP, Ca^{2+} or both were added the driving force was not changed when compared with the standard case. This means that the driving force is not responsible for the change in the amplitude of fluctuations. Therefore, these cases are discussed in the effect of membrane conductance, in the next section.

The membrane potential obtained from the control case is consistent with the results that were obtained by Fraser et al. [196]. The membrane potential obtained by Fraser et al. was -32.6mV and the standard deviation was 1.9 mV.

Effect of the membrane conductance

To test our hypothesis the intracellular solution was changed using different groups of jurkat cells, by introducing molecules that might change the membrane conductance. Due to the complexity of the transport system in jurkat T cells, interpretation of the results was simplified to one of the most relevant transporters.

In one of the groups, 1 μM Ca^{2+} was introduced in the pipette, which is the saturation value that may be fully activating the KCa channels [192]. Unsurprisingly, the observed hyperpolarization of the membrane and the largest amplitude of the fluctuation may be attributed to the full activation of KCa channels and,

as a result, to the increase in the membrane conductance to K^+ ions.

In another group of jurkat cells, ATP was introduced. The membrane potential remains close to the control. Since it is well known that Na^+/K^+-ATPase (pump) contribute significantly in the generation of the membrane potential, but it is not clear that this pump is the only transporter that may be activated when ATP was added. But, it seems possible that this result is due to the diffusion of Na^+ and K^+ from the pipette to cells, therefore, the operation of the pump is not required to move these cations against their gradients on the expense of ATP hydrolysis. Surprisingly, the amplitude of the fluctuation increases from 1.869 to 2.32 mV. This is expected if the pump is operating. Therefore, this result suggests that ATP may activate another ion channel, such as Cl^- channel. Future study of the effect of ATP is recommended, by blocking the pump using inhibitors when ATP is introduced, to test the effect of ATP in generating the membrane potential in jurkat cells and to test the role of ATP in magnification of the amplitude of the fluctuations.

The last test for the effect of the conductance on the amplitude of the fluctuation was by introducing ATP and Ca^{2+} simultaneously. The membrane potential, as expected, hyperpolarised due to the activation of KCa channels. Ca^{2+} insignificantly reduced the amplitude of the fluctuation generated by ATP ($p= 0.366$). This result can be attributed to the inhibitory effect of Ca^{2+} on the pump [215, 216, 217], or a sodium channel is activated and result in the reduction of the net current through the plasma membrane. Surprisingly, ATP significantly reduced the amplitude of the fluctuation generated by Ca^{2+} ($p=0.015$). Since no inhibitory effect to ATP on channels activated by Ca^{2+}, it may be attributed to an effect from the activation of other ions channels. Further studies, which take these results into account, are required to be taken.

5.1.8 Summary

With respect to the hypotheses presented previously, clear differences have been demonstrated in the resting membrane potential and its dynamics, at steady state, between standard (control condition) and altered state, contributing to our standing of the physiological sources of membrane potential dynamics. Most previous studies consider these dynamics as noise [14, 1]. Verheugen et al. and Nakaoka et al reported that these fluctuations are due to intrinsic properties of the membrane [171, 15]. In this study, we demonstrate that these fluctuations are not only connected to intrinsic properties of the membrane but also connected to the composition of ions concentrations inside and outside the cell.

It was observed that the dynamics of membrane potential in resting jurkat cells had significantly higher amplitude when solutions containing ATP or Ca^{2+} introduced inside K^{+}-dominant jurkat T cells compared to control case. This is attributed to the activation of ion channels with ATP or with Ca^{2+}, which result in an increase of the net current through the plasma membrane and, as a result, an increase in the amplitude of the fluctuations in the resting membrane potential.

In Cl^{-}-dominant cells (discussed in appendix 8.2.3), ATP and both ATP and Ca^{2+}, when introduced inside the cells, show the higher amplitude of the resting membrane potential dynamics compared to control case. These results mean that the addition of these materials result in activation of ions transporters which result in an increase in the net current through the plasma membrane and an increase in the amplitude of fluctuations. But, in Na^{+}-dominant cells (discussed in appendix 8.2.3) neither of these solutions show a higher amplitude in the dynamics of the membrane potential compared to control case, which is expected. The case which was expected to increase the amplitude of fluctuations in membrane potential, using Na^{+}-dominant cells, was when Ca^{2+} is added inside cells. There were difficulties in recording of the membrane potential in this case because of inactivation of Nav1.5 channels by Ca^{2+} [403]. Therefore, this case was excluded from

our study. The significant increase in the amplitude of fluctuations is contributed to the activation of ion channels by the addition of these molecules inside the cells. As a result, the conductance increased and this support the idea that these fluctuations are generated by opening and closing of gated ion channels [404].

In addition, it was shown that the amplitude of these dynamics was increasing and decreasing with the driving force which acts on ions that generate these fluctuations when compared to ion driving force in control case. In K^+-dominant jurkat cells, the elevation of extracellular K^+ concentration results in a decrease of K^+-driving force despite the intracellular solution was used. As a result, the amplitude of the membrane potential dynamics decreases significantly relative to control. These results support our hypothesis that the driving force is one of two essential factors that generate the dynamics in the membrane potential of resting jurkat cells.

In Cl^--dominant, the reduction of extracellular Cl^- concentration results in an increase in the driving force of Cl^- ions. Therefore, the increase in the amplitude of membrane potential dynamics was expected. Similar to K^+-dominant, the driving force in Na^+ altered state decreases. As a result, the amplitude of fluctuations in the membrane potential decreases relative to control. The change was significant in only one case in which, the intracellular solution was the control. In the other two cases, the decrease in the amplitude of fluctuation was insignificant.

Returning to the hypotheses posed at the beginning of this chapter, it is now possible to state that the dynamics (fluctuations) in the membrane conductance, due to opening and closing of gated ion channels, with the driving force of permeable ions formulate the sources of membrane potential dynamics in resting jurkat cells. This research may serve as a base for future studies of membrane potential fluctuations or oscillations and the role of these dynamics in cell functional processes.

The findings in this study are subject at least to two limitations. First, the

intracellular solution cannot be edited or replaced within recordings. Second, the extracellular solution was difficult to be replaced more than once due to the limited lifetime of jurkat cells. These limitations prevent measurements in different cases to be proceeded using the same group of cells.

In conclusions, this study showed changes in the membrane potential and membrane potential dynamics in resting jurkat T cells in altered states compared to control state. When the altered states have effects on the membrane conductance or the driving force of the ions, it generates changes in the membrane potential and in the amplitude of membrane potential dynamics in resting jurkat cells. Whilst these results are very promising, further research is needed using inhibitors of several types of ion channels to study the contribution of each ion in the membrane potential dynamics, and using different combinations of extracellular ions concentrations that may eliminate the driving force of part of the ions to observe the contributions of each ion in these dynamics. Doing so may provide confirmation of our results.

5.2 Coherence between NADH and the mitochondrial membrane potential or pH

5.2.1 Introduction

Glycolytic oscillations were discussed in section 2.8. It was shown that the frequencies of the oscillations change due to the feeding method, pH and temperature. Olsen et. al., [4] show that NADH are driving the mitochondrial membrane potential (MMP) oscillations. In this work, the frequency of the main mode of NADH and MMP which were measured simultaneously was found to be around 0.026 Hz. Whereas, the frequency of the main mode of NADH and pH which were measured simultaneously was found to be around 0.031 Hz. It was found, by detecting higher

harmonics in all the data, that the mitochondrial ATPase, F_0F_1-ATPase, might be responsible of any possible interaction between glycolysis, pH and the MMP. To confirm this result, azide (an inhibitor of F_0F_1-ATPase) was used and result in diminishing the higher harmonics from the MMP data. These results suggest that this ATPase may be responsible of the coherence between the signals, may couple them, and may lead glycolysis to drive MMP and pH oscillations.

5.2.2 Hypotheses

The time-domain, the time-frequency representation, time-averaged phase coherence, the windowed wavelet coherence, and the higher harmonics finder tool provide the tools to test the hypotheses:

1) Glycolysis and the mitochondria membrane potential (MMP) are coherent.

2) Glycolysis is in coherence with the intracellular pH.

3) Glycolysis is interacting with all other processes in the cell.

4) The source of this coherence might be the F_0F_1-ATPase which cause glycolysis to drive both MMP and pH oscillations.

5.2.3 Experimental Protocol

To test our hypotheses, the fluorescence of NADH and the fluorescence of DiOC2(3) (a dye used to measure the MMP) were measured simultaneously from a suspended population of S. cerevisiae yeast cells. The fluorescence of NADH, a glycolytic metabolite, represents the glycolytic process. Similar measurements were done between the intracellular pH and NADH to test the second hypothesis. Another measurement was done using nanoparticles with aptamers, a truncated DNA linked from one side to a quencher and linked from the other side with a fluorophore, to measure ATP concentration in the cytosol. The measurement of ATP, similar to NADH, represents the glycolytic oscillation in the culture of the yeast suspension.

Several inhibitors of proteins or metabolites, which were involved in these oscillations, were used to support the previous measurements with piece of evidence of the existence of a possible interaction between these processes. Iodoacetate, sodium azide, FCCP and omeprazole were used to test whether glycolytic oscillations are driving both intracellular pH and MMP. Whereas, azide were used to inhibit F_0F_1-ATPase and to test if this ATPase play a role in the coupling between glycolysis, pH and MMP oscillations.

The oscillations in the fluorescence of pH, NADH, MMP, and ATP were recorded for 1500, 2000, 2500 seconds depend on the oscillation's period in the case. The sampling frequency was 0.5 Hz for MMP and NADH simultaneous measurements and 1 Hz for ATP and the simultaneous measurements of pH and NADH.

5.2.4 Analysis

Preprocessing

The measurements usually start before the addition of glucose and KCN, which is required to initiate the oscillations. Since the full range of data precede the initiation of oscillations, the first part of the data contains no information about the glycolytic oscillations, therefore, these data were omitted before the analysis. Then, the data were detrended using a moving average of 100 sec to remove any trend in the data that does not affect the behaviour of the oscillations. Matlab was used with codes that I wrote to perform the analysis.

Statistics

Through the analysis, coherence and higher harmonics require statistical tests, which was done using data surrogates. Since nonlinearity is the main feature we are testing, iterated amplitude adjusted Fourier transform (IAAFT) surrogate is

required. In this surrogate, the phase was randomized keeping other linear features of the data non-altered to destroy the nonlinearity from the surrogates. In the case of coherence, 200 surrogates were generated from each data and the coherence between the surrogates of the two processes was calculated. The 95th percentile of the coherence of the surrogates was compared with the coherence between the original data. The coherence was considered significant when the coherence of the original data is higher than that of the 95th percentile of the surrogates in the region of the frequencies of interest.

In a higher harmonic finder tool, the AAFT surrogate was used since we are still investigating nonlinearity. The time-frequency representation (TFR) was used with the original data and the surrogates. Then the phases were extracted from the ridges of the TFR and were divided into bins. The mutual information between the phase of the main mode and the higher ones were calculated and plotted for both the original data and the surrogates. When the original data mutual information was higher than that of the surrogates plus five standard deviation it was considered to be statistical significance.

All Matlab codes used here were generated by students in biomedical group at Lancaster University [8, 380, 390, 379, 7, 385, 9] and I edited it to work with my signals.

Analysis

A suspension of yeast cells, S. cerevisiae, was used to measure the fluorescence of NADH and the mitochondrial membrane potential (MMP) simultaneously. The green fluorescence of the carbocyanine dye $DiOC_2(3)$ was used to measure the MMP. A 30 mM of glucose was added to the suspension followed by 5 mM of KCN to initiate the glycolytic oscillations. The results, obtained from the experiment, represent the average of the fluorescence of NADH and $DiOC_2(3)$ that produced by the yeast population. Figure 5.9(A, and B) show the time representation of

the fluorescence of NADH and $DiOC_2(3)$. The time frequency representations of the results are shown in figure 5.9 (C, and D). The oscillations in both were sustained until glucose was consumed. Both, NADH and $DiOC_2(3)$ fluorescence were oscillating at the same frequencies, the frequency of the main mode was around 0.026 Hz and the second was around 0.052 Hz (figure 5.9 (H)). It appears from the identical frequencies that NADH and the MMP may be tightly coupled. To check for a possible interaction between them, coherence is used, and it was found that they are fully coherent in the frequency region of the oscillatory modes (figure 5.9 (G)). To check if the second frequency is an independent mode or a higher harmonic of the first mode, a harmonic finder method, based on the information theory, is used (see chapter 4). It was found that the second frequency (0.052 Hz) is a higher harmonic of the main mode (0.026 Hz), which results from the nonlinearity that generated from the interaction of the intracellular processes (figure 5.9 (E, F)). The second frequency does not appear clearly in NADH; therefore, the higher harmonic does not exist in the relevant figure.

In a separate experiment the average of ATP concentration from a population of yeasts was measured using new biosensors. This biosensor composed of an aptamer inserted in nanoparticles. The aptamer is a truncated DNA linked from one side to a quencher and linked from the other side to a fluorophore (see chapter 2). The nanoparticles were inserted into the cells using electroporation method. The data obtained were used, as illustrated in chapter 2, to calculate the concentration of ATP. The results are represented as a time series in figure 5.10 (B). the time-frequency representation (TFR) of the results is shown in figure 5.10 (D). In (A) and (C) from the same figure, NADH fluorescence is shown. This data was measured from a different experiment, therefore, the frequencies extracted from the ridges in the TFR of (A) and (B) are not completely identical (figure 5.10 (F)) and this results in no coherence between them (not shown). But, it is clear from the TFR that ATP oscillations contain the same pair of frequencies that was found in MMP and it contains a main mode with frequency 0.026 Hz and a higher

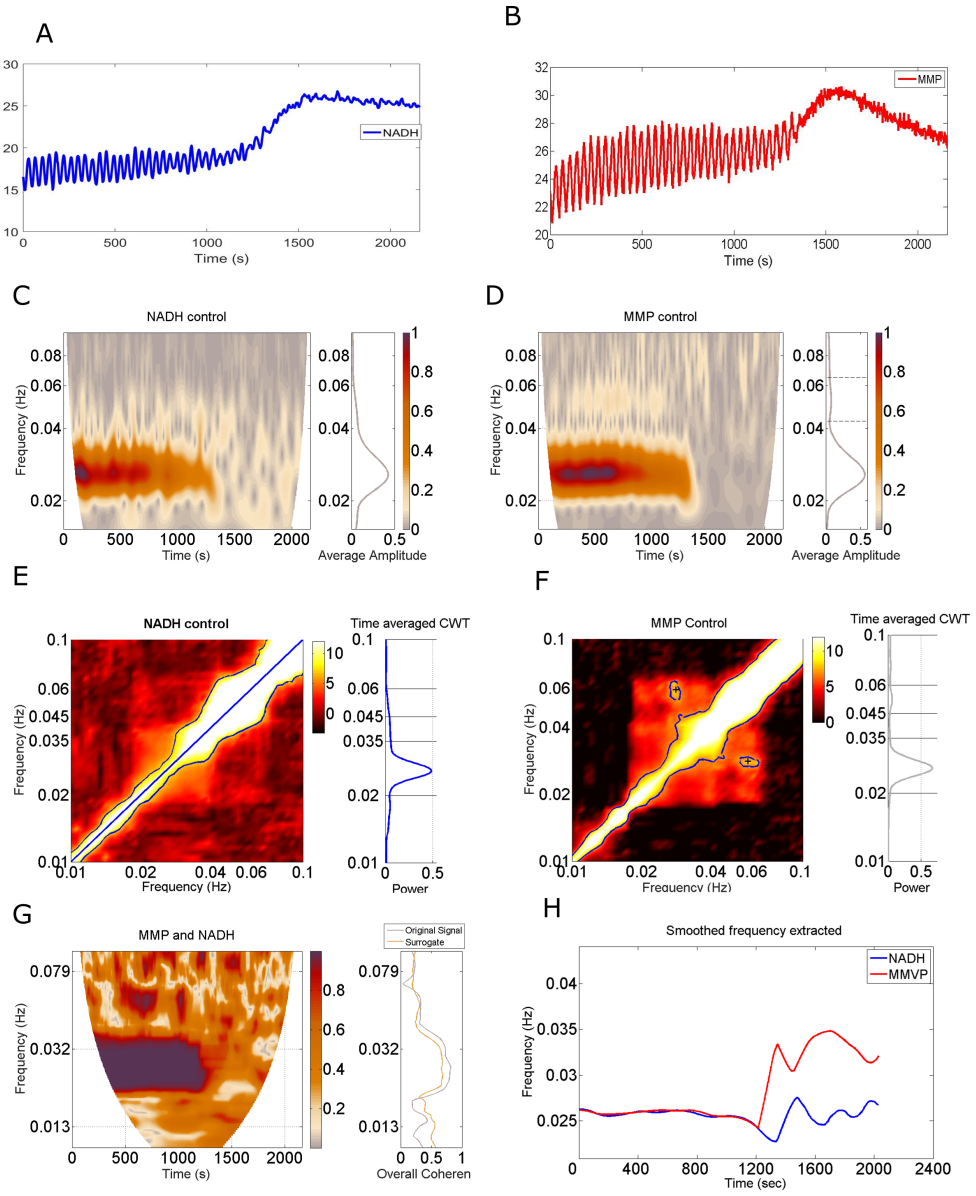

Figure 5.9: Yeast cells were suspended to a density of 10% wet weight in 100 mM phosphate buffer and $DiOC_2(3)$. Oscillations were initiated by the addition of 30 mM glucose followed by 5 mM KCN. A) Time series of NADH fluorescence. B) Time series of $DiOC_2(3)$ fluorescence. C and D) Time-frequency representation of A and B respectively. E and F) the mutual information plot relative to the mean and standard deviation of the surrogates. Regions more than 5σ above the surrogate mean are marked with blue, and local maxima are marked with +. G) The windowed phase coherence between NADH and MMP, left and on the right is the time-averaged wavelet phase coherence. The significance is shown when the coherence of the original data (black line) is higher than the 95th percentile of 200 pairs of IAAFT surrogates (brown line). H) the extracted and smoothed frequency from ridges in TFR of both signals. The window that is used in smoothing is equivalent to the three slowest oscillations in the data. Morlet wavelet is used with central frequency of 2 except for E and F the central frequency is 1.

harmonic at 0.052 Hz, figure 5.10 (E).

From another population of yeasts, pH and NADH were measured simultaneously (see measurements methods). The time series of the original data is represented in figure 5.11 (A and B). The TFR of these data is represented in figure 5.11 (C and D). The frequencies of these data are 0.031 Hz (the main mode) and 0.062 Hz (higher mode). From the analysis of the mutual information between the phases extracted from the TFR representation, it is found that the first frequency represents a main mode and the other one represents a higher harmonic of that mode (figure 5.11 E, F). The frequencies of pH and NADH of the main modes are identical and they are found to be coherent as shown in figure 5.11 (G and H).

Cells were incubated in 250nM, 500nM and 1μM of carbonilcyanide p-triflouromethoxyphenylhydrazone (FCCP) for 10 min before being transferred, to uncouple glycolysis from the MMP with very low concentrations of a substrate that redistribute H^+ between the compartments of the cell and even its medium. The signals measured are shown in figures (8.18 - 8.20, presented in appendix C 8.3 in A and B for NADH and MMP time series respectively). The main difference from figure 5.9 (the control) is that the MMP depolarises while NADH signals are not affected. Therefore, the TFR (figures 8.18 - 8.20 C and D) show no difference from the control (figure 5.9 C and D). The frequencies of the main mode are identical (figures 8.18 - 8.20 H), and the higher harmonics appear in the TFR and disappear in the harmonic finder representations (figures 8.18 - 8.20 E and F). The signal for all concentrations of FCCP show coherence between NADH and MMP (figures 8.18 - 8.20, G). This means that FCCP at low concentrations fails to affect the frequencies of the oscillations in both NADH and the MMP and fail to decouple them. It was reported that FCCP cause annihilation of the oscillations of both MMP and NADH, at high concentrations (>5 uM) [4].

To investigate if the F_0F_1 -ATPase is involved in the mechanism responsible for a coupling between the oscillations of the MMP and NADH, cells were incubated

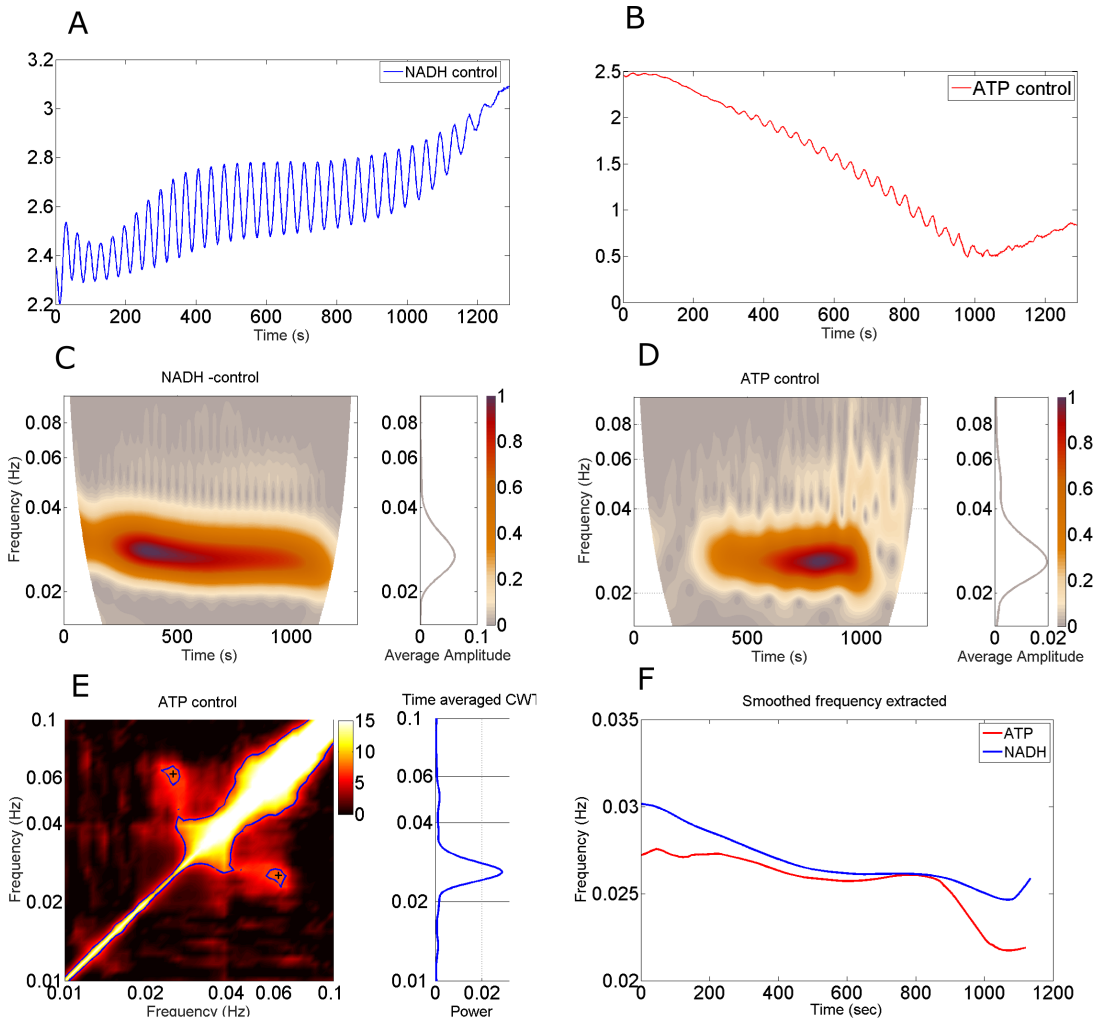

Figure 5.10: Yeast cells were suspended to a density of 10% wet weight in 100 mM phosphate buffer and $DiOC_2(3)$. Oscillations were initiated by the addition of 30 mM glucose followed by 5 mM KCN. A) Time series of NADH fluorescence. B) Time series of ATP concentrations. C and D) Time-frequency representation of A and B respectively. E) the mutual information plot relative to the mean and standard deviation of the surrogates. Regions more than 5σ above the surrogate mean are marked with blue, and local maxima are marked with +. F) the extracted and smoothed frequency from ridges in TFR of both signals. Morlet wavelet is used with central frequency of 2, except for E, the central frequency is 1.

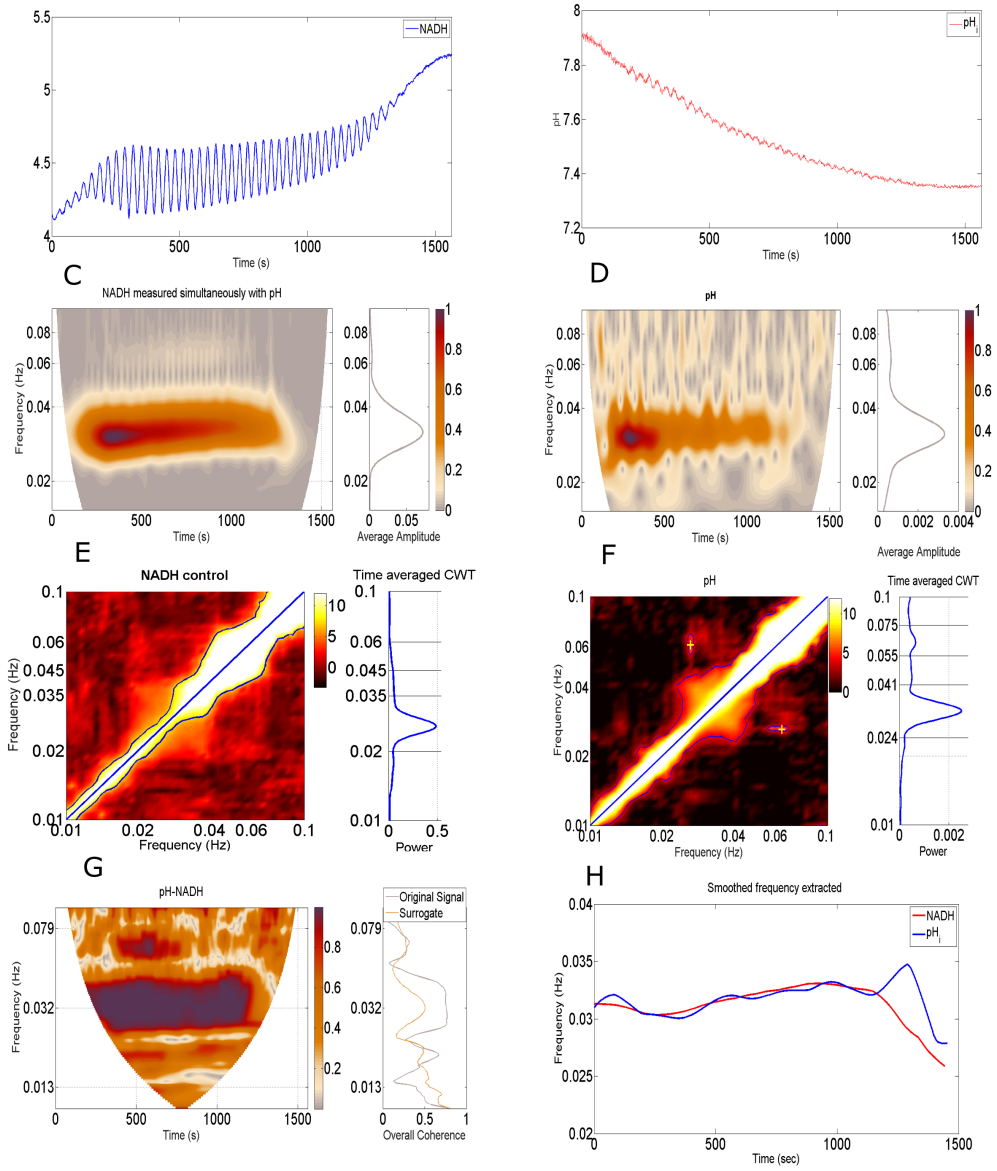

Figure 5.11: Yeast cells were suspended to a density of 10% wet weight in 100 mM phosphate buffer and $DiOC_2(3)$. Oscillations were initiated by the addition of 30 mM glucose followed by 5 mM KCN. A) the time series of pH. B) the time series of NADH fluorescence. C and D) Time-frequency representation of A and B respectively. E and F) the mutual information plot relative to the mean and standard deviation of the surrogates. Regions more than 5σ above the surrogate mean are marked with blue, and local maxima are marked with +. G) The windowed phase coherence between NADH and MMP, left and on the right is the time-averaged wavelet phase coherence. The significance is shown when the coherence of the original data (black line) is higher than the 95th percentile of 200 pairs of IAAFT surrogates (brown line). H) the extracted and smoothed frequency from ridges in TFR of both signals. Morlet wavelet is used with central frequency of 2, except for E and F, the central frequency is 1.

in 100 μM, 200 μM and 400 μM of azide, an inhibitor of that ATPase. It is observed that azide affects the amplitude of both the MMP and NADH. As the concentration of azide increases, the oscillations of both NADH and the MMP last less and the frequencies appear to be not identical. Therefore, the coherence between these oscillations annihilated more quickly. The higher harmonics also disappear when the concentration of azide increases to 200 μM and 400 μM (see figures 5.12 - 5.14). These results are in consistence with the inhibition of the oscillations of NADH and the MMP using a higher azide concentration, 5 mM [4].

Measurement of ATP after the addition of 2mM of sodium azide, which precede the addition of glycose and KCN, result in complete elimination of the oscillations and a change in the decline of ATP level. These results are consistent with the inhibition of that ATPase and the reduction of ATP hydrolysis. As seen in figure 8.17 (A-D) in appendix C 8.3, the oscillations exist in the absence of the inhibitor and ceased in the presence of the inhibitor, which suggest a main role of the F_0F_1-ATPase in the oscillations of ATP concentrations.

To test if glycolysis is driving the MMP and pH, iodoacetate was used. Iodoacetate is an inhibitor of glycolysis through the inhibition of glyceraldehyde-3- phosphate dehydrogenase. 20 mM iodoacetate was added to an oscillating suspension at t=1000; it appears at t=700 sec due to truncation of usefulness data when metabolism was shifted by the addition of glucose followed by KCN. The results show that iodoacetate has eliminated the oscillations in NADH, MMP, ATP and pH (figures 8.21 - 5.16) and uncouple the frequencies of the main mode between NADH and MMP as well as in NADH and pH. The coherence between NADH and MMP was eliminated as well as between NADH and pH.

To investigate the role of the plasma membrane H^+-ATPase (pma1), omeprazole, an inhibitor of the pma1, was used. But, it wasn't easy to measure NADH fluorescence because omeprazole can absorb UV emissions, therefore, it absorbs most of the NADH fluorescence. The results show that the oscillations in the

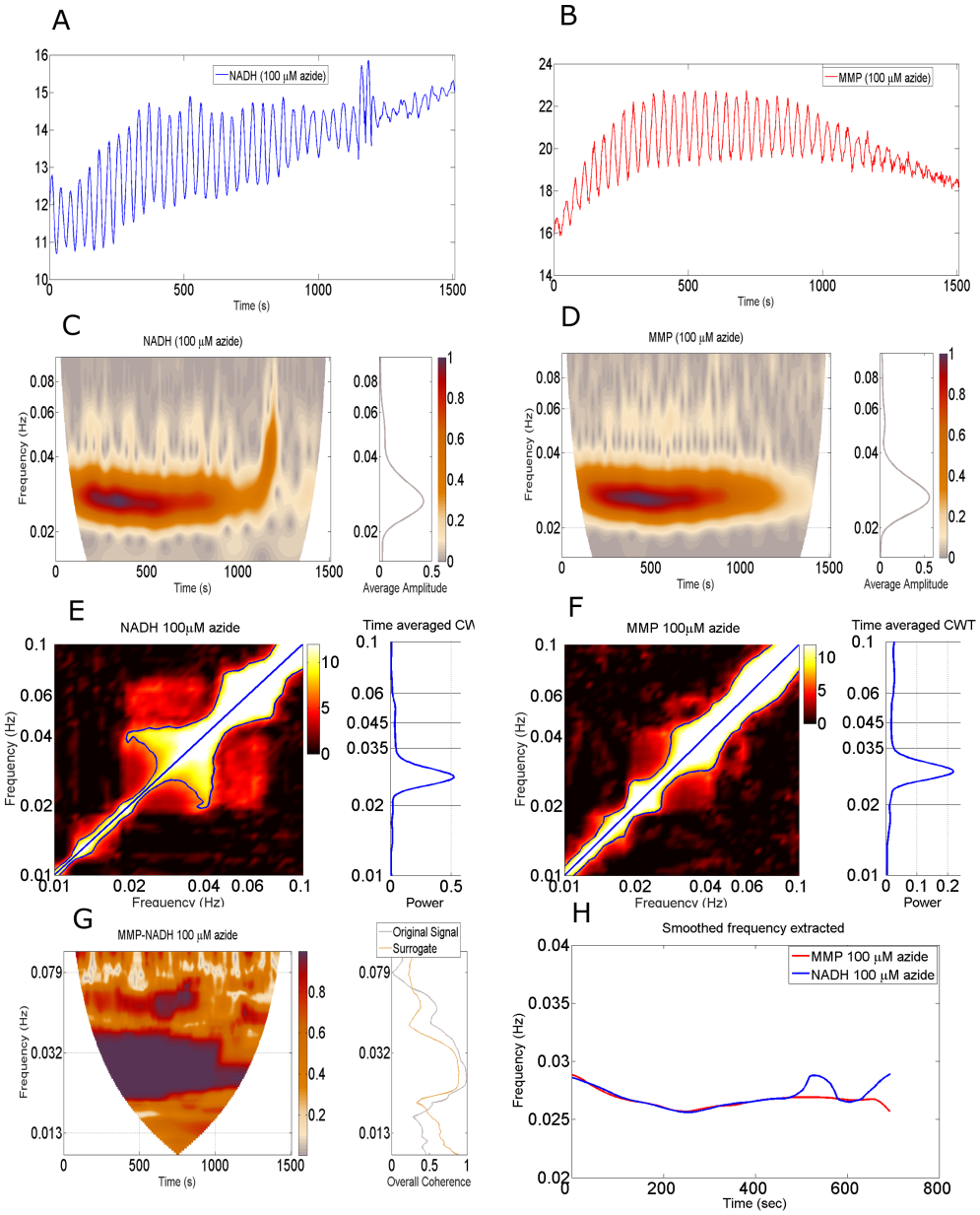

Figure 5.12: Yeast cells were suspended to a density of 10% wet weight in 100 mM phosphate buffer and cells were incubated for 10 min in 100μM of sodium azide before being transferred. Oscillations were initiated by the addition of 30 mM glucose followed by 5 mM KCN. A) Time series of NADH fluorescence. B) Time series of $DiOC_2(3)$ fluorescence. C and D) Time-frequency representation of A and B respectively. E and F) the mutual information plot relative to the mean and standard deviation of the surrogates. Regions more than 5σ above the surrogate mean are marked with blue, and local maxima are marked with +. G) The windowed phase coherence between NADH and MMP, left and on the right is the time-averaged wavelet phase coherence. The significance is shown when the coherence of the original data (black line) is higher than the 95th percentile of 200 pairs of IAAFT surrogates (brown line). H) the extracted and smoothed frequency from ridges in TFR of both signals. Morlet wavelet is used with central frequency of 2, except for E and F, the central frequency is 1.

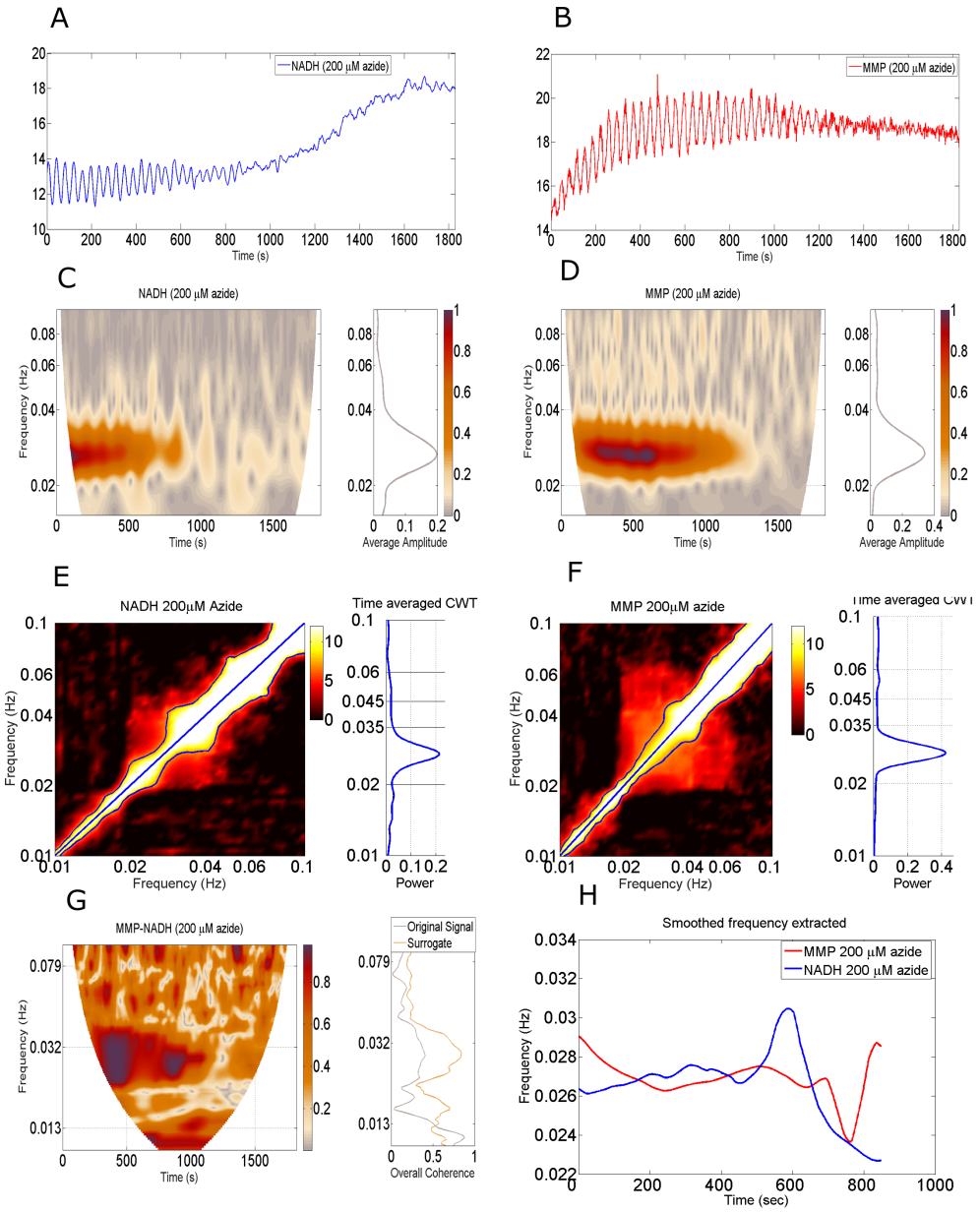

Figure 5.13: Yeast cells were suspended to a density of 10% wet weight in 100 mM phosphate buffer and cells were incubated for 10 min in 200μM of sodium azide before being transferred. Oscillations were initiated by the addition of 30 mM glucose followed by 5 mM KCN. A) Time series of NADH fluorescence. B) Time series of $DiOC_2(3)$ fluorescence. C and D) Time-frequency representation of A and B respectively. E and F) the mutual information plot relative to the mean and standard deviation of the surrogates. Regions more than 5σ above the surrogate mean are marked with blue, and local maxima are marked with +. G) The windowed phase coherence between NADH and MMP, left and on the right is the time-averaged wavelet phase coherence. The significance is shown when the coherence of the original data (black line) is higher than the 95th percentile of 200 pairs of IAAFT surrogates (brown line). H) the extracted and smoothed frequency from ridges in TFR of both signals. Morlet wavelet is used with central frequency of 2, except for E and F, the central frequency is 1.

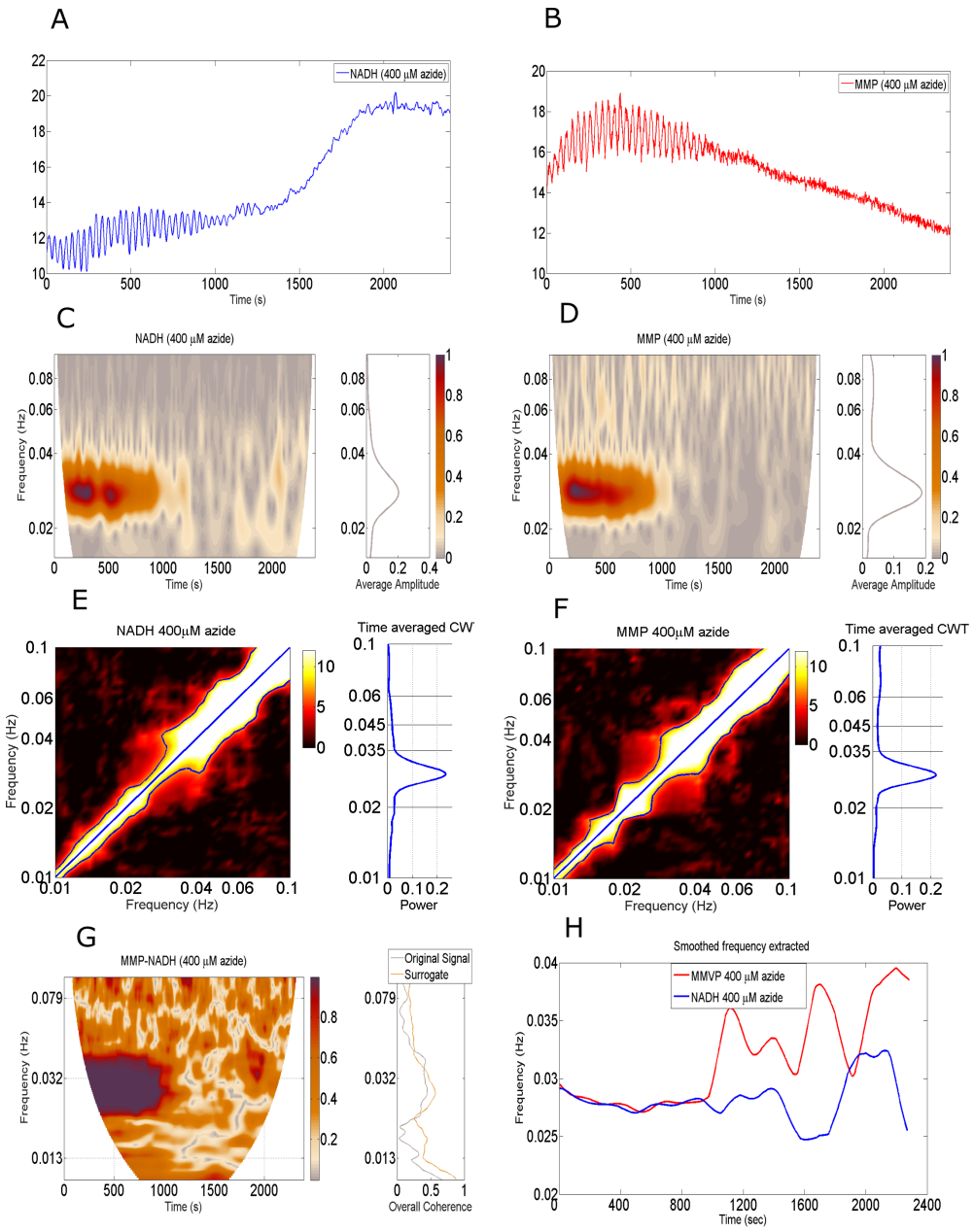

Figure 5.14: Yeast cells were suspended to a density of 10% wet weight in 100 mM phosphate buffer and cells were incubated for 10 min in 400μM of sodium azide before being transferred. Oscillations were initiated by the addition of 30 mM glucose followed by 5 mM KCN. A) Time series of NADH fluorescence. B) Time series of $DiOC_2(3)$ fluorescence. C and D) Time-frequency representation of A and B respectively. E and F) the mutual information plot relative to the mean and standard deviation of the surrogates. Regions more than 5σ above the surrogate mean are marked with blue, and local maxima are marked with +. G) The windowed phase coherence between NADH and MMP, left and on the right is the time-averaged wavelet phase coherence. The significance is shown when the coherence of the original data (black line) is higher than the 95th percentile of 200 pairs of IAAFT surrogates (brown line). H) the extracted and smoothed frequency from ridges in TFR of both signals. Morlet wavelet is used with central frequency of 2, except for E and F, the central frequency is 1.

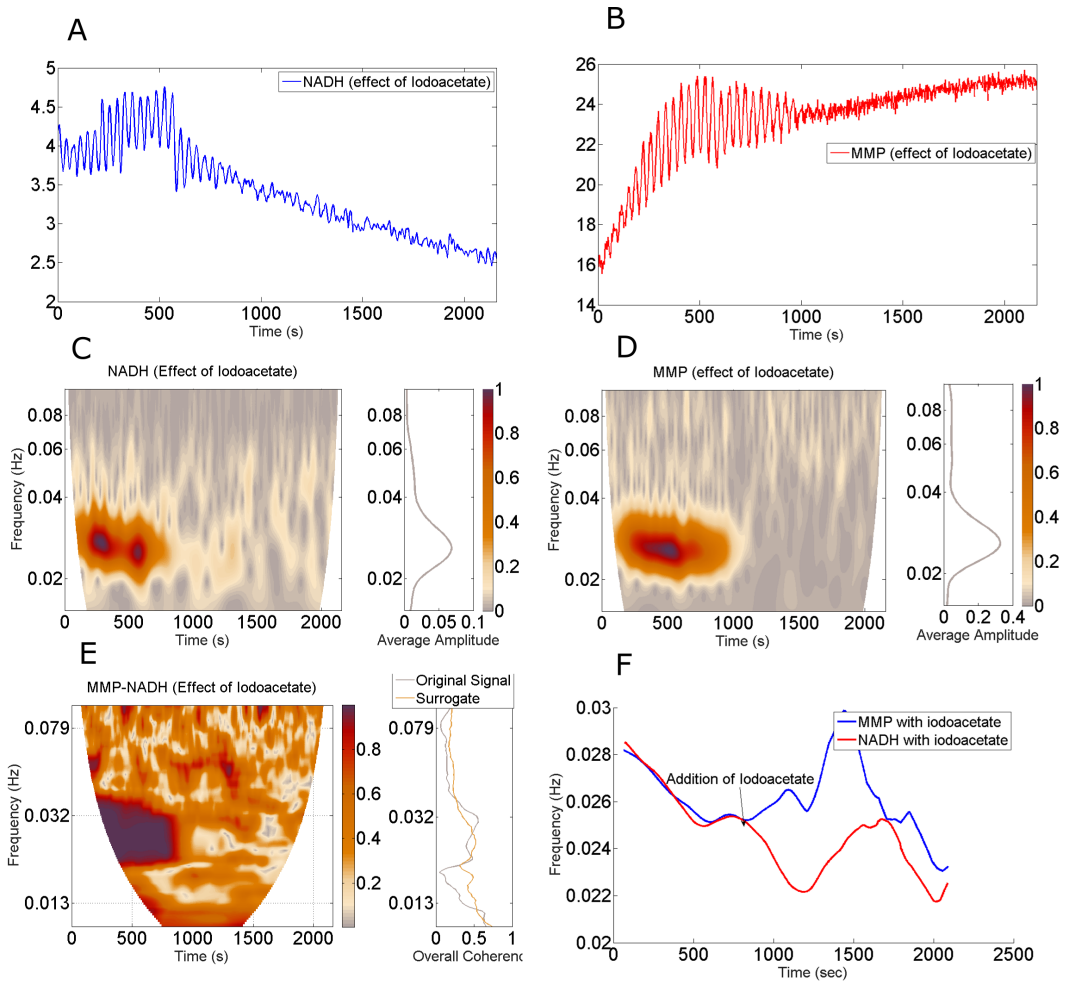

Figure 5.15: The effect of iodoacetate on the oscillations of NADH and MMP. Yeast cells were suspended to a density of 10% wet weight in 100 mM phosphate buffer and $DiOC_2(3)$, glucose and KCN were added as described in Fig. 5.9. At time 1000 s, 20 mM iodoacetate was added to the suspension; it appears at t=700 sec due to truncation of usefulness data when metabolism was shifted by the addition of glucose followed by KCN. A and B show the time series of NADH and MMP respectively. C and D show the TFR of A and B. E) he coherence between the data in A and B. F) the extracted frequencies from C and D using the ridges in the TFR. Morlet wavelet is used with central frequency of 2.

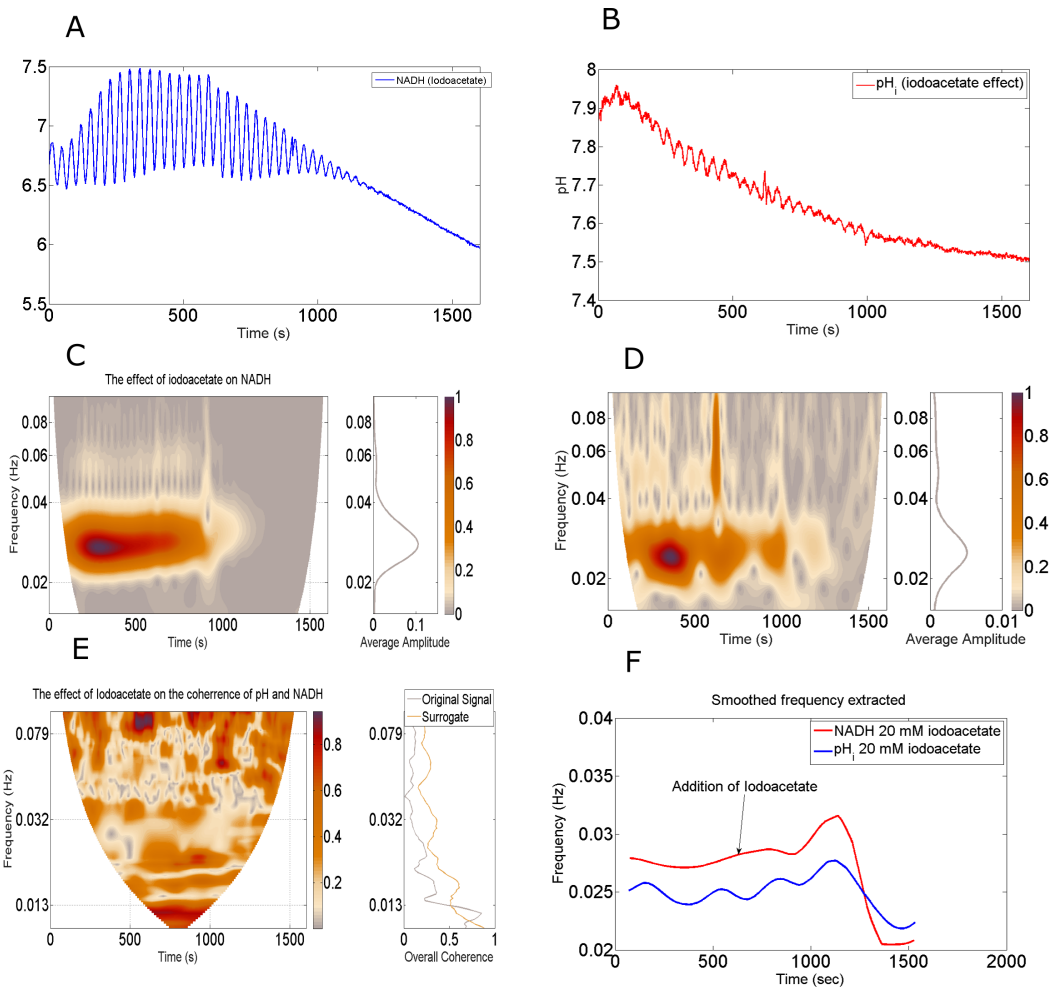

Figure 5.16: The effect of iodoacetate on the oscillations of NADH and pH. Yeast cells were suspended to a density of 10% wet weight in 100 mM phosphate buffer), glucose and KCN were added as described in Figure 5.9. At time 1000 s, 20 mM iodoacetate was added to the suspension; it appears at t=700 sec due to truncation of usefulness data when metabolism was shifted by the addition of glucose followed by KCN. A and B represent the time series of NADH and pH respectively. C and D the TFR of A and B. E) the coherence between the data from A and B. F) the extracted frequencies from the ridges in the TFR in C and D. Morlet wavelet is used with central frequency of 2.

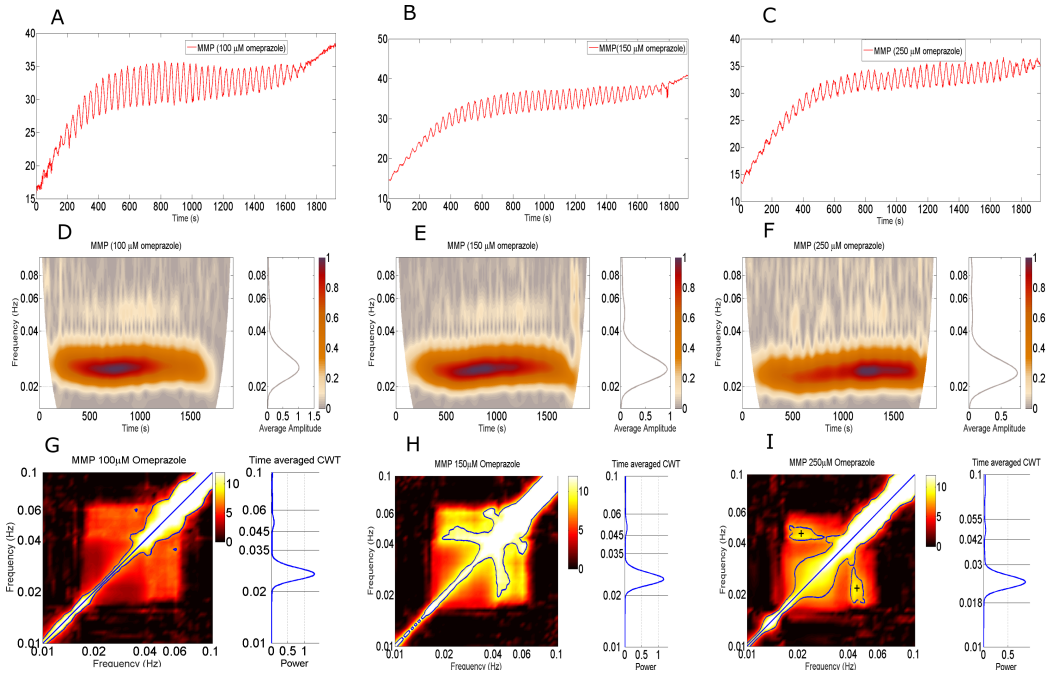

Figure 5.17: The effect of omeprazole on the oscillations of MMP. Yeast cells were suspended to a density of 10% wet weight in 100 mM phosphate buffer and $DiOC_2(3)$. Then cells were incubated in omeprazole (100 μM, 150 μM and 250 μM) glucose and KCN were added as described in Figure 5.9. A-C) Time series of MMP. D-F) TFR of A-C. G-I) the mutual information plot relative to the mean and standard deviation of the surrogates. Regions more than 5σ above the surrogate mean are marked with blue, and local maxima are marked with +. Morlet wavelet is used with central frequency of 2, except for G, H and I, the central frequency is 1.

MMP sustained more as the concentration of omeprazole increases (figure 5.17) and the higher harmonics maintained as in the control case figure 5.9. These results are consistent with the inhibition of the ATP hydrolysis through the pma1 inhibition, since the MMP is usually proportional with the level of ATP in the cytosol.

Measurements of pH from a yeast population in the presence and absence of omeprazole (250 uM) is shown in figure 5.18. The oscillation of pH annihilated in the presence of omeprazole compared with the control. pH also decreases to become more acidic in the presence of omeprazole which is consistent with the inhibition of the proton pump.

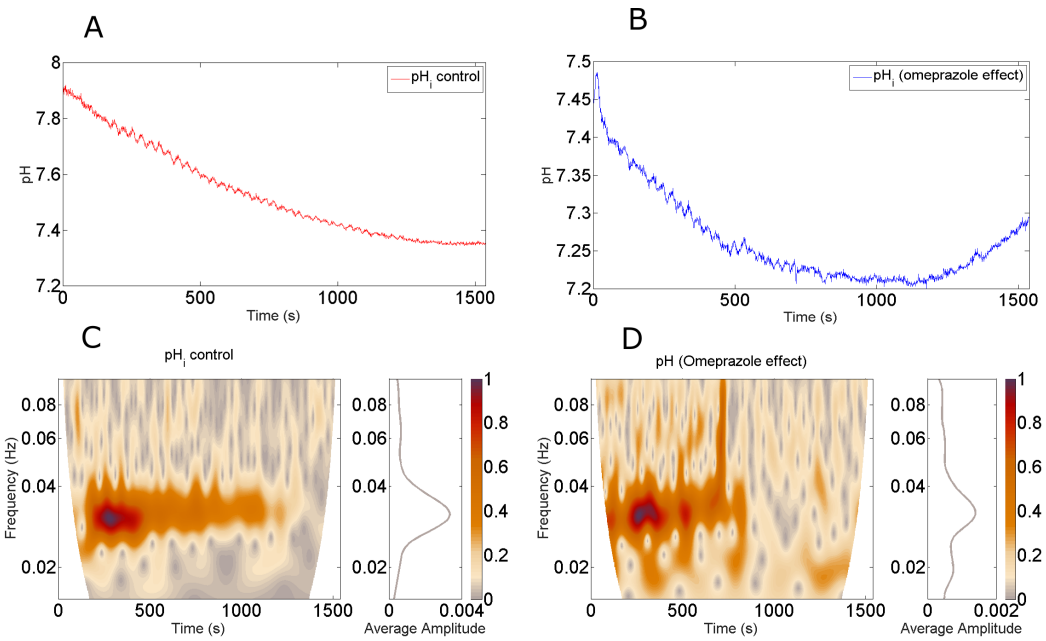

Figure 5.18: The effect of omeprazole on the oscillations of pH. Yeast cells were suspended to a density of 10% wet weight in 100 mM phosphate buffer. Then cells were incubated in omeprazole, glucose and KCN were added as described in Figure 5.9. A) ATP control time series. B) ATP time series in the presence of omeprazole (250 μM). C and D) The TFR of A and B respectively. Morlet wavelet is used with central frequency of 2.

5.2.5 Discussion

The analysis of the fluorescence of NADH and the MMP, which was measured from intact yeast cells, shows that both fluorescence oscillates with the same frequencies, 0.026 Hz and 0.052 Hz. The extracted frequencies from the ridges of the TFR of NADH and the MMP were found to be functions of time and completely identical. It was also reported that they were oscillating in phase [4]. This may suggest that these oscillations are coupled. To investigate a possible interaction between these oscillations, the phase coherence and widowed wavelet phase coherence were calculated. The results (figure 5.9, G) show that the oscillations of the fluorescence of NADH and the MMP were coherent. The windowed wavelet phase coherence shows the time variability of the coherence between them. It is clear that coherence exists in the regions where they oscillate and disappear when the oscillations end. The interaction of these processes results in a complexity and a nonlinearity in

the dynamics of each metabolite. To find out the existence of the nonlinearity, higher harmonics finder based on the mutual information theory was used. This tool extracted the phases from the TFR of the signal and divided them into bins and then calculate the mutual information (M(φ1,φ2)) between pairs of phases, when the mutual information is very high then the phases are highly dependent. The method is applicable to relatively short signals which contain frequencies that are time variables [379]. Figure 5.9 (E, F) shows the higher harmonics in both NADH and the MMP fluorescence. In the MMP, the higher harmonics are clear, while in NADH, there are no higher harmonics.

Unfortunately, the length of the data is too short to apply Bayesian techniques [405], which can be used to find the coupling and its direction.

From two separate populations of intact yeast cells NADH fluorescence and ATP concentrations were measured. As reported by Ozalp et al. [5], they were oscillating out of phase at 150-180 degree. The TFR of these oscillations (figure 5.10 C, D) show that both have two frequencies, the main mode is around 0.026 Hz and the second is around 0.052 Hz. But, the extracted frequencies from the TFR of these data show that the frequencies are not identical, and this may be due to separately measured data. The nonlinearity in ATP due to the interaction with other processes was checked using the higher harmonics finder. ATP has also a main mode at 0.026 Hz and a higher harmonic at 0.052 Hz, exactly as in the MMP, which is expected since the MMP is known to be proportional to the ATP level in the cytosol.

pH was measured simultaneously with NADH, and it is shown in figure 5.11 that the fluorescence of NADH and the dye used to measure pH exhibit oscillations with the same frequencies. However, the frequencies of NADH when measured simultaneously with pH was different from that of NADH when measured simultaneously with MMP, see figures 5.9 and 5.11. The frequencies of both are around 0.031 Hz and around 0.062 Hz. This shift may be interpreted in two ways; first,

it is likely to be due to the effect of the dye used to measure pH since glycolysis is sensitive to pH and it was reported that the frequency of glycolytic oscillation is pH dependent [336]. Second, it may be interpreted as pH here drives glycolysis by affecting PFK and shifts the frequency of the glycolysis towards the frequency of pH. PFK is known to be regulated by pH; very low pH inhibits PFK and high pH enhance PFK. The time variability of the extracted frequency of both pH and NADH was found to be identical and they are found to be coherent in the region of their frequencies of interest (figure 5.11 G,H). The interaction between pH and other intracellular processes was found through the higher harmonic's finder tool (figure 5.11, E).

It was reported that high concentration of FCCP (>5 μM) can annihilate the oscillations in both NADH and the MMP. This uncoupler can dissipate the proton gradient across membranes by redistribution of protons between cytosol and the mitochondrial matrix [406]. In this experiment, the data was measured from yeast populations, which were incubated in very low concentrations of FCCP (250 nM, 500 nM, and 1 μM). The analysis of these results shows that very low concentrations of FCCP have no effect on the oscillations of both NADH and the MMP and their frequencies do not change. The possible interaction between NADH and the MMP also does not change as shown from the coherence analysis (see figures 8.18 - 8.20). FCCP redistributes H^+ and disturb the proton gradients across the membranes. Therefore, the effect on the MMP appears through the depolarization of the MMP which is consistent with the dissipation of the proton gradient. Azide decouples NADH and the MMP as seen from the extracted frequencies from the ridges of the TFR of both data measured in the presence of azide. Also, from their coherence analysis, coherence does not exist when cells were incubated in azide, which means that azide reduces the interaction between the two processes through the annihilation of the oscillations.

The F_0F_1-ATPase is a protein turbine that uses the proton gradient across the inner membrane of the mitochondria to synthesize ATP. When the metabolism

shifts from aerobic to anaerobic, which is required to initiate the oscillations, F_0F_1-ATPase start hydrolysing ATP to pump protons to let the mitochondria maintain its membrane potential. To test the role of this ATPase in the mechanism of the oscillations of NADH and the MMP, cells were incubated in (100 uM, 200 uM, and 400 uM) sodium azide, an inhibitor of F_0F_1-ATPase. The results show that azide annihilate the oscillations in both NADH and the MMP. As the concentration of azide increases the effect on the oscillations increases. These results suggest that the F_0F_1-ATPase plays a crucial role in the glycolytic oscillations though the hydrolysis of ATP and forms a main part of the mechanism of the MMP oscillations through pumping protons out of the mitochondrial matrix towards the cytosol (figures 5.12 - 5.14).

Azide is an inhibitor of several processes in the mitochondria: (1) it inhibits respiration at complex IV (cytochrome c oxidase) [407]; (2) it inhibits "nonrespiratory oxygen consumption" in S. cerevisiae [408]; and (3) it is an inhibitor of ATP hydrolysis by F0F1-ATPase [409]. Concerning an effect on complex IV, cyanide was added, which blocks respiration. And according to Olsen et al. [4], no oxygen consumption by the yeast cells in the presence of 5 mM cyanide, and further addition of azide could not increase this inhibition. And they also reported that addition of 5 mM salicylhydroxamic acid, which is an inhibitor of nonrespiratory oxygen consumption [408], did not have any effect on the glycolytic oscillations. This leaves us with the effect of azide on the activity of F0F1-ATPase.

To confirm the role of azide-inhibited ATPase in the glycolytic oscillations, the oscillations in the concentration of ATP was measured in the presence of 2 mM of azide. The result (figure 8.17) shows that azide has eliminated the oscillation from ATP completely, which is consistent with F_oF_1-ATPase as a main consumer of ATP. These results show that there is a possible interaction between NADH and MMP and this interaction might be driven by the F_0F_1-ATPase and the ATP/ADP antiporter which is reported by Olsen et al [4]. This antiporter can be considered as a facilitator for the interaction through the exchange of ATP for ADP; a transport

of ATP from the cytosol to the mitochondrial matrix and ADP from the matrix to the cytosol. Since this transport is electrogenic, it may also participate in the generation of the MMP.

To test the role of glycolysis in the oscillations of the MMP and pH, iodoacetate, an inhibitor of glycolysis, was added to oscillating populations of yeasts. The results, shown in figures 8.21 - 5.16, show that iodoacetate annihilate the oscillations in NADH, ATP, ADP, pH and the MMP, which suggests that glycolysis might be the driver of the oscillations in pH and the MMP. Iodoacetate uncouples the frequencies of the NADH and MMP which were measured simultaneously as well as for NADH and pH and completely become incoherent.

Finally, the H^+-ATPase (pma1) role in the mechanism of these oscillations was tested by the addition of omeprazole, an inhibitor of pma1. The effect of omeprazole on the MMP oscillations was clear (figure 5.17). Omeprazole inhibits the proton pump which result in an increase in the ATP level and an increase in the MMP fluorescence. It was observed that the oscillations of the MMP sustained more in the presence of omeprazole relative to the control measurements in figure 5.9. Omeprazole also annihilate the pH oscillations and change the decline of the slope of pH which is consistent in inhibition of proton pumping shown in the decrease in pH value (figure 5.18). The main problem was in the measurements of NADH fluorescence due to the absorbency of omeprazole to NADH fluorescence. This problem makes it complex to interpret the main role of pma1 in the glycolytic oscillations. But, as a major consumer of ATP (20-60%), pma1 is expected to play a major role in the mechanism of glycolytic oscillations. In addition, it may play a crucial role in pH oscillations since it is one of the main regulators of the cytosolic pH. To confirm the role of pma1 in glycolytic oscillations, it is required to introduce an inhibitor of the pma1, which is not an absorber of NADH UV fluorescence. other inhibitors of pma1 are NSC11668, hitachimycin [410] and Tetrahydrocarbazoles [411]. These inhibitors require to be identified if they are absorbers of UV light or not in order to get an optimal inhibitor which can be used with UV fluorescence.

In summary, the intracellular processes are in an appropriate interaction which makes these processes cooperate in the face of external stresses. The sum of all cooperative processes results in a stronger cell to survive the challenges that it may face through the changes in the medium structure due to natural changes. If these processes are operating separately, the cell may not survive any simple challenge. This means that these possible interactions make the cell more efficient in regulating its life. The mechanisms that the cell develop to be cooperative are present mainly in the transport system that the cell has, such as ATP/ADP antiporter, F_0F_1-ATPase and pma1.

5.2.6 Summary

The primary aim of this part of this work was to investigate possible interactions between metabolism and MMP or pH in yeast cells, when metabolism was shifted from aerobic to an anaerobic state. Phase coherence and higher harmonic finder were the appropriate tools to be used in the analysis to test the existence of the proposed interaction between the fluorescence recorded from each of these processes and to determine a possible mechanism for these interactions. The time-frequency representation was necessary for the analysis since it facilitates the extraction of the frequency which was integrated to get the phase from each data. Those phases were used in the calculations of phase coherence or in the mutual information between the phases to find the higher harmonics.

From the analysis, ATP, NADH, and MMP were oscillating with the same frequencies (0.026 Hz and 0.052 Hz) while the pH and NADH which were measured simultaneously were oscillating with a slightly different frequencies (0.031 Hz and 0.062 Hz) may be due to the effect of pH on the glycolytic frequency caused by the shift in pH due to the dye which was used to measure pH inside the cells. Oscillating with the same frequencies might be a sign of coherence if the phase difference is constant. Therefore, phase coherence was used to test the presence

of possible interaction between the data which was measured simultaneously. It was found that both MMP and pH are in coherence with NADH, which represents the glycolytic oscillations. The interaction between the processes may appear as a nonlinearity in the data. Therefore, the higher harmonics finder was used to explore the existence of this nonlinearity. It was found that ATP, pH, and MMP have the same main mode and the same higher harmonic frequency. These three processes share the protein F0F1-ATPase which is located in the inner membrane of the mitochondria, which shows through the analysis using inhibitors that it plays a role in the oscillations of each of these processes. Since this protein is hydrolysing ATP to pump protons out of the mitochondrial matrix into the cytosol and results in MMP build up, these results suggest that the higher harmonic found to be common might be linked to that protein. And this ATPase may represent the parameter that couples MMP and pH to glycolytic oscillations and may represent the mechanism by which glycolysis drive both pH and MMP oscillations.

The analysis of the recorded fluorescence using the inhibitor of glycolysis (iodoacetate), the H^+ redistributor (FCCP) and the inhibitor of F_0F_1-ATPase (azide) shows that glycolysis is driving both pH and the MMP and suggest F_0F_1-ATPase to be used in the mechanism.

Chapter 6

Modelling of the interaction between glycolysis and both cytosolic pH and the mitochondrial membrane potential

In this chapter the interactions of the glycolytic oscillations with both cytosolic pH and the mitochondrial membrane potential are modelled. The model based on the measured data presented and analysed in chapter (5). In addition, information which were discussed in chapter (2) were considered in this model.

6.1 The model

In this model, we consider glycolytic oscillation, which is represented by the oscillations of ATP or NADH, as an oscillator GO. In addition, the mitochondrial membrane potential and the cytosolic pH are considered as oscillators MMO and

pHO respectively. This model is an extension of the model presented by Lancaster et al. [412], where they modelled the energy metabolism by two coupled oscillators and show that chronotaxicity could be used to distinguish a healthy state of the cell from an altered state. In our model, the mitochondria are in an altered state only, and so, the input is ATP from glycolysis. The input of the GO is glucose while the input for the pHO is CO_2 produced by GO when the pyruvate is fermented by the yeast cells. Here, the availability of ATP produced by GO is considered as the most primary influence on the mitochondrial membrane potential oscillator. Pyruvate, produced by glycolysis, is fermented to produce ethanol and CO_2 where the later might be converted into hydrogen ions and bicarbonate. The oscillation in ATP is a result of production by glycolysis and consumption by ATPases [4]. The first ATPase (H^+pump) involved in ATP consumption is F_0F_1ATPase, which is located in the inner mitochondrial membrane and consumes ATP to pump protons out of the mitochondrial matrix to build up the mitochondrial membrane potential. The second ATPase is located in the plasma membrane (PMA1) and consumes ATP to regulate the cytosolic pH by pumping protons from the cytosol into the medium of the cell. It is obvious that both ATPases (pumps) are involved in regulation of the cytosolic pH and affect the glycolytic oscillations [4]. The regulation of any oscillator is controlled by the availability of substrates. The change in pH may occur due to an increase in the rate of glycolysis, the activity of PMA1, and the activity of F_0F_1ATPase.

Glycolysis is affected by cytosolic pH due to the inhibitory effect of acidity on PFK [413] which may result in greater decrease in pH. The short-term regulation of pH relies on the cell buffer capacity, which represents all proteins and metabolites located in the cytosol; for more information see section 2.6.4. Therefore, the buffer capacity could be seen partially as the external input to the pHO oscillator, while CO_2 represents the output of fermentation which is required by pHO.

We modelled the oscillators using phase oscillators since we are interested in the time variability of their frequencies and not their amplitudes. The model

composed of three differential equations, each equation representing one of the oscillators,

$$\dot{X}_{GO} = \omega_{GO} + \epsilon_1 \sin(X_{GO} - X_{pHO}) - \epsilon_4 \sin(X_{GO} - \omega_G t) + \sigma\eta(t) \tag{6.1}$$

$$\dot{X}_{pHO} = \omega_{pHO} - \epsilon_2 \sin(X_{pHO} - X_{GO}) - \epsilon_6 \sin(X_{pHO} - X_{MMO}) - \epsilon_5 \sin(X_{pHO} - \omega_b t) + \sigma\eta(t) \tag{6.2}$$

$$\dot{X}_{MMO} = \omega_{MMO} - \epsilon_3 \sin(X_{MMO} - X_{GO}) + \sigma\eta(t) \tag{6.3}$$

where X_{GO}, X_{pHO} and X_{MMO} are the instantaneous phases of GO, pHO and MMO respectively, ω_{GO}, ω_{pHO} and ω_{MMO} are the natural frequencies of GO, pHO and MMO, ω_G and ω_b are the frequencies of the external drivers of GO and pHO oscillators, and $\eta(t)$ is white Gaussian noise. We represent GO and pHO as bidirectionally coupled oscillators since they are continuously interacting as discussed before, with coupling strengths ϵ_1 and ϵ_2 which may vary with time to represent different metabolic states. On the other hand, MMO is represented as unidirectionally coupled to both GO and pHO to represent the effect of GO on MMO and the effect of MMO on pHO with coupling strengths ϵ_3 and ϵ_6 respectively. The inhibitory effect of pH on glycolysis is represented in the model by a repulsive coupling while the excitatory nature of glycolytic oscillations on both the mitochondrial oscillator and pH oscillator is represented by attractive couplings. In addition, the mitochondrial effect on pH is also represented by an attractive coupling. In the model, the substrate of the glycolytic oscillator is glucose, while pH can be linked to the buffer capacity of the cytosol. The external influences on the GO and pHO are represented as unidirectionally coupled drivers, with coupling strengths ϵ_4 and ϵ_5 for glucose and buffer capacity respectively, which may also vary with time.

The oscillators discussed before can be represented as in figure 6.1. Our model is represented as in figure 6.2.

The model is used to regenerate the signals extracted from yeast cells. The

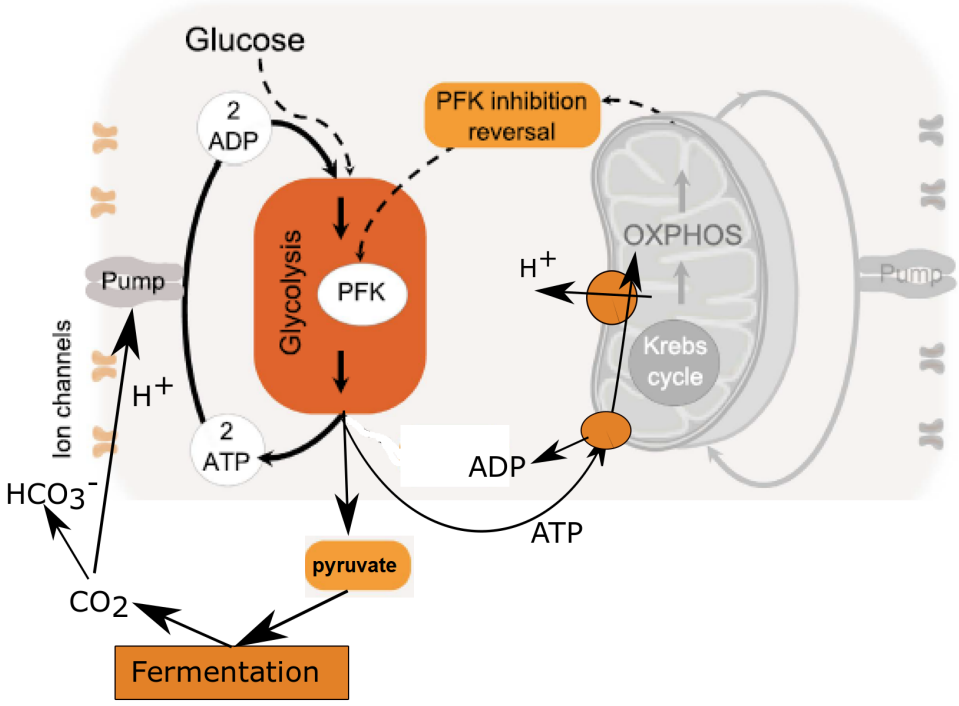

Figure 6.1: Metabolic process in yeast when respiration is inhibited using KCN after the addition of glucose to starved yeast cells. Glycolysis is the main source of cytosolic ATP. Pyruvate that produced by glycolysis is fermented and CO_2 is produced and converted to protons and bicarbonate. The generation of the mitochondrial membrane potential require ATP which is transported from the cytosol. pH is regulated by the pumps which utilise ATP to pump protons out of the mitochondrial matrix. Another pump is located in the plasma membrane which pump protons to the medium. The signals of ATP, cytosolic pH and the mitochondrial membrane potential are oscillating.

signals produced by the model are represented as time series and as time-frequency representation using the continuous wavelet transform. Figures (6.3-6.5) show comparisons between the original signals and the model results represented in time series and time-frequency representation using the Morlet wavelet transform with central frequency, f_0=1.

6.2 Discussion

In this model, the oscillations in glycolysis, the mitochondrial membrane potential (MMP) and the cytosolic pH were considered as three biological oscillators which

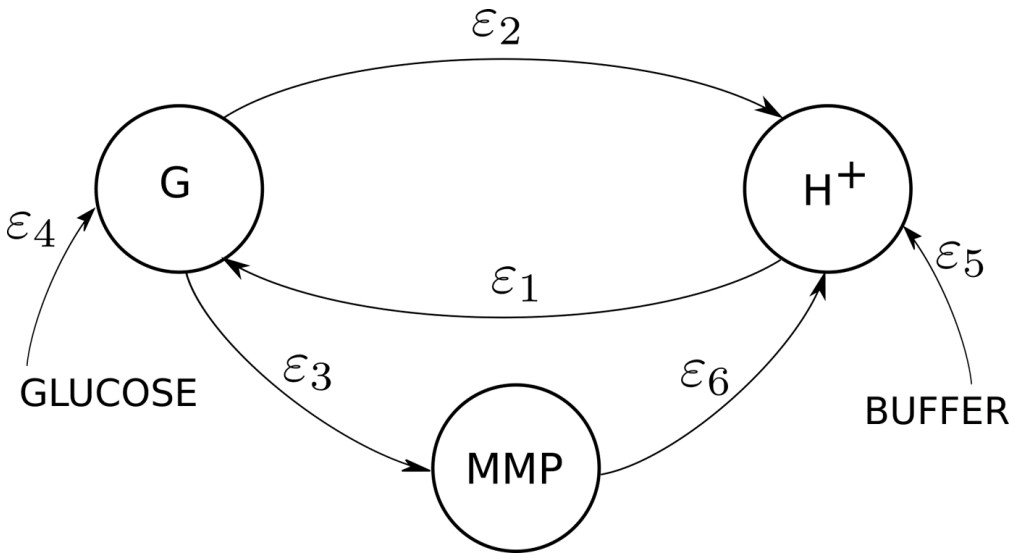

Figure 6.2: The model of the oscillatory processes in yeast cells in an altered state, where respiration is inhibited. The glycolytic and mitochondrial oscillators GO and MO, are coupled via an attractive coupling strength ϵ_3 (due to excitatory influence of GO on MO). GO and pHO are coupled to each others via a repulsive coupling strength ϵ_1 due to inhibitory effect of pH on glycolysis and an attractive coupling strength ϵ_2 due to the excitatory effect of glycolysis on cytosolic pH. pHO is also coupled to the mitochondrial membrane potential (MO) via an attractive coupling strength ϵ_6. The external drivers are coupled to their oscillators via attractive coupling strengths ϵ_4 and ϵ_5 for GO and pHO respectively.

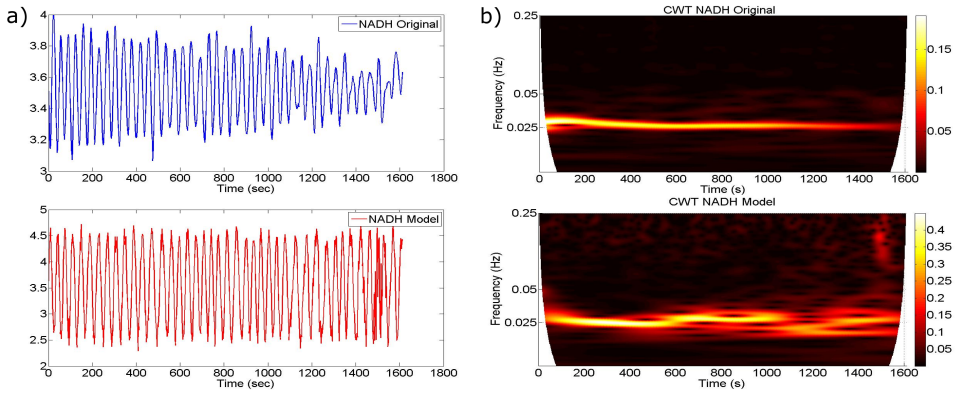

Figure 6.3: a) A comparison between the time series of the original data of the NADH fluorescence measured as the average from a population of synchronized yeast cells with an altered metabolism state and the time series resulted from the model. b) The time-frequency representation of the signals in (a) using the continuous wavelet transform with central frequency f_0=2 and using the Morlet wavelet type.

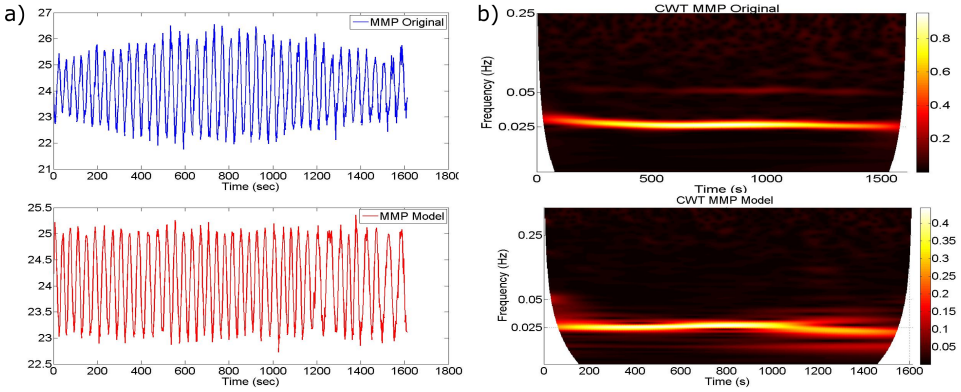

Figure 6.4: a) A comparison between the time series of the original data of the mitochondrial membrane potential (MMP) fluorescence measured as the average from a population of synchronized yeast cells with an altered metabolism state and the time series resulted from the model using the frequency extracted from the original data. b) The time-frequency representation of the signals in (a) using the continuous wavelet transform with central frequency f_0=2 and using the morlet wavelet type.

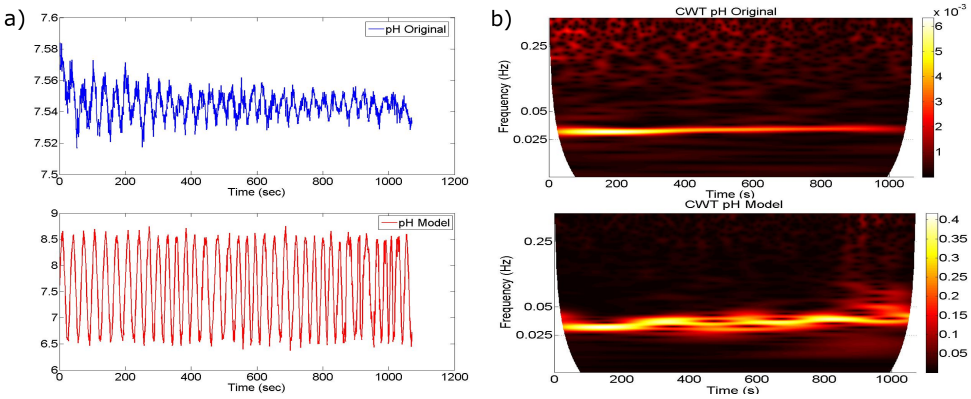

Figure 6.5: a) A comparison between the time series of the original data of the cytosolic pH fluorescence measured as the average from a population of synchronized yeast cells with an altered metabolism state and the time series resulted from the model using the frequency extracted from the original data. b) The time-frequency representation of the signals in (a) using the continuous wavelet transform with central frequency f_0=2 and using the morlet wavelet type.

are confined in the cell. Each oscillator was represented by its natural frequency and terms that represent the interaction with other oscillators. Glucose represents an external driver to glycolysis. It appears from the data simulated from the model that glycolysis is driving both oscillations in pH and oscillations MMP. Glycolysis provides MMP with ATP which is required to operate F_0F_1ATPase that hydrolyse the ATP to pump H^+ out of the mitochondrial matrix. At the same time, glycolysis results in H^+ which result in cytosolic pH change. When glucose is added, the glycolysis rate increases, and so, cytosolic pH increases [4]. Then, the activity of the H^+-ATPase, which is located in the plasma membrane, increases and results in consumption of ATP and decrease in H^+ in the cytosol. The regulation of pH appears to be driven by glycolysis which provides the ATPases with ATP to pump the protons.

The model can regenerate the signals measured from yeast cells and show the same main mode frequency. The signals were represented in the time domain and in the time-frequency domain. It appears that the representation of the signals resulting from the model are similar to those measured from yeast cells. The main difference between the original and the model signals is the second mode which does not appear in the time-frequency representations.

This model could be considered as a milestone of future modelling that may include healthy and altered state of cells, where pH, MMP and ATP could be measured simultaneously when that becomes possible. In addition, when cell volume is measured accurately from cells where glycolysis is oscillating, it might be added to the model as an oscillator if it is oscillating.

6.3 Summary

Glycolytic oscillations in yeasts with altered state are modelled to represent the energy state of the cell. In this model, cytosolic pH was modelled as an oscillator

which interacts with the energy state of the cell. Since pH regulation requires the consumption of ATP to pump protons out of the cytosol, it will reduce the concentration of ATP in the cytosol, resulting in an increase of the glycolysis rate through the interaction of ATP concentration with PFK enzyme. The ATPase activity increases when pH in the cytosol decreases, and it results in the reduction of glycolysis rate to prevent further pH decrease. It is obvious that the interaction between glycolysis and pH is substantial to prevent extreme change in pH. Any increase in pH results in an increase in PFK activity and glycolysis rate and the production of protons. This results in pH reduction which prevents further increase in pH. Whereas, a decrease in pH will affect PFK enzyme activity and result in a reduction of glycolysis rate. This results in reduction of proton production which prevent extreme decrease in pH. In the model, these interactions were represented as a bidirectional coupling between the two oscillators.

Chapter 7

Conclusions

The primary aim of the current work was to investigate how metabolism might be involved in the maintenance of the membrane potential and its dynamics (fluctuations). In addition, the interaction of the glycolysis with the intracellular pH and the mitochondrial membrane potential in a shifted yeast culture from aerobic to an anaerobic state was investigated.

The fluctuations in the resting membrane potential

The dynamics in the resting MP recorded from Jurkat T cells in standard and altered states were investigated. The investigation included alteration of the extracellular concentration of the major ions that generate the resting membrane potential of cells (Na^+, K^+, and Cl^-).

The effect of the driving force The concentration of K^+ was increased while the concentrations of the other two ions were lowered. These changes result in alteration of the equilibrium potential of the altered ion and change the recorded membrane potential and, therefore, results in a change in the driving force of each ion. It was found that the amplitude of the fluctuation is directly proportional to the driving force in every case.

The effect of the membrane conductance The other factor, that was investigated, if it has an effect on the amplitude of the fluctuation in the resting membrane potential, was the membrane conductance. Introducing Ca^{2+} into the intrapipette solution was found to increase the conductance of the membrane through the activation of transporters in the plasma membrane of the cell. One possible transporter that may be activated by Ca^{2+} is the Ca^{2+}-gated K^+ channels. The addition of Ca^{2+} results in an extreme increase in the amplitude of the fluctuations. And this can be due to a change in the membrane conductance due to the activation of transporters when Ca^{2+} was added. In addition, introducing ATP also results in a significant increase in the amplitude of the fluctuations. This increase is linked to the role of metabolism in the maintenance of the membrane potential and the magnification of the fluctuations amplitude through the activation pumps (Primary active transporters). One possible pump is the Na^+, K^+ pump, which hydrolyses ATP to pump these ions against their electrochemical gradient. Since, the membrane does not change significantly while the fluctuations significantly increases, the addition of ATP may activate other transporter (or pump). On the other hand, introducing both Ca^{2+} and ATP shows no significant effect upon the amplitude of the fluctuations and this might be due to the inhibitory effect of Ca^{+2} on the Na^+, K^+-pump. This protein (the pump) represents the missing element in the Hodgkin-Huxley model which is necessary to make the model more realistic.

These results show that the fluctuations of the resting membrane potential are generated by the opening and closing of the gated ion channels, and that two factors can change their amplitude: the ionic driving force (the electrochemical gradient which represents an extrinsic property of the membrane) and the conductance of the membrane (which represents an intrinsic property of the membrane).

Interaction between metabolism, intracellular pH and the mitochondrial membrane potential

The analysis of the fluorescence of glycolytic oscillations, represented by NADH or ATP, intracellular pH and the dye used to measure the mitochondrial membrane potential (MMP) show a possible interaction between these processes which might be inevitable but also crucial for cells to survive in the face of environmental challenges. The extracted frequencies from the ridges of the time-frequency representation of the recorded data were found to be identical in the data measured simultaneously from two processes.

Phase coherence Phase coherence was detected between each pair of data to investigate the existence of an interaction between any two signals measured simultaneously. The results show that glycolysis was in coherence both with pH and with the MMP. The interaction between these processes might result in a nonlinearity of the recorded data. This nonlinearity was detected using harmonics finder tool.

Harmonics detection To detect nonlinearity in the signals under study, mutual information theory was exploited in a tool used to find higher harmonics from the data. The results show a common main mode in all data and a common higher harmonics in ATP, intracellular pH, and the MMP. Whereas, the higher harmonic does not appear in NADH signal. These results may suggest that these higher harmonics are linked to the mitochondrial pump (F_0F_1-ATPase). This pump plays a role in the oscillations of each of these three data sets by hydrolysing ATP to pump proton from the mitochondrial matrix into the cytosol and result in building up the mitochondrial membrane potential. The analysis using inhibitors shows that glycolytic oscillations are driving the oscillations in both intracellular pH and the MMP. Since inhibition of glycolysis using iodoacetate results in inhibition of all oscillations. While the inhibition of oscillations in pH and MMP using FCCP

(>20 μM) does not inhibit the glycolytic oscillations.

In summary, metabolism appears to be involved in some way in the generation of the membrane potential and its dynamics. Metabolism also plays a role in the magnification of the amplitude of the fluctuations in the resting membrane potential; this might be through the activation of the Na^+, K^+-ATPase. This work also shows that metabolism is involved in other cellular processes such as intracellular pH and the MMP. These results suggest that metabolism might be the main process that is crucial for other regulatory processes through the coupling factor, ATP which is a product of metabolism and a necessary element in other regulatory processes such as; ion homoeostasis, maintenance of the plasma membrane potential, intracellular pH regulation, the generation and maintenance of the MMP and the cell volume regulation.

7.1 Original contributions

The original contributions of this work are listed below:

- It was shown that the dynamics in the resting membrane potential are not noise, but represent an important feature of the resting membrane potential in jurkat T cells.
- It was shown that metabolism, represented by cytosolic ATP, is involved in the generation of the dynamics in the resting membrane potential in jurkat T cells.
- The conductance of the plasma membrane was shown to be a factor that magnifies the fluctuations in the membrane potential.
- The driving force of ions that cross the plasma membrane represent another factor that generates the fluctuations in the resting membrane potential. Therefore, increasing the driving force of the dominant ions may magnify

the amplitude of the fluctuations in the resting membrane potential.

- It was shown that the average fluorescence of NADH, ATP, and the mitochondrial membrane potential, from a population of yeast cells, oscillate with the same main frequency of 0.026 Hz.
- It was shown that NADH and intracellular pH measured simultaneously from a population of yeast cells oscillate with the same main frequency of 0.031 Hz.
- NADH was shown to be in coherence with intracellular pH and NADH also was shown to be in coherence with the mitochondrial membrane potential. These signals were measured simultaneously.
- The frequency of each signal was extracted as a function of time. It was shown that the frequencies of the data measured simultaneously were identical.
- It was found that ATP, intracellular pH and the mitochondrial membrane potential contain higher harmonics with a frequency equal to twice the main frequency.
- It was shown that F_0F_1-ATPase may be involved in a coupling between glycolytic oscillations and the oscillations in cytosolic pH and the mitochondrial membrane potential oscillations.
- It was found that glycolysis drives the oscillations in both intracellular pH and the mitochondrial membrane potential in yeast cells, where respiration is inhibited.
- The interaction between glycolysis and both cytosolic pH and the mitochondrial membrane potential were modelled.

Altogether, we have investigated the role of metabolism in the generation of the resting membrane potential and in the dynamics of the resting membrane potential. In addition, the role of glycolytic oscillations in the oscillations of both intracellular

pH and the mitochondrial membrane potential was investigated. It was shown that metabolism is crucial for other cellular processes.

7.2 Future Directions

The work in the present thesis provides the first evidence of the involvement of the metabolism in most cellular processes in standard and altered states. Cell volume recordings that are simultaneous with recordings of other cellular processes do not exist, and so, a natural next step would be recommended to measure the cell volume simultaneously with NADH fluorescence to investigate how metabolism is involved in cell volume regulatory mechanisms.

Chapter 8

Appendices

8.1 Appendix A: Derivation of Goldman-Hodgkin-Katz equation

The total flux of any ion across the membrane is given by Nernst-Plank equation [414],

$$J_{total} = -D\frac{\partial[C]}{\partial x} - \mu z[C]\frac{\partial V}{\partial x} \tag{8.1}$$

The first term on the right side represent Fick's law of diffusion [415]and the second term represent the microscopic version of Ohm's law [416]. Where D is the diffusion constant with units of length2/sec,$\partial[C]/\partial x$ is the ion concentration gradient, µ is the mobility of the ions, z is the valence of ion, [C] concentration of ions and $\partial V/\partial x$ is the potential gradient.

Using Einstein's relation that connects the diffusion coefficient with the mobility [417]

$$D = \frac{kT}{q}\mu \tag{8.2}$$

Where q is the charge in coulombs and k is Boltzmann's constant in J/K. the total

flux can be written as,

$$J_{total} = -\frac{kT}{q}\mu\frac{\partial[C]}{\partial x} - \mu z[C]\frac{\partial V}{\partial x} \tag{8.3}$$

Substituting $\frac{kT}{q} = F$, Faraday is constant and using a current flux (I/area) by multiplying the flux by the valence and Faraday's constant yields,

$$I = -(uzRT\frac{\partial[C]}{\partial x} - uz^2F[C]\frac{\partial V}{\partial x}) \tag{8.4}$$

where u is the molar mobility (μ/N_A). This equation is the Nernst-Plank equation. The Nernst equation can be obtained by setting the current equal to zero. Substituting the constant field $\frac{dV}{dx} = \frac{V_m}{l}$ where l represents the membrane thickness. Solving the Nernst-Plank equation with boundary conditions of the concentrations to be $[C]_i$ and $[C]_o$ and define$\beta = \frac{zFV_m}{RT}$ the result is,

$$I = \frac{uz^2FV_m}{l}(\frac{[C]_oe^{-\beta} - [C]_i}{e^{-\beta} - 1}) \tag{8.5}$$

The permeability is defined as

$$P = \frac{\mu RT}{lF} \tag{8.6}$$

P has dimensions of length/sec Substituting in terms of the permeability in equation 8.5 gives,

$$I = PzF\beta(\frac{[C]_oe^{-\beta} - [C]_i}{e^{-\beta} - 1}) \tag{8.7}$$

In real cells, the current composed of several ionic species. Therefore, the total current is the sum of the individual currents. This is because they assume that the ions move independently, do not interact. Assume that the current composed

only of K^+, Na^+ and Cl^-, the total current is given by

$$I_{total} = I_K + I_{Na} + I_{Cl} \tag{8.8}$$

And each of these currents can be represented by the Nernst-Plank equation. At steady state, the total current is zero, so the resting potential of the membrane is given by

$$V_m = \frac{RT}{F}(ln\frac{P_K[K^+]_o + P_Na[Na^+]_o + P_{Cl}[Cl^-]_i}{P_K[K^+]_i + P_Na[Na^+]_i + P_{Cl}[Cl^-]_o}) \tag{8.9}$$

which is known as Goldman-Hodgkin-Katz equation [185].

8.2 Appendix B: Fluctuations in membrane potentials

Jurkat T cells were categorized into three cohorts, the first one was analysed and discussed in chapter 5 while the other two cohorts, which represent supporting material to our hypotheses test, are analysed and present in this appendix.

8.2.1 Cohort 2: Cl^--dominant

As in K^+-dominant cells, measurements and analysis were done to study the factors that create and affect the dynamics in the resting membrane potential in Cl^--dominant jurkat T cells. The main difference between the solutions used with cohort1 and cohort2 is the altered bath: in cohort1, the extracellular K^+ is elevated from 6 mM to 60 mM, but in cohort2, the extracellular Cl^- is lowered from 162 mM to 6 mM. Therefore, the equilibrium potential of that ion is altered and so the resting membrane potential is shifted in parallel. As in cohort1, 4 groups of Jurkat T lymphocytes were used with whole-cell patch-clamp configuration to measure the resting membrane potential.

The mean and the standard deviation in the resting membrane potential recorded from jurkat T cells are present in table (8.1). The significance between groups and within groups, when altering the intracellular or extracellular solutions or both, are checked using Wilcoxon signed-rank test with paired and Wilcoxon sum-ranked test with unpaired data. The significant difference was considered between two cases for p <0.05. The calculated p-values are present in (figure 8.1).

Figure (8.2a) show the resting membrane potential recorded from group1 (GCl1). The solution used in the pipette is standard and also the bath, this case is considered as control. The mean is found to be -3.895 mV and the standard deviation is 0.968 mV. The bath solution was replaced by a solution with low extracellular concentration of Cl^-. The concentration of Cl^- in the bath was lowered from 162 mM to 6 mM and the pipette solution is kept standard. The measurements are repeated with the new configuration. The mean of the resting membrane potential increased insignificantly to 15.559 mV (p= 0.1) and the standard deviation is magnified to 1.6778 mV (p=0.4).

Table 8.1: Resting membrane potential and standard deviation in Cl^--dominant jurkat T cells (Cohort2), LCl: low $[Cl^-]_o$

Solution	Membrane potential mV (Mean ±SEM)	Standard Deviation mV (Mean ±SEM)
Standard (I1+ E1)	-3.985±1.737	0.968±0.531
LCl (I1+ E2)	+15.559±8.155	1.678±0.443
Ca^{2+} (I2+ E1)	0.546±2.884	0.734±0.241
Ca^{2+}-LCl (I2+ E2)	+22.980±4.891	1.264±0.277
ATP (I3+ E1)	-6.031±1.496	1.331±0.422
ATP-LCl (I3+ E2)	+9.485±1.710	2.272±0.422
Ca^{2+}+ATP (I4+ E1)	-15.094±3.517	1.352±0.213
Ca^{2+}+ATP-LCl (I4+ E2)	+4.964±3.92	2.210±0.36

Figure (8.3a) represents the resting membrane potential recorded from group (GCl2). The pipette solution contain an additional 1 μM Ca^{2+} and the medium (bath) is standard. The calculated mean of the resting membrane potential is relatively depolarized with respect to the control case (MP= 0.546 mV, p=0.18).

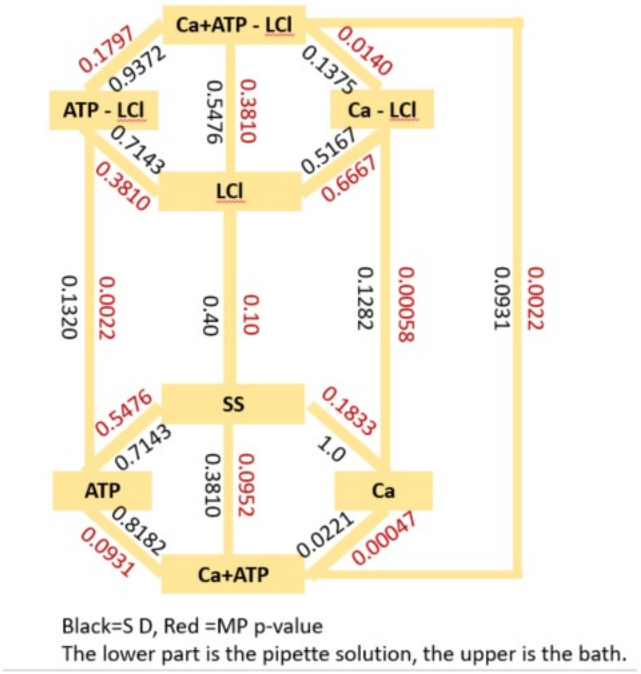

Figure 8.1: Significance between each two cases in Cl-dominant groups of Jurkat T cells was checked using Wilcoxon signed-rank test and the significant value is considered for p <0.05, SD:standard deviation (p-value in black) and MP: membrane potential (p-value in red), abbreviations as in figure 5.1 and LCl: lowering Cl^- in the bath from 162 to 6mM

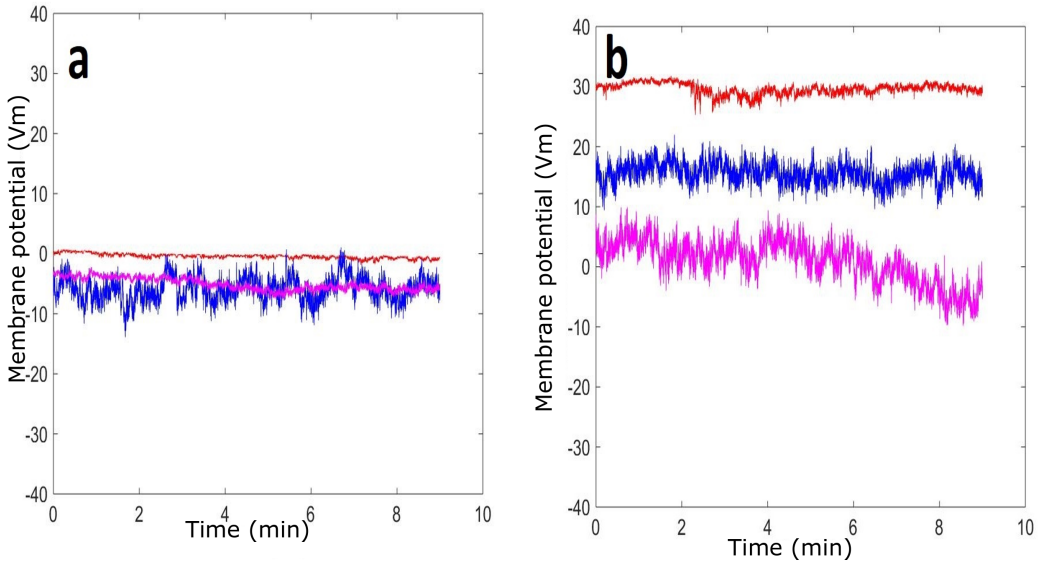

Figure 8.2: Recordings of the resting membrane potential of Jurkat T cells group GCl1 using whole-cell patch-clamp, a) the pipette solution is standard (I1) and the bath is standard (E1), b) the pipette solution is standard (I1) , and the bath with low extracellular concentration of Cl^- (E2), N=3, p=0.1

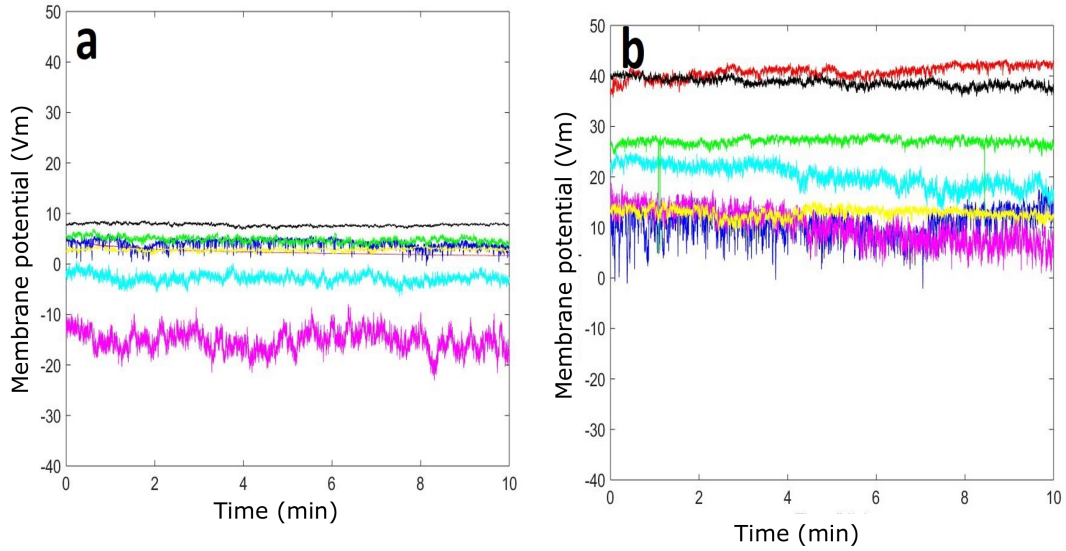

Figure 8.3: Recordings of the resting membrane potential of Jurkat T cells group GCl2 using whole-cell patch-clamp, a) the pipette solution is standard+ 1μM Ca^{2+} (I2) and the bath is standard (E1), b) the pipette solution is standard +1μM Ca^{2+}(I2) , and the bath with low extracellular concentration of Cl^- (E2Cl), N=7, p=0.00058

The extracellular Cl^- is lowered in the bath solution and the pipette solution still contains 1μM Ca^{2+}. The calculated mean of the resting membrane potential, from figure (8.3b), is significantly depolarized to +22.98 mV (p=0.00058) and the standard deviation magnified insignificantly to 1.264 mV (p =0.093).

The standard solution of the pipette is replaced by ATP solution (I3) and the bath solution remain standard. A new group (GCl3) of Jurlat cells is used in the measurements. The results are plotted in figure (8.4a) and the mean and the standard deviation were calculated. The mean is slightly hyperpolarised to -6.03 mV (p=0.548) and the standard deviation increases insignificantly to 1.33 mV (p= 0.714). Figure (8.4b) shows the recordings from the same group after decreasing the extracellular Cl^-. The calculated mean of the resting membrane potential becomes significantly depolarized (MP=9.458 mV, p= 0.0022) and the standard deviation magnified to its highest value (sd=2.27 mV, p=0.132).

In the last group (GCl4), both ATP and Ca^{2+} are introduced in the pipette solutions and the resting membrane potential is recorded for each cell. The record-

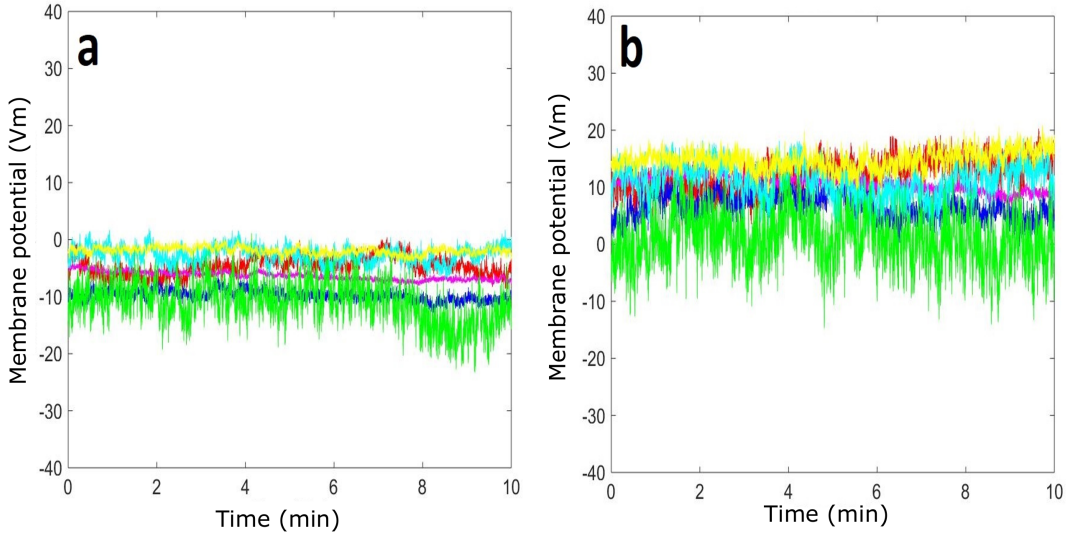

Figure 8.4: Recordings of the resting membrane potential of Jurkat T cells group GCl3 using whole-cell patch-clamp, a) the pipette solution is standard +ATP(I3) and the bath is standard (E1), b) the pipette solution is standard +ATP(I3), and the bath with low extracellular concentration of Cl^- (E2Cl), N=6, p=0.0022

ings are represented in figure (8.5a). The mean and the standard deviation of the steady state of the membrane potential are calculated. The membrane is hyperpolarised to its largest value (-15.09 mV), (p=0.095) and the standard deviation insignificantly increases to 1.35 mV (p=0.38). Recordings are continued by replacing the bath to lower extracellular Cl^- to 6mM. The calculated mean of the membrane potential is significantly depolarized to 4.96 mV (p=0.0022) and the standard deviation increases to 2.21 mV (p=0.093).

8.2.2 Cohort 3: Na^+-dominant

In this work, Jurkat T lymphocytes are categorized into three groups, the third one is Na^+-dominant (cohort3) in which 3 groups of cells are used to do measurements, because it is not easy to measure the membrane potential introducing Ca^{2+} in Na^+-dominant cells. The pipette solutions used are I1, I3 and I4 and the bath solutions are the standard (E1) and a lowered extracellular Na^+ solution (ENa2). Calculation of the mean and the standard deviation of the steady value of the

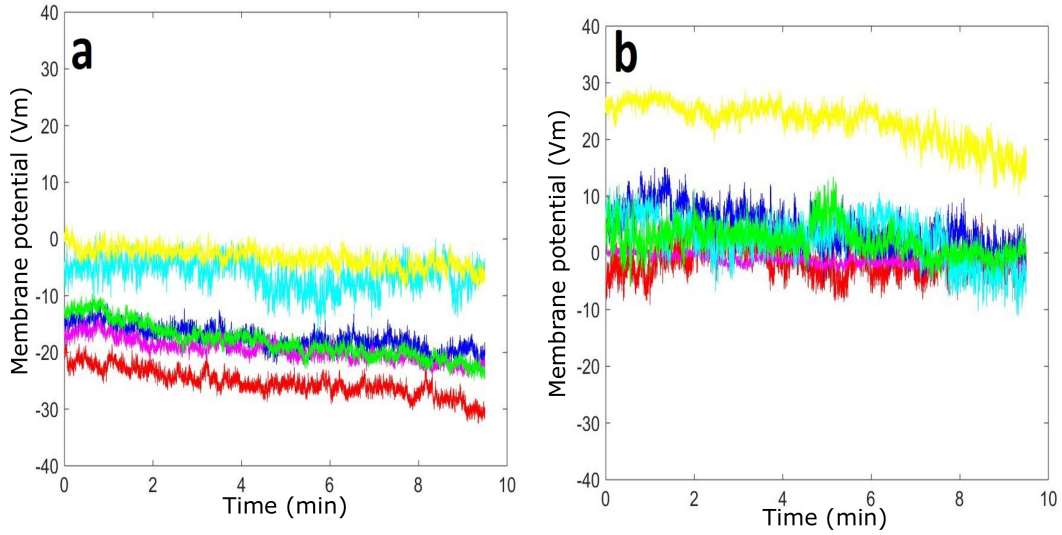

Figure 8.5: Recordings of the resting membrane potential of Jurkat T cells group GCl4 using whole-cell patch-clamp, a) the pipette solution is standard +ATP +1μM Ca^{2+}(I4) and the bath is standard (E1), b) the pipette solution is standard +ATP +1μM Ca^{2+}(I4) , and the bath with low extracellular concentration of Cl^{-} (E2Cl), N=6, p=0.0022

membrane potential are done and presented in table (8.2) as Mean ±SEM. Significance between cases are tested using Wilcoxon signed-rank test and significant values were considered for p <0.05.

Figure (8.7a) shows the resting membrane potential from group (GNa1), with which the pipettes solution is standard (I1) and the bath is standard (E1). This group is considered as the control. The calculated mean of the resting membrane potential and the standard deviation are -7.489 mV and 1.955 mV respectively. The bath solution is replaced by the solution (ENa2), extracellular Na^{+} concentration is lowered from 150 mM to 10 mM, and the recordings are continued and then plotted in figure (8.7b). The mean and the standard deviation in the resting membrane potential are calculated. A significant hyperpolarization is observed (MP =-21.0087 mV, p=0.026) and the standard deviation deceased significantly to 0.684 mV (p= 0.004).

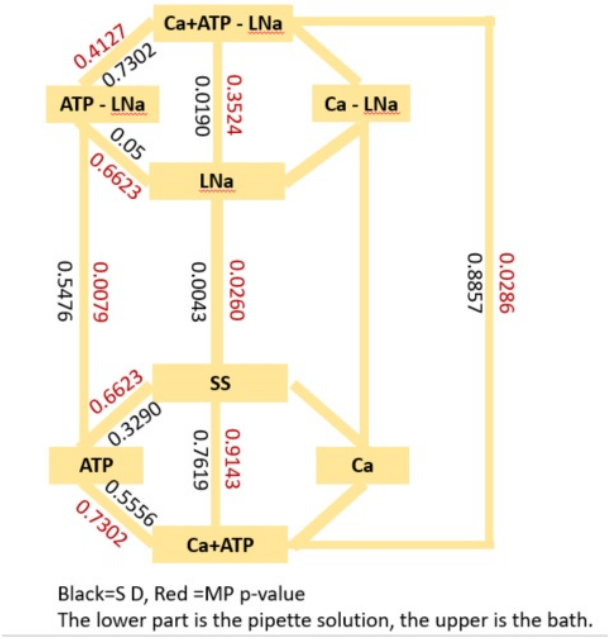

Figure 8.6: Significance between each two cases in Na-dominant groups of Jurkat T cells was checked using the Wilcoxon signed-rank test and the significant value is considered for p <0.05, SD:standard deviation (p-value in black) and MP: membrane potential (p-value in red), abbreviations as in figure 5.1 and LNa: lowering Na^+ in the bath from 150 to 10 mM

Table 8.2: Resting membrane potential and standard deviation in Na^+-dominant jurkat T cells (Cohort3), LNa: low $[Na^+]_o$

Solution	Membrane potential mV (Mean ±SEM)	Standard Deviation mV (Mean ±SEM)
Standard (I1+ E1)	-7.489±3.303	1.955±0.316
LNa (I1+ ENa2)	-21.008±1.394	0.684±0.112
ATP (I3+ E1)	-5.565±3.511	1.554±0.836
ATP-LNa (I3+ ENa2)	-19.296±1.889	1.585±0.474
Ca^{2+}+ATP (I4+ E1)	-6.966±0.828	1.525±0.301
Ca^{2+}+ATP-LNa (I4+ ENa2)	-17.168±3.010	1.41±0.138

ATP is introduced in the pipette solution(I3) and is used with a standard bath (E1) to record the resting membrane potential from a new group of Jurkat T cells (GNa2). The data is plotted in figure (8.8a). The calculated mean and the standard deviation of the resting potential are respectively, -5.565 mV and 1.554 mV and the p-values are 0.66 and 0.329 respectively. The recordings are continued after lowering the extracellular Na^+ concentration from 150 mM to 10

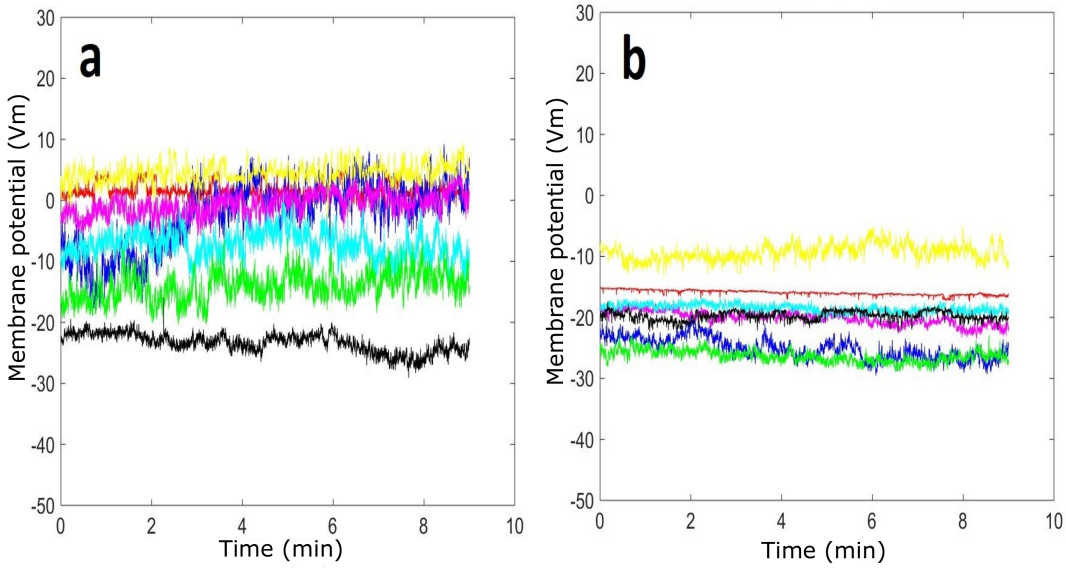

Figure 8.7: Recordings of the resting membrane potential of Jurkat T cells group GNa1 using whole-cell patch-clamp, a) the pipette solution is standard (I1) and the bath is standard (E1), b) the pipette solution is standard0. (I1) , and the bath with low extracellular concentration of Na^+ (ENa2), N=7, p=0.026

mM. The steady value of the membrane potential is -19.296 mV (p=0.0079) and the standard deviation is 1.585 mV (p=0.548), see figure (8.8b). The last group of Na^+-dominant Jurkat cells used in measurements was introduced to a pipette solution (I4), which contains ATP and Ca^{2+}. The recorded membrane potentials are represented in figure (8.9a). The membrane potential is closed to the control (MP= -6.966 mV, p=0.914) and the standard deviation is slightly smaller compared to the control (sd= 1.525 mV, p=0.762). After replacement of the medium by ENa2 (low $[Na^+]_o$), recordings of the steady membrane potential is continued. The mean of the membrane potential hyperpolarised significantly (p=0.0286) and the standard deviation insignificantly decreased to 1.41 mV (p= 0.886).

8.2.3 Discussion of cohort2 and cohort 3

Cl^--dominant)

As mentioned before, previous studies reported that jurkat cells, under physiological conditions, are dominated by voltage-gated K^+ channels (Kv1.3). But. in this

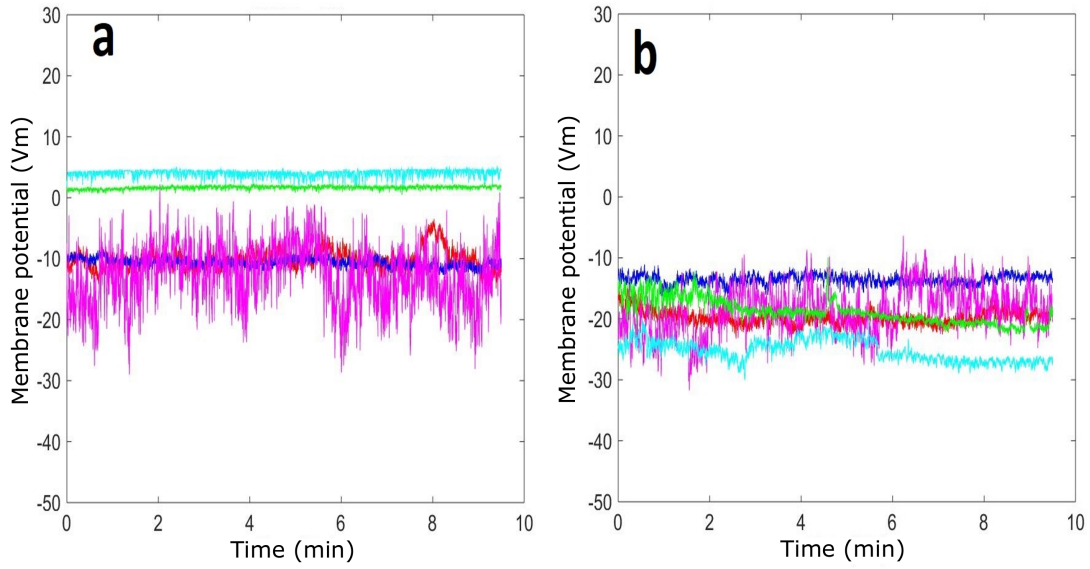

Figure 8.8: Recordings of the resting membrane potential of Jurkat T cells group GNa2 using whole-cell patch-clamp, a) the pipette solution is standard +ATP (I3) and the bath is standard (E1), b) the pipette solution is standard + ATP (I3) , and the bath with low extracellular concentration of Na^+ (ENa2), N=5, p=0.0079

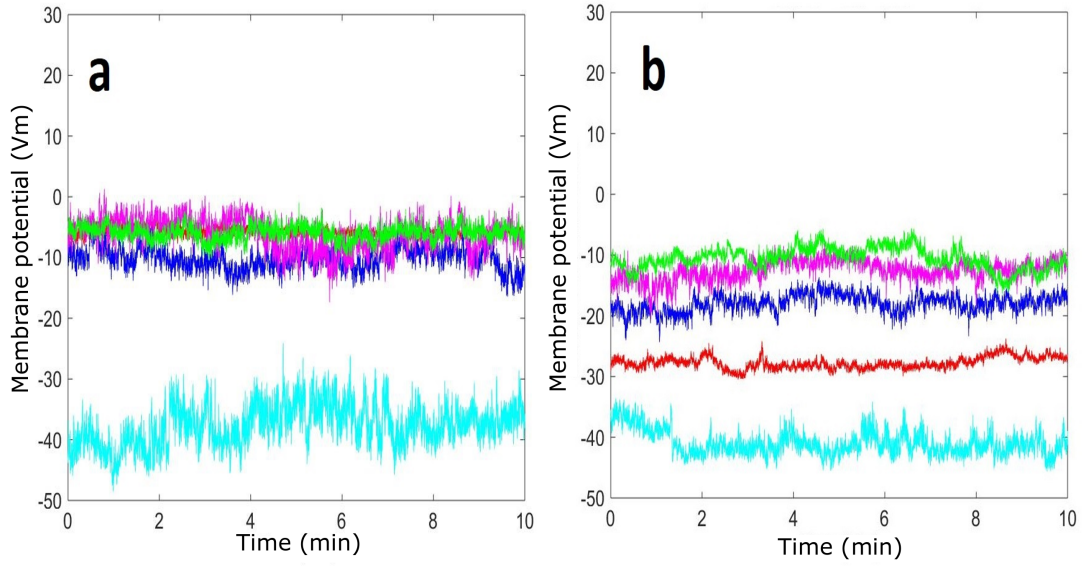

Figure 8.9: Recordings of the resting membrane potential of Jurkat T cells group GNa3 using whole-cell patch-clamp, a) the pipette solution is standard +ATP $+1\mu$M Ca^{2+} (I4) and the bath is standard (E1), b) the pipette solution is standard + ATP $+1\mu$M Ca^{2+} (I4 , and the bath with low extracellular concentration of Na^+ (ENa2), N=5, p=0.0286

work we show that jurkat cells are 3 cohorts; the first is the one discussed, K^+ -dominant, the second is Cl^--dominant and the third is Na^+-dominant.

Table 8.3: Driving force and the amplitude of fluctuation in Cl^--dominant jurkat T cells (Cohort2), LCl: low $[Cl^-]_o$

Solution	Driving Force (mV)	Amplitude of fluctuations (mV)
Standard (I1+ E1)	-0.35	0.968
LCl (I1+ E2)	-63.19	1.678
Ca^{2+} (I2+ E1)	+4.2	0.734
Ca^{2+}-LCl (I2+ E2)	-55.77	1.264
ATP (I3+ E1)	-2.38	1.331
ATP-LCl (I3+ E2)	-69.26	2.272
Ca^{2+}+ATP (I4+ E1)	-11.45	1.352
Ca^{2+}+ATP-LCl (I4+ E2)	-73.79	2.210

To confirm the hypotheses of this work, all cohorts were used in measurements. The intracellular solutions used in the pipette were the same with all cohorts; standard (I1), 1 μM Ca^{2+} was added (I2), 4mM ATP was added (I3) and both 4mM ATP and 1 μM Ca^{2+} were added together (I4). But, the medium (bath) solutions were used with all cohorts are the standard and another altered bath in which the extracellular concentration of K^+, Cl^- or Na^+ was altered depends on the group of cells.

In cohort2, comparing the mean of the measured membrane potential using standard bath with measurement from cells in an altered bath (Cl^- was lowered from 162 mM to 6 mM), despite what intracellular solution was used, shows significant depolarization and shows an increase in the amplitude of the fluctuation, which is proportional to the driving force of Cl^- ions. Table (8.3) shows the calculated driving forces of Cl^- ion in all cases and the amplitude of fluctuations. Plotting the driving force vs the amplitude of fluctuations in all cases measured with an altered medium show a linear relationship (see figure 8.10). In these cases, the membrane was depolarized and the membrane conductance was approximately constant. This result suggests that Cl^--dominant jurkat cells have no ion channels

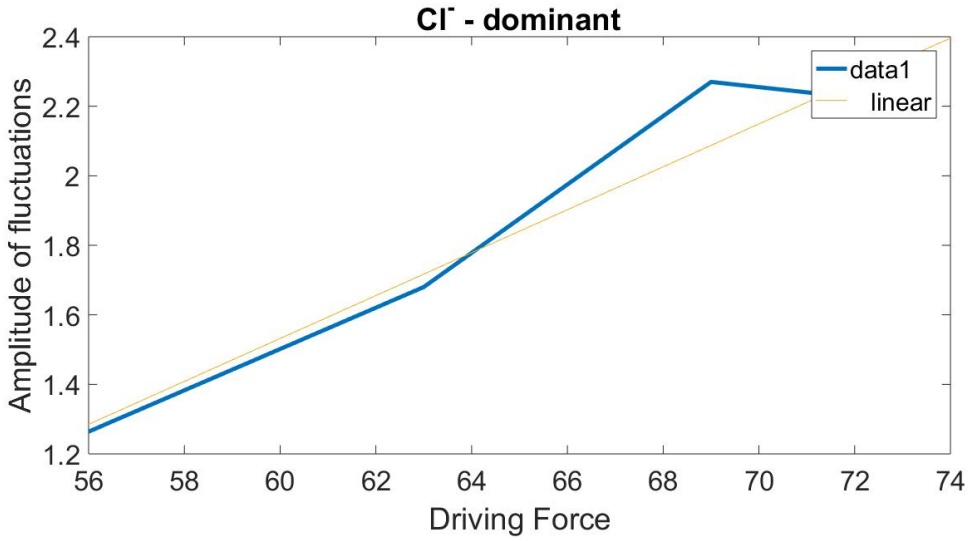

Figure 8.10: Relationship between the amplitude of the resting membrane potential of Jurkat T cells vs driving force of Cl^- ions measured from cells with altered medium to a low concentration of Cl^- (6mM), the pipette solution was I1, I2, I3, and I4

that show voltage dependence in this work, which is consistent with Cl^- diffusion.

As shown in the table (8.3), the driving force of Cl^- ions are negative in approximately every case. This sign means that Cl^- ions are moving out of the cell to the extracellular medium in the direction of the electric force, which dominates the chemical force. Since lymphocytes possess higher intracellular Cl^- concentrations relative to the equilibrium value [418], it is recommended to have an active mechanism to regulate Cl^- ions. This mechanism uses the antiporter $Cl^-/HCO_3{}^-$, which is usually essential in pH and cell volume regulation [246]. It was reported that this antiporter is Na^+-dependent [419], then by the same authors and after 13 years, they contradict their first results by reporting that $Cl^-/HCO_3{}^-$ is independent of extracellular Na^+.

When Ca^{2+} was introduced in the pipette, the driving force becomes positive, which means that Cl^- ions are moving into the cell. An insignificant decrease in the amplitude of fluctuation from 0.968 to 0.734 mV appears, which opposes the effect of activation of CFTR channels by Ca^{2+} [191]

ATP is known to activate Cl^-_{mini} [193]. Therefore, when ATP was added to the pipette, the membrane hyperpolarised to -6.03 mV and the amplitude of the fluctuation increased due to an increase in the membrane conductance. But, since the driving force is negative, it was expected to depolarize the membrane. This result may suggest a movement of K^+ ions in parallel to Cl^-, to verify neutrality.

But, when both Ca^{2+} and ATP were added to the pipette solution, the membrane was hyperpolarised to -15.094 mV, which is expected, because the activation of Cl^-_{mini} is enhanced when both ATP and Ca^{2+} exist together [218]. The amplitude of the fluctuation, in this case, is approximately the same as in the case when ATP been added alone. This result is difficult to be explained because it was expected to magnify the amplitude due to the increase in the membrane conductance caused by Cl^-_{mini} activation.

Na^+-dominant

The third group of jurkat cells reported in this work is Na^+-dominant. The current in this group is dominated by the sodium current over other ions. Measurements were done as before using the same intracellular solutions except for I2, in which Ca^{2+} is to be introduced. It was difficult to get recordings of the membrane potential from Na^+-dominant cells when Ca^{2+} was added inside the cells. Two extracellular mediums were used in the measurements; one is the standard solution E1 and the another is ENa2, in which Na^+ concentration was lowered from 150 mM to 10 mM.

Significances in the membrane potential were obtained when the extracellular solution was ENa2. This suggests that the hyperpolarization observed in the recordings of the membrane potential is due to the shift in Na^+ equilibrium potential. There were no significances in the membrane potential when ATP or ATP with Ca^{2+} was added inside the cells. Surprisingly, ATP causes approximately no change in the membrane potential. An effect which is not expected by

the Na^+/K^+-ATPase (pump). The pump usually hyperpolarizes the membrane through the extrusion of $3Na^+$ and taken in $2K^+$ in each cycle exploiting the energy from the hydrolysis of ATP. No Na^+ ion channel is known to be activated by ATP. This result may be interpreted by the diffusion of Na^+ and K^+ from the pipette to the cell, therefore, there is no need to fuel the pump with ATP to move these ions against their gradients. The same result was obtained when ATP and Ca^{2+} were added simultaneously to the intracellular solution. This result is may be due to the activation of TRPM4 by Ca^{2+} and inactivation of Nav1.5 also by Ca^{2+} [191, 403]

Table 8.4: Driving force and the amplitude of fluctuation in Na^+-dominant jurkat T cells (Cohort3), LNa: low $[Na^+]_o$

Solution	Driving Force (mV)	Amplitude of fluctuations (mV)
Standard (I1+ E1)	-56.2	1.955
LNa (I1+ ENa2)	-2.05	0.684
ATP (I3+ E1)	-55.96	1.554
ATP-LNa (I3+ ENa2)	-2	1.585
Ca^{2+}+ATP (I4+ E1)	-63.52	1.525
Ca^{2+}+ATP-LNa (I4+ ENa2)	-4.7	1.41

The depolarization in the membrane potential, when ATP or ATP with Ca^{2+} were added inside cells, may be due to an activation of Cl^- channel by ATP and activation of K^+ channels by Ca^{2+} (KCa).

The amplitude of the fluctuations change significantly when the standard medium of the control cells are replaced by ENa2 (Low extracellular Na^+). This suggests that this change is due to the change in the driving force of Cl^- ions (see table 8.4). Two other cases in which the amplitude of the fluctuations changes significantly. In these cases ATP and both ATP with Ca^{2+} were introduced in the intracellular solution and when the extracellular solution was ENa2. The driving force and the membrane potential were approximately constants in both cases. Therefore, we have to exclude the effects of the driving force and the activation

of voltage-gated Na^+ channels (such as Nav1.5 which was found in 10% of jurkat cells). These results suggest that ATP may have an effect on an ion channel in an altered medium with low extracellular Na^+.

When ATP and Ca^{2+} are introduced inside the cells in the standard medium, the amplitude of the fluctuation decreases insignificantly. Therefore, the results obtained from the cells after the addition of ATP with or without Ca^{2+} inside cells are difficult to be explained. Because in literature there is no Na^+ ion channel which is activated by ATP in low Na^+ concentrations.

A future work is needed to be taken to study the effect of ATP and Ca^{2+} on Na^+-dominant jurkat cells.

The analysis of the data using time-averaged wavelet power (TAWP) confirms our hypotheses. In cohort 1, the elevation of extracellular K^+ significantly changes the time-averaged wavelet power of the spectrum. This result supports that the driving force change causes this effect. In the same cohort, the addition of ATP or Ca^{2+} causes also a significant change in the TAWP, which supports the effect of the membrane conductance on the dynamics of the resting membrane potential.

in cohort 2, when the chloride was lowered in the bath their was an insignificant increase in the TAWP. This increase was accompanied by an increase in the driving force of Cl^- ions. When ATP was added to the pipette solution, an insignificant increase in the TAWP was obtained. This increase in TAWP may be attributed to the increase in conductance of the membrane to chloride ions due to activation of Cl^--mini channel by ATP. This result can be confirmed by the addition of Ca^{2+} simultaneously with ATP because the presence of Ca^{2+} enhances the activation of Cl^--mini by ATP. The result of the addition of Ca^{2+} simultaneously with ATP to the pipette positively affects the TAWP. The TAWP increases as a result of an increase in open Cl^--mini channels.

In cohort 3, the alteration of extracellular Na^+ causes a significant decrease in TAWP only when the pipette solution was standard. But when the pipette solution

was altered by the addition of ATP or ATP with calcium, the decrease in TAWP was insignificant. This decrease may be interpreted by the decrease in the driving force of Na^+ ions, which cause a decrease in the amplitude of the dynamics in the resting membrane potential. There was no evidence that the added molecules to the pipette cause any change in the membrane conductance to Na^+ ions. The only one was expected to cause a change in conductance is Ca^{2+}, which was difficult to give recordings of the membrane potential. The difficulty may be attributed to the inhibitory effect of Ca^{2+} on Na^+ channels.

In conclusion, the data recorded from Na^+-dominant jurkat cells supports the hypothesis of this work, that the driving force has a substantial effect on the amplitude of the membrane potential. But, it was difficult to interpret the effect of the added molecules on the conductance of the membrane. therefore, it was difficult to test the second hypothesis using the data from Na^+-dominant jurkat cells because it was difficult to do recordings when Ca^{2+} was introduced. Ca^{2+} is known to activate TRPM4 channels, which is selective to Na^+ over other cations [191]. Another difficulty in testing the second hypothesis was due to the significant effect of ATP on the amplitude of the fluctuations, which is not expected because ATP is not known to activate Na^+ channels.

8.2.4 Time-averaged wavelet power of cohorts 2 And 3)

The same calculations were done with all signals from Cl^--dominant jurkat cells. The mean of time-averaged wavelet power over all frequencies of interest (0.01-10 Hz) was calculated and the significance between all cases was checked using Wilcoxon signed-rank and sum-rank tests, as mentioned previously. The results are tabulated in table 8.5 and the values were considered significant for $p < 0.05$ and highlighted in orange.

As shown in table 8.5, despite the significance in resting membrane potential

and in the amplitude of fluctuations discussed in previous sections, there was no significance change in the time-averaged wavelet power in all cases of Cl^--dominant jurkat cells. Figures (8.11 - 8.13) show the spectrum obtained for each pair of signals to compare between different cases.

Table 8.5: The mean of time averaged wavelet power calculated to each case in jurkat T cells (Cohort2) and the significance between each two cases was calculated using Wilcoxon signed-rank test , LCl: Low $[Cl^-]_o$, SS:standard solution, SCa: Ca^{2+} was added to pipette,ATP: ATP was added to pipette, CaATP: Ca and ATP were added to the pipette, CaCl: Ca was added to the pipette and Cl^- was lowered in the medium, ATPCl: ATP was added to the pipette and Cl^- was lowered in the medium, CaATPCl: Ca and ATP were added to the pipette and Cl^- was lowered in the medium. Significant differences ($p < 0.05$) are highlighted in orange.

Solutions (X-Y) (i.e. X=SS and Y=LCl in first row)	Mean of the time averaged wavelet power of X mV^2/s	Mean of the time averaged wavelet power of Y mV^2/s	p-value
SS-LCl	0.0878	0.1684	0.4000
ATP-ATPCl	0.1383	0.2484	0.0931
Ca-CaCl	0.0695	0.1285	0.0931
CaATP-CaATPCl	0.1434	0.2126	0.1282
SS-Ca	0.0878	0.0695	1.000
SS-ATP	0.0878	0.1383	0.5476
SS-CaATP	0.0878	0.1434	0.3810
LCl-CaCl	0.1684	0.1285	1.000
LCl-ATPCl	0.1684	0.2484	0.5476
LCl-CaATPCl	0.1684	0.2126	0.3810
Ca-CaATP	0.0695	0.1434	0.1375
ATP-CaATP	0.1383	0.1434	0.6991
Ca-CaATPCl	0.0695	0.2126	0.2949
ATP-CaATPCl	0.1383	0.2126	0.5887

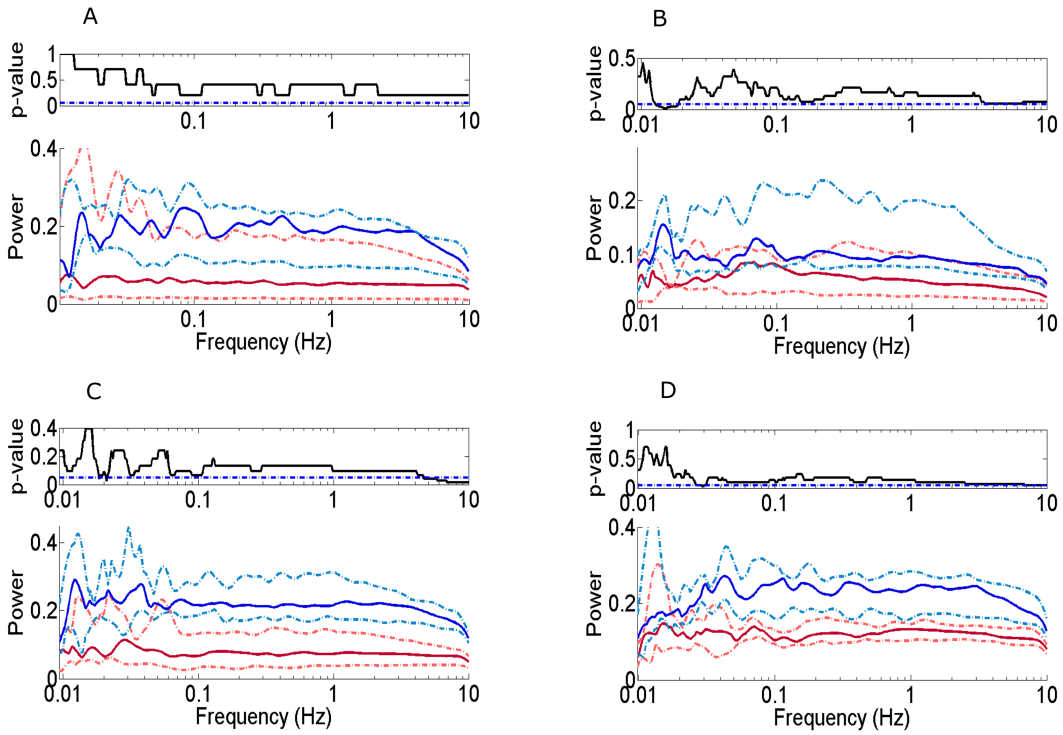

Figure 8.11: Time-averaged wavelet power resting membrane potential of Cl^--dominant jurkat cells. The median for each group is plotted and the dashed lines represent the 25% and the 75% quantiles A) Standard pipette solution with standard bath (red) compared with standard pipette solution with altered bath (Cl^- lowered from 162 mM to 6 mM) (blue). B) Calcium is added to the pipette solution with standard bath data (red) compared with the same pipette solution with altered Cl^- in the bath (blue). C) ATP is added to the pipette solution with standard bath data (red) compared with the same pipette solution with altered Cl^- in the bath (blue). D) ATP and Calcium are added together to the pipette solution with standard bath data (red) compared with the same pipette solution with altered Cl^- in the bath (blue). Significance is plotted separately over each graph in the figure. The p-value <0.05 was considered as significant (dashed-blue line) (See table 8.5). Morlet wavelet is used with central frequency 1.

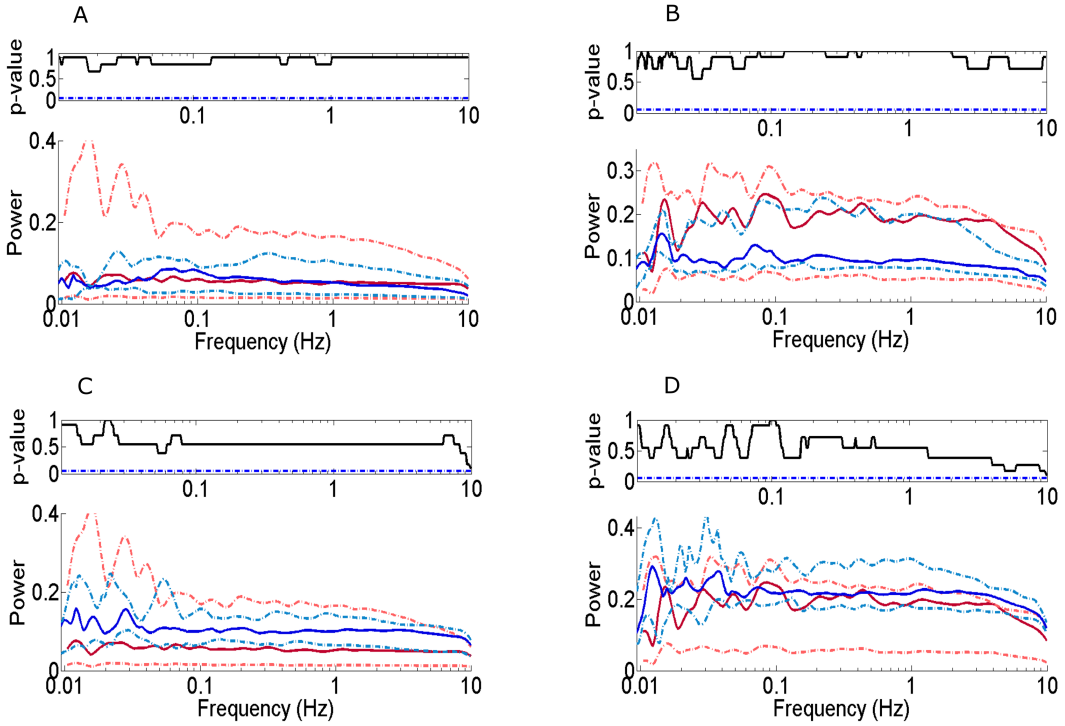

Figure 8.12: Time-averaged wavelet power resting membrane potential of Cl^--dominant jurkat cells. The median for each group is plotted and the dashed lines represent the 25% and the 75% quantiles A) The addition of calcium with standard bath (blue) compared to the control case (red). B) The addition of calcium with altered chloride in the bath (blue) compared with the standard pipette with altered bath (red). C) The addition of ATP with standard bath compared (blue) to the control case (red). D) The addition of ATP with altered chloride in the bath (blue) compared with the standard pipette with altered bath (red). Significance is plotted separately over each graph in the figure. The p-value <0.05 was considered as significant (dashed-blue line) (See table 8.5). Morlet wavelet is used with central frequency 1.

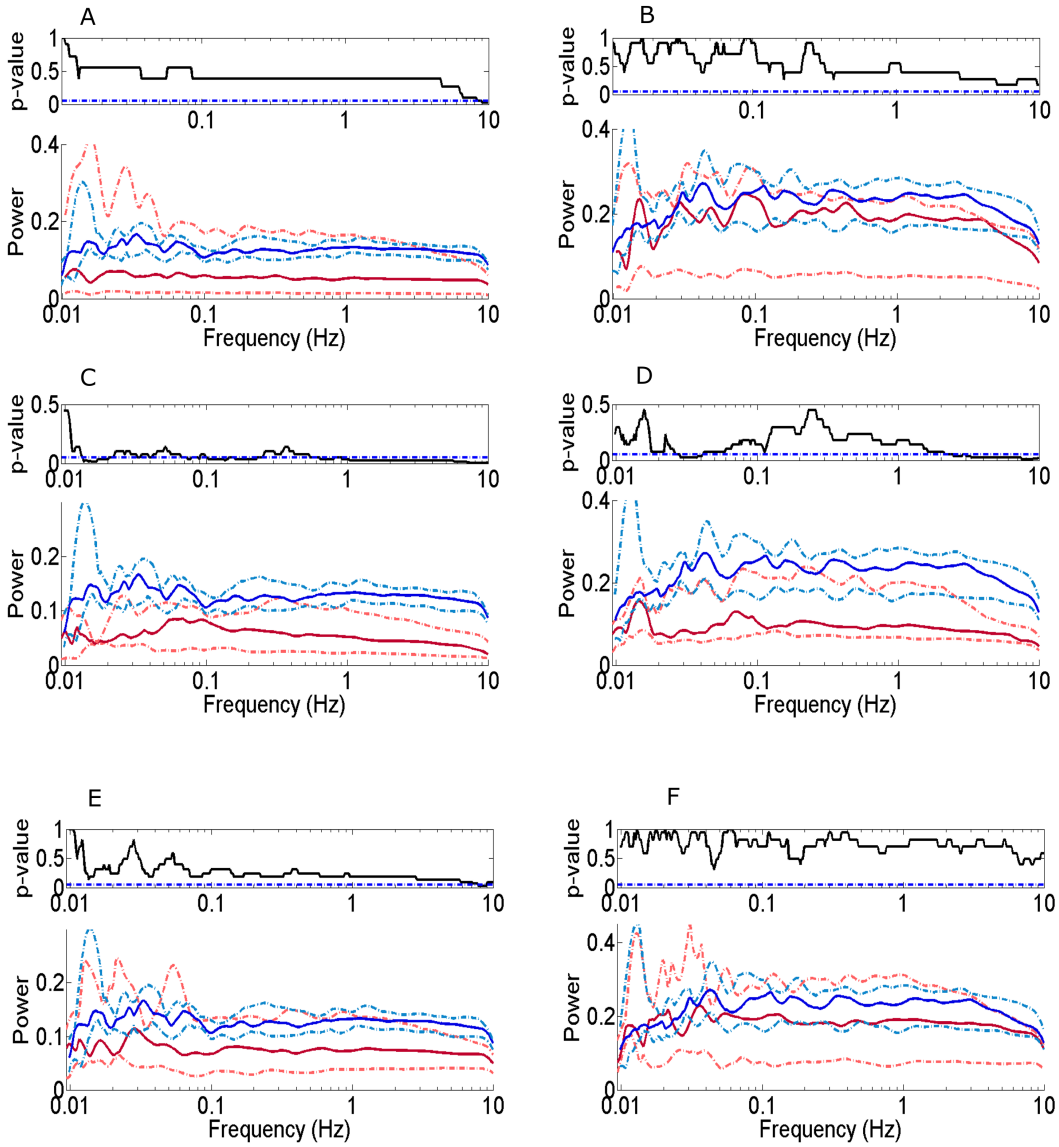

Figure 8.13: Time-averaged wavelet power resting membrane potential of Cl^--dominant jurkat cells. The median for each group is plotted and the dashed lines represent the 25% and the 75% quantiles A) The addition of both ATP and calcium with standard bath (blue) compared with the control (red). B) The addition of both ATP and calcium with altered bath (Chloride is lowered from 162 mM to 6 mM) (blue) compared with standard pipette solution with altered bath (red). C) The addition of calcium with standard bath (red) compared to the addition of both ATP and calcium with standard bath (blue). D) The addition of calcium with altered bath (red) compared to the addition of both ATP and calcium with altered bath (blue). E) The addition of ATP with standard bath (red) compared to the addition of both ATP and calcium with standard bath (blue). F) The addition of ATP with altered bath (red) compared to the addition of both ATP and calcium with altered bath (blue). Significance is plotted separately over each graph in the figure. The p-value <0.05 was considered as significant (dashed-blue line) (See table 8.5). Morlet wavelet is used with central frequency 1.

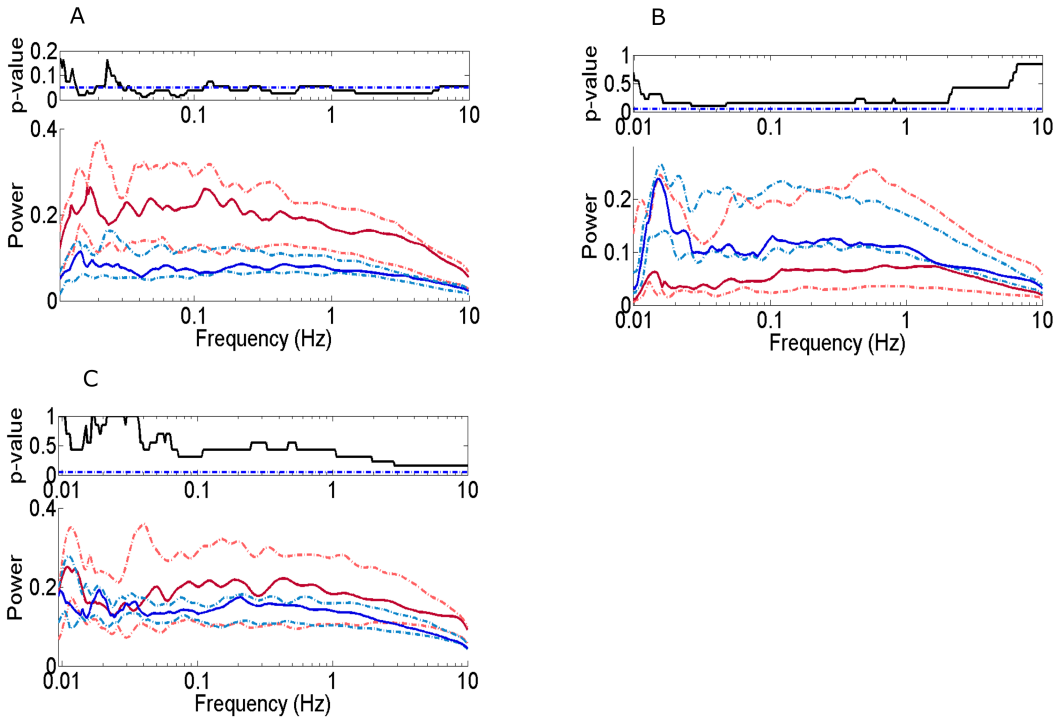

Figure 8.14: Time-averaged wavelet power resting membrane potential of Na^+-dominant jurkat cells. The median, 25% Quantile and 75% Quantile are plotted for each group A) The control case (red) compared with the lowered sodium (blue) in the bath with the standard pipette solution. B) The addition of ATP to the pipette with standard bath (red) compared with the same case with an altered sodium in the bath (blue), (Sodium was lowered from 150 mM to 10 mM). C) The addition of both ATP and calcium with standard bath (red) compared with the same solution with altered bath (blue). Significance is plotted separately over each graph in the figure. The p-value <0.05 was considered as significant (dashed-blue line) (See table 8.6). Morlet wavelet is used with central frequency 1.

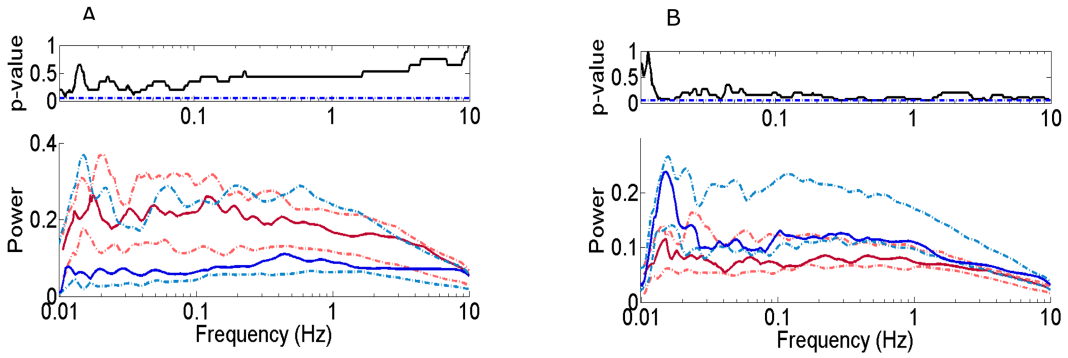

Figure 8.15: Time-averaged wavelet power resting membrane potential of Na^+-dominant jurkat cells. The median, 25% Quantile and 75% Quantile are plotted for each group A) The addition of ATP with standard bath (blue) compared with the control (red). B) The addition of ATP with altered sodium in the bath (blue) compared with the standard pipette solution with altered bath (red) . Significance is plotted separately over each graph in the figure. The p-value <0.05 was considered as significant (dashed-blue line) (See table 8.6). Morlet wavelet is used with central frequency 1.

Table 8.6: The mean of time averaged wavelet power calculated to each case in jurkat T cells (Cohort3) and the significance between each two cases was calculated using Wilcoxon signed-rank test , LNa: Low $[Na^+]_o$, SS:standard solution, ATP: ATP was added to pipette, CaATP: Ca and ATP were added to the pipette, ATPNa: ATP was added to the pipette and Na^+ was lowered in the medium, CaATPNa: Ca and ATP were added to the pipette and Na^+ was lowered in the medium. Significant differences (p <0.05) are highlighted in orange.

Solutions (X-Y) (i.e. X=SS and Y=LCl in first row)	Mean of the time averaged wavelet power of X mV^2/s	Mean of the time averaged wavelet power of Y mV^2/s	p-value
SS-ATP	0.1774	0.1678	0.4318
SS-CaATP	0.1774	0.1938	0.7551
Na-ATPNa	0.0751	0.1519	0.1490
Na-CaATPNa	0.0751	0.1290	0.0480
SS-Na	0.1774	0.0751	0.0041
ATP-ATPNa	0.1678	0.1519	0.1508
CaATP-CaATPNa	0.1938	0.1290	0.4206
CaATP-ATP	0.1938	0.1678	0.5476
ATPNa-CaATPNa	0.1519	0.1290	0.5476

The recordings of the resting membrane potential of cohort 3 (Na^+-dominant) of jurkat cells were analyzed using time domain analysis. In this section, the time-averaged wavelet power is used to analyze the fluctuation in the frequency range 0.01-10 Hz. The mean of time-averaged wavelet power was calculated for each case

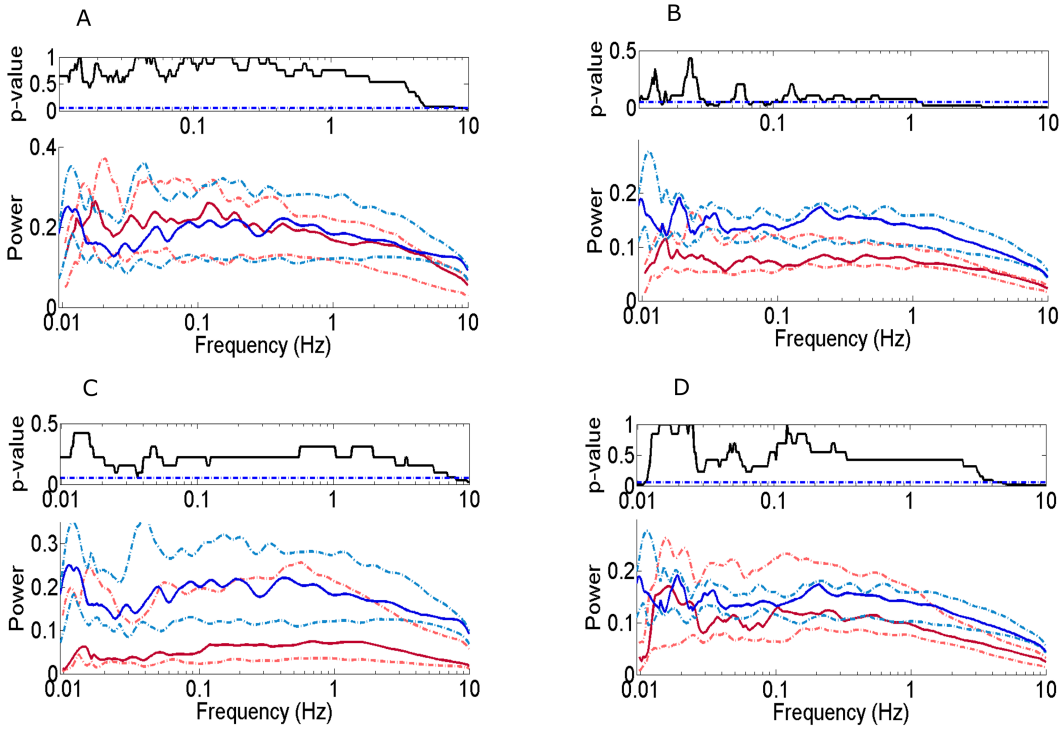

Figure 8.16: Time-averaged wavelet power resting membrane potential of Na^+-dominant jurkat cells. The median, 25% Quantile and 75% Quantile are plotted for each group A) The addition of both ATP and calcium with standard bath (blue) compared with the control (red). B) The addition of both ATP and calcium with altered sodium in the bath (blue) compared with the standard pipette solution with altered bath (red). C) The addition of ATP with standard bath (red) compared with the addition of both ATP and calcium with standard bath (blue). D) The addition of ATP with altered bath (red) compared with the addition of both ATP and calcium with altered bath (blue). Significance is plotted separately over each graph in the figure. The p-value <0.05 was considered as significant (dashed-blue line) (See table 8.6). Morlet wavelet is used with central frequency 1.

and the significance was calculated using Wilcoxon signed-rank and the sum-rank tests for paired and unpaired groups. The results are tabulated in table 8.6.

In two cases, the difference in the time-averaged wavelet power was significant. In one of them, when the control was compared with the case in which the bath was altered to a lower extracellular sodium (from 150 mM to 10 mM). Another case, when the bath was altered while the pipette solution was standard compared to the addition of both ATP and calcium to the pipette, see table 8.6.

In the rest of the cases, the comparison between time-averaged wavelet power was insignificant, see figures (8.14-8.16).

8.3 Appendix C: Coherence between NADH and MMP or pH

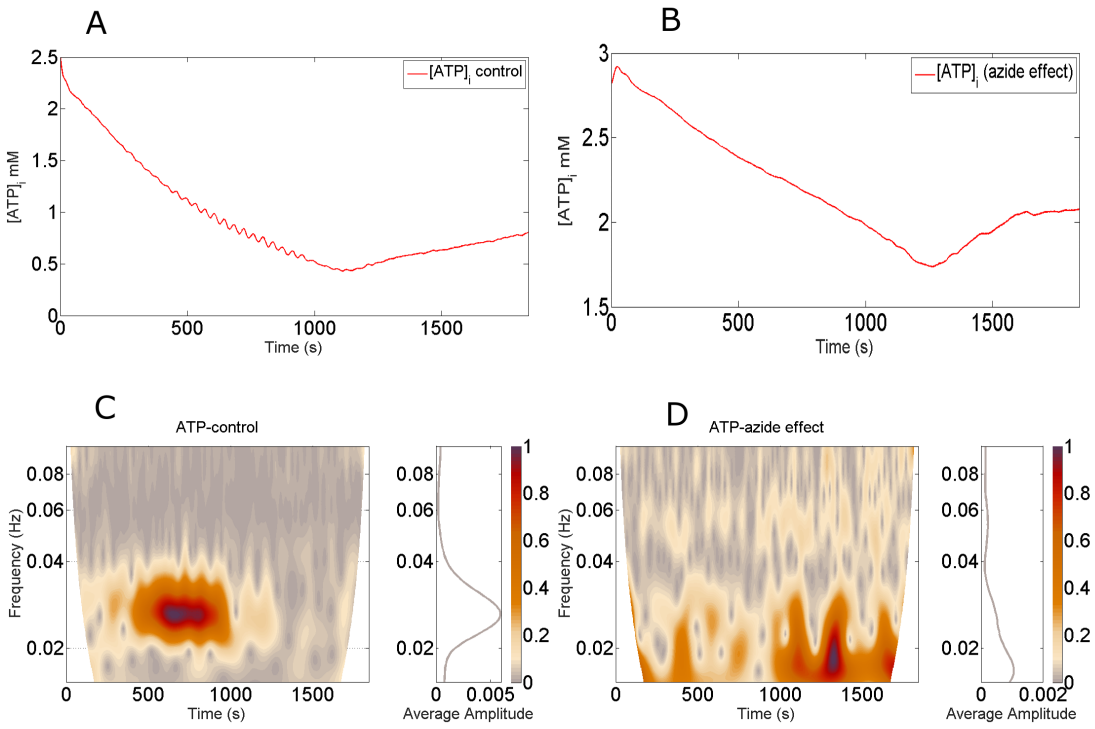

Figure 8.17: The effect of azide on the dynamics of intracellular ATP in yeast cells. Yeast cells were incubated for 10 min in 2mM sodium azide. In the absence (A: time series and C: TFR) or presence (B: time series and D: TFR) of 2mM sodium azide before addition of 30mM glucose and 5mM KCN. Morlet wavelet is used in TFR with central frequency 2.

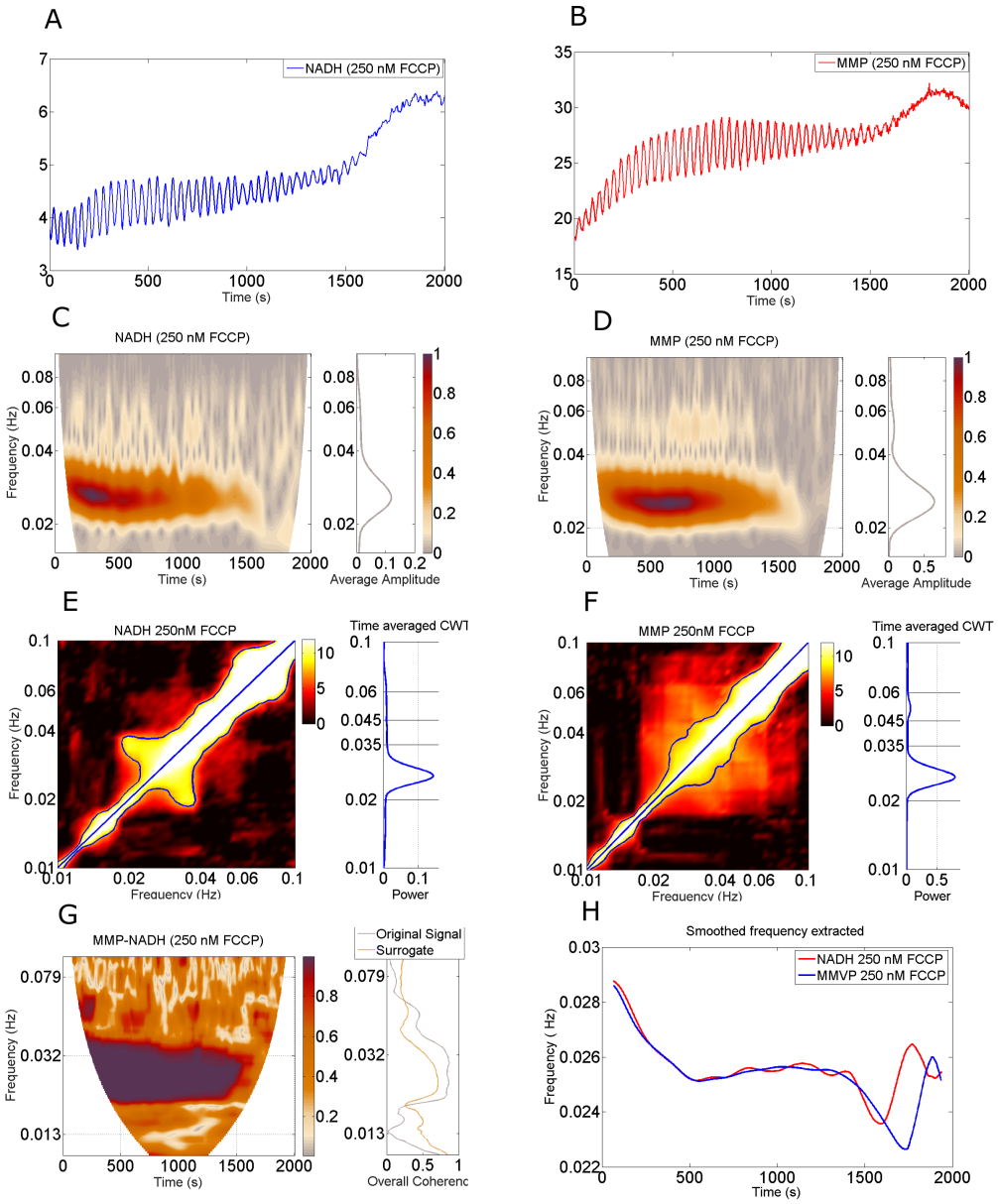

Figure 8.18: Yeast cells were suspended to a density of 10% wet weight in 100 mM phosphate buffer, and cells were incubated for 10 min in 250 nM of FCCP before being transferred. Oscillations were initiated by the addition of 30 mM glucose followed by 5 mM KCN. A) time series of NADH fluorescence. B) time series of $DiOC_2(3)$ fluorescence. C and D) time-frequency representation of A and B respectively. E and F) the mutual information plot relative to the mean and standard deviation of the surrogates. Regions more than 5σ above the surrogate mean are marked with blue, and local maxima are marked with +. G) The windowed phase coherence between NADH and MMP, and the time-averaged wavelet phase coherence. The significance is shown when the coherence of the original data (black line) is higher than the 95th percentile of 200 pairs of IAAFT surrogates (brown line). H) the extracted and smoothed frequency from ridges in TFR of both signals. Morlet wavelet is used in TFR with central frequency of 2, except for E and F the central frequency is 1.

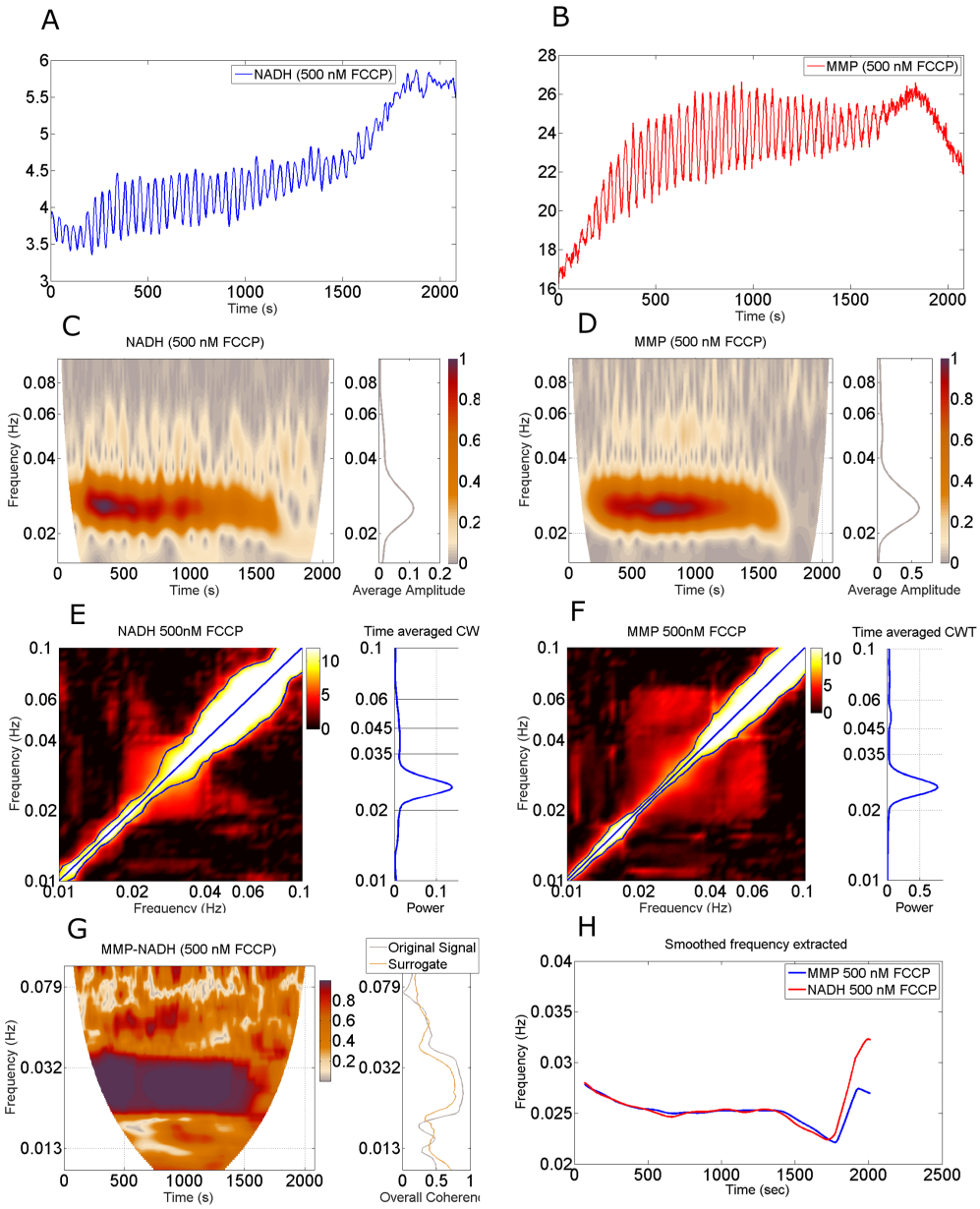

Figure 8.19: Yeast cells were suspended to a density of 10% wet weight in 100 mM phosphate buffer and cells were incubated for 10 min in 500 nM of FCCP before being transferred. Oscillations were initiated by the addition of 30 mM glucose followed by 5 mM KCN. A) time series of NADH fluorescence. B) time series of $DiOC_2(3)$ fluorescence. C and D) time-frequency representation of A and B respectively. E and F) the mutual information plot relative to the mean and standard deviation of the surrogates. Regions more than 5σ above the surrogate mean are marked with blue, and local maxima are marked with +. G) The windowed phase coherence between NADH and MMP, and the time-averaged wavelet phase coherence. The significance is shown when the coherence of the original data (black line) is higher than the 95th percentile of 200 pairs of IAAFT surrogates (brown line). H) the extracted and smoothed frequency from ridges in TFR of both signals. Morlet wavelet is used in TFR with central frequency of 2, except for E and F the central frequency is 1.

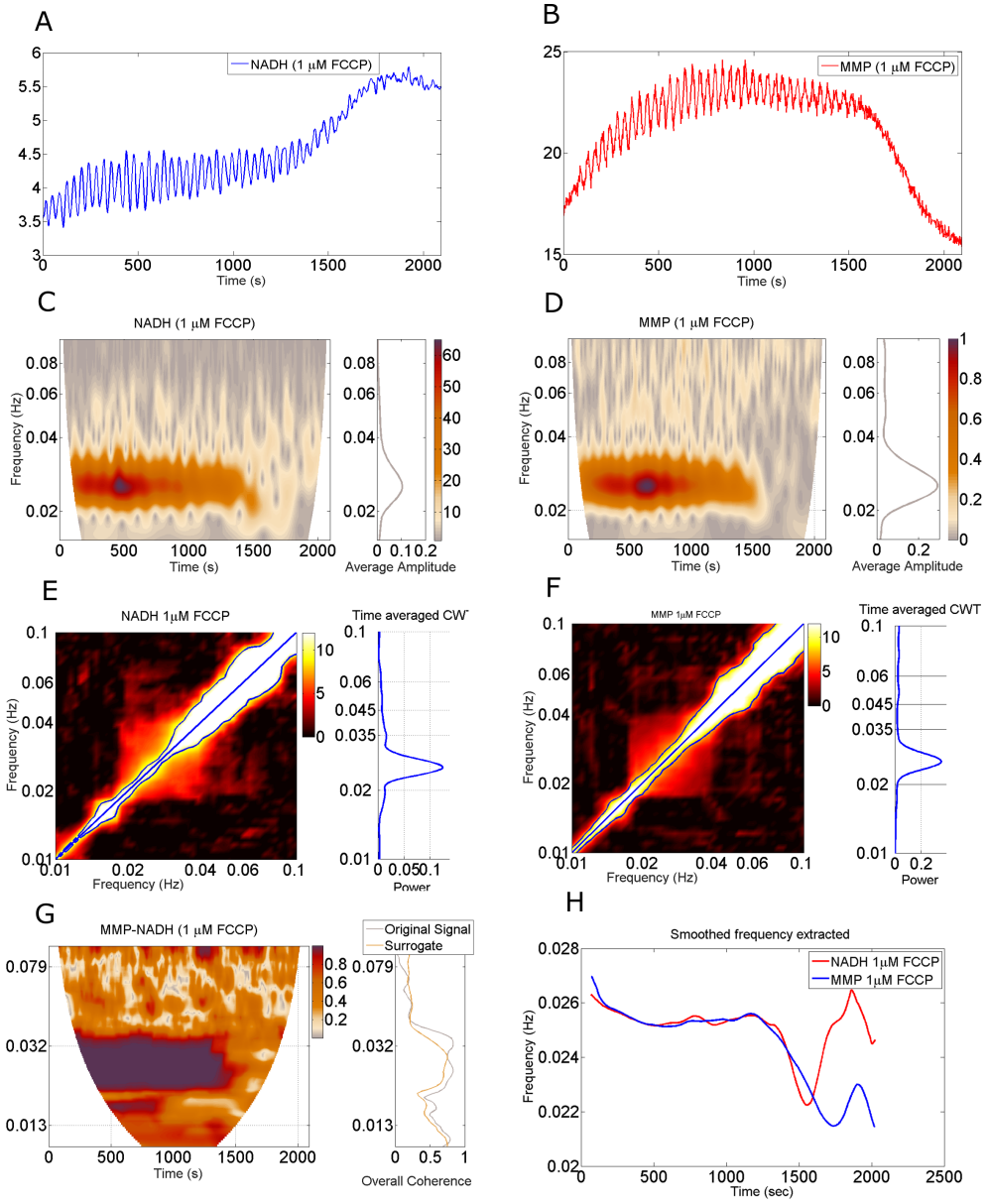

Figure 8.20: Yeast cells were suspended to a density of 10% wet weight in 100 mM phosphate buffer and cells were incubated for 10 min in 1μM of FCCP before being transferred. Oscillations were initiated by the addition of 30 mM glucose followed by 5 mM KCN. A) time series of NADH fluorescence. B) time series of $DiOC_2(3)$ fluorescence. C and D) time-frequency representation of A and B respectively. E and F) the mutual information plot relative to the mean and standard deviation of the surrogates. Regions more than 5σ above the surrogate mean are marked with blue, and local maxima are marked with +. G) The windowed phase coherence between NADH and MMP, and the time-averaged wavelet phase coherence. The significance is shown when the coherence of the original data (black line) is higher than the 95th percentile of 200 pairs of IAAFT surrogates (brown line). H) the extracted and smoothed frequency from ridges in TFR of both signals. Morlet wavelet is used in TFR with central frequency of 2, except for E and F the central frequency is 1.

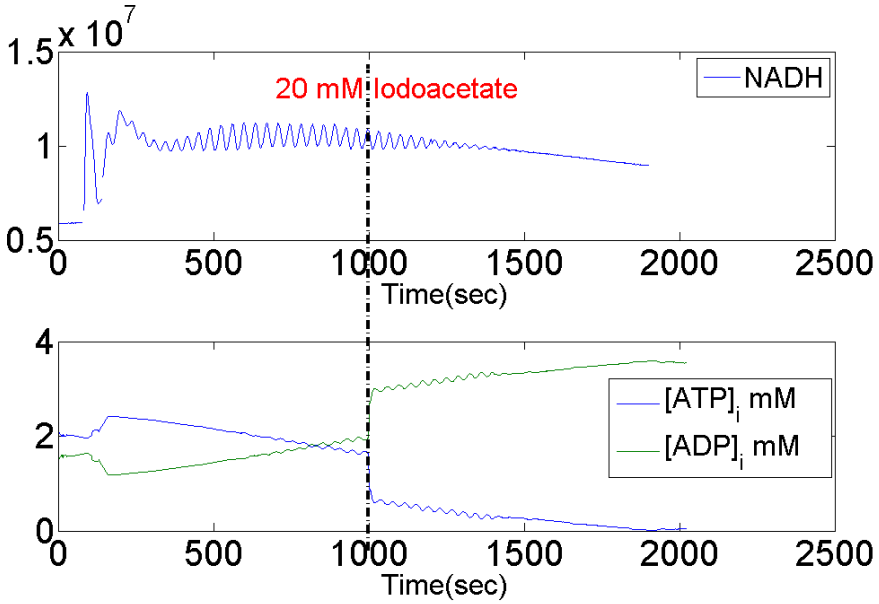

Figure 8.21: The effect of iodoacetate on the oscillations of NADH, ATP, and ADP. Yeast cells were suspended to a density of 10% wet weight in 100 mM phosphate buffer). Glucose and KCN were added as described in Fig. 1. At time 1000 s, 20 mM iodoacetate was added to the suspension. Up) NADH fluorescence time series. Down) ATP and ADP time series.

Bibliography

[1] A. L. Hodgkin and A. F. Huxley, "A quantitative description of membrane current and its application to conduction and excitation in nerve," *J. Physiol.*, vol. 117, no. 4, pp. 500–544, 1952.

[2] S. Patel, *The role of membrane potential dynamics in cell behaviours: investigating the membrane potential dynamics in the Jurkat and HMEC-1 cell lines using the continuous wavelet transform.* PhD thesis, Lancaster University, 2016.

[3] S. P. Yu, "Na^+, K^+-ATPase: the new face of an old player in pathogenesis and apoptotic/hybrid cell death," *Biochem. Pharmacol.*, vol. 66, no. 8, pp. 1601–1609, 2003.

[4] L. F. Olsen, A. Z. Andersen, A. Lunding, J. C. Brasen, and A. K. Poulsen, "Regulation of glycolytic oscillations by mitochondrial and plasma membrane H^+-ATPases," *Biophys. J.*, vol. 96, no. 9, pp. 3850–3861, 2009.

[5] V. C. Özalp, T. R. Pedersen, L. J. Nielsen, and L. F. Olsen, "Time-resolved measurements of intracellular ATP in the yeast Saccharomyces cerevisiae using a new type of nanobiosensor," *J. Biol. Chem.*, vol. 285, no. 48, pp. 37579–37588, 2010.

[6] L. Duysens and J. Amesz, "Fluorescence spectrophotometry of reduced phosphopyridine nucleotide in intact cells in the near-ultraviolet and visible region," *Bioch. et Biophys. Acta*, vol. 24, pp. 19–26, 1957.

[7] P. T. Clemson and A. Stefanovska, "Discerning non-autonomous dynamics," *Phys. Rep.*, vol. 542, no. 4, pp. 297–368, 2014.

[8] D. Iatsenko, P. V. McClintock, and A. Stefanovska, "Nonlinear mode decomposition: a noise-robust, adaptive decomposition method," *Phys. Rev. E*, vol. 92, no. 3, p. 032916, 2015.

[9] G. Lancaster, D. Iatsenko, A. Pidde, V. Ticcinelli, and A. Stefanovska, "Surrogate data for hypothesis testing of physical systems," *Phys. Rep.*, 2018.

[10] D. Tosteson and J. Hoffman, "Regulation of cell volume by active cation transport in high and low potassium sheep red cells," *J. Gen. Physiol.*, vol. 44, no. 1, pp. 169–194, 1960.

[11] E. Jakobsson, "Interactions of cell volume, membrane potential, and membrane transport parameters," *American Journal of Physiology-Cell Physiology*, vol. 238, no. 5, pp. C196–C206, 1980.

[12] C. M. Armstrong, "The Na/K pump, Cl ion, and osmotic stabilization of cells," *PNAS*, vol. 100, no. 10, pp. 6257–6262, 2003.

[13] J. A. Fraser and C. L.-H. Huang, "A quantitative analysis of cell volume and resting potential determination and regulation in excitable cells," *J. Physiol.*, vol. 559, no. 2, pp. 459–478, 2004.

[14] W. Moolenaar, J. De Goede, and A. Verveen, "Membrane noise in paramecium," *Nature*, vol. 260, no. 5549, p. 344, 1976.

[15] Y. Nakaoka, T. Imaji, M. Hara, and N. Hashimoto, "Spontaneous fluctuation of the resting membrane potential in paramecium: amplification caused by intracellular Ca^{2+}," *J. Exp. Biol.*, vol. 212, no. 2, pp. 270–276, 2009.

[16] T. Majima, "Membrane potential fluctuation in Paramecium," *Biophys. Chem.*, vol. 11, no. 1, pp. 101–108, 1980.

[17] F. Oosawa, "Spontaneous signal generation in living cells," *Bull. Math. Biol.*, vol. 63, no. 4, pp. 643–654, 2001.

[18] B. Alberts, D. Bray, K. Hopkin, A. Johnson, J. Lewis, M. Raff, K. Roberts, and P. Walter, *Essential cell biology*. Garland Science, 2013.

[19] A. Bekatorou, C. Psarianos, and A. A. Koutinas, "Production of food grade yeasts.," *Food Technol. Biotechnol.*, vol. 44, no. 3, 2006.

[20] R. Zadrag, M. Kwolek-Mirek, G. Bartosz, and T. Bilinski, "Relationship between the replicative age and cell volume in saccharomyces cerevisiae," *Acta Biochim. Pol.*, vol. 53, no. 4, p. 747, 2006.

[21] D. Leister and J. M. Herrmann, *Mitochondria: practical protocols*, vol. 372. Springer Science & Business Media, 2007.

[22] J. Rine, "The yeast Saccharomyces cerevisiae in molecular and cellular biology: a smaller but not lower eucaryote," *Am. Zoologist*, vol. 29, no. 2, pp. 605–616, 1989.

[23] P.-A. Marechal and P. Gervais, "Yeast viability related to water potential variation: influence of the transient phase," *Appl. Microbiol. Biotechnol.*, vol. 42, no. 4, pp. 617–622, 1994.

[24] B. Shen, S. Hohmann, R. G. Jensen, and H. J. Bohnert, "Roles of sugar alcohols in osmotic stress adaptation. Replacement of glycerol by mannitol and sorbitol in yeast," *Plant Physiol.*, vol. 121, no. 1, pp. 45–52, 1999.

[25] A. Blomberg, "Metabolic surprises in Saccharomyces cerevisiae during adaptation to saline conditions: questions, some answers and a model," *FEMS Microbiol. Letters*, vol. 182, no. 1, pp. 1–8, 2000.

[26] N. Abdel and E. Moghaz, "Comparative study of salt tolerance in Saccharomyces cerevisiae and Pichia pastoris yeast strains," *Adv. Biores.*, vol. 1, pp. 170–7, 2010.

[27] H. Saito and F. Posas, "Response to hyperosmotic stress," *Genetics*, vol. 192, no. 2, pp. 289–318, 2012.

[28] C. Bermejo, E. Rodríguez, R. García, J. M. Rodríguez-Peña, M. L. Rodríguez de la Concepción, C. Rivas, P. Arias, C. Nombela, F. Posas, and J. Arroyo, "The sequential activation of the yeast HOG and SLT2 pathways is required for cell survival to cell wall stress," *Mol. Biol. Cell*, vol. 19, no. 3, pp. 1113–1124, 2008.

[29] A. K. Poulsen, F. R. Lauritsen, and L. Folke Olsen, "Sustained glycolytic oscillations–no need for cyanide," *FEMS Microbiol. Letters*, vol. 236, no. 2, pp. 261–266, 2004.

[30] A. K. Poulsen, M. Ø. Petersen, and L. F. Olsen, "Single cell studies and simulation of cell–cell interactions using oscillating glycolysis in yeast cells," *Biophys. Chem.*, vol. 125, no. 2-3, pp. 275–280, 2007.

[31] A. K. Poulsen, A. Z. Andersen, J. C. Brasen, A. M. Scharff-Poulsen, and L. F. Olsen, "Probing glycolytic and membrane potential oscillations in Saccharomyces cerevisiae," *Biochemistry*, vol. 47, no. 28, pp. 7477–7484, 2008.

[32] A. Z. Andersen, A. K. Poulsen, J. C. Brasen, and L. F. Olsen, "On-line measurements of oscillating mitochondrial membrane potential in glucose-fermenting Saccharomyces cerevisiae," *Yeast*, vol. 24, no. 9, pp. 731–739, 2007.

[33] L. J. Nielsen, L. F. Olsen, and V. C. Ozalp, "Aptamers embedded in polyacrylamide nanoparticles: a tool for in vivo metabolite sensing," *Acs Nano*, vol. 4, no. 8, pp. 4361–4370, 2010.

[34] C. K. Ytting, A. T. Fuglsang, J. K. Hiltunen, A. J. Kastaniotis, V. C. Özalp, L. J. Nielsen, and L. F. Olsen, "Measurements of intracellular ATP provide new insight into the regulation of glycolysis in the yeast Saccharomyces cerevisiae," *Integrative Biol.*, vol. 4, no. 1, pp. 99–107, 2012.

[35] S. L. Forsburg, "The art and design of genetic screens: yeast," *Nat. Rev. Genetics*, vol. 2, no. 9, p. 659, 2001.

[36] S. L. Forsburg, "The yeasts saccharomyces cerevisiae and Schizosaccharomyces pombe: models for cell biology research," *Gravit. Space Res.*, vol. 18, no. 2, 2007.

[37] H. Karathia, E. Vilaprinyo, A. Sorribas, and R. Alves, "Saccharomyces cerevisiae as a model organism: a comparative study," *PloS One*, vol. 6, no. 2, p. e16015, 2011.

[38] A. Martini, "Origin and domestication of the wine yeast Saccharomyces cerevisiae," *J. Wine Res.*, vol. 4, no. 3, pp. 165–176, 1993.

[39] E. Cabib, D.-H. Roh, M. Schmidt, L. B. Crotti, and A. Varma, "The yeast cell wall and septum as paradigms of cell growth and morphogenesis," *J. Biol. Chem.*, vol. 276, no. 23, pp. 19679–19682, 2001.

[40] M. Osumi, "The ultrastructure of yeast: cell wall structure and formation," *Micron*, vol. 29, no. 2-3, pp. 207–233, 1998.

[41] M. Yamaguchi, Y. Namiki, H. Okada, Y. Mori, H. Furukawa, J. Wang, M. Ohkusu, and S. Kawamoto, "Structome of Saccharomyces cerevisiae determined by freeze-substitution and serial ultrathin-sectioning electron microscopy," *J. Electron Microscopy*, vol. 60, no. 5, pp. 321–335, 2011.

[42] M. Ingram *et al.*, "An introduction to the biology of yeasts.," *An introduction to the Biology of Yeasts.*, 1955.

[43] P. Orlean, J. Pringle, J. Broach, and E. Jones, "The molecular and cellular biology of the yeast Saccharomyces. Cell cycle and cell biology," 1997.

[44] D. M. Smith, K. McKenna, and C. J. Thompson, "Hyponatraemia," *Clin. Endocrinol.*, vol. 52, no. 6, pp. 667–678, 2000.

[45] W. N. Arnold and J. S. Lacy, "Permeability of the cell envelope and osmotic behavior in Saccharomyces cerevisiae," *J. Bacteriol.*, vol. 131, no. 2, pp. 564–571, 1977.

[46] G. M. Walker, *Yeast Physiology and Biotechnology*. John Wiley & Sons, 1998.

[47] J. Ramos, H. Sychrová, and M. Kschischo, *Yeast membrane transport*. Springer, 2016.

[48] W. Dowhan and M. Bogdanov, "Functional roles of lipids in membranes," in *New Comprehensive Biochemistry*, vol. 36, pp. 1–35, Elsevier, 2002.

[49] M. Burger, E. E. Bacon, and J. Bacon, "Some observations on the form and location of invertase in the yeast cell," *Biochem. J.*, vol. 78, no. 3, p. 504, 1961.

[50] R. Kollár, E. Petráková, G. Ashwell, P. W. Robbins, and E. Cabib, "Architecture of the yeast cell wall the linkage between chitin and β (13)-glucan," *J. Biol. Chem.*, vol. 270, no. 3, pp. 1170–1178, 1995.

[51] R. Kollár, B. B. Reinhold, E. Petráková, H. J. Yeh, G. Ashwell, J. Drgonová, J. C. Kapteyn, F. M. Klis, and E. Cabib, "Architecture of the yeast cell wall β (1$\rightarrow$ 6)-glucan interconnects mannoprotein, β (1$\rightarrow$ 3)-glucan, and chitin," *J. Biol. Chem.*, vol. 272, no. 28, pp. 17762–17775, 1997.

[52] R. Vuković and V. Mrša, "Structure of the Saccharomyces cerevisiae cell wall," *Croat. Chem. Acta*, vol. 68, no. 3, pp. 597–605, 1995.

[53] E. Cabib and B. Bowers, "Chitin and yeast budding localization of chitin in yeast bud scars," *J. Biol. Chem.*, vol. 246, no. 1, pp. 152–159, 1971.

[54] P. N. Lipke and R. Ovalle, "Cell wall architecture in yeast: new structure and new challenges," *J. Bacteriol.*, vol. 180, no. 15, pp. 3735–3740, 1998.

[55] J. A. Shaw, P. C. Mol, B. Bowers, S. J. Silverman, M. H. Valdivieso, A. Durán, and E. Cabib, "The function of chitin synthases 2 and 3 in the Saccharomyces cerevisiae cell cycle.," *J. Cell Biol.*, vol. 114, no. 1, pp. 111–123, 1991.

[56] F. M. Klis, P. Mol, K. Hellingwerf, and S. Brul, "Dynamics of cell wall structure in Saccharomyces cerevisiae," *FEMS Microbiol. Rev.*, vol. 26, no. 3, pp. 239–256, 2002.

[57] K. Altmann, M. Dürr, and B. Westermann, "Saccharomyces cerevisiae as a model organism to study mitochondrial biology," in *Mitochondria*, pp. 81–90, Springer, 2007.

[58] A. A. Eddy and J. A. Barnett, "A history of research on yeasts 11. the study of solute transport: the first 90 years, simple and facilitated diffusion1," *Yeast*, vol. 24, no. 12, pp. 1023–1059, 2007.

[59] J. E. Karpel and L. F. Bisson, "Aquaporins in saccharomyces cerevisiae wine yeast," *FEMS microbiology letters*, vol. 257, no. 1, pp. 117–123, 2006.

[60] E. J. Luard and D. Griffin, "Effect of water potential on fungal growth and turgor," *Trans. Br. Mycol. Soc.*, vol. 76, no. 1, pp. 33–40, 1981.

[61] S. Törnroth-Horsefield and R. Neutze, "Opening and closing the metabolite gate," *PNAS*, pp. pnas–0810654106, 2008.

[62] S. J. Ralph, S. Rodríguez-Enríquez, J. Neuzil, E. Saavedra, and R. Moreno-Sánchez, "The causes of cancer revisited:"mitochondrial malignancy" and ros-induced oncogenic transformation–why mitochondria are targets for cancer therapy," *Mol. Aspects Med.*, vol. 31, no. 2, pp. 145–170, 2010.

[63] G. Kroemer and J. Pouyssegur, "Tumor cell metabolism: cancer's achilles' heel," *Cancer Cell*, vol. 13, no. 6, pp. 472–482, 2008.

[64] T. N. Seyfried and L. M. Shelton, "Cancer as a metabolic disease," *Nutrition & Metabolism*, vol. 7, no. 1, p. 7, 2010.

[65] D. C. Wallace, "Mitochondria and cancer," *Nat. Rev. Cancer*, vol. 12, no. 10, p. 685, 2012.

[66] S. M. Cloonan and A. M. Choi, "Mitochondria: commanders of innate immunity and disease," *Curr. Opin. Immunol.*, vol. 24, no. 1, pp. 32–40, 2012.

[67] M. G. Vander Heiden, L. C. Cantley, and C. B. Thompson, "Understanding the Warburg effect: the metabolic requirements of cell proliferation," *Science*, vol. 324, no. 5930, pp. 1029–1033, 2009.

[68] R. Diaz-Ruiz, S. Uribe-Carvajal, A. Devin, and M. Rigoulet, "Tumor cell energy metabolism and its common features with yeast metabolism," *Biochim. Biophys. Acta - Rev. Cancer*, vol. 1796, no. 2, pp. 252–265, 2009.

[69] R. Diaz-Ruiz, M. Rigoulet, and A. Devin, "The warburg and crabtree effects: On the origin of cancer cell energy metabolism and of yeast glucose repression," *Biochimica et Biophysica Acta (BBA)-Bioenergetics*, vol. 1807, no. 6, pp. 568–576, 2011.

[70] C. Ruckenstuhl, S. Büttner, D. Carmona-Gutierrez, T. Eisenberg, G. Kroemer, S. J. Sigrist, K.-U. Fröhlich, and F. Madeo, "The warburg effect suppresses oxidative stress induced apoptosis in a yeast model for cancer," *PloS one*, vol. 4, no. 2, p. e4592, 2009.

[71] K. Natter and S. D. Kohlwein, "Yeast and cancer cells–common principles in lipid metabolism," *Biochim. Biophys. Acta - Mol. Cell Biol. Lipids*, vol. 1831, no. 2, pp. 314–326, 2013.

[72] S. Dequin and S. Casaregola, "The genomes of fermentative Saccharomyces," *C. R. Biol.*, vol. 334, no. 8-9, pp. 687–693, 2011.

[73] J. Piškur, E. Rozpędowska, S. Polakova, A. Merico, and C. Compagno, "How did Saccharomyces evolve to become a good brewer?," *TRENDS Genet.*, vol. 22, no. 4, pp. 183–186, 2006.

[74] R. S. Zitomer, P. Carrico, and J. Deckert, "Regulation of hypoxic gene expression in yeast," *Kidney international*, vol. 51, no. 2, pp. 507–513, 1997.

[75] M. Molon, M. Szajwaj, M. Tchorzewski, A. Skoczowski, E. Niewiadomska, and R. Zadrag-Tecza, "The rate of metabolism as a factor determining longevity of the saccharomyces cerevisiae yeast," *Age*, vol. 38, no. 1, p. 11, 2016.

[76] A. Berk, S. Zipursky, and H. Lodish, "Molecular Cell Biology 4th edition," 2000.

[77] G. Kopperschläger, R. Freyer, W. Diezel, and E. Hofmann, "Some kinetic and molecular properties of yeast phosphofructokinase," *FEBS letters*, vol. 1, no. 3, pp. 137–141, 1968.

[78] W. Atzpodien and H. Bode, "Purification and Regulatory Properties of ATP-Sensitive Phosphofructokinase from Yeast," *Eur. J. Biochem.*, vol. 12, no. 1, pp. 126–132, 1970.

[79] A. Ramaiah, J. A. Hathaway, and D. E. Atkinson, "Adenylate as a metabolic regulator effect on yeast phosphofructokinase kinetics," *J. Biol. Chem.*, vol. 239, no. 11, pp. 3619–3622, 1964.

[80] J. A. Muntz *et al.*, "The role of potassium and ammonium ions in alcoholic fermentation," *J. biol. Chem*, vol. 171, pp. 653–665, 1947.

[81] R. Bartrons, E. Van Schaftingen, S. Vissers, and H.-G. Hers, "The stimulation of yeast phosphofructokinase by fructose 2, 6-bisphosphate," *FEBS letters*, vol. 143, no. 1, pp. 137–140, 1982.

[82] A. Sols and M. L. Salas, "[77c] phosphofructokinase: Iii. yeast," in *Methods in enzymology*, vol. 9, pp. 436–442, Elsevier, 1966.

[83] A. Nilsson and J. Nielsen, "Metabolic trade-offs in yeast are caused by f1f0-atp synthase," *Scientific reports*, vol. 6, p. 22264, 2016.

[84] R. N. Bento, M. A. Rendas, V. A. Semedo, C. E. Bernardes, M. E. Piedade, and F. Antunes, "The metabolic profile of lag and exponential phases of Saccharomyces cerevisiae growth changes continuously," *bioRxiv*, p. 063909, 2016.

[85] E. Boles, F. Schulte, T. Miosga, K. Freidel, E. Schlüter, F. K. Zimmermann, C. P. Hollenberg, and J. J. Heinisch, "Characterization of a glucose-repressed pyruvate kinase (pyk2p) in saccharomyces cerevisiae that is catalytically insensitive to fructose-1, 6-bisphosphate.," *Journal of bacteriology*, vol. 179, no. 9, pp. 2987–2993, 1997.

[86] J. M. Thevelein and S. Hohmann, "Trehalose synthase: guard to the gate of glycolysis in yeast?," *Trends Biochem. Sci.*, vol. 20, no. 1, pp. 3–10, 1995.

[87] M. Peak, M. Al-Habori, and L. Agius, "Regulation of glycogen synthesis and glycolysis by insulin, ph and cell volume. interactions between swelling and alkalinization in mediating the effects of insulin," *Biochem. J.*, vol. 282, no. 3, pp. 797–805, 1992.

[88] J. T. Pronk, H. Yde Steensma, and J. P. van Dijken, "Pyruvate metabolism in Saccharomyces cerevisiae," *Yeast*, vol. 12, no. 16, pp. 1607–1633, 1996.

[89] J. A. Barnett, "A history of research on yeasts 5: the fermentation pathway," *Yeast*, vol. 20, no. 6, pp. 509–543, 2003.

[90] K. Otterstedt, C. Larsson, R. M. Bill, A. Ståhlberg, E. Boles, S. Hohmann, and L. Gustafsson, "Switching the mode of metabolism in the yeast Saccharomyces cerevisiae," *EMBO Rep.*, vol. 5, no. 5, pp. 532–537, 2004.

[91] J. Van den Brink, A. B. Canelas, W. M. Van Gulik, J. T. Pronk, J. J. Heijnen, J. H. De Winde, and P. Daran-Lapujade, "Dynamics of glycolytic regulation during adaptation of Saccharomyces cerevisiae to fermentative metabolism," *Appl. Env. Microbiol.*, vol. 74, no. 18, pp. 5710–5723, 2008.

[92] C. Verduyn, T. P. Zomerdijk, J. P. van Dijken, and W. A. Scheffers, "Continuous measurement of ethanol production by aerobic yeast suspensions with an enzyme electrode," *Appl. Microbiol. Biotechnol.*, vol. 19, no. 3, pp. 181–185, 1984.

[93] T. Walther, M. Novo, K. Rössger, F. Létisse, M.-O. Loret, J.-C. Portais, and J.-M. François, "Control of atp homeostasis during the respiro-fermentative transition in yeast," *Mol. Syst. Biol.*, vol. 6, no. 1, p. 344, 2010.

[94] D. Molenaar, R. Van Berlo, D. De Ridder, and B. Teusink, "Shifts in growth strategies reflect tradeoffs in cellular economics," *Mol. Syst. Biol.*, vol. 5, no. 1, p. 323, 2009.

[95] A. Betz and B. Chance, "Influence of inhibitors and temperature on the oscillation of reduced pyridine nucleotides in yeast cells," *Arch. Biochem. Biophys.*, vol. 109, no. 3, pp. 579–584, 1965.

[96] D. Reibstein, J. Den Hollander, S. Pilkis, and R. Shulman, "Studies on the regulation of yeast phosphofructo-1-kinase: its role in aerobic and anaerobic glycolysis," *Biochemistry*, vol. 25, no. 1, pp. 219–227, 1986.

[97] A. Rodríguez-Navarro *et al.*, "Potassium transport in fungi and plants.," *Biochim. Biophys. Acta, Rev. Biomembr.*, vol. 1469, no. 1, pp. 1–30, 2000.

[98] H. Sychrova, "Yeast as a model organism to study transport and homeostasis of alkali metal cations," *Physiol. Res.*, vol. 53, pp. S91–98, 2004.

[99] R. R. Lew, N. N. Levina, L. Shabala, M. I. Anderca, and S. N. Shabala, "Role of a mitogen-activated protein kinase cascade in ion flux-mediated turgor regulation in fungi," *Eukaryotic Cell*, vol. 5, no. 3, pp. 480–487, 2006.

[100] J. Ariño, J. Ramos, and H. Sychrová, "Alkali metal cation transport and homeostasis in yeasts," *Microbiol. Mol. Biol. Rev.*, vol. 74, no. 1, pp. 95–120, 2010.

[101] J. Ramos and A. Rodríguez-Navarro, "Regulation and interconversion of the potassium transport systems of Saccharomyces cerevisiae as revealed by rubidium transport," *Eur. J. Biochem.*, vol. 154, no. 2, pp. 307–311, 1986.

[102] R. SERRANO, "Plasma membrane ATPase of fungi and plants as a novel type of proton pump," in *Curr. Top. Cell Regul.*, vol. 23, pp. 87–126, Elsevier, 1984.

[103] R. Serrano, "Effect of ATPase inhibitors on the proton pump of respiratory-deficient yeast," *Eur. J. Biochem.*, vol. 105, no. 2, pp. 419–424, 1980.

[104] D. Gradmann, U.-P. Hansen, W. S. Long, C. L. Slayman, and J. Warncke, "Current-voltage relationships for the plasma membrane and its principal electrogenic pump in Neurospora crassa: I. Steady-state conditions," *J. Membr. Miol.*, vol. 39, no. 4, pp. 333–367, 1978.

[105] R. Serrano and A. Rodriguez-Navarro, "Ion homeostasis during salt stress in plants," *Curr. Opin. Cell Biol.*, vol. 13, no. 4, pp. 399–404, 2001.

[106] A. Pena, G. Cinco, A. Gómez-Puyou, and M. Tuena, "Effect of the pH of the incubation medium on glycolysis and respiration in Saccharomyces cerevisiae," *Arch. Biochem. Biophys.*, vol. 153, no. 2, pp. 413–425, 1972.

[107] A. Peña, G. Cinco, A. G. Puyou, and M. Tuena, "Studies on the mechanism of the stimulation of glycolysis and respiration by K^+ in Saccharomyces cerevisiae," *Biochim. Biophys. Acta Bioenerg.*, vol. 180, no. 1, pp. 1–8, 1969.

[108] B. C. Monk, A. B. Mason, G. Abramochkin, J. E. Haber, D. Seto-Young, and D. S. Perlin, "The yeast plasma membrane proton pumping ATPase is a viable antifungal target. i. Effects of the cysteine-modifying reagent omeprazole," *Biochim. Biophys. Acta -Biomembr.*, vol. 1239, no. 1, pp. 81–90, 1995.

[109] G. Curti, F. Massardi, and P. Lado, "Synergistic activation of plasma membrane H^+-ATPase in Arabidopsis thaliana cells by turgor decrease and by fusicoccin," *Physiologia Plantarum*, vol. 87, no. 4, pp. 592–600, 1993.

[110] D. Bracey, C. Holyoak, and P. Coote, "Comparison of the inhibitory effect of sorbic acid and amphotericin B on Saccharomyces cerevisiae: is growth inhibition dependent on reduced intracellular pH?," *J. Appl. Microbiol.*, vol. 85, no. 6, pp. 1056–1066, 1998.

[111] R. Gillies, K. Ugurbil, J. Den Hollander, and R. Shulman, "31P NMR studies of intracellular pH and phosphate metabolism during cell division cycle of Saccharomyces cerevisiae," *PNAS*, vol. 78, no. 4, pp. 2125–2129, 1981.

[112] E. Conway and T. Brady, "Biological production of acid and alkali. 1. Quantitative relations of succinic and carbonic acids to the potassium and hydrogen ion exchange in fermenting yeast," *Biochem. J.*, vol. 47, no. 3, p. 360, 1950.

[113] A. F. Duro and R. Serrano, "Inhibition of succinate production during yeast fermentation by deenergization of the plasma membrane," *Curr. Microbiol.*, vol. 6, no. 2, pp. 111–113, 1981.

[114] C. Prior, S. Potier, J.-L. Souciet, and H. Sychrova, "Characterization of the Nha1 gene encoding a Na^+/H^+-antiporter of the yeast Saccharomyces cerevisiae," *FEBS Lett.*, vol. 387, no. 1, pp. 89–93, 1996.

[115] M. Kahm, C. Navarrete, V. Llopis-Torregrosa, R. Herrera, L. Barreto, L. Yenush, J. Ariño, J. Ramos, and M. Kschischo, "Potassium starvation in yeast: mechanisms of homeostasis revealed by mathematical modeling," *PLoS Comput. Biol.*, vol. 8, no. 6, p. e1002548, 2012.

[116] M. Kahm, *A Mathematical Model of the Potassium Homeostasis in Saccharomyces cerevisiae*. PhD thesis, Universitäts-und Landesbibliothek Bonn, 2012.

[117] R. Ohgaki, N. Nakamura, K. Mitsui, and H. Kanazawa, "Characterization of the ion transport activity of the budding yeast Na^+/H^+ antiporter, Nha1p, using isolated secretory vesicles," *Biochim. Biophys. Acta -Biomembr.*, vol. 1712, no. 2, pp. 185–196, 2005.

[118] O. Kinclova-Zimmermannova and H. Sychrova, "Functional study of the Nha1p C-terminus: involvement in cell response to changes in external osmolarity," *Current Genetics*, vol. 49, no. 4, pp. 229–236, 2006.

[119] O. Kinclova-Zimmermannova, D. Gaskova, and H. Sychrova, "The Na^+, K^+/H^+-antiporter Nha1 influences the plasma membrane potential of Saccharomyces cerevisiae," *FEMS Yeast Res.*, vol. 6, no. 5, pp. 792–800, 2006.

[120] J. Pattison-Granberg and B. L. Persson, "Regulation of cation-coupled high-affinity phosphate uptake in the yeast Saccharomyces cerevisiae," *J. Bacteriol.*, vol. 182, no. 17, pp. 5017–5019, 2000.

[121] G. Borst-Pauwels, "Ion Transport in Yeast," *Biochim. Biophys. Acta -Rev. Biomembr.*, vol. 650, no. 2-3, pp. 88–127, 1981.

[122] M. Cockburn, P. Earnshaw, and A. Eddy, "The stoicheiometry of the absorption of protons with phosphate and L-glutamate by yeasts of the genus Saccharomyces," *Biochem. J.*, vol. 146, no. 3, pp. 705–712, 1975.

[123] G. Roomans and G. Borst-Pauwels, "Interaction of cations with phosphate uptake by Saccharomyces cerevisiae. Effects of surface potential," *Biochem. J.*, vol. 178, no. 3, pp. 521–527, 1979.

[124] R. F. Gaber, C. A. Styles, and G. R. Fink, "Trk1 encodes a plasma membrane protein required for high-affinity potassium transport in saccharomyces cerevisiae.," *Molecular and Cellular Biology*, vol. 8, no. 7, pp. 2848–2859, 1988.

[125] B. Benito, B. Garciadeblás, A. Fraile-Escanciano, and A. Rodríguez-Navarro, "Potassium and sodium uptake systems in fungi. the transporter diversity of Magnaporthe oryzae," *Fungal Genet. Biol.*, vol. 48, no. 8, pp. 812–822, 2011.

[126] R. Haro and A. Rodrı-guez-Navarro, "Molecular analysis of the mechanism of potassium uptake through the TRK1 transporter of Saccharomyces cerevisiae," *Biochim. Biophys. Acta -Biomembr.*, vol. 1564, no. 1, pp. 114–122, 2002.

[127] A. Rivetta, C. Slayman, and T. Kuroda, "Quantitative modeling of chloride conductance in yeast TRK potassium transporters," *Biophys. J.*, vol. 89, no. 4, pp. 2412–2426, 2005.

[128] T. Kuroda, H. Bihler, E. Bashi, C. Slayman, and A. Rivetta, "Chloride channel function in the yeast TRK-potassium transporters," *J. Membr. Biol.*, vol. 198, no. 3, pp. 177–192, 2004.

[129] C. Corratgé-Faillie, M. Jabnoune, S. Zimmermann, A.-A. Véry, C. Fizames, and H. Sentenac, "Potassium and sodium transport in non-animal cells: the Trk/Ktr/HKT transporter family," *Cell. Mol. Life Sci.*, vol. 67, no. 15, pp. 2511–2532, 2010.

[130] R. Madrid, M. J. Gómez, J. Ramos, and A. Rodríguez-Navarro, "Ectopic potassium uptake in trk1 trk2 mutants of Saccharomyces cerevisiae correlates with a highly hyperpolarized membrane potential," *J. Biol. Chem.*, vol. 273, no. 24, pp. 14838–14844, 1998.

[131] H. Lalucque and P. Silar, "Incomplete penetrance and variable expressivity of a growth defect as a consequence of knocking out two K^+ transporters in the euascomycete fungus podospora anserina," *Genetics*, vol. 166, no. 1, pp. 125–133, 2004.

[132] H. Findon, A.-M. Calcagno-Pizarelli, J. L. Martínez, A. Spielvogel, A. Markina-Iñarrairaegui, T. Indrakumar, J. Ramos, M. A. Peñalva, E. A. Espeso, and H. N. Arst Jr, "Analysis of a novel calcium auxotrophy in aspergillus nidulans," *Fungal Genet. Biol.*, vol. 47, no. 7, pp. 647–655, 2010.

[133] H. Bihler, C. L. Slayman, and A. Bertl, "NSC1: a novel high-current inward rectifier for cations in the plasma membrane of Saccharomyces cerevisiae," *FEBS Lett.*, vol. 432, no. 1-2, pp. 59–64, 1998.

[134] H. Bihler, R. F. Gaber, C. L. Slayman, and A. Bertl, "The presumed potassium carrier Trk2p in Saccharomyces cerevisiae determines an H^+-dependent, K^+-independent current," *FEBS Lett.*, vol. 447, no. 1, pp. 115–120, 1999.

[135] H. Bihler, C. L. Slayman, and A. Bertl, "Low-affinity potassium uptake by Saccharomyces cerevisiae is mediated by NSC1, a calcium-blocked non-specific cation channel," *Biochim. Biophys. Acta -Biomembr.*, vol. 1558, no. 2, pp. 109–118, 2002.

[136] D. Sanders, U.-P. Hansen, and C. L. Slayman, "Role of the plasma membrane proton pump in pH regulation in non-animal cells," *PNAS*, vol. 78, no. 9, pp. 5903–5907, 1981.

[137] M. R. Blatt and C. L. Slayman, "Role of" active" potassium transport in the regulation of cytoplasmic pH by nonanimal cells," *PNAS*, vol. 84, no. 9, pp. 2737–2741, 1987.

[138] A. Rodriguez-Navarro and J. Ramos, "Dual system for potassium transport in Saccharomyces cerevisiae.," *J. Bacteriol.*, vol. 159, no. 3, pp. 940–945, 1984.

[139] F. Rubio, W. Gassmann, and J. I. Schroeder, "Sodium-driven potassium uptake by the plant potassium transporter HKT1 and mutations conferring salt tolerance," *Science*, vol. 270, no. 5242, pp. 1660–1663, 1995.

[140] A. Bertl, C. L. Slayman, and D. Gradmann, "Gating and conductance in an outward-rectifying K^+ channel from the plasma membrane of Saccharomyces cerevisiae," *J. Membr. Biol.*, vol. 132, no. 3, pp. 183–199, 1993.

[141] S. H. Loukin, B. Vaillant, X.-L. Zhou, E. P. Spalding, C. Kung, and Y. Saimi, "Random mutagenesis reveals a region important for gating of the yeast K^+ channel Ykc1," *EMBO J.*, vol. 16, no. 16, pp. 4817–4825, 1997.

[142] P. Vergani, T. Miosga, S. M. Jarvis, and M. R. Blatt, "Extracellular K^+ and Ba^{2+} mediate voltage-dependent inactivation of the outward-rectifying K^+ channel encoded by the yeast gene TOK1," *FEBS Lett.*, vol. 405, no. 3, pp. 337–344, 1997.

[143] C. Fairman, X.-L. Zhou, and C. Kung, "Potassium uptake through the TOK1 K^+ channel in the budding yeast," *J. Membr. Biol.*, vol. 168, no. 2, pp. 149–157, 1999.

[144] R. Haro, B. Garciadeblas, and A. Rodriguez-Navarro, "A novel P-type AT-Pase from yeast involved in sodium transport," *FEBS Lett.*, vol. 291, no. 2, pp. 189–191, 1991.

[145] M. A. BaAueIos, H. Sychrova, C. Bleykasten-Grosshans, J.-L. Souciet, and S. Potier, "The Nhal antiporter of Saccharomyces cerevisiae mediates sodium and potassium efflux," *Microbiology*, vol. 144, no. 10, pp. 2749–2758, 1998.

[146] M. A. Bañuelos, M. C. Ruiz, A. Jiménez, J.-L. Souciet, S. Potier, and J. Ramos, "Role of the Nha1 antiporter in regulating K^+ influx in Saccharomyces cerevisiae," *Yeast*, vol. 19, no. 1, pp. 9–15, 2002.

[147] L. Maresova and H. Sychrova, "Physiological characterization of Saccharomyces cerevisiae kha1 deletion mutants," *Mol. Microbiol.*, vol. 55, no. 2, pp. 588–600, 2005.

[148] M. Boutry, F. Foury, and A. Goffeau, "Energy-dependent uptake of calcium by the yeast Schizosaccharomyces pombe," *Biochim. Biophys. Acta -Biomembr.*, vol. 464, no. 3, pp. 602–612, 1977.

[149] A. Miseta, R. Kellermayer, D. P. Aiello, L. Fu, and D. M. Bedwell, "The vacuolar ca2+/h+ exchanger vcx1p/hum1p tightly controls cytosolic ca2+ levels in s. cerevisiae," *FEBS letters*, vol. 451, no. 2, pp. 132–136, 1999.

[150] V. Denis and M. S. Cyert, "Internal Ca^{2+} release in yeast is triggered by hypertonic shock and mediated by a TRP channel homologue," *J. Cell Biol.*, vol. 156, no. 1, pp. 29–34, 2002.

[151] M. Fischer, N. Schnell, J. Chattaway, P. Davies, G. Dixon, and D. Sanders, "The saccharomyces cerevisiae cch1 gene is involved in calcium influx and mating," *Febs Letters*, vol. 419, no. 2-3, pp. 259–262, 1997.

[152] C. P. Palmer, X.-L. Zhou, J. Lin, S. H. Loukin, C. Kung, and Y. Saimi, "A trp homolog in saccharomyces cerevisiae forms an intracellular ca2+-permeable channel in the yeast vacuolar membrane," *Proceedings of the National Academy of Sciences*, vol. 98, no. 14, pp. 7801–7805, 2001.

[153] T. Dunn, K. Gable, and T. Beeler, "Regulation of cellular ca2+ by yeast vacuoles.," *Journal of Biological Chemistry*, vol. 269, no. 10, pp. 7273–7278, 1994.

[154] C. L. Brett, D. N. Tukaye, S. Mukherjee, and R. Rao, "The yeast endosomalNa^+ $(K^+)/H^+$ exchanger Nhx1 regulates cellular pH to control vesicle trafficking," *Mol. Biol. Cell*, vol. 16, no. 3, pp. 1396–1405, 2005.

[155] L. Přibylová, K. Papoušková, M. Zavřel, J.-L. Souciet, and H. Sychrova, "Exploration of yeast alkali metal cation/H^+ antiporters: sequence and structure comparison," *Folia Microbiol.*, vol. 51, no. 5, pp. 413–424, 2006.

[156] S. S. Samarão, C. E. Teodoro, F. E. Silva, C. C. Ribeiro, T. M. Granato, N. R. Bernardes, C. A. Retamal, A. R. Façanha, A. L. Okorokova-Façanha, and L. A. Okorokov, "V H^+-ATPase along the yeast secretory pathway: energization of the ER and Golgi membranes," *Biochim. Biophys. Acta - Biomembr.*, vol. 1788, no. 2, pp. 303–313, 2009.

[157] O. Cagnac, M. Leterrier, M. Yeager, and E. Blumwald, "Identification and characterization of Vnx1p, a novel type of vacuolar monovalent cation/H+ antiporter of Saccharomyces cerevisiae," *J. Biol. Chem.*, 2007.

[158] F. J. Quintero, M. R. Blatt, and J. M. Pardo, "Functional conservation between yeast and plant endosomal Na^+/H^+ antiporters 1," *FEBS Lett.*, vol. 471, no. 2-3, pp. 224–228, 2000.

[159] R. Nass, K. W. Cunningham, and R. Rao, "Intracellular sequestration of sodium by a novel Na^+/H^+ exchanger in yeast is enhanced by mutations in the plasma membrane H^+-ATPase insights into mechanisms of sodium tolerance," *J. Biol. Chem.*, vol. 272, no. 42, pp. 26145–26152, 1997.

[160] R. Nass and R. Rao, "The yeast endosomal Na^+/H^+ exchanger, Nhx1, confers osmotolerance following acute hypertonic shock," *Microbiology*, vol. 145, no. 11, pp. 3221–3228, 1999.

[161] K. Bowers, B. P. Levi, F. I. Patel, and T. H. Stevens, "The Sodium/Proton Exchanger Nhx1p Is Required for Endosomal Protein Trafficking in the Yeast, Saccharomyces cerevisiae," *Mol. Biol. Cell*, vol. 11, p. 4277–4294, 2000.

[162] P. Mitchell, "Coupling of phosphorylation to electron and hydrogen transfer by a chemi-osmotic type of mechanism," *Nature*, vol. 191, no. 4784, pp. 144–148, 1961.

[163] M. S. Cyert and C. C. Philpott, "Regulation of cation balance in Saccharomyces cerevisiae," *Genetics*, vol. 193, no. 3, pp. 677–713, 2013.

[164] H. Lodish, A. Berk, S. L. Zipursky, P. Matsudaira, D. Baltimore, and J. Darnell, "Molecular Cell Biology 4th edition," *NCBI, Bookshelf*, 2000.

[165] A. V. Holden, "Models of the Stochastic Activity of Neural Aggregates," in *Models of the Stochastic Activity of Neurones*, pp. 286–333, Springer, 1976.

[166] H. Kutchai, "Resting Membrane Potentials," 1977.

[167] C.-L. Li and H. McIlwain, "Maintenance of resting membrane potentials in slices of mammalian cerebral cortex and other tissues in vitro," *J. Physiol.*, vol. 139, no. 2, pp. 178–190, 1957.

[168] T. Doan and D. Kunze, "Contribution of the hyperpolarization-activated current to the resting membrane potential of rat nodose sensory neurons," *J. Physiol.*, vol. 514, no. 1, pp. 125–138, 1999.

[169] S. M. Felber and M. D. Brand, "Factors determining the plasma-membrane potential of lymphocytes.," *Biochem. J.*, vol. 204, no. 2, p. 577, 1982.

[170] J. Hoffman and P. Laris, "Determination of membrane potentials in human and amphiuma red blood cells by means of a fluorescent probe," *The Journal of Physiology*, vol. 239, no. 3, pp. 519–552, 1974.

[171] J. A. Verheugen, H. Vijverberg, M. Oortgiesen, and M. Cahalan, "Voltage-gated and Ca^{2+}-activated K^+ channels in intact human T lymphocytes. noninvasive measurements of membrane currents, membrane potential, and intracellular calcium," *J. Gen. Physiol.*, vol. 105, no. 6, pp. 765–794, 1995.

[172] B. Dworakowska and K. Dołowy, "Ion channels-related diseases.," *Acta Biochim. Polonica*, vol. 47, no. 3, p. 685, 2000.

[173] C. A. Hübner and T. J. Jentsch, "Ion channel diseases," *Hum. Mol. Gen.*, vol. 11, no. 20, pp. 2435–2445, 2002.

[174] F. M. Ashcroft, *Ion Channels and Disease*. Academic Press, 1999.

[175] A. Molleman, *Patch Clamping: an introductory guide to patch clamp electrophysiology*. John Wiley & Sons, 2003.

[176] A. L. Olson and J. E. Pessin, "Structure, function, and regulation of the mammalian facilitative glucose transporter gene family," *Ann. rev. Nutr.*, vol. 16, no. 1, pp. 235–256, 1996.

[177] R. J. Alpern and M. Chambers, "Basolateral membrane Cl^-/HCO_3^- exchange in the rat proximal convoluted tubule. Na-dependent and-independent modes.," *J. Gen. Physiol.*, vol. 89, no. 4, pp. 581–598, 1987.

[178] D. Gleeson, "Acid-base transport systems in gastrointestinal epithelia.," *Gut*, vol. 33, no. 8, p. 1134, 1992.

[179] P. Geck and E. Heinz, "Secondary active transport: introductory remarks," *Kidney Int.*, vol. 36, no. 3, pp. 334–341, 1989.

[180] C. Slayman, W. Long, and C.-H. Lu, "The relationship between ATP and an electrogenic pump in the plasma membrane ofneurospora crassa," *J. Membr. Biol.*, vol. 14, no. 1, pp. 305–338, 1973.

[181] R. Thomas, "The role of bicarbonate, chloride and sodium ions in the regulation of intracellular pH in snail neurones," *J. Physiol.*, vol. 273, no. 1, pp. 317–338, 1977.

[182] O. Christensen, "Mediation of cell volume regulation by Ca^{2+} influx through stretch-activated channels," *Nature*, vol. 330, no. 6143, p. 66, 1987.

[183] Y. Ishida and T. Chused, "Lack of voltage sensitive potassium channels and generation of membrane potential by sodium potassium ATPase in murine T lymphocytes.," *J. Immunol.*, vol. 151, no. 2, pp. 610–620, 1993.

[184] G. B. Ermentrout and D. H. Terman, *Mathematical foundations of neuroscience*, vol. 35. Springer Science & Business Media, 2010.

[185] A. L. Hodgkin and B. Katz, "The effect of sodium ions on the electrical activity of the giant axon of the squid," *J. Physiol.*, vol. 108, no. 1, pp. 37–77, 1949.

[186] M. Nelson and J. Rinzel, "The hodgkin-huxley model," in *The Book of Genesis*, pp. 29–49, Springer, 1998.

[187] A. Schwab, H.-J. Westphale, L. Wojnowski, S. Wünsch, and H. Oberleithner, "Spontaneously oscillating k+ channel activity in transformed madin-darby canine kidney cells.," *The Journal of clinical investigation*, vol. 92, no. 1, pp. 218–223, 1993.

[188] H.-J. Westphale, L. Wojnowski, A. Schwab, and H. Oberleithner, "Spontaneous membrane potential oscillations in madin-darby canine kidney cells transformed by alkaline stress," *Pflügers Archiv*, vol. 421, no. 2-3, pp. 218–223, 1992.

[189] A. Pandiella, M. Magni, D. Lovisolo, and J. Meldolesi, "The effect of epidermal growth factor on membrane potential. rapid hyperpolarization followed by persistent fluctuations.," *Journal of Biological Chemistry*, vol. 264, no. 22, pp. 12914–12921, 1989.

[190] M. Cahalan, K. Chandy, T. DeCoursey, and S. Gupta, "A voltage-gated potassium channel in human T lymphocytes.," *J. Physiol.*, vol. 358, no. 1, pp. 197–237, 1985.

[191] S. Feske, H. Wulff, and E. Y. Skolnik, "Ion channels in innate and adaptive immunity," *Ann. Rev. Immunol.*, vol. 33, pp. 291–353, 2015.

[192] S. Grissmer, R. S. Lewis, and M. D. Cahalan, "Ca^{2+}-activated K^+ channels in human leukemic T cells.," *J. Gen. Physiol.*, vol. 99, no. 1, pp. 63–84, 1992.

[193] R. S. Lewis, P. E. Ross, and M. D. Cahalan, "Chloride channels activated by osmotic stress in T lymphocytes.," *J. Gen. Physiol.*, vol. 101, no. 6, pp. 801–826, 1993.

[194] E. J. Tarcha, C. M. Olsen, P. Probst, D. Peckham, E. J. Muñoz-Elías, J. G. Kruger, and S. P. Iadonato, "Safety and pharmacodynamics of dalazatide, a Kv1. 3 channel inhibitor, in the treatment of plaque psoriasis: A randomized phase 1b trial," *PloS One*, vol. 12, no. 7, p. e0180762, 2017.

[195] R. S. Lewis and M. D. Cahalan, "Potassium and calcium channels in lymphocytes," *Ann. Rev. Immunol.*, vol. 13, no. 1, pp. 623–653, 1995.

[196] S. P. Fraser, J. K. Diss, L. J. Lloyd, F. Pani, A.-M. Chioni, A. J. George, and M. Djamgoz, "T-lymphocyte invasiveness: control by voltage-gated Na^+ channel activity," *FEBS Lett.*, vol. 569, no. 1-3, pp. 191–194, 2004.

[197] G. Grafton and L. Thwaite, "Calcium channels in lymphocytes," *Immunology*, vol. 104, no. 2, pp. 119–126, 2001.

[198] A. Brueggemann, M. George, M. Klau, M. Beckler, J. Steindl, J. Behrends, and N. Fertig, "Ion channel drug discovery and research: The automated nano-patch-clampo technology," *Curr. Drug Discov. Tech.*, vol. 1, no. 1, pp. 91–96, 2004.

[199] E. Neher and B. Sakmann, "The patch clamp technique," *Sci. Am.*, vol. 266, no. 3, pp. 44–51, 1992.

[200] C. P. Moore, A. King, and I. O. Sutherland, "Ion-sensitive dyes," June 24 1997. US Patent 5,641,684.

[201] A. Waggoner, "Dye indicators of membrane potential," *Ann. Rev. Biophys. Bioeng.*, vol. 8, no. 1, pp. 47–68, 1979.

[202] J. E. Gonzalez and R. Y. Tsien, "Voltage sensing by fluorescence resonance energy transfer in single cells," *Biophys. J.*, vol. 69, no. 4, pp. 1272–1280, 1995.

[203] J. Xu, X. Wang, B. Ensign, M. Li, L. Wu, A. Guia, and J. Xu, "Ion-channel assay technologies: quo vadis?," *Drug Discov. Today*, vol. 6, no. 24, pp. 1278–1287, 2001.

[204] H.-b. Yu, M. Li, W.-p. Wang, and X.-l. Wang, "High throughput screening technologies for ion channels," *Acta Pharmacol. Sinica*, vol. 37, no. 1, pp. 34–43, 2016.

[205] Y. Okada, *Patch Clamp Techniques: from Beginning to Advanced Protocols*. Springer, 2012.

[206] P. Pahapill and L. Schlichter, "Modulation of potassium channels in human T lymphocytes: effects of temperature.," *J. Physiology*, vol. 422, no. 1, pp. 103–126, 1990.

[207] R. S. Lewis and M. D. Cahalan, "Ion channels and signal transduction in lymphocytes," *Ann. Rev. Physiol.*, vol. 52, no. 1, pp. 415–430, 1990.

[208] P. Hou, R. Zhang, Y. Liu, J. Feng, W. Wang, Y. Wu, and J. Ding, "Physiological role of Kv1. 3 channel in T lymphocyte cell investigated quantitatively by kinetic modeling," *PloS One*, vol. 9, no. 3, p. e89975, 2014.

[209] W. Huang, C. Lu, Y. Wu, S. Ouyang, and Y. Chen, "Identification and functional characterization of voltage-gated sodium channels in lymphocytes," *Biochem. Biophys. Res. Commun.*, vol. 458, no. 2, pp. 294–299, 2015.

[210] Z. Su, X. Guo, D. S. Barker, R. L. Shoemaker, R. B. Marchase, and J. E. Blalock, "A store-operated nonselective cation channel in human lymphocytes," *Cell. Mol. Neurobiol.*, vol. 25, no. 3, pp. 625–647, 2005.

[211] H. H. Kerschbaum and M. D. Cahalan, "Single-channel recording of a store-operated Ca^{2+} channel in jurkat T lymphocytes," *Science*, vol. 283, no. 5403, pp. 836–839, 1999.

[212] G. B. Segel, W. Simon, and M. A. Lichtman, "Regulation of sodium and potassium transport in phytohemagglutinin-stimulated human blood lymphocytes," *J. Clin. Inves.*, vol. 64, no. 3, pp. 834–841, 1979.

[213] I. Marakhova, A. Vereninov, F. Toropova, and T. Vinogradova, "Long-term enhancement of Na, K-ATPase pump during blasttransformation of human lymphocytes is controlled first by translational, then by transcriptional mechanisms," *FEBS Lett.*, vol. 368, no. 1, pp. 110–112, 1995.

[214] I. I. Marakhova, A. A. Vereninov, F. V. Toropova, and T. A. Vinogradova, "Na, K-ATPase pump in activated human lymphocytes: on the mechanisms of rapid and long-term increase in K influxes during the initiation of phytohemagglutinin-induced proliferation," *Biochim. Biophys. Acta -Biomembr.*, vol. 1368, no. 1, pp. 61–72, 1998.

[215] E. Dunham and I. Glynn, "Adenosinetriphosphatase activity and the active movements of alkali metal ions," *J. Physiol.*, vol. 156, no. 2, pp. 274–293, 1961.

[216] F. Epstein and R. Whittam, "The mode of inhibition by calcium of cell-membrane adenosine-triphosphatase activity," *Biochem. J.*, vol. 99, no. 1, p. 232, 1966.

[217] A. Brown and V. Lew, "The effect of intracellular calcium on the sodium pump of human red cells.," *J. Physiol.*, vol. 343, no. 1, pp. 455–493, 1983.

[218] J. H. Chen, H. Schulman, and P. Gardner, "A cAMP-regulated chloride channel in lymphocytes that is affected in cystic fibrosis," *Science*, vol. 243, no. 4891, pp. 657–661, 1989.

[219] W. B. Guggino, "Outwardly rectifying chloride channels and CF: a divorce and remarriage," *J. Bioenerg. Biomembr.*, vol. 25, no. 1, pp. 27–35, 1993.

[220] S. S. Garber, "Outwardly rectifying chloride channels in lymphocytes," *J. Membr. Biol.*, vol. 127, no. 1, pp. 49–56, 1992.

[221] K. Khodakhah, A. Melishchuk, and C. M. Armstrong, "Killing k channels with tea+," *Proceedings of the National Academy of Sciences*, vol. 94, no. 24, pp. 13335–13338, 1997.

[222] I. S. Oliveira, I. G. Ferreira, G. M. Alexandre-Silva, F. A. Cerni, C. M. Cremonez, E. C. Arantes, U. Zottich, and M. B. Pucca, "Scorpion toxins targeting kv1. 3 channels: insights into immunosuppression," *Journal of Venomous Animals and Toxins including Tropical Diseases*, vol. 25, 2019.

[223] H. Jäger, J. P. Adelman, and S. Grissmer, "SK2 encodes the apamin-sensitive Ca^{2+}-activated K^+ channels in the human leukemic T cell line, jurkat," *FEBS Lett.*, vol. 469, no. 2-3, pp. 196–202, 2000.

[224] J. J. Agarwal, Y. Zhu, Q.-Y. Zhang, A. A. Mongin, and L. B. Hough, "Tram-34, a putatively selective blocker of intermediate-conductance, calcium-activated potassium channels, inhibits cytochrome p450 activity," *PloS one*, vol. 8, no. 5, p. e63028, 2013.

[225] A. Hermann and C. Erxleben, "Charybdotoxin selectively blocks small ca-activated k channels in aplysia neurons.," *The Journal of general physiology*, vol. 90, no. 1, pp. 27–47, 1987.

[226] M. D. Cahalan, "Stimulating store-operated Ca^{2+} entry," *Nat. Cell Biol.*, vol. 11, no. 6, pp. 669–677, 2009.

[227] R. H. Chokshi, A. T. Larsen, B. Bhayana, and J. F. Cotten, "Breathing stimulant compounds inhibit task-3 potassium channel function likely by binding at a common site in the channel pore," *Molecular pharmacology*, vol. 88, no. 5, pp. 926–934, 2015.

[228] Y. Xiao, J. Tang, Y. Yang, M. Wang, W. Hu, J. Xie, X. Zeng, and S. Liang, "Jingzhaotoxin-iii, a novel spider toxin inhibiting activation of voltage-gated sodium channel in rat cardiac myocytes," *Journal of Biological Chemistry*, vol. 279, no. 25, pp. 26220–26226, 2004.

[229] A. Gasser, G. Glassmeier, R. Fliegert, M. F. Langhorst, S. Meinke, D. Hein, S. Krüger, K. Weber, I. Heiner, N. Oppenheimer, *et al.*, "Activation of T cell calcium influx by the second messenger ADP-ribose," *J. Biol. Chem.*, vol. 281, no. 5, pp. 2489–2496, 2006.

[230] R. Kraft, C. Grimm, H. Frenzel, and C. Harteneck, "Inhibition of trpm2 cation channels by n-(p-amylcinnamoyl) anthranilic acid," *British journal of pharmacology*, vol. 148, no. 3, pp. 264–273, 2006.

[231] R. Guinamard, T. Hof, and C. Del Negro, "The trpm 4 channel inhibitor 9-phenanthrol," *British journal of pharmacology*, vol. 171, no. 7, pp. 1600–1613, 2014.

[232] G. Panyi, Z. Varga, and R. Gáspár, "Ion channels and lymphocyte activation," *Immunol. Lett.*, vol. 92, no. 1, pp. 55–66, 2004.

[233] M. Prakriya, "The molecular physiology of CRAC channels," *Immunol. Rev.*, vol. 231, no. 1, pp. 88–98, 2009.

[234] X. Hou, L. Pedi, M. M. Diver, and S. B. Long, "Crystal structure of the calcium release–activated calcium channel Orai," *Science*, vol. 338, no. 6112, pp. 1308–1313, 2012.

[235] C. Tian, L. Du, Y. Zhou, and M. Li, "Store-operated crac channel inhibitors: opportunities and challenges," *Future medicinal chemistry*, vol. 8, no. 7, pp. 817–832, 2016.

[236] R. Chokshi, M. Matsushita, and J. A. Kozak, "Sensitivity of TRPM7 channels to Mg^{2+} characterized in cell-free patches of jurkat T lymphocytes," *Am. J. Physiol. Cell Physiol.*, vol. 302, no. 11, pp. C1642–C1651, 2012.

[237] M. Parnas, M. Peters, D. Dadon, S. Lev, I. Vertkin, I. Slutsky, and B. Minke, "Carvacrol is a novel inhibitor of drosophila trpl and mammalian trpm7 channels," *Cell calcium*, vol. 45, no. 3, pp. 300–309, 2009.

[238] D. M. Bautista, M. Hoth, and R. S. Lewis, "Enhancement of calcium signalling dynamics and stability by delayed modulation of the plasma-membrane calcium-ATPase in human T cells," *J. Physiol.*, vol. 541, no. 3, pp. 877–894, 2002.

[239] J. Chaudhary, M. Walia, J. Matharu, E. Escher, and A. K. Grover, "Caloxin: a novel plasma membrane ca2+ pump inhibitor," *American Journal of Physiology-Cell Physiology*, vol. 280, no. 4, pp. C1027–C1030, 2001.

[240] J. J. Densmore, G. Szabo, and L. S. Gray, "A voltage-gated calcium channel is linked to the antigen receptor in jurkat T lymphocytes," *FEBS Lett.*, vol. 312, no. 2-3, pp. 161–164, 1992.

[241] R. S. Chuang, H. Jaffe, L. Cribbs, E. Perez-Reyes, and K. J. Swartz, "Inhibition of t-type voltage-gated calcium channels by a new scorpion toxin," *Nature neuroscience*, vol. 1, no. 8, p. 668, 1998.

[242] F. Michelangeli and J. M. East, "A diversity of serca ca2+ pump inhibitors," 2011.

[243] P. Linsdell, "Cystic fibrosis transmembrane conductance regulator chloride channel blockers: pharmacological, biophysical and physiological relevance," *World journal of biological chemistry*, vol. 5, no. 1, p. 26, 2014.

[244] M. Sakaguchi, H. Matsuura, and T. Ehara, "Swelling-induced cl- current in guinea-pig atrial myocytes: inhibition by glibenclamide," *The Journal of physiology*, vol. 505, no. 1, pp. 41–52, 1997.

[245] P. Krogsgaard-Larsen, "Inhibitors of the gaba uptake systems," *Molecular and cellular biochemistry*, vol. 31, no. 2, pp. 105–121, 1980.

[246] F. Lang, E. Gulbins, I. Szabo, A. Lepple-Wienhues, S. M. Huber, C. Duranton, K. S. Lang, P. A. Lang, and T. Wieder, "Cell volume and the regulation of apoptotic cell death," *J. Mol. Recog.*, vol. 17, no. 5, pp. 473–480, 2004.

[247] L. Reuss, "Cyclic amp inhibits cl-/hco3-exchange at the apical membrane of necturus gallbladder epithelium.," *The Journal of general physiology*, vol. 90, no. 2, pp. 173–196, 1987.

[248] F. Lang, J. Madlung, J. Bock, U. Lükewille, S. Kaltenbach, K. Lang, C. Belka, C. Wagner, H. Lang, E. Gulbins, *et al.*, "Inhibition of jurkat-T-lymphocyte Na^+/H^+-exchanger by CD95 (Fas/Apo-1)-receptor stimulation," *Pflügers Archiv Eur. J. Physiol.*, vol. 440, no. 6, pp. 902–907, 2000.

[249] Y. Hotta, J. Nakagawa, N. Ishikawa, Y. Wakida, H. Ando, K. Takeya, N. Ohashi, and K. Matsui, "Protective effect of sm-20550, a selective na+-h+ exchange inhibitor, on ischemia-reperfusion-injured hearts," *Journal of cardiovascular pharmacology*, vol. 37, no. 2, pp. 143–154, 2001.

[250] A. Asuaje, P. Smaldini, P. Martín, N. Enrique, A. Orlowski, E. A. Aiello, C. G. León, G. Docena, and V. Milesi, "The inhibition of voltage-gated H^+ channel (HVCN1) induces acidification of leukemic jurkat T cells promoting cell death by apoptosis," *Pflügers Archiv-Eur. J. Physiol.*, vol. 469, no. 2, pp. 251–261, 2017.

[251] T. Schilling, A. Gratopp, T. E. DeCoursey, and C. Eder, "Voltage-activated proton currents in human lymphocytes," *J. Physiol.*, vol. 545, no. 1, pp. 93–105, 2002.

[252] V. V. Cherny and T. E. DeCoursey, "ph-dependent inhibition of voltage-gated h+ currents in rat alveolar epithelial cells by zn2+ and other divalent cations," *The Journal of general physiology*, vol. 114, no. 6, pp. 819–838, 1999.

[253] A.-N. T. Nguyen, D. P. Wallace, and G. Blanco, "Ouabain binds with high affinity to the na, k-atpase in human polycystic kidney cells and induces extracellular signal–regulated kinase activation and cell proliferation," *Journal of the American Society of Nephrology*, vol. 18, no. 1, pp. 46–57, 2007.

[254] L. Yip, C. W. Cheung, R. Corriden, Y. Chen, P. A. Insel, and W. G. Junger, "Hypertonic stress regulates T-cell function by the opposing actions of extracellular adenosine triphosphate and adenosine," *Shock*, vol. 27, no. 3, pp. 242–250, 2007.

[255] L. Yip, T. Woehrle, R. Corriden, M. Hirsh, Y. Chen, Y. Inoue, V. Ferrari, P. A. Insel, and W. G. Junger, "Autocrine regulation of T-cell activation by ATP release and P2X7 receptors," *FASEB J.*, vol. 23, no. 6, pp. 1685–1693, 2009.

[256] T. Woehrle, L. Yip, A. Elkhal, Y. Sumi, Y. Chen, Y. Yao, P. A. Insel, and W. G. Junger, "Pannexin-1 hemichannel–mediated ATP release together with P2X1 and P2X4 receptors regulate T-cell activation at the immune synapse," *Blood*, vol. 116, no. 18, pp. 3475–3484, 2010.

[257] T. Woehrle, L. Yip, M. Manohar, Y. Sumi, Y. Yao, Y. Chen, and W. G. Junger, "Hypertonic stress regulates T cell function via pannexin-1 hemichannels and P2X receptors," *J Leuk. Biol.*, vol. 88, no. 6, pp. 1181–1189, 2010.

[258] A. W. Lohman, J. L. Weaver, M. Billaud, J. K. Sandilos, R. Griffiths, A. C. Straub, S. Penuela, N. Leitinger, D. W. Laird, D. A. Bayliss, *et al.*, "S-nitrosylation inhibits pannexin 1 channel function," *Journal of Biological Chemistry*, vol. 287, no. 47, pp. 39602–39612, 2012.

[259] W. H. Loomis, S. Namiki, R. S. Ostrom, P. A. Insel, and W. G. Junger, "Hypertonic stress increases T cell interleukin-2 expression through a mechanism that involves ATP release, P2 receptor, and p38 MAPK activation," *J. Biol. Chem.*, vol. 278, no. 7, pp. 4590–4596, 2003.

[260] D. Stakišaitis, V. Meilus, A. Juška, P. Matusevičius, and J. Didžiapetrienė, "Sodium is not required for chloride efflux via chloride/bicarbonate exchanger from rat thymic lymphocytes," *BioMed Res. Int.*, vol. 2014, 2014.

[261] S. Feske, E. Y. Skolnik, and M. Prakriya, "Ion channels and transporters in lymphocyte function and immunity," *Nat. Rev. Immunol.*, vol. 12, no. 7, p. 532, 2012.

[262] L. Stokes, J. Gordon, and G. Grafton, "Non-voltage-gated L-type Ca^{2+} channels in human T cells pharmacology and molecular characterization of the major α pore-forming and auxiliary β-subunits," *J. Biol. Chem.*, vol. 279, no. 19, pp. 19566–19573, 2004.

[263] K. Hill, S. McNulty, and A. Randall, "Inhibition of TRPM2 channels by the antifungal agents clotrimazole and econazole," *Naunyn. Schmiedebergs. Arch. Pharmacol.*, vol. 370, no. 4, pp. 227–237, 2004.

[264] K. Togashi, H. Inada, and M. Tominaga, "Inhibition of the transient receptor potential cation channel TRPM2 by 2-aminoethoxydiphenyl borate (2-APB)," *British J. Pharmacol.*, vol. 153, no. 6, pp. 1324–1330, 2008.

[265] E. Donnadieu, G. Bismuth, and A. Trautmann, "Calcium fluxes in T lymphocytes.," *J. Biol. Chem.*, vol. 267, no. 36, pp. 25864–25872, 1992.

[266] L. Fierro, P.-E. Lund, and A. B. Parekh, "Comparison of the activation of the Ca^{2+} release-activated Ca^{2+} current i CRAC to $InsP_3$ in jurkat T-lymphocytes, pulmonary artery endothelia and RBL-1 cells," *Pflügers Archiv*, vol. 440, no. 4, pp. 580–587, 2000.

[267] J. G. Bilmen, S. Z. Khan, M.-u.-H. Javed, and F. Michelangeli, "Inhibition of the SERCA Ca^{2+} pumps by curcumin," *FEBS J.*, vol. 268, no. 23, pp. 6318–6327, 2001.

[268] C. D. Bortner, M. Gómez-Angelats, and J. A. Cidlowski, "Plasma membrane depolarization without repolarization is an early molecular event in anti-fas-induced apoptosis," *J. Biol. Chem.*, vol. 276, no. 6, pp. 4304–4314, 2001.

[269] R. Franco, C. Bortner, and J. Cidlowski, "Potential roles of electrogenic ion transport and plasma membrane depolarization in apoptosis," *J. Membr. Biol.*, vol. 209, no. 1, pp. 43–58, 2006.

[270] F. Nolte, O. Friedrich, M. Rojewski, R. H. Fink, H. Schrezenmeier, and S. Körper, "Depolarisation of the plasma membrane in the arsenic trioxide (As2o3)-and anti-CD95-induced apoptosis in myeloid cells," *FEBS Lett.*, vol. 578, no. 1-2, pp. 85–89, 2004.

[271] G. Barbiero, F. Duranti, G. Bonelli, J. S. Amenta, and F. M. Baccino, "Intracellular ionic variations in the apoptotic death of L cells by inhibitors of cell cycle progression," *Exp. Cell Res.*, vol. 217, no. 2, pp. 410–418, 1995.

[272] F. Beauvais, L. Michel, and L. Dubertret, "Human eosinophils in culture undergo a striking and rapid shrinkage during apoptosis. Role of K^+ channels," *J. Leuk. Biol.*, vol. 57, no. 6, pp. 851–855, 1995.

[273] C. D. Bortner, F. M. Hughes, and J. A. Cidlowski, "A primary role for K^+ and Na^+ efflux in the activation of apoptosis," *J. Biol. Chem.*, vol. 272, no. 51, pp. 32436–32442, 1997.

[274] B. Dallaporta, P. Marchetti, M. A. De Pablo, C. Maisse, H.-T. Duc, D. Métivier, N. Zamzami, M. Geuskens, and G. Kroemer, "Plasma membrane potential in thymocyte apoptosis," *J. Immunol.*, vol. 162, no. 11, pp. 6534–6542, 1999.

[275] F. M. Hughes, C. D. Bortner, G. D. Purdy, and J. A. Cidlowski, "Intracellular K^+ suppresses the activation of apoptosis in lymphocytes," *J. Biol. Chem.*, vol. 272, no. 48, pp. 30567–30576, 1997.

[276] C. S. I. Nobel, J. K. Aronson, D. J. Van Den Dobbelsteen, and A. F. Slater, "Inhibition of Na^+/K^+-ATPase may be one mechanism contributing

to potassium efflux and cell shrinkage in cd95-induced apoptosis," *Apoptosis*, vol. 5, no. 2, pp. 153–163, 2000.

[277] M. Lobikin, B. Chernet, D. Lobo, and M. Levin, "Resting potential, oncogene-induced tumorigenesis, and metastasis: the bioelectric basis of cancer in vivo," *Phys. Biol.*, vol. 9, no. 6, p. 065002, 2012.

[278] M. Borgnia, S. Nielsen, A. Engel, and P. Agre, "Cellular and molecular biology of the aquaporin water channels," *Ann. Rev. Biochem.*, vol. 68, no. 1, pp. 425–458, 1999.

[279] D. Brown, "The ins and outs of aquaporin-2 trafficking," *Am. J. Physiol. Renal Physiol.*, vol. 284, no. 5, pp. F893–F901, 2003.

[280] D. Brown, T. Katsura, and C. E. Gustafson, "Cellular mechanisms of aquaporin trafficking," *Am. J. Physiol. Renal Physiol.*, vol. 275, no. 3, pp. F328–F331, 1998.

[281] L. S. King, M. Yasui, and P. Agre, "Aquaporins in health and disease," *Mol. Med. Today*, vol. 6, no. 2, pp. 60–65, 2000.

[282] C. D. Cone Jr, "Unified theory on the basic mechanism of normal mitotic control and oncogenesis," -*J. Theor. Biol.*, vol. 30, no. 1, pp. 151–181, 1971.

[283] N. R. Smith, R. L. Sparks, T. B. Pool, and I. L. Cameron, "Differences in the intracellular concentration of elements in normal and cancerous liver cells as determined by X-ray microanalysis," *Cancer Res.*, vol. 38, no. 7, pp. 1952–1959, 1978.

[284] R. Sparks, T. Pool, N. Smith, and I. Cameron, "Effects of amiloride on tumor growth and intracellular element content of tumor cells in vivo," *Cancer Res.*, vol. 43, no. 1, pp. 73–77, 1983.

[285] R. G. Bates and A. K. Vijh, "Determination of pH: theory and practice," *J. Electrochem. Soc.*, vol. 120, no. 8, pp. 263C–263C, 1973.

[286] A. K. Covington, R. Bates, and R. Durst, "Definition of pH scales, standard reference values, measurement of pH and related terminology (Recommendations 1984)," *Pure Appl. Chem.*, vol. 57, no. 3, pp. 531–542, 1985.

[287] K. F. Lim, "Negative pH does exist," *J. Chem. Edu.*, vol. 83, no. 10, p. 1465, 2006.

[288] F. Sherman, "Getting started with yeast," in *Methods Enzymol.*, vol. 350, pp. 3–41, Elsevier, 2002.

[289] A. Perktold, B. Zechmann, G. Daum, and G. Zellnig, "Organelle association visualized by three dimensional ultrastructural imaging of the yeast cell," *FEMS Yeast Res.*, vol. 7, no. 4, pp. 629–638, 2007.

[290] R. Orij, J. Postmus, A. Ter Beek, S. Brul, and G. J. Smits, "In vivo measurement of cytosolic and mitochondrial pH using a pH-sensitive GFP derivative in Saccharomyces cerevisiae reveals a relation between intracellular pH and growth," *Microbiology*, vol. 155, no. 1, pp. 268–278, 2009.

[291] W.-K. Huh, J. V. Falvo, L. C. Gerke, A. S. Carroll, R. W. Howson, J. S. Weissman, and E. K. O'shea, "Global analysis of protein localization in budding yeast," *Nature*, vol. 425, no. 6959, p. 686, 2003.

[292] K. van Eunen, J. Bouwman, P. Daran-Lapujade, J. Postmus, A. B. Canelas, F. I. Mensonides, R. Orij, I. Tuzun, J. van den Brink, G. J. Smits, *et al.*, "Measuring enzyme activities under standardized in vivo-like conditions for systems biology," *FEBS J.*, vol. 277, no. 3, pp. 749–760, 2010.

[293] T. Imai and T. Ohno, "The relationship between viability and intracellular pH in the yeast Saccharomyces cerevisiae.," *Appl. Env. Microbiol.*, vol. 61, no. 10, pp. 3604–3608, 1995.

[294] M. Pampulha and M. Loureiro-Dias, "Combined effect of acetic acid, pH and ethanol on intracellular pH of fermenting yeast," *Appl. Microbiol. Biotechnol.*, vol. 31, no. 5-6, pp. 547–550, 1989.

[295] R. Orij, S. Brul, and G. J. Smits, "Intracellular pH is a tightly controlled signal in yeast," *Biochim. Biophys. Acta -Gen. Subj.*, vol. 1810, no. 10, pp. 933–944, 2011.

[296] T. Ferreira, A. B. Mason, and C. W. Slayman, "The yeast Pma1 proton pump: a model for understanding the biogenesis of plasma membrane proteins," *J. Biol. Chem.*, vol. 276, no. 32, pp. 29613–29616, 2001.

[297] R. Serrano, "In vivo glucose activation of the yeast plasma membrane ATPase," *FEBS Lett.*, vol. 156, no. 1, pp. 11–14, 1983.

[298] A. Peña, N. S. Sánchez, H. Álvarez, M. Calahorra, and J. Ramírez, "Effects of high medium ph on growth, metabolism and transport in saccharomyces cerevisiae," *FEMS yeast research*, vol. 15, no. 2, 2015.

[299] J. François, E. Van Schaftingen, and H.-G. HERS, "Effect of benzoate on the metabolism of fructose 2, 6-bisphosphate in yeast," *Eur. J. Biochem.*, vol. 154, no. 1, pp. 141–145, 1986.

[300] S. Anand and R. Prasad, "Rise in intracellular pH is concurrent with 'start'progression of Saccharomyces cerevisiae," *Microbiology*, vol. 135, no. 8, pp. 2173–2179, 1989.

[301] S. Lindquist and E. Craig, "The heat-shock proteins," *Ann. Rev. Genetics*, vol. 22, no. 1, pp. 631–677, 1988.

[302] P. Coote, M. Cole, and M. Jones, "Induction of increased thermotolerance in Saccharomyces cerevisiae may be triggered by a mechanism involving intracellular pH," *Microbiology*, vol. 137, no. 7, pp. 1701–1708, 1991.

[303] P. Coote, M. Jones, I. Seymour, D. Rowe, D. Ferdinando, A. McArthur, and M. Cole, "Activity of the plasma membrane H^+-ATPase is a key physiological determinant of thermotolerance in Saccharomyces cerevisiae," *Microbiology*, vol. 140, no. 8, pp. 1881–1890, 1994.

[304] R. Serrano, "Structure and function of proton translocating ATPase in plasma membranes of plants and fungi," *Biochim. Biophys. Acta -Rev. Biomembr.*, vol. 947, no. 1, pp. 1–28, 1988.

[305] L. Maresova, E. Urbankova, D. Gaskova, and H. Sychrova, "Measurements of plasma membrane potential changes in Saccharomyces cerevisiae cells reveal the importance of the Tok1 channel in membrane potential maintenance," *FEMS Yeast Res.*, vol. 6, no. 7, pp. 1039–1046, 2006.

[306] F. Rolland, J. H. De Winde, K. Lemaire, E. Boles, J. M. Thevelein, and J. Winderickx, "Glucose-induced cAMP signalling in yeast requires both a G-protein coupled receptor system for extracellular glucose detection and a separable hexose kinase-dependent sensing process," *Mol. Microbiol.*, vol. 38, no. 2, pp. 348–358, 2000.

[307] G. A. Martinez-Munoz and P. Kane, "Vacuolar and plasma membrane proton pumps collaborate to achieve cytosolic ph homeostasis in yeast," *Journal of Biological Chemistry*, vol. 283, no. 29, pp. 20309–20319, 2008.

[308] P. M. Kane, C. Yamashiro, and T. Stevens, "Biochemical characterization of the yeast vacuolar H^+-atpase.," *J. Biol. Chem.*, vol. 264, no. 32, pp. 19236–19244, 1989.

[309] M. Futai and H. Kanazawa, "Structure and function of proton-translocating adenosine triphosphatase (F0F1): biochemical and molecular biological approaches.," *Microbiol. Rev.*, vol. 47, no. 3, p. 285, 1983.

[310] M. D. Ortega and A. Rodríguez-Navarro, "Potassium and rubidium effluxes in Saccharomyces cerevisiae," *Z. Naturforsch. C*, vol. 40, no. 9-10, pp. 721–725, 1985.

[311] O. Kinclová, J. Ramos, S. Potier, and H. Sychrová, "Functional study of the Saccharomyces cerevisiae Nha1p C-terminus," *Mol. Microbiol.*, vol. 40, no. 3, pp. 656–668, 2001.

[312] I. C. West and P. Mitchell, "Proton/sodium ion antiport in Escherichia coli," *Biochem. J.*, vol. 144, no. 1, pp. 87–90, 1974.

[313] R. Ros, C. Montesinos, A. Rimon, E. Padan, and R. Serrano, "Altered Na^+ and Li^+ homeostasis in Saccharomyces cerevisiae cells expressing the bacterial cation antiporter NhaA," *J. Bacteriol.*, vol. 180, no. 12, pp. 3131–3136, 1998.

[314] E. Padan, M. Venturi, Y. Gerchman, and N. Dover, "Na^+/H^+ antiporters," *Biochim. Biophys. Acta -Bioenergetics*, vol. 1505, no. 1, pp. 144–157, 2001.

[315] D. Taglicht, E. Padan, and S. Schuldiner, "Overproduction and purification of a functional Na^+/H^+ antiporter coded by NhaA (ant) from Escherichia coli.," *J. Biol. Chem.*, vol. 266, no. 17, pp. 11289–11294, 1991.

[316] P. Mitchell, "Chemiosmotic coupling in oxidative and photosynthetic phosphorylation," *Biol. Rev.*, vol. 41, no. 3, pp. 445–501, 1966.

[317] P. D. Boyer, B. Chance, L. Ernster, P. Mitchell, E. Racker, and E. C. Slater, "Oxidative phosphorylation and photophosphorylation," *Ann. Rev. Biochem.*, vol. 46, no. 1, pp. 955–966, 1977.

[318] M. D. Lane, P. L. Pedersen, and A. S. Mildvan, "The mitochondrian updated," *Science*, vol. 234, pp. 526–528, 1986.

[319] M. P. Murphy and M. D. Brand, "Variable stoichiometry of proton pumping by the mitochondrial respiratory chain," *Nature*, vol. 329, no. 6135, pp. 170–172, 1987.

[320] P. Mitchell, "Keilin's respiratory chain concept and its chemiosmotic consequences," *Science*, vol. 206, no. 4423, pp. 1148–1159, 1979.

[321] P. D. Boyer, "The unusual enzymology of ATP synthase," *Biochemistry*, vol. 26, no. 26, pp. 8503–8507, 1987.

[322] P. L. Pedersen, N. Williams, and J. Hullihen, "Mitochondrial ATP synthase: dramatic magnesium-induced alterations in the structure and function of the F1-ATPase moiety," *Biochemistry*, vol. 26, no. 26, pp. 8631–8637, 1987.

[323] A. J. Lotka, "Undamped oscillations derived from the law of mass action.," *J. Am. Chem. Soc.*, vol. 42, no. 8, pp. 1595–1599, 1920.

[324] B. Hess and A. Boiteux, "Oscillatory phenomena in biochemistry," *Ann. Rev. Biochem.*, vol. 40, no. 1, pp. 237–258, 1971.

[325] B. Chance, B. Schoener, and S. Elsaesser, "Control of the waveform of oscillations of the reduced pyridine nucleotide level in a cell-free extract," *PNAS*, vol. 52, no. 2, pp. 337–341, 1964.

[326] B. Chance, R. W. Estabrook, and A. Ghosh, "Damped sinusoidal oscillations of cytoplasmic reduced pyridine nucleotide in yeast cells," *PNAS*, vol. 51, no. 6, pp. 1244–1251, 1964.

[327] M. A. Aon, S. Cortassa, H. V. Westerhoff, and K. Van Dam, "Synchrony and mutual stimulation of yeast cells during fast glycolytic oscillations," *Microbiology*, vol. 138, no. 10, pp. 2219–2227, 1992.

[328] P. Richard, B. Teusink, H. V. Westerhoff, and K. van Dam, "Around the growth phase transition s. cerevisiae's make-up favours sustained oscillations of intracellular metabolites," *FEBS Lett.*, vol. 318, no. 1, pp. 80–82, 1993.

[329] P. Richard, J. A. Diderich, B. M. Bakker, B. Teusink, K. van Dam, and H. V. Westerhoff, "Yeast cells with a specific cellular make-up and an environment that removes acetaldehyde are prone to sustained glycolytic oscillations," *FEBS Lett.*, vol. 341, no. 2-3, pp. 223–226, 1994.

[330] P. Richard, B. M. Bakker, B. Teusink, K. Van Dam, and H. V. Westerhoff, "Acetaldehyde mediates the synchronization of sustained glycolytic oscillations in populations of yeast cells," *Eur. J. Biochem.*, vol. 235, no. 1-2, pp. 238–241, 1996.

[331] P. Richard, B. Teusink, M. B. Hemker, K. van Dam, and H. V. Westerhoff, "Sustained oscillations in free-energy state and hexose phosphates in yeast," *Yeast*, vol. 12, no. 8, pp. 731–740, 1996.

[332] S. Danø, P. G. Sørensen, and F. Hynne, "Sustained oscillations in living cells," *Nature*, vol. 402, no. 6759, p. 320, 1999.

[333] A. Kloster and L. F. Olsen, "Oscillations in glycolysis in Saccharomyces cerevisiae: the role of autocatalysis and intracellular ATPase activity," *Biophys. Chem.*, vol. 165, pp. 39–47, 2012.

[334] B. J. Dodd and J. M. Kralj, "Live Cell Imaging Reveals pH Oscillations in Saccharomyces cerevisiae During Metabolic Transitions," *Sci. Rep.*, vol. 7, no. 1, p. 13922, 2017.

[335] A.-K. Gustavsson, D. D. van Niekerk, C. B. Adiels, F. B. du Preez, M. Goksör, and J. L. Snoep, "Sustained glycolytic oscillations in individual isolated yeast cells," *FEBS J.*, vol. 279, no. 16, pp. 2837–2847, 2012.

[336] J. DAS and H.-G. BUSSE, "Long term oscillation in glycolysis," *J. of Biochem.*, vol. 97, no. 3, pp. 719–727, 1985.

[337] E. Neher and B. Sakmann, "Single-channel currents recorded from membrane of denervated frog muscle fibres," *Nature*, vol. 260, no. 5554, p. 799, 1976.

[338] D. Yprey and L. J. Defelice, "The patch-clamp technique explained and exercised with the use of simple electrical equivalent circuits," *Elec. Prop. Cells; Springer: Boston, MA, USA*, p. 7, 2000.

[339] D. Ogden and P. STANFIELD, "Patch clamp techniques for single channel and whole-cell recording," in *Microelectrode techniques: the Plymouth Workshop Handbook*, vol. 2, 1994.

[340] M. Pusch and E. Neher, "Rates of diffusional exchange between small cells and a measuring patch pipette," *Pflügers Archiv*, vol. 411, no. 2, pp. 204–211, 1988.

[341] W. Walz, A. A. Boulton, and G. B. Baker, *Patch-Clamp Analysis: advanced techniques*. No. 35, Springer Science & Business Media, 2002.

[342] A. Korngreen, *Advanced Patch-clamp Analysis for Neuroscientists*. Springer, 2016.

[343] C. Albrecht, "Joseph r. lakowicz: Principles of fluorescence spectroscopy," *Analyt. Bioanalyt. Chem.*, vol. 390, no. 5, pp. 1223–1224, 2008.

[344] P. Maechler, H. Wang, and C. B. Wollheim, "Continuous monitoring of ATP levels in living insulin secreting cells expressing cytosolic firefly luciferase," *FEBS Lett.*, vol. 422, no. 3, pp. 328–332, 1998.

[345] K. Salin, E. M. Villasevil, S. K. Auer, G. J. Anderson, C. Selman, N. B. Metcalfe, and C. Chinopoulos, "Simultaneous measurement of mitochondrial respiration and ATP production in tissue homogenates and calculation of effective P/O ratios," *Physiol. Rep.*, vol. 4, no. 20, 2016.

[346] B. Strehler, E. Harvey, J. Chang, and M. Cormier, "The luminescent oxidation of reduced riboflavin or reduced riboflavin phosphate in the bacterial luciferin-luciferase reaction," *PNAS*, vol. 40, no. 1, pp. 10–12, 1954.

[347] A. Leyssens, A. V. Nowicky, L. Patterson, M. Crompton, and M. Duchen, "The relationship between mitochondrial state, ATP hydrolysis,$[Mg^{2+}]_i$ and $[Ca^{2+}]_i$ studied in isolated rat cardiomyocytes.," *J. Physiol.*, vol. 496, no. 1, pp. 111–128, 1996.

[348] J. Wang, Y. Jiang, C. Zhou, and X. Fang, "Aptamer-based ATP assay using a luminescent light switching complex," *Anal. Chem.*, vol. 77, no. 11, pp. 3542–3546, 2005.

[349] J.-H. Kim, J.-H. Ahn, P. W. Barone, H. Jin, J. Zhang, D. A. Heller, and M. S. Strano, "A luciferase/single-walled carbon nanotube conjugate for near-infrared fluorescent detection of cellular ATP," *Angew. Chem. Int. Ed.*, vol. 49, no. 8, pp. 1456–1459, 2010.

[350] M. Nakano, H. Imamura, T. Nagai, and H. Noji, "Ca^{2+} regulation of mitochondrial ATP synthesis visualized at the single cell level," *ACS Chem. Biol.*, vol. 6, no. 7, pp. 709–715, 2011.

[351] H. Yaginuma, S. Kawai, K. V. Tabata, K. Tomiyama, A. Kakizuka, T. Komatsuzaki, H. Noji, and H. Imamura, "Diversity in ATP concentrations in a single bacterial cell population revealed by quantitative single-cell imaging," *Scientific Rep.*, vol. 4, p. 6522, 2014.

[352] S. P. Adderley, M. Sridharan, E. A. Bowles, A. H. Stephenson, R. S. Sprague, and M. L. Ellsworth, "Inhibition of ATP release from erythrocytes: a role for EPACs and PKC," *Microcirculation*, vol. 18, no. 2, pp. 128–135, 2011.

[353] M. Abelho, "Extraction and quantification of ATP as a measure of microbial biomass," in *Methods to Study Litter Decomposition*, pp. 223–229, Springer, 2005.

[354] G. Manfredi, L. Yang, C. D. Gajewski, and M. Mattiazzi, "Measurements of ATP in mammalian cells," *Methods*, vol. 26, no. 4, pp. 317–326, 2002.

[355] B. F. Milne, M. A. Marques, and F. Nogueira, "Fragment molecular orbital investigation of the role of AMP protonation in firefly luciferase pH-sensitivity," *Phys. Chem. Chem. Phys.*, vol. 12, no. 42, pp. 14285–14293, 2010.

[356] C. Chinopoulos, S. Vajda, L. Csanády, M. Mándi, K. Mathe, and V. Adam-Vizi, "A novel kinetic assay of mitochondrial ATP-ADP exchange rate mediated by the ANT," *Biophys. J.*, vol. 96, no. 6, pp. 2490–2504, 2009.

[357] C. Chinopoulos, G. Kiss, H. Kawamata, and A. A. Starkov, "Measurement of ADP-ATP exchange in relation to mitochondrial transmembrane potential and oxygen consumption," in *Methods in Enzymology*, vol. 542, pp. 333–348, Elsevier, 2014.

[358] R. B. Sekar and A. Periasamy, "Fluorescence resonance energy transfer (FRET) microscopy imaging of live cell protein localizations," *J. Cell Biol.*, vol. 160, no. 5, pp. 629–633, 2003.

[359] H. Imamura, K. P. H. Nhat, H. Togawa, K. Saito, R. Iino, Y. Kato-Yamada, T. Nagai, and H. Noji, "Visualization of ATP levels inside single living cells with fluorescence resonance energy transfer-based genetically encoded indicators," *PNAS*, vol. 106, no. 37, pp. 15651–15656, 2009.

[360] A. D. Ellington and J. W. Szostak, "In vitro selection of RNA molecules that bind specific ligands," *Nature*, vol. 346, no. 6287, p. 818, 1990.

[361] C. Tuerk and L. Gold, "Systematic evolution of ligands by exponential enrichment: RNA ligands to bacteriophage T4 DNA polymerase," *Science*, vol. 249, no. 4968, pp. 505–510, 1990.

[362] S. Song, L. Wang, J. Li, C. Fan, and J. Zhao, "Aptamer-based biosensors," *TrAC Trends Analyt. Chem.*, vol. 27, no. 2, pp. 108–117, 2008.

[363] T. Nguyen, J. P. Hilton, and Q. Lin, "Emerging applications of aptamers to micro-and nanoscale biosensing," *Microfluid. Nanofluidics*, vol. 6, no. 3, p. 347, 2009.

[364] E. J. Cho, J.-W. Lee, and A. D. Ellington, "Applications of aptamers as sensors," *Ann. Rev. Analyt. Chem.*, vol. 2, pp. 241–264, 2009.

[365] L. Gold, B. Polisky, O. Uhlenbeck, and M. Yarus, "Diversity of oligonucleotide functions," *Ann. Rev. Biochem.*, vol. 64, no. 1, pp. 763–797, 1995.

[366] J. Gehl, "Electroporation: theory and methods, perspectives for drug delivery, gene therapy and research," *Acta Physiol.*, vol. 177, no. 4, pp. 437–447, 2003.

[367] M. Halm, T. Hornbaek, N. Arneborg, S. Sefa-Dedeh, and L. Jespersen, "Lactic acid tolerance determined by measurement of intracellular pH of single cells of candida krusei and Saccharomyces cerevisiae isolated from fermented maize dough," *Int. J. Food Microbiol.*, vol. 94, no. 1, pp. 97–103, 2004.

[368] A. G. Hills, "pH and the henderson-hasselbalch equation," *Am. J. Med.*, vol. 55, no. 2, pp. 131–133, 1973.

[369] H. N. Po and N. Senozan, "The henderson-hasselbalch equation: its history and limitations," *J. Chem. Edu.*, vol. 78, no. 11, p. 1499, 2001.

[370] S. De Monte, F. d'Ovidio, S. Danø, and P. G. Sørensen, "Dynamical quorum sensing: Population density encoded in cellular dynamics," *PNAS*, vol. 104, no. 47, pp. 18377–18381, 2007.

[371] N. D. Virgo, *Thermodynamics and the structure of living systems.* PhD thesis, University of Sussex, 2011.

[372] S. Strogatz, "Nonlinear dynamics and chaos: With applications to physics, biology, chemistry, and engineering (boulder, co," 2001.

[373] A. Goldbeter, *Biochemical oscillations and cellular rhythms: the molecular bases of periodic and chaotic behaviour*. Cambridge university press, 1997.

[374] J. D. Murray, "Mathematical biology. i, volume 17 of interdisciplinary applied mathematics," 2002.

[375] P. E. Kloeden and C. Pötzsche, "Nonautonomous dynamical systems in the life sciences," in *Nonautonomous Dynamical Systems in the Life Sciences*, pp. 3–39, Springer, 2013.

[376] C. Chatfield, *The analysis of time series: an introduction*. CRC press, 2016.

[377] M. Heideman, D. Johnson, and C. Burrus, "Gauss and the history of the fast fourier transform," *IEEE ASSP Mag.*, vol. 1, no. 4, pp. 14–21, 1984.

[378] D. Gabor, "Theory of communication. part 1: The analysis of information," *J. Instit. Elect. Eng.-Part III: Radio Commun. Eng.*, vol. 93, no. 26, pp. 429–441, 1946.

[379] L. Sheppard, A. Stefanovska, and P. McClintock, "Detecting the harmonics of oscillations with time-variable frequencies," *Phys. Rev. E*, vol. 83, no. 1, p. 016206, 2011.

[380] D. Iatsenko, P. V. McClintock, and A. Stefanovska, "Extraction of instantaneous frequencies from ridges in time-frequency representations of signals," *Signal Process.*, vol. 125, pp. 290–303, 2016.

[381] A. Bandrivskyy, A. Bernjak, P. McClintock, and A. Stefanovska, "Wavelet phase coherence analysis: application to skin temperature and blood flow," *Cardiovasc. Eng. int. j.*, vol. 4, no. 1, pp. 89–93, 2004.

[382] J. Jamšek, M. Paluš, and A. Stefanovska, "Detecting couplings between interacting oscillators with time-varying basic frequencies: Instantaneous wavelet bispectrum and information theoretic approach," *Phys. Rev. E*, vol. 81, no. 3, p. 036207, 2010.

[383] A. Duggento, T. Stankovski, P. V. McClintock, and A. Stefanovska, "Dynamical bayesian inference of time-evolving interactions: From a pair of coupled oscillators to networks of oscillators," *Phys. Rev. E*, vol. 86, no. 6, p. 061126, 2012.

[384] L. Keselbrener and S. Akselrod, "Selective discrete fourier transform algorithm for time-frequency analysis: method and application on simulated and cardiovascular signals," *IEEE Trans. Biomed. Eng.*, vol. 43, no. 8, pp. 789–802, 1996.

[385] P. Clemson, G. Lancaster, and A. Stefanovska, "Reconstructing time-dependent dynamics," *Proc. IEEE*, vol. 104, no. 2, pp. 223–241, 2016.

[386] G. Kaiser, "Chapter 10 in" A Friendly Guide to Wavelets," 1994.

[387] A. Pikovsky, M. Rosenblum, J. Kurths, and J. Kurths, *Synchronization: a universal concept in nonlinear sciences*, vol. 12. Cambridge university press, 2003.

[388] J. Theiler, S. Eubank, A. Longtin, B. Galdrikian, and J. D. Farmer, "Testing for nonlinearity in time series: the method of surrogate data," *Physica D: Nonlinear Phenomena*, vol. 58, no. 1-4, pp. 77–94, 1992.

[389] M. Paluš, "From nonlinearity to causality: statistical testing and inference of physical mechanisms underlying complex dynamics," *Contemporary Phys.*, vol. 48, no. 6, pp. 307–348, 2007.

[390] L. Sheppard, A. Stefanovska, and P. McClintock, "Testing for time-localized coherence in bivariate data," *Phys. Rev. E*, vol. 85, no. 4, p. 046205, 2012.

[391] F. Wilcoxon, "Individual comparisons by ranking methods," *Biometr. bull.*, vol. 1, no. 6, pp. 80–83, 1945.

[392] B. Rosner, R. J. Glynn, and M.-L. T. Lee, "The Wilcoxon signed rank test for paired comparisons of clustered data," *Biometrics*, vol. 62, no. 1, pp. 185–192, 2006.

[393] J. H. McDonald, *Handbook of biological statistics*, vol. 2. Sparky House Publishing Baltimore, MD, 2009.

[394] J. D. Gibbons and S. Chakraborti, "Nonparametric statistical inference marcel dekker," *Inc. New York*, 2003.

[395] D. Kugiumtzis, "Surrogate data test on time series," in *Modelling and Forecasting Financial Data*, pp. 267–282, Springer, 2002.

[396] D. G. Lopeza, A. Gutierrez, and E. Trejos, "A new surrogate data method for non-stationary time series," *Nonlinear Anal. -Real*, 2010.

[397] T. Schreiber and A. Schmitz, "Surrogate time series," *Physica D: Nonlinear Phenomena*, vol. 142, no. 3-4, pp. 346–382, 2000.

[398] C. Raeth and R. Monetti, "Surrogates with random fourier phases," in *Topics On Chaotic Systems: Selected Papers from CHAOS 2008 International Conference*, pp. 274–285, World Scientific, 2009.

[399] P. Szendro, G. Vincze, and A. Szasz, "Bio-response to white noise excitation," *Electro-and Magnetobiology*, vol. 20, no. 2, pp. 215–229, 2001.

[400] L. Mullins and K. Noda, "The influence of sodium-free solutions on the membrane potential of frog muscle fibers," *The Journal of general physiology*, vol. 47, no. 1, pp. 117–132, 1963.

[401] R. Moreton, "An investigation of the electrogenic sodium pump in snail neurones, using the constant-field theory," *Journal of Experimental Biology*, vol. 51, no. 1, pp. 181–201, 1969.

[402] C. Poignard, A. Silve, F. Campion, L. M. Mir, O. Saut, and L. Schwartz, "Ion fluxes, transmembrane potential, and osmotic stabilization: a new dynamic electrophysiological model for eukaryotic cells," *European Biophysics Journal*, vol. 40, no. 3, pp. 235–246, 2011.

[403] C. Armstrong and G. Cota, "Calcium block of Na^+ channels and its effect on closing rate," *Proc. Nat. Acad. Sci.*, vol. 96, no. 7, pp. 4154–4157, 1999.

[404] C. C. Chow and J. A. White, "Spontaneous action potentials due to channel fluctuations," *Biophys. J.*, vol. 71, no. 6, pp. 3013–3021, 1996.

[405] T. Stankovski, A. Duggento, P. V. McClintock, and A. Stefanovska, "A tutorial on time-evolving dynamical Bayesian inference," *The Eur. Phys. J. Spec. Topics*, vol. 223, no. 13, pp. 2685–2703, 2014.

[406] P. G. Heytler, "[58] uncouplers of oxidative phosphorylation," in *Methods in enzymology*, vol. 55, pp. 462–472, Elsevier, 1979.

[407] D. Keilin, E. F. Hartree, and E. Hartree, "Cytochrome and cytochrome oxidase," *Proceedings of the Royal Society of London. Series B-Biological Sciences*, vol. 127, no. 847, pp. 167–191, 1939.

[408] E. Rosenfeld, B. Beauvoit, M. Rigoulet, and J.-M. Salmon, "Non-respiratory oxygen consumption pathways in anaerobically-grown saccharomyces cerevisiae: evidence and partial characterization," *Yeast*, vol. 19, no. 15, pp. 1299–1321, 2002.

[409] D. A. Harris, "Azide as a probe of co-operative interactions in the mitochondrial f1-atpase," *Biochimica et Biophysica Acta (BBA)-Bioenergetics*, vol. 974, no. 2, pp. 156–162, 1989.

[410] S. Ottilie, G. M. Goldgof, A. L. Cheung, J. L. Walker, E. Vigil, K. E. Allen, Y. Antonova-Koch, C. W. Slayman, Y. Suzuki, and J. D. Durrant, "Two inhibitors of yeast plasma membrane atpase 1 (sc pma1p): toward the development of novel antifungal therapies," *Journal of cheminformatics*, vol. 10, no. 1, p. 6, 2018.

[411] M. Bublitz, L. Kjellerup, K. O. Cohrt, S. Gordon, A. L. Mortensen, J. D. Clausen, T. D. Pallin, J. B. Hansen, A. T. Fuglsang, W. Dalby-Brown, *et al.*, "Tetrahydrocarbazoles are a novel class of potent p-type atpase inhibitors with antifungal activity," *PloS one*, vol. 13, no. 1, p. e0188620, 2018.

[412] G. Lancaster, Y. F. Suprunenko, K. Jenkins, and A. Stefanovska, "Modelling chronotaxicity of cellular energy metabolism to facilitate the identification of altered metabolic states," *Scientific reports*, vol. 6, p. 29584, 2016.

[413] B. Trivedi and W. H. Danforth, "Effect of pH on the kinetics of frog muscle phosphofructokinase," *J. Biol. Chem.*, vol. 241, no. 17, pp. 4110–4114, 1966.

[414] H. Cohen and J. Cooley, "The numerical solution of the time-dependent Nernst-Planck equations," *Biophys. J.*, vol. 5, no. 2, pp. 145–162, 1965.

[415] M. H. Lee, "Fick's law, Green-Kubo formula, and Heisenberg's equation of motion," *Phys. Rev. L.*, vol. 85, no. 12, p. 2422, 2000.

[416] Y. V. Nazarov, "Generalized Ohm's Law," in *Quantum Dynamics of Submicron Structures*, pp. 687–704, Springer, 1995.

[417] Q. Gu, E. Schiff, S. Grebner, F. Wang, and R. Schwarz, "Non-Gaussian transport measurements and the Einstein relation in amorphous silicon," *Phys. Rev. L.*, vol. 76, no. 17, p. 3196, 1996.

[418] J. Garcia-Soto and S. Grinstein, "Determinants of the transmembrane distribution of chloride in rat lymphocytes: role of Cl^- - $HCO_3{}^-$ exchange," *Am. J. Physiol. Cell Physiol.*, vol. 258, no. 6, pp. C1108–C1116, 1990.

[419] D. Stakisaitis, M. S. Lapointe, and D. Batlle, "Mechanisms of chloride transport in thymic lymphocytes," *Am. J. Physiol. Renal Physiol.*, vol. 280, no. 2, pp. F314–F324, 2001.